

# SURFACE PRESSURE AND WIND LOAD CHARACTERISTICS ON PRISMS IMMERSED IN A TRANSIENT GUST FRONT FLOW FIELD

Kyle Butler<sup>\*</sup>, Shuyang Cao<sup>†</sup>, Yukio Tamura<sup>†</sup>, Ahsan Kareem<sup>\*</sup>, Shigehira Ozono<sup>‡</sup>

<sup>\*</sup>NatHaz Modeling Laboratory  
University of Notre Dame, Notre Dame, IN 46545, USA  
e-mails: kbutler3@nd.edu, kareem@nd.edu

<sup>†</sup>Wind Engineering Research Center  
Tokyo Polytechnic University, Kanagawa 243-02, Japan  
e-mails: cao@arch.t-kougei.ac.jp, yukio@arch.t-kougei.ac.jp

<sup>‡</sup>Department of Applied Physics, Faculty of Engineering  
University of Miyazaki, 889-2192, Japan  
e-mail: ozono@phys.miyazaki-u.ac.jp

**Keywords:** Gust fronts, multiple fan wind tunnel, transient surface pressures.

**Abstract:** *Thunderstorm generated gust fronts are responsible for various degrees of structural damage in many areas of the world. However, the resulting impact of gust front winds is not fully understood to such a level that their flow kinematics, dynamics and impact on structures can be quantified with some certainty. Gust front winds are transient in nature and have a flow profile which differs significantly from a typical boundary layer flow field. This study focuses on investigating the effects of this flow profile and its transient nature on the aerodynamics of bluff, prismatic bodies. A gust front type flow field is generated using a multiple fan wind tunnel and the resulting surface pressures are captured on a suite of prismatic models, which vary in size in relationship to the oncoming wind profile. The temporal variations in surface pressures are analyzed using traditional time, frequency and time-frequency domain schemes. Results indicate the changing nature of the surface pressure field in time, highlighting both qualitative and quantitative differences between local and area-averaged pressures under a host of flow profiles.*

## 1 INTRODUCTION

Many severe wind events are not caused by typical boundary layer type winds and associated fluctuating components, but by large scale transient phenomena. Thunderstorms, downburst outflows and gust fronts constitute various extreme wind events that cause significant damage and result in loss of lives and property, particularly to low or mid-rise buildings, transmission lines, industrial structures and, potentially, long span bridges. Studies have shown that thunderstorm winds are the prevailing design wind speeds for higher recurrence intervals of many locations in the United States (e.g. Twisdale and Vickery 1992), highlighting the need for more fundamental studies of the flow behavior. Thus, new simulation and

modeling techniques are required to capture thunderstorm and gust front characteristics. Some characteristics of these events are, primarily, their respective horizontal wind velocity profiles near the ground surface and their short life span. However, the impacts of such events are not as easily quantified as is the impact of typical synoptic boundary layer flow fields, and little is understood about the true nature of their aerodynamic behavior.

The simulation of downbursts and gust fronts has been attempted through various physical and numerical techniques including impinging jets (e.g. Chay and Letchford 2002), large vortex generators (Sarkar et al. 2006), wall jets (Lin and Savory 2006), and a flat plate at high incidence (Butler and Kareem 2007), along with numerical models aimed at reproducing storm event time histories (e.g. Wood et al. 2001). This work presents the use of a new facility to the study gust front wind loads on structures. As opposed to recreating the entire thunderstorm or downburst structure (ie. a descending core column of air), a more basic approach was undertaken to investigate the broader impacts of the ground level outflow from these events, identifying features in the resulting surface pressure field that distinguish these events from impacts due to synoptic flow systems. In order to accomplish this, a newly designed wind tunnel was employed to isolate the impact of two distinct features of gust front flows: the near ground flow profile shape and the rapid, transient changes. The impact of these conditions were captured on multiple square cross-section, prismatic models, to better understand the basic underlying mechanisms that result from the impact of gust front type flow fields and to compare them with the existing body of research about flows around simple prismatic shapes (e.g. Kareem and Cermak 1984, Lin et. al. 2005). The results presented consider both qualitative and quantitative measures to expose the underlying aerodynamics involved.

Beyond the basic bluff body aerodynamics viewpoint, these experimental results build upon the body of knowledge that is currently being incorporated into a new design framework. The Gust Front Factor (GFF) based approach (Kwon and Kareem 2007) centers around the delineation of the impact of the features commonly associated with gust front type flows. The GFF approach, akin to the gust loading factor approach, provides a framework for the codification of the gust front load effects in building design codes. The factor encapsulates static and dynamic characteristics of gust-front wind effects through their distinguishing features: variation in the vertical velocity profile; dynamic effects induced by the sudden rise in wind speed; non-stationarity of turbulence in gust-front wind; transient aerodynamics. This experimental program attempts to address two of these features: the kinematic effects resulting from the velocity pressure relationship in the profile shape and the transient aerodynamic effects resulting from the rapidly varying flow field.

## 2 EXPERIMENTAL SETUP

Experiments were carried out in the 3-D multiple-fan wind tunnel constructed at the University of Miyazaki, a description of which is given in Fig. 1a. It is comprised of a series of 99 fans arranged in a grid-like pattern, each individually controlled through separate AC servo-motors. The development of this facility from a 2-D to 3-D domain and subsequent experiments utilizing this facility have shown its efficacy in generating and reproducing various statistical characteristics of atmospheric flows (e.g. Nishi and Miyagi 1995, Cao et al. 2001, 2002, Ozono et al. 2006). The test section measures 15.5m long (adjustable), 2.6m wide and 1.8m high. Based on the dynamic nature of this system, and its inherent capability to tailor flow fields, it was presented as an ideal choice to aid in the modeling of gust front type outflows.

In this study, emphasis was placed on generating a transient variation of the mean flow profile while also replicating the general shape of a gust front outflow for detailed surface pres-

sure measurements. The objective was to capture various trends in the pressure response of a prismatic cylinder to both the inflow profile shape and the concurrent increase in flow speed. Surface pressures were monitored on three prismatic models (a general layout of the measurement locations is shown in Fig. 1b) and each varied in height with respect to the height of the level of maximum outflow in the gust profile. The first model (M1) was designed such that the roof level was above the height of the maximum outflow, and contained 176 pressure measurement locations distributed over the windward, side and leeward surfaces. The second prismatic model (M2) was designed such that its height was closest to the level of maximum outflow, and the third prismatic model (M3) was reduced such that its roof level height was below the level of maximum outflow. On each model, pressure measurements were taken at various levels, with 20 pressure measurement locations evenly distributed on each level. Therefore, the smallest model had 60 pressure measurement locations and the mid-height model had 120 measurement locations.

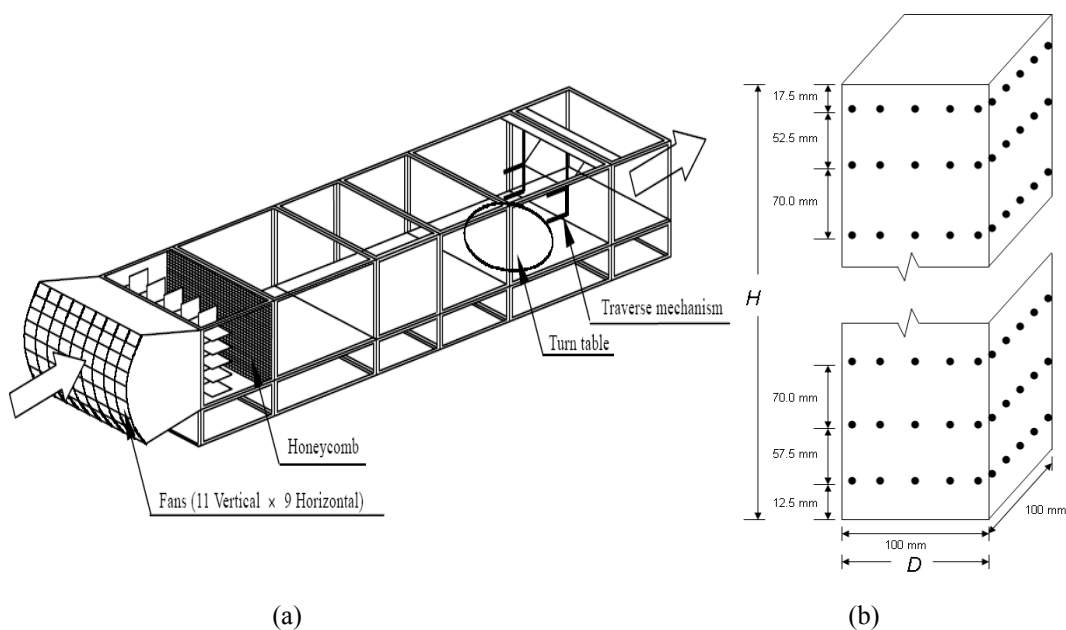


Figure 1: a) Multiple fan wind tunnel setup (Cao et al. 2002) and b) a general schematic of pressure measurement locations on prismatic model.

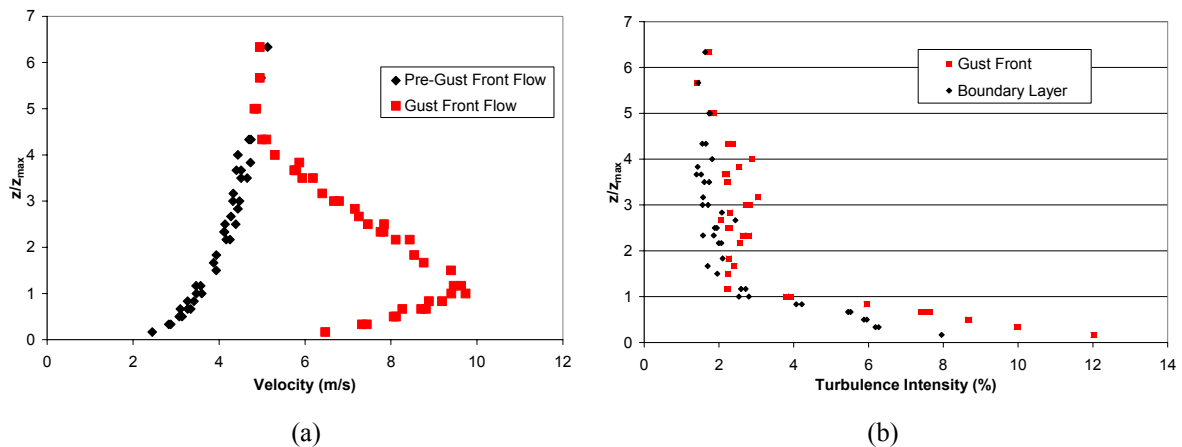


Figure 2: a) Velocity profile of the initial boundary layer flow and the subsequent gust front outflow and b) the turbulence intensity profile of both the boundary layer and gust front flows.

In each test case presented, the velocity variation at the height of maximum outflow between the boundary layer condition and the gust front condition remained fixed and was approximately 7m/s. Each model was subjected to the same, repeated time history of flow conditions and the angle of attack of each model was varied between  $0^\circ$  and  $45^\circ$ . The mean flow profile and the turbulence intensity profiles of both the boundary layer and gust front flow conditions are presented in Fig. 2a and 2b, where  $z$  is the height above the surface and  $z_{max}$  is the height at which the maximum velocity occurs.

Statistics for the mean profile and turbulence intensity were assessed in the time periods before and after the flow acceleration/deceleration, thus the transient segment is not included. The mean gust front outflow exhibits the characteristic “nose” shape in the near ground region and matches the existing flow regime at the boundary layer height, one of the methods of velocity assessment presented in the GFF framework. The higher turbulence intensity values occur within the region of the increasing flow gradients near ground, while only a slight increase is evident above the maximum outflow. Although there are measurements of turbulence intensity profiles in relation to impinging jets and wall jets (i.e. Chay and Letchford 2002, Lin and Savory 2006), used within a similar context, and through some full scale captures of gust fronts and downbursts (e.g. Orwig and Schroeder 2007), there is little information regarding the full behavior of the gust front profile from which to draw accurate comparisons, particularly regarding the turbulence profile or the transient development of the profile.

### 3 RESULTS AND DISCUSSION

Each prismatic model studied was exposed to a gust front like event, where the wind speed was accelerated to induce changes in the flow profile that recreated the profile generated from full scale investigations. In this case, the prismatic models were exposed to a boundary layer flow field before a gust front like profile was induced for approximately 80 seconds ending with the wind speed profile given in the initial flow condition, i.e. the boundary layer flow profile. Fig. 3a shows an example time history of the velocity at the maximum outflow level.

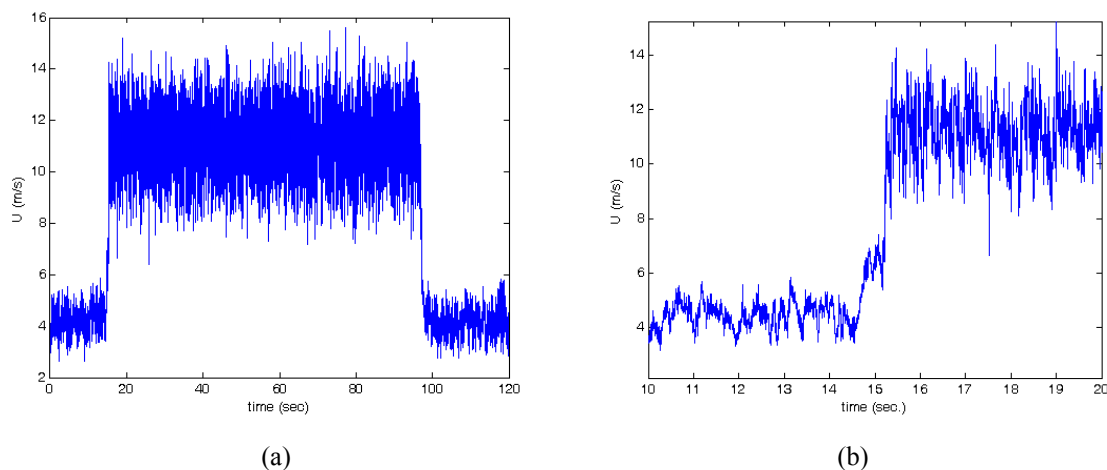


Figure 3: a) Example time history of velocity at maximum outflow and b) cutaway of initial velocity increase.

The scaling of extreme gust events can be based on any number of parameters, e.g. downburst outflow radius or maximum velocity height. In this particular case, the gust scale must be based on the profile shape and the length of the event occurrence. Fujita catalogued various different downburst cases, which can provide a basis for scaling experimental conditions. The downburst profiles examined by Fujita (1985, 1990) identified maximum outflow velocity heights between 30m and 100m and maximum speeds up to approximately 75m/s. Based

on this particular full scale information, length scales linked to the height of maximum outflow produced in the wind tunnel approximately range between 1/120 and 1/400. Velocity scales based on a maximum outflow speed of 11m/s is approximately 1/7, yielding a range of time scales between 1/17 and 1/57. Assuming gust events occur over an interval of 1s to 2s, as presented in this study (a sample time history of which is shown in Fig. 3b, along with a pressure response in Fig. 4b), this represents extreme events lasting 20s to 120s. For comparison, the classic Andrews Air Force Base event in 1983 experienced an increase in velocity from the ambient condition to maximum gust speed occurred within a window of approximately two minutes. However, continued analysis of gust front events will certainly introduce new scaling challenges.

Comparisons of the mean surface pressures within each of the two flow profiles showed variations in both the level of pressure increase and regions of dominant impact. The results for the boundary layer case compare well with other experimental data for tall and low-rise structures (e.g. Surry and Djakovich 1995, Tamura et al. 1997). The mean pressure coefficient on the windward surface of M1, shown in Fig. 4a, indicates a shift in the location of the maximum pressure and an increase in pressures, compared to the initial boundary layer flow, in the lower region of the model surface (where  $z$  is the vertical direction,  $x$  is the horizontal direction and  $H$  and  $D$  are the height and width of the model, respectively). In the boundary layer flow, the mean pressure coefficients on the side faces were more negative than that experienced in the gust front flow. Similar trends were also observed on the leeward surface. This may indicate a more coherent flow field around the prism surface, considering there was no significant change in the turbulence intensity above the maximum outflow level. Mean pressures on the low and mid-rise structures behaved in much the same fashion as they do around the taller model. Pressure coefficients on the leeward surface were more negative in the boundary layer flow when compared to the gust flow regime over the entirety of the surface, indicating possible suppressed vortex development that generally occurs with square cylinders.

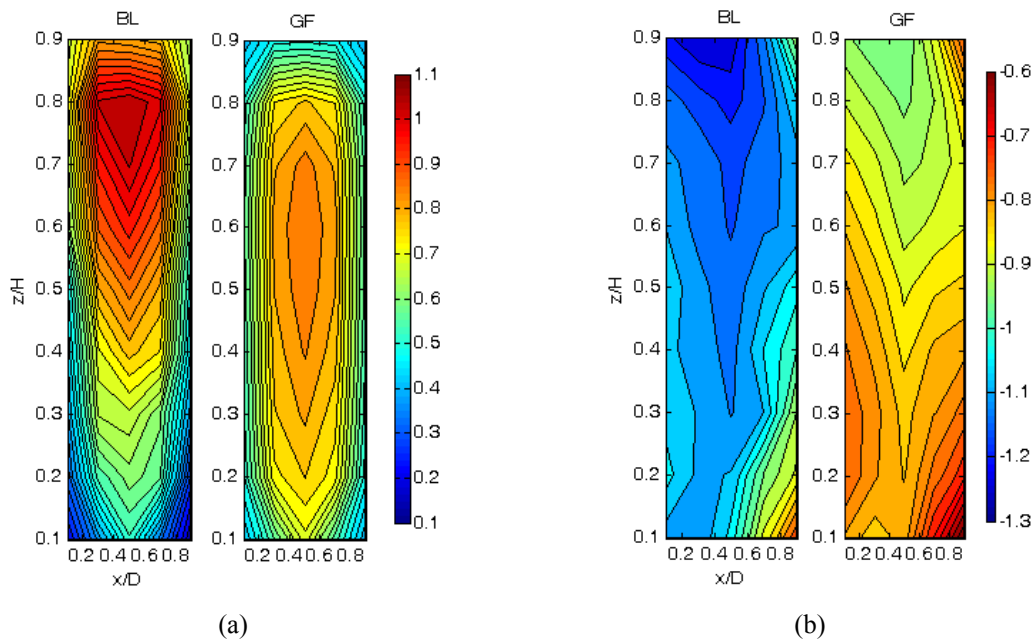


Figure 4: Contours of the mean pressure coefficient on model M1 on (a) windward and (b) side face in both boundary layer (left) and gust front (right) outflows.

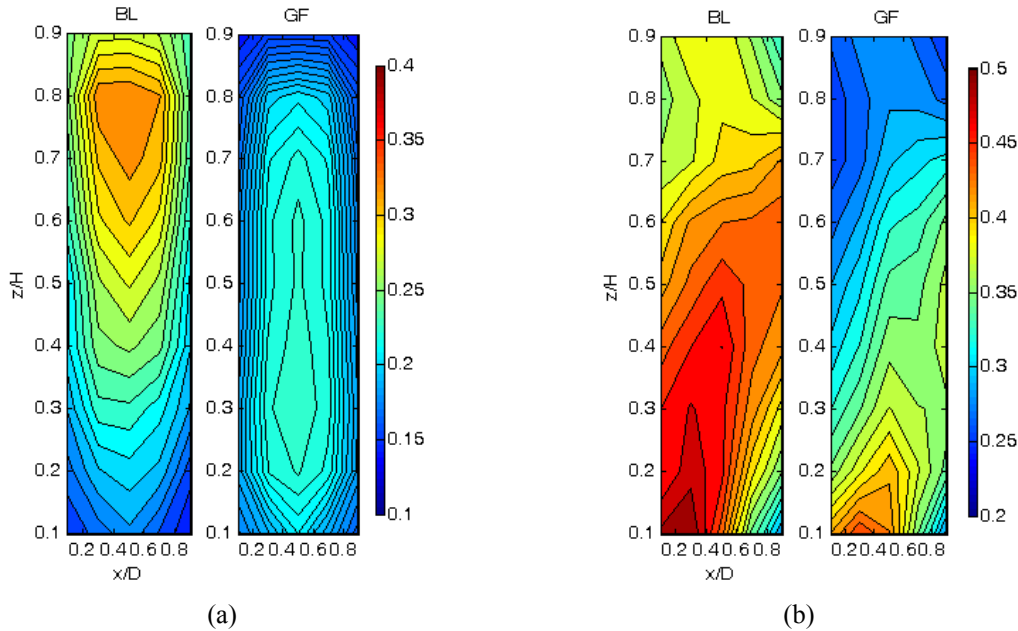


Figure 5: Contours of the RMS of pressure coefficients on model M1 on (a) windward and (b) side face in both boundary layer (rightleft) and gust front (leftright) outflows.

However, in similar studies regarding gust front flows and their impacts on prismatic models (e.g. Letchford and Chay 2002), it has been identified that the gust event can induce situations where the pressure coefficients achieve an absolute value larger than that given by a quasi-steady estimate. The increase in the pressure coefficients on the side surfaces in the gust flow field, when compared to boundary layer flows for the examined prisms, as well as the concomitant increase in the windward and leeward surfaces, indicates a self-similar nature in the gust front flow profile that exists independently of the approach flow profile.

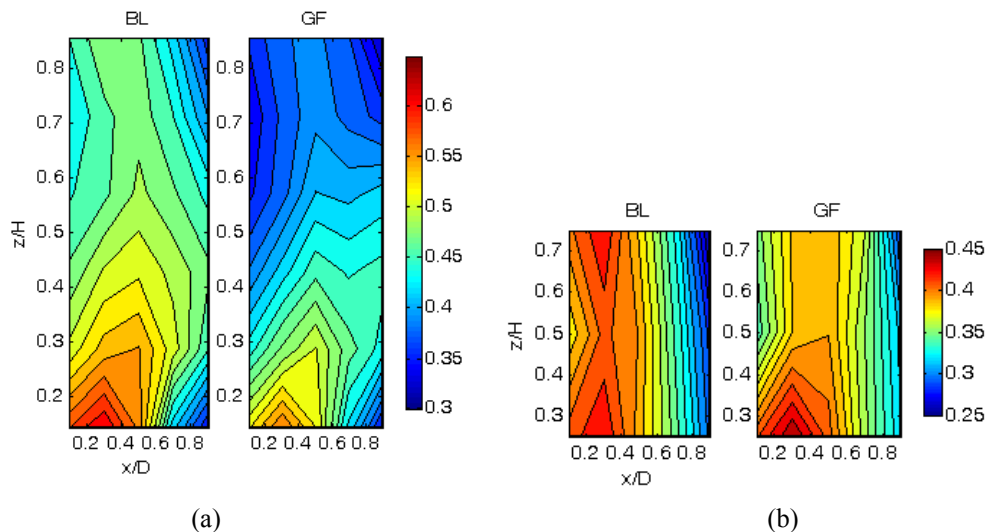


Figure 6: Contours of the RMS of pressure coefficients on the side faces of (a) M2 and (b) M3 in both boundary layer (rightleft) and gust front (leftright) outflows.

The RMS of the surface pressure fluctuations on M1, shown in Fig. 5b, indicated decreased variability in the pressure coefficient on the side face when the prism was subjected to the gust front flow than compared to the boundary layer flow. Additionally, the variation in pressure coefficient on the mid-rise and low-rise prisms, shown in Fig. 6a and 6b respectively, did show similarity in the distribution of the RMS of pressures corresponding with the height of

the model. The roof level of the mid-rise structure is approximately in line with the height of maximum outflow, and results showed that the mid-rise model had higher pressure coefficient fluctuations on the side face than did that of the high and low-rise models. This could be explained as a result of the nature of opposing gradients in the flow field. The high-rise model experiences both flow gradients, the opposition of which could have a moderating effect on fluctuations on the model surface, and could potentially be responsible for the higher correlations experienced on the side faces. The mid-rise model is subject to the near ground surface velocity gradient, and is indirectly influenced by the opposing velocity gradient not impacted by the model surface. On the other hand, the low-rise model is immersed within the lower half of the velocity gradient and is not influenced by the upper half of the gust front gradient, therefore experiencing lower levels of fluctuations.

Apart from the mean distribution resulting from each profile, the pressure coefficient distribution during the velocity increase reveals more about the impact of the flow structure. Fig. 7 shows the maximum, or minimum, pressure coefficient during the period of accelerated velocity. The windward surface (Fig. 7a) of prism M1 shows two distinct regions of increasing pressure resulting from the dual gradient, while a region of decreasing pressure appears on the trailing edge of the side surface (Fig. 7b) at the height of maximum outflow velocity in the gust profile. The distribution of extreme pressures is altered by the changing flow field, primarily the large velocity gradients which modify the aerodynamics of the surrounding flow.

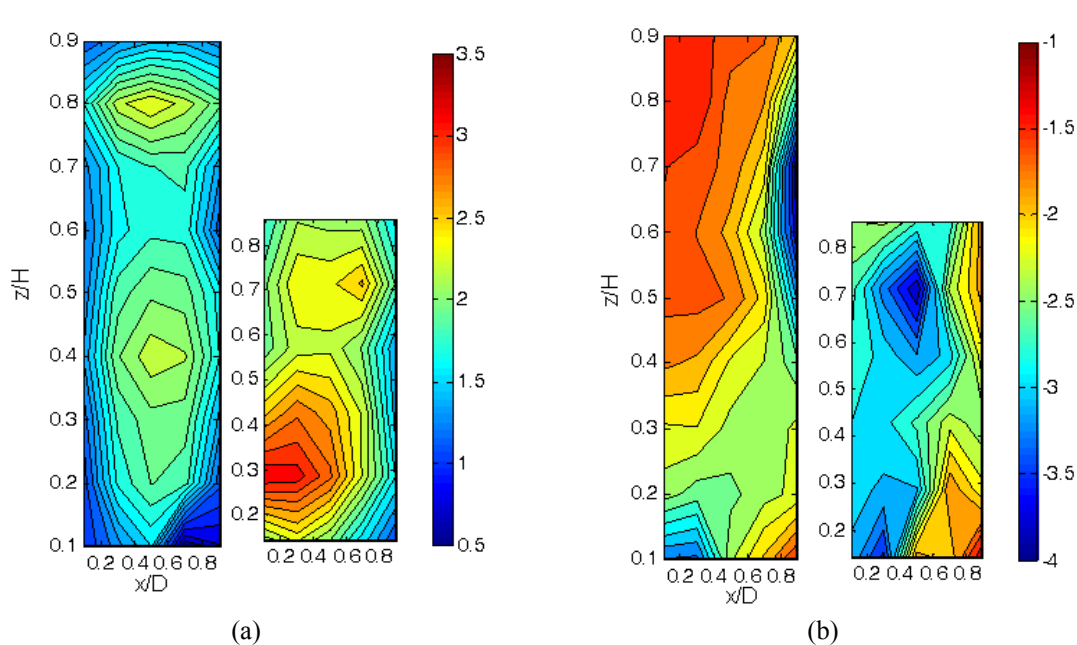


Figure 7: Contours of the instantaneous maximum / minimum pressure coefficients on the (a) windward and (b) side surfaces of M1 and M2 during the velocity rise period.

Correlations of pressures in the chordwise and spanwise directions reveal distinctions regarding both the prism height and inflow profile shape. The spanwise correlation taken at the leading edge (Fig. 8a) indicates that the gust front outflow decreases the level of correlation over the height of the structures, though the level of which is dictated by the prism height. Correlation measures taken along the trailing edge (Fig. 8b) when compared to those taken on the leading edge, show that the subsistence of correlation measures in the gust front flow do not occur, as values decrease more rapidly for prism M1 when compared to the smaller prisms. It is interesting to note, however, when moving from leading edge to trailing edge, that spanwise correlations for the mid and low-rise prisms show that the values for the gust front flow become larger than those of the boundary layer flow at the trailing edge. The

marked difference in the correlations of M1 over the height is indicative of the differing velocity gradients that are experienced.

Similar plots of the chordwise correlation taken at mid-level height, shown in Fig. 9a, on each model prism shows higher correlations for the gust front profile, compared to the boundary layer profile, for M1 than for M2 or M3, where the gust profile correlations are lower. This again may indicate that the large scale flow structure is more coherent within the gust front flow field. Additionally, the spanwise correlation of the profiles along the center line of the windward surface shows that the gust flow profile has a negative correlation in the lower portion of the profile, indicating an opposing flow structure derived from the dual gradients in the flow profile.

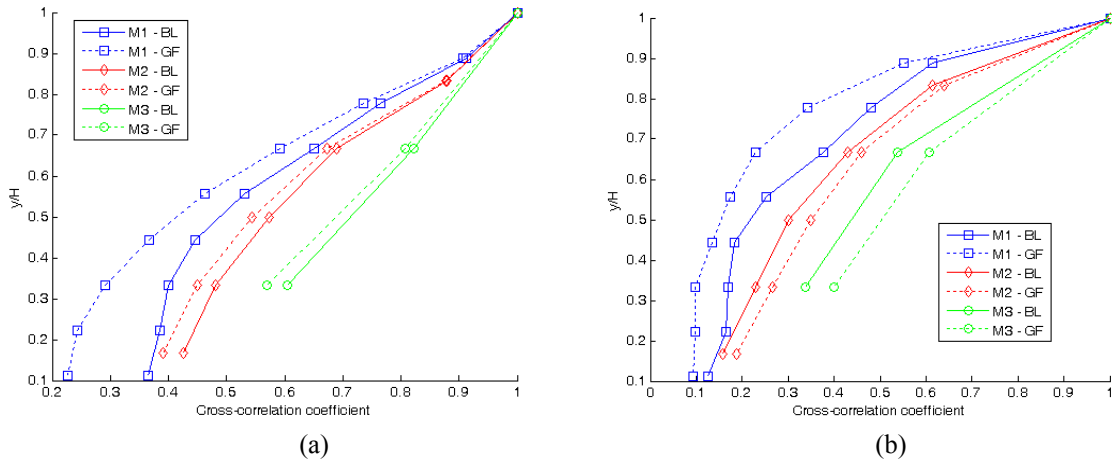


Figure 8: Correlations in the (a) spanwise direction along the leading edge and (b) in the spanwise direction along the trailing edge on prism side face.

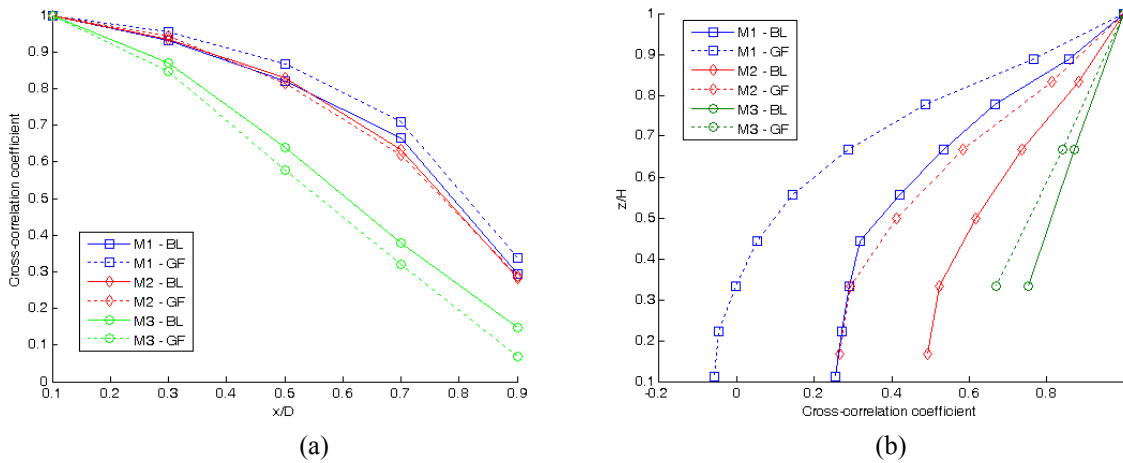


Figure 9: Correlations of pressures taken in the (a) chordwise at mid level height and (b) spanwise along the center line of the windward surface.

Other statistical features, such as the power spectral density (PSD), showed variation in the frequency content at individual pressure measurement locations as result of the changing flow velocity. What is of interest is how the height of the building modifies the frequency component of the resulting flow field as a result of the gust front profile. In similar studies (Butler and Kareem 2007), the effect of turbulence had a spatial evolution with observations from the windward to side face at the leading corner. As mentioned earlier, the height wise dual gradient nature of the flow field has the potential of inducing dual natured effects within the sur-

face pressure regime developed by the existing boundary layer flow. The PSD at mid-level height in the high-rise model, making observations from the leading edge to the trailing edge, shows a peaked nature that becomes more defined with the increasing velocity. There is no shift in the non-dimensional frequency, possibly indicating that the gust front flow profile does not directly change the vortex development around the prism, but that it may be a transient factor.

Comparing the frequency profile of the high-rise structure with that of the mid-rise structure, it is observed that the frequency content changes in much the same manner, though with less relative energy. In addition, the low-rise model has markedly less energy than the taller two models in either flow regime, as development of any stable flow structure is muted with the truncated prism length.

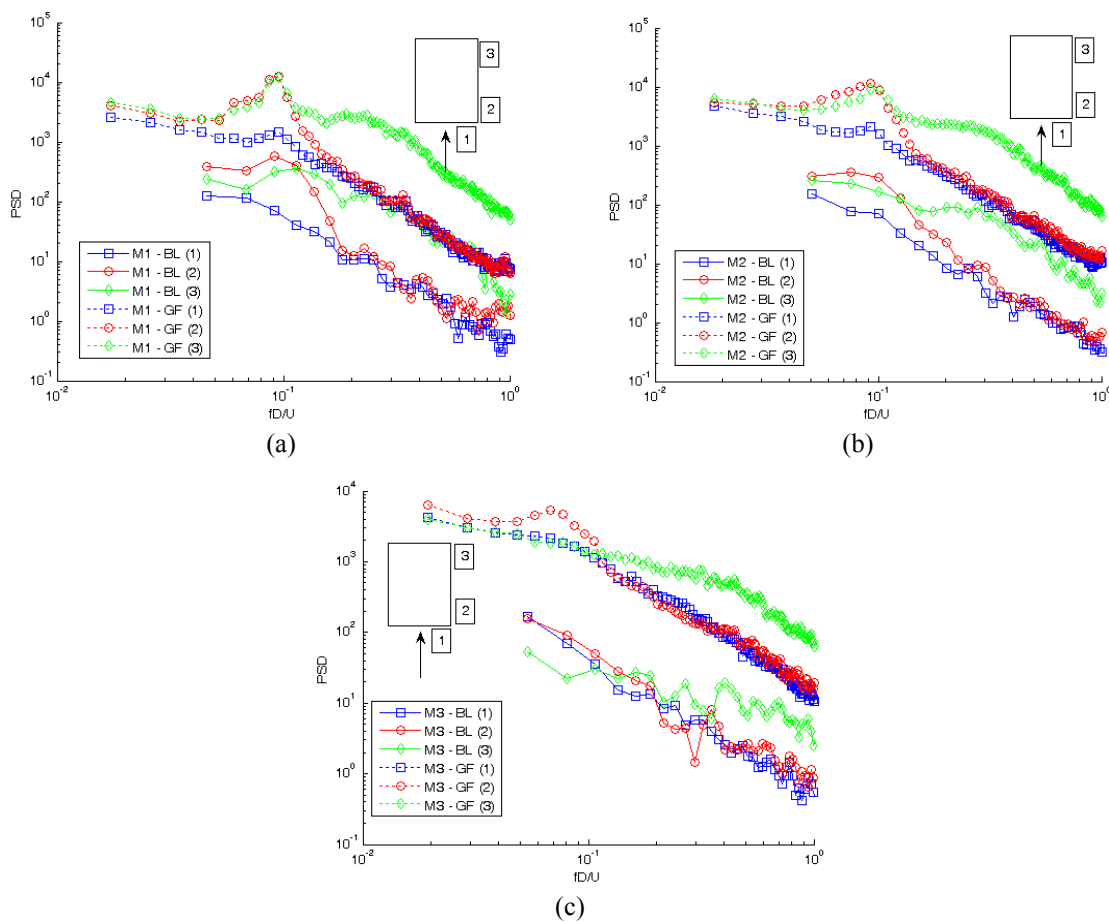


Figure 10: PSD of mid-level pressure measurements on the leading edge and side face for (a) M1, (b) M2 and (c) M3.

Examination of global forces, such as lift and drag, offer more intriguing results. The drag and lift force coefficient generated by the tallest prismatic model, a time history of which is shown in Fig.11a and 12a respectively, reveals no obvious impact in the intensity of either drag or lift due to the changing inflow field. A probability distribution for each force component shows normally distributed lift and a positively skewed distribution for drag. The time history of drag shows a slightly higher shift in the mean value for the boundary layer flow condition, indicating that the gust inflow profile potentially moderates the level of suction on the leeward surface, as well as the level of spanwise vortex formation.

The corresponding wavelet scalograms for the drag and lift time history, shown in Fig. 11b and 12b respectively, reveals frequency content changes, primarily as a result of the changing flow speed. What is interesting to note is that the intensity of the wavelet scalogram for the lift force coefficient decreases once exposed to the gust front profile flow, compared to the boundary layer flow at the beginning and end of each experimental run. Since the intensity of fluctuating lift was not impacted by the changing flow profile, though the wavelet intensity was comparatively reduced, it is estimated that a broader range of frequencies was introduced with the gust front profile. Additionally, there is no identifiable frequency content in the scalogram at the instant of flow acceleration or deceleration, possibly due to the inability of the surrounding flow field to instantaneously adapt to the change in velocity and profile shape.

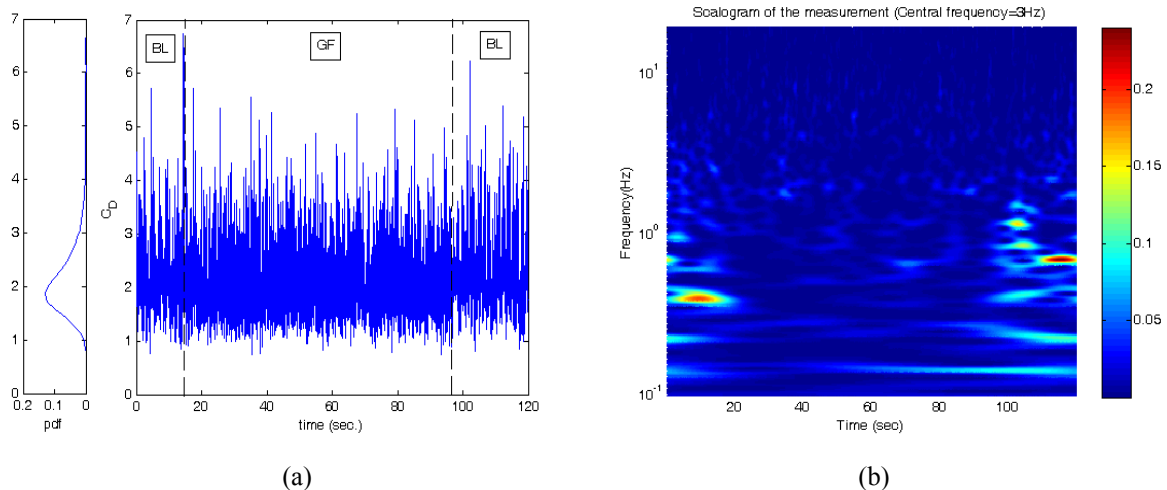


Figure 11: (a) Time history of the drag coefficient for M1 and (b) corresponding wavelet scalogram.

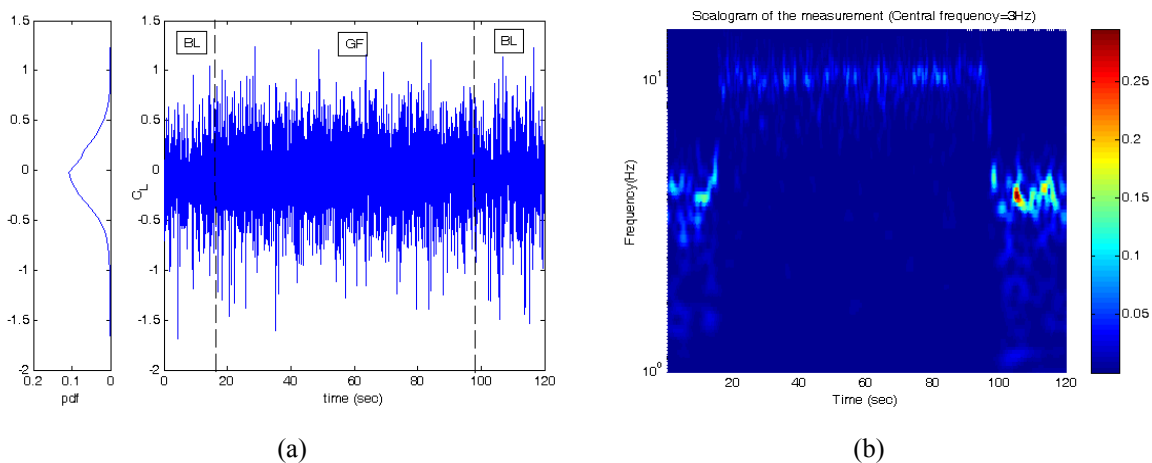


Figure 12: (a) Time history of the lift coefficient for M1 and (b) corresponding wavelet scalogram

Comparing wavelet scalograms for the resulting forces on various prisms, there is a particular trend that becomes apparent in two instances. In both the case of resulting drag and lift behaviors, the occurrence of dominant wavelet scalogram energies occurs before and after the boundary layer flow profile is shifted to the gust flow profile shape. It is worth noting that the turbulence intensity of the gust front inflow profile above the maximum outflow level remains at similar levels, while exhibiting an increase below this level for the gust front flow. It is possible that the turbulence encountered by the model at the lower heights, below the maximum outflow, may impact the level of organized structure development needed for stable vor-

tex shedding over the prism length and the sustenance of frequency contents during the gust front profile flow.

In order to understand the impact of a non-stationary process, different techniques are required beyond traditional stationary analysis schemes. A short-time correlation analysis was performed to uncover the short time behavior of the system. Fig. 13 shows the correlation between two pressure measurement locations on the side face at mid-level height (13a) and the correlation between the oncoming flow and a pressure measurement on the leeward surface (13b). Higher correlation coefficients occurred during the instances of accelerated/decelerated flow. By comparing global attributes, such as lift, and local features, it is apparent that the gust front flow field induces higher correlation of pressures around the model surfaces during significant flow changes, and that the changed flow field also reduced the global pressure impact. Expanding from this, the higher global correlations during the velocity acceleration may attribute to the fact that there are no major frequency contributions during this exchange.

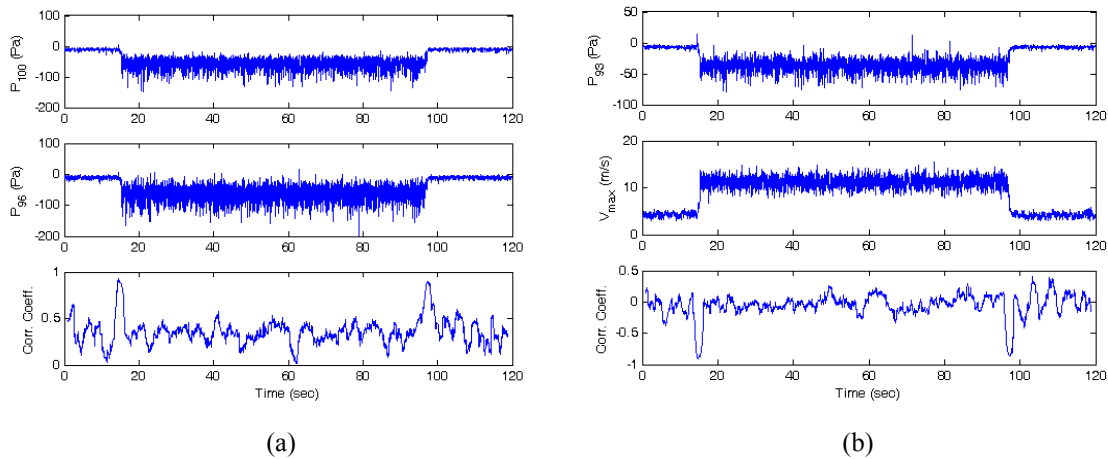


Figure 13: Correlation of a) surface pressures along the side face at mid-level height and b) between the oncoming flow and rear surface pressures.

From global trends to temporally localized behavior, wavelets can again prove useful in uncovering instantaneous behavioral trends in an event. Early research on impulsive flows around circular cylinders (Sarpkaya 1966) showed evidence of a peak in the drag force estimate above the steady state level after the initiation of a transient event, while more recent work has highlighted changes in the drag force frequency content (Matsumoto et al. 2007) for rectangular prisms as well. Fig. 14a and 14b shows zoomed wavelet scalograms of the drag and lift force coefficients respectively, within a 10 second window around the instant of the velocity increase in the gust front flow field occurring on prism M1. In the zoomed wavelet scalogram of the lift coefficient, Fig. 14b, over the velocity increase event, it is noted that the frequency tends to change with the increase in speed, as shown in the time history in Fig. 3a, and this occurs in both the pre and post-gust front events. However, the corresponding drag force coefficient wavelet scalogram, Fig. 14a, shows a brief appearance of two peaks in frequency, similar to that indicated in Fig. 14c observed by Matsumoto et al. 2007, occurring just after the velocity change has reached its steady state level. It was concluded that such a shift was the result of a brief change in the vortex development process (Sarpkaya 1966), though the extent of those changes may be muted in this case considering that there was a pre-existing flow which established a stable vortex development regime and it can be further influenced by other turbulence variations primarily resulting from the dual gradient profile. The

higher intensity content of frequency in the boundary layer flow field compared to the gust front field does suggest that stable vortex development is dependent upon the approach flow topology.

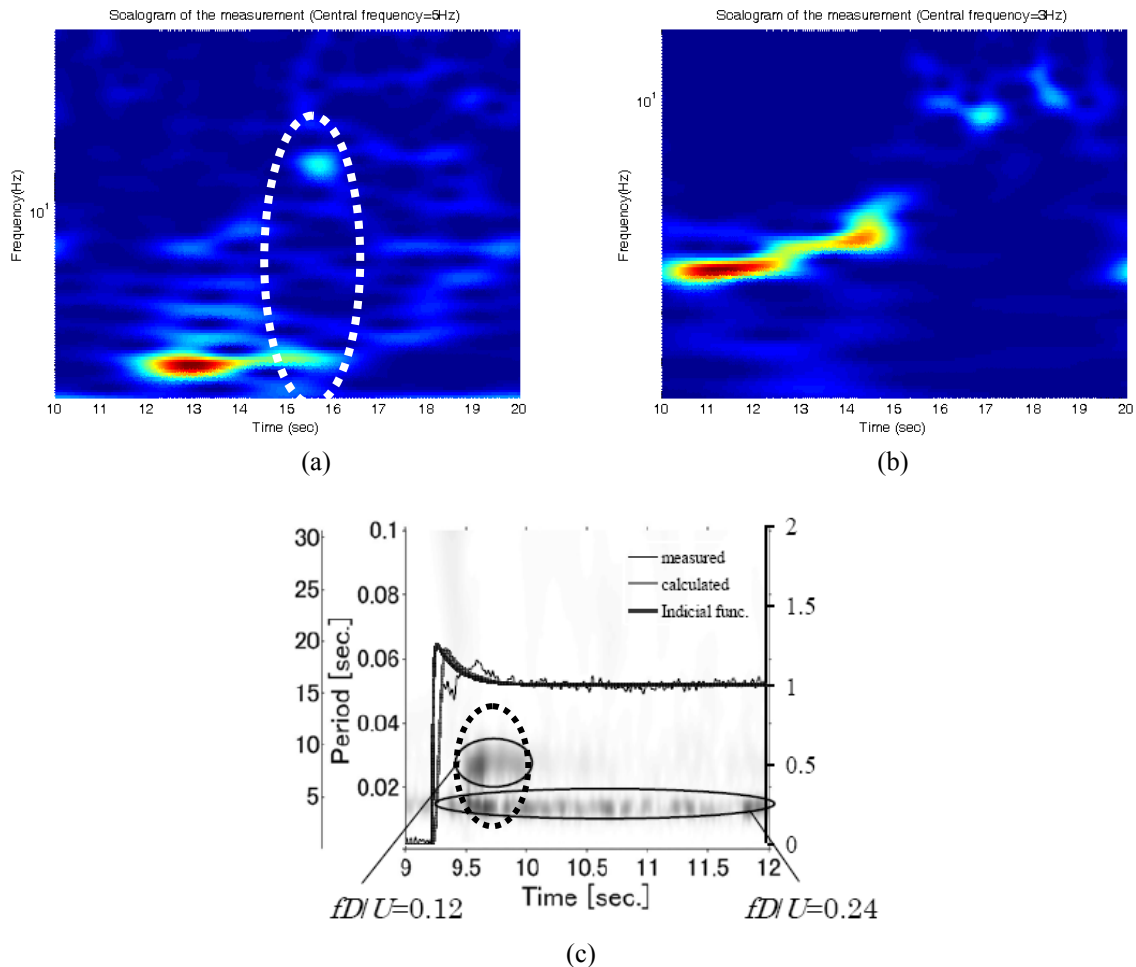


Figure 14: Temporally localized wavelet scalograms of (a) drag force coefficient, (b) lift force coefficient at the instant of gust velocity increase and (c) wavelet scalogram for drag force on a prismatic cylinder with  $B/D = 1.0$  (Matsumoto et al. 2007).

For angles of attack beyond  $15^\circ$ , there is little information that can be derived from the frequency domain. As in the case of boundary layer flow (Butler and Kareem 2007), angles of attack beyond approximately  $30^\circ$  have the effect of diminishing the spectral content of the shedding frequency. As shown in Fig. 15, the frequency content for the lift force coefficient is dramatically shifted once the prismatic model is oriented beyond a  $0^\circ$  incidence. There are spectral peaks that remain for the  $15^\circ$  incidence angle, while no dominant frequency component occurs at  $30^\circ$  and  $45^\circ$  incidence.

Assessment of the larger scale flow structure was investigated through the use of co-spectral analysis. The co-spectra between pressure measurement locations on M1 in both the spanwise and chordwise directions were examined. Fig. 16a shows the normalized co-spectra between measurement locations along the leading edge of the side face in the spanwise direction during exposure to the boundary layer type profile. Fig. 16b shows similar information for measurement locations exposed to the gust front flow field. In both cases, the dominant frequency content exists nearest the presumed Strouhal value for the prism. Although conventional co-spectral analysis does not portray the time dependence of embedded correlations

in the pressure field, it is interesting to note that the co-spectral content during exposure to the gust front flow shows more focused content at the Strouhal value when compared to the same content resulting from the boundary layer flow field.

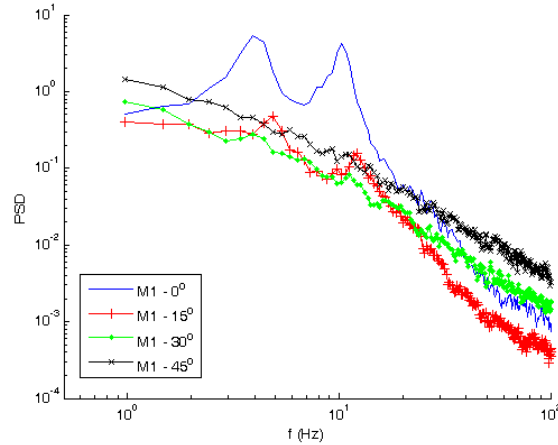


Figure 15: PSD of the lift force coefficient for prism M1 at varying angles of attack.

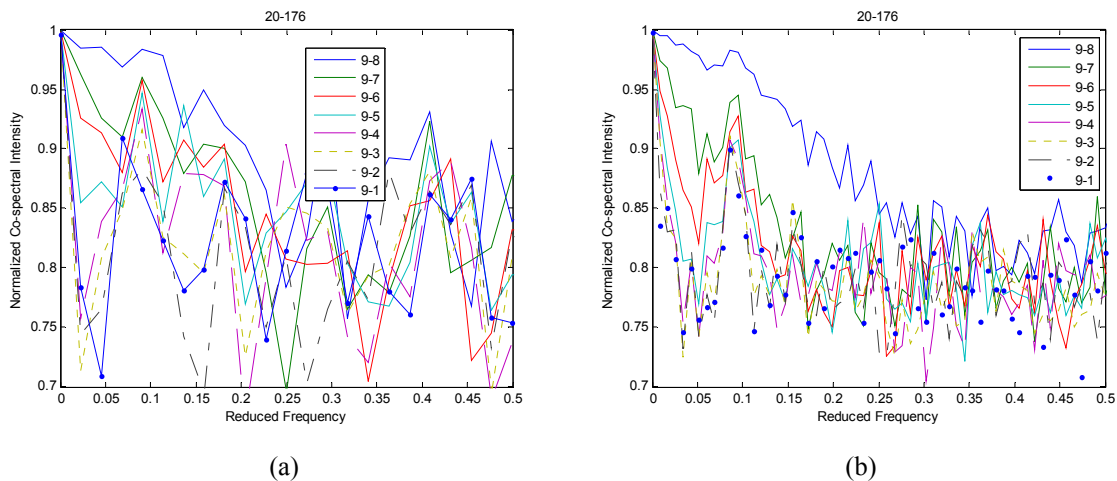


Figure 16: Co-spectra of pressure measurement locations in the spanwise direction along the leading edge due to exposure to the (a) boundary layer flow field and (b) gust front flow field.

Wavelets, similar to those used to examine drag and lift coefficients, were also used to investigate local variations in the dominant frequency content of pressures in time. In this analysis, wavelets were used to examine changes in fluctuating surface pressure frequency. Wavelet co-scalograms were used to identify common frequency content between pressure measurement locations as a function of time, and as a function of the pressure measurement location varying in downstream distance along the side face, at various levels. Fig. 17a shows the wavelet co-spectra for two adjacent pressure locations on the side face (separated by 2 cm.), in the chordwise direction, at midlevel starting at the leading edge. Higher intensity bursts occur intermittently throughout the duration of the gust front profile exposure, and these bursts occur through a range of frequencies with dominant peaks centered on the same frequency as that noted in the lift force, observed in Figure 12b. Similarly, Figure 17b shows a similar wavelet co-spectra between pressure locations at the leading and trailing edge (separated by 8 cm.) on the side face. In this case, the intermittent bursts of frequency occur at the same dominant frequency as noted in Figure 17a, with slightly less intensity in other frequency ranges. It is interesting to note that given the level of velocity fluctuations during the gust

front event, compared to that at the beginning and end of the time series, there are prominent similarities in the frequency content of surface pressures even with an increase in the separation between the points examined. However, there is more intense frequency content when observing the resultant forces, lift force in this case, within the lower velocity flow events before and after the gust front. This observation highlights the peculiarities between the integral pressure fluctuations and the global force, which are being further examined to better understand the interaction of gust front flow topology with the prismatic shape.

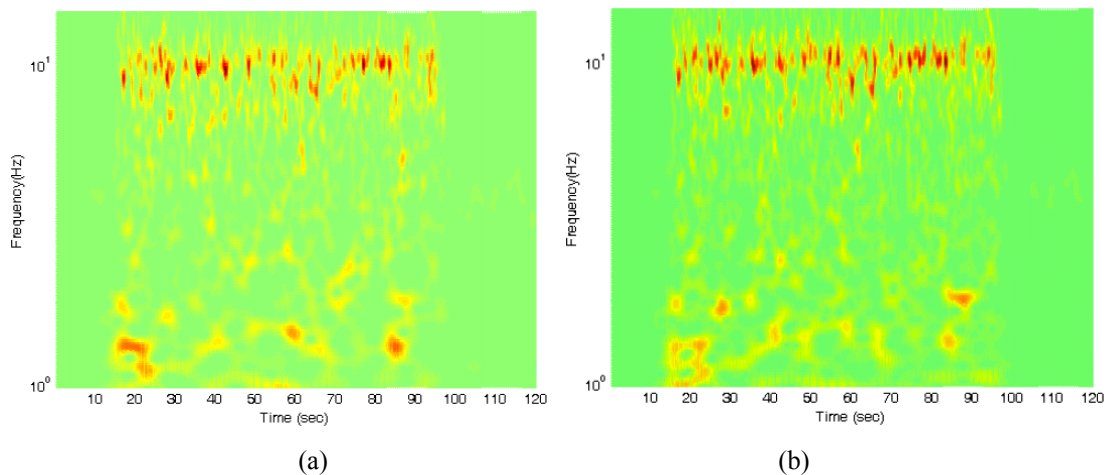


Figure 17: Wavlet Co-scalograms between pressure measurement locations at mid-level height with x/d separation of a) 0.2 and b) 0.8 (with central frequency of 3Hz in both cases).

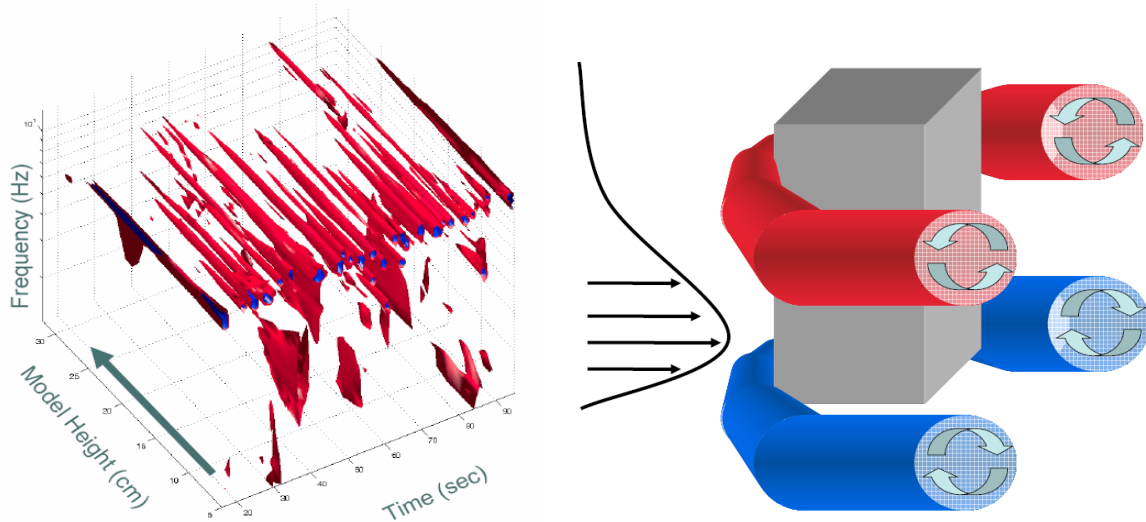


Figure 18: a) 3-dimensional wavelet scalogram generated in the spanwise direction along the leading edge and b) caricature of idealized flow structure resulting from gust front flow.

To assess the nature of the time-frequency variations in surface pressure within a spatial context, scalograms were analyzed at critical points, such as leading and trailing edge corners. Data was organized using a 3-dimensional representation of the wavelet scalogram, where the scalogram was generated for each surface measurement in the spanwise direction and interpolated connections between corresponding values of intensity were drawn. Fig. 18a demonstrates the multi-dimensional wavelet scalogram along with a caricature of gust front type flow field as it wraps around a prism. This allowed for a spatial view of the scalogram energy, to uncover where and when particular frequency contents appeared or ceased to exist.

This representation is aimed at examining the wavelet scalograms to uncover possible transient flow structures, as indicated in Fig. 18b, such as zones of flow separation and rotation where horseshoe type vortices, typical of near surface flows, develop as a pair of contra-rotating vortices possibly as a result of double flow gradients in the oncoming profile. During exposure to the gust flow profile, intermittent high frequency pressure zones, associated with the increased velocity, at the leading edge appear over much of the prism height, while brief low frequency regions appear over the lower height levels. The dual vortex structure may be identified through these low frequency zones, and further refinement of the wavelet scaling could reveal the corresponding zones at the higher levels. This multi-level wavelet scalogram may serve as a critical tool to delineate transient spatio-temporal structures in the pressure field.

#### 4 CONCLUSIONS

A fundamental study aimed at delineating the kinematic and transient effects of variations within the boundary layer flow field on the surface pressures of prismatic models is presented. A multiple fan wind tunnel was employed to simulate a transient gust front flow field with changing flow profile shape. Surface pressures were examined on a suite of prismatic models, capturing transient changes within the flow field. The results of this experiment were examined through traditional statistical methods, and more recent analysis techniques that involve time-frequency domain realizations. It was noted that the correlation of surface pressure around the model surfaces was markedly higher during the flow field acceleration, and the surface pressures extremes revealed characteristics driven by the dual flow profile gradients, compared to the synoptic boundary layer flows before and after, while wavelet scalograms showed marked differences between the typical boundary layer flow field and the gust front profile. Further analysis of these experiments will continue mapping the effects of the gust front flow on the surrounding flow field within a spatio-temporal context.

#### ACKNOWLEDGEMENTS

The authors would like to thank University of Miyazaki and the Center of Excellence: Wind Effects in Urban Areas and the Global Center of Excellence: New Frontier of Education and Research in Wind Engineering at the Tokyo Polytechnic University for participating in this collaborative effort, as well as NSF Grant CMS 03-24331.

#### REFERENCES

- [1] L. Twisdale, P. Vickery, Research on thunderstorm wind design parameters, *Journal of Wind Engineering and Industrial Aerodynamics*, 41 (1992) 545-556.
- [2] M. Chay, C. Letchford, Pressure distributions on a cube in a simulated thunderstorm downburst – Part A: stationary downburst observations, *Journal of Wind Engineering and Industrial Aerodynamics*, 90 (2002) 711-732.
- [3] P. Sarkar, F. Haan, V. Balaramudu, A. Sengupta, Laboratory simulation of tornado and microburst to assess wind loads on buildings, *ASCE Structures Congress*, May 17<sup>th</sup>-19<sup>th</sup>, 2006, St. Louis, MO, USA.
- [4] W. Lin, E. Savory, Large-scale quasi-steady modeling of a downburst outflow using a slot jet, *Wind and Structures*, 9 (2006) 419-440.
- [5] K. Butler, A. Kareem, Physical and numerical modeling of downburst generated gust fronts, *Proc. 12th International Conference on Wind Engineering*, Cairns, Australia, July 1-6, 2007.

- [6] G. Wood, K. C. S. Kwok, N. Motteram, D. Fletcher, Physical and numerical modeling of thunderstorm downbursts, *Journal of Wind Engineering and Industrial Aerodynamics*, 89 (2001) 535-552.
- [7] A. Kareem, J. Cermak, Pressure fluctuations on a square building model in boundary-layer flows, *Journal of Wind Engineering and Industrial Aerodynamics*, 36 (1990) 589-599.
- [8] N. Lin, C. Letchford, Y. Tamura, B. Liang, O. Nakamura, Characteristics of wind forces acting on tall buildings, *Journal of Wind Engineering and Industrial Aerodynamics*, 93 (2005) 217-242.
- [9] D. Surry, D. Djakovich, Fluctuating pressure on models of tall buildings, *Journal of Wind Engineering and Industrial Aerodynamics*, 58 (1995) 81-112.
- [10] Y. Tamura, H. Ueda, H. Kikuchi, K. Hibi, S. Suganuma, B. Bienkiewicz, Proper orthogonal decomposition study of approach wind-building pressure correlation, *Journal of Wind Engineering and Industrial Aerodynamics*, 72 (1997) 421-431.
- [11] D. Kwon, A. Kareem, Gust-front factor: A new framework for the analysis of wind load effects in gust-fronts, *Proc. 12th International Conference on Wind Engineering*, Cairns, Australia, July 1-6, 2007.
- [12] A. Nishi, H. Miyagi, Computer-controlled wind tunnel for wind-engineering applications, *Journal of Wind Engineering and Industrial Aerodynamics*, 54/55 (1995) 493-504.
- [13] S. Cao, A. Nishi, K. Hirano, S. Ozono, H. Miyagi, H. Kikugawa, Y. Matsuda, Y. Wakasugi, An actively controlled wind tunnel and its application to the reproduction of the atmospheric boundary layer, *Boundary-Layer Meteorology*, 101 (2001) 61-76.
- [14] S. Cao, A. Nishi, H. Kikugawa, Y. Matsuda, Reproduction of wind velocity history in a multiple fan wind tunnel, *Journal of Wind Engineering and Industrial Aerodynamics*, 90 (2002) 1719-1729.
- [15] S. Ozono, A. Nishi, H. Miyagi, Turbulence generated by a wind tunnel of multi-fan type in uniformly active and quasi-grid modes, *Journal of Wind Engineering and Industrial Aerodynamics*, 94 (2006) 225-240.
- [16] K. Orwig, J. Schroeder, Near-surface wind characteristics of extreme thunderstorm winds, *Journal of Wind Engineering and Industrial Aerodynamics*, 95 (2007) 565-584.
- [17] T. T. Fujita, *The downburst: microburst and macroburst*, University of Chicago Press, Chicago, Illinois, 1985, 122p.
- [18] T. T. Fujita, Downbursts: meteorological features and wind field characteristics, *Journal of Wind Engineering and Industrial Aerodynamics*, 36 (1990) 75-86.
- [19] C. Letchford and M. Chay, Pressure distributions on a cube in a simulated thunderstorm downburst – Part B: moving downburst observations. *Journal of Wind Engineering and Industrial Aerodynamics*, 90 (2002) 733-753.
- [20] T. Sarpkaya, Separated flow about lifting bodies and impulsive flow about cylinders, *AIAA Journal*, 4 (1966) 414-420.
- [21] K. Butler, A. Kareem (2007), Characteristics of pressure and integral loads on prisms in boundary layer flows, *Proc. 12th International Conference on Wind Engineering*, Cairns, Australia, July 1-6, 2007.
- [22] M. Matsumoto, M. Shimamura, T. Meada, H. Shirato, T. Yagi, K. Hori, Y. Kawashima, M. Hashimoto, Drag forces on 2-D cylinders due to sudden increase of wind velocity, *Proc. 12th International Conference on Wind Engineering*, Cairns, Australia, July 1-6, 2007.

# How hybrid GPS-based surveying techniques can further assist with structural design and construction

Xiaojing LI<sup>1,2</sup>, Akihito YOSHIDA<sup>2</sup>, Yukio TAMURA<sup>2</sup>, Chris RIZOS<sup>1</sup>, Linlin GE<sup>1</sup> and Ryuji IMAI<sup>3</sup>

<sup>1</sup> *School of Surveying & Spatial Information Systems, University of New South Wales, Australia*

<sup>2</sup> *Wind Engineering Research Centre, Tokyo Polytechnic University, Japan*

<sup>3</sup> *Urban Renaissance Agency, Japan*

## BIOGRAPHY

Dr Xiaojing LI, as a JSPS Research Fellow, conducts her joint research with her host Professor Yukio Tamura in the Tokyo Polytechnic University (TPU). She is a Research Fellow working in the University of New South Wales (UNSW). Her research interests include surveying system design and data analysis, integration of GPS and other sensors for full-scale structural monitoring and advanced digital signal processing.

Dr Akihito YOSHIDA is an Associate Professor at TPU. His research interests include structural design and wind tunnel test for scaled structural modeling, full-scale structural monitoring and analysis for structural design improvement.

Dr Yukio TAMURA is a Professor and Director of the Global Centre of Excellence on Wind Engineering at TPU. His research interests include structural design, wind resistance design and structural response to wind load.

Dr Chris RIZOS is a Professor and Head of the School of Surveying & Spatial Information Systems, University of New South Wales (UNSW). His research interests include positioning and navigation with GNSS, and geodesy.

Dr Linlin GE is an Associate Professor at UNSW and Project Leader in the CRC for Spatial Information. His research interests include integration of GNSS with radar interferometry and GIS.

## ABSTRACT

Resistance to seismic forces is a requirement for almost all tall Japanese buildings, which tend to be designed as light-weight and flexible as possible, and thus are vulnerable to wind-induced vibrations. This issue is not only a challenge for Japan's tall buildings, but a worldwide problem due to the growing concern of increased extreme weather conditions because of climate change. Therefore the focus of the research undertaken by the authors has been on the testing of full-scale buildings, in addition to their model analysis in wind tunnels. The first mode of deformation is the dominant one in wind-induced responses of tall

buildings, and sufficient information for evaluating habitability and wind-resistance can be obtained from monitoring the displacement of the top of the building. This is the main reason for the installation of GPS receivers on the top of tall buildings.

Wind-induced responses of tall buildings consist of three components: static, quasi-static, and resonant. Consequently displacements of the top building can be decomposed into these three components. It is not possible to use accelerometers alone to measure all three of these components. Not surprisingly GPS technology has been introduced because of its high positioning accuracy and ease of installation. However, because this satellite-based technology is less accurate for static and quasi-static displacement measurement of a vibrating structure, as well as problems of resolution for higher-mode vibrations, a *hybrid* sensor system to complement individual shortcomings of GPS and accelerometers is necessary. This paper will discuss the contribution of the inclination sensor "Nivel" for quasi-static displacement evaluation in combination with GPS and accelerometer. The authors will present results from data measured using Nivel, accelerometer and GPS sensors on a tall office tower in Yokohama, Japan.

## INTRODUCTION

Large-scale engineering structures are critical parts of a nation's infrastructure, often iconic in nature (world's tallest building, longest bridge, etc), and hence any failure could cause significant damage to the economy, as well as to property and amenity, and even lead to loss of life. These structures are designed using the principles of material and structural mechanics. Numerical modelling using the finite element method and testing on scale models are often employed to assist structural design (e.g. Wolf and Song 1996).

Damping of these structures is a very complex phenomena controlled by a number of mechanisms. Extensive studies have been conducted involving numerous buildings to estimate damping (e.g. Tamura and Suganuma, 1996; Jeary, 1997; Satake et al, 2003). Recent trends in wind resistant design of tall buildings suggest the future of tall building design include the use of monitoring systems on the buildings themselves (Tamura, 2007).

One aspect of building design is related to the external forces acting on structures. A maximum acceleration of  $818\text{cm/sec}^2$  was recorded in 1995 during the Kobe earthquake in Japan. A peak gust of  $88.8\text{m/sec}$  was recorded when Typhoon No.19 hit the Japanese Shimokoshiki Island in 1991. These forces caused severe damage to buildings and infrastructure. The recent 12 May 2008 Sichuan earthquake in China flattened many townships and killed approximately 80,000 people just a week after the Burma (Myanmar) cyclone catastrophe. The current worldwide concern of increased extreme weather conditions has put structural design and monitoring on centre stage.

Tall buildings in Japan have to resist two different kinds of (opposite) extreme design forces: strong winds and earthquakes. The seismic force must be withstood by all tall Japanese buildings, hence they tend to be designed as light-weight and flexible. However, they are then vulnerable to wind-induced vibrations. Essentially the design of buildings higher than 60m requires dynamic response analysis in time domain. In addition, in order not to alter the wind environment around a tall building, causing discomfort and risks to pedestrians and other buildings, the Metropolis of Tokyo has a municipal bylaw for environmental assessment requiring wind tunnel or CFD (Computational Fluid Dynamic) predictions and field measurements before and after construction of any building higher than 100m and with a total floor area larger than  $10^5$  square metres.

Structural damping is the most important, but most uncertain, parameter influencing dynamic response of a building. This uncertainty significantly reduces the reliability of structural design for dynamic effects. Accurate determination of structural damping is very important, not only for evaluating structural responses, but also for designing damping devices to be installed in buildings and structures. However, there is no theoretical method for estimating damping in buildings. Thus, damping has been estimated on the basis of actual measurements of buildings with widely varying damping ratios.

The tip displacement and fundamental structural natural frequencies are the core measurements for evaluating the building's first mode responses of deformation and damping ratios. Structural damping is amplitude dependent. Tip resonant displacement and the building's height are the key quantities for predicting a building's damping design characteristics. The proposed integrated GPS-based system would ensure the accuracy of measurements for damping analysis.

#### **GPS ADVANTAGE FOR STATIC LEAN**

Wind-induced responses on structure consist mainly of three components: static, quasi-static, and resonant. The static displacement by the structure means its static lean. The 'static lean' of a building will alter the stiction so its damping should be different. It is not possible to use accelerometers to measure static and quasi-static displacement. This is the main reason that GPS

technology has been increasingly used for structural monitoring (e.g. Ashkenazi & Roberts, 1997; Brownjohn et al, 1998; Tamura et al, 2002; Kilpatrick et al, 2003; Li, 2004; Li et al, 2006). However, a GPS-based hybrid sensor system is necessary due to limitations of accuracy and resolution in GPS.

GPS measurement gives the direct total displacement in response to the forces acting on the building when installed on top. It is well known that GPS measurement is contaminated by baseline error and has difficulty in detecting displacements under a centimetre in magnitude (Parkinson & Spilker, 1996). But GPS can measure the absolute displacement with defined origin of its coordinates. Furthermore, the extraction of resonant displacement from GPS measurement of the top of a building will help us to detail damping analysis. The selected test site is a steel building, the Yokohama Island Tower, where the rover GPS antenna (Figure 1) was installed at a height of 119m with open sky view.



**Figure 1 Rover GPS on top of Yokohama Island Tower**

#### **GPS SYSTEM RELIABILITY VERIFICATION**

In order to verify that the displacement with resonant natural frequencies of the Yokohama building can be measured with long baseline, on 28<sup>th</sup> Dec. 2007, a free vibration monitoring experiment was taken place. A Z-XII3 Ashtech GPS antenna the same as the Rover GPS was mounted firmly on top of a one dimensional steel building model as shown in Figures 3. The reference GPS was set up 34km away, and the GPS sampling rate was 10Hz. The accelerometer was collocated with the GPS. It is LS-10C Servo type from RION Company, Japan. The accelerometer sampling rate was set at 100Hz. A total of five experimental sessions were conducted with different initial displacements applied to the building model. Then the free vibrating result - in displacement and acceleration - were measured by the GPS and accelerometer sensors respectively. The last three excitation results (Experiments 3, 4 and 5 with initial input displacement of 8cm, 4cm and 3cm respectively) were analysed. Figures 4, 5 and 6 are plots of the results from the free vibration experiments 5, 4 and 3 respectively.



**Figure 2 Yokohama Island Tower**

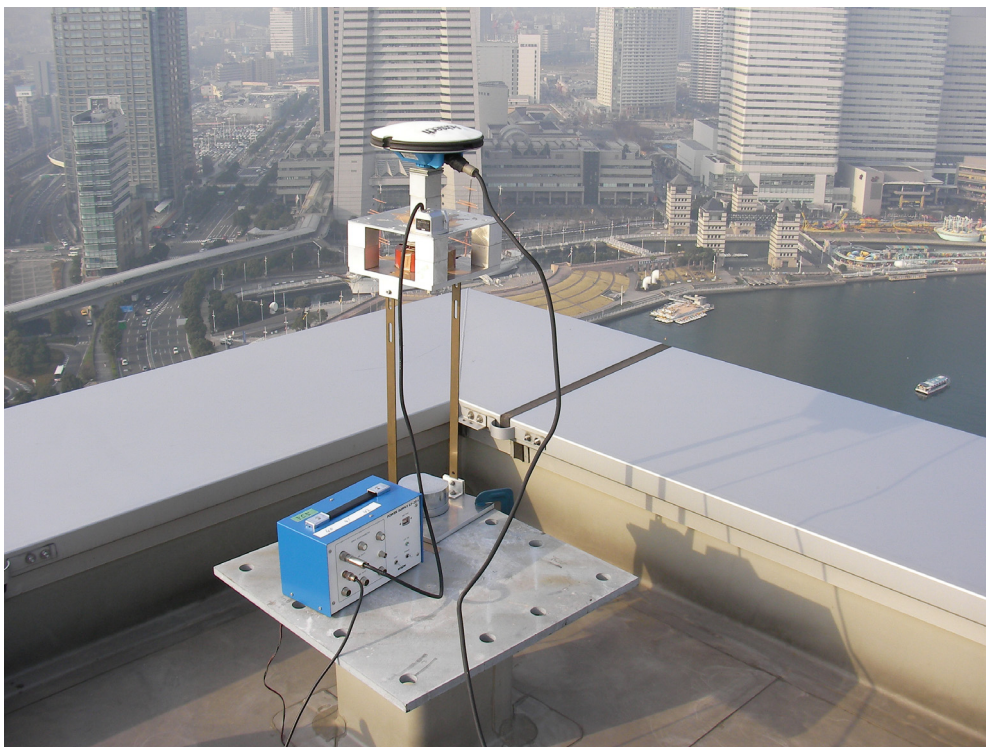
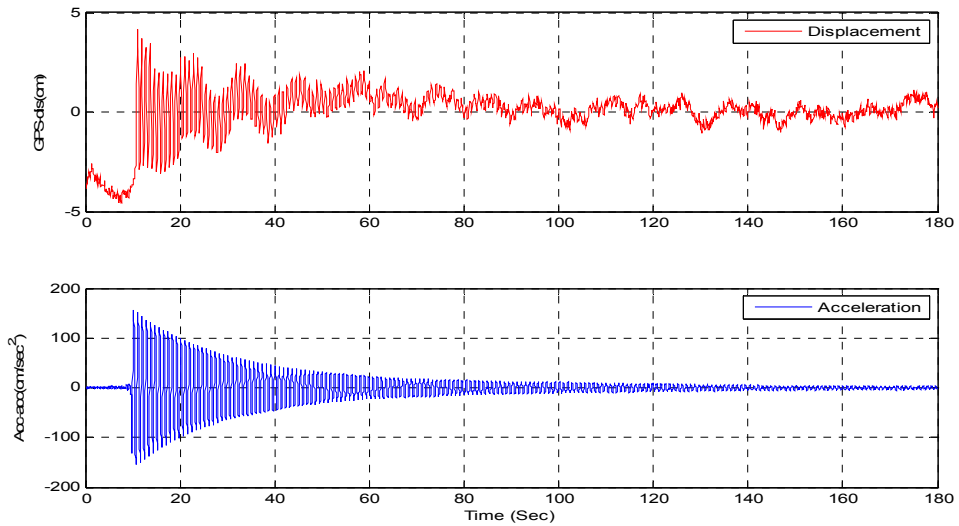
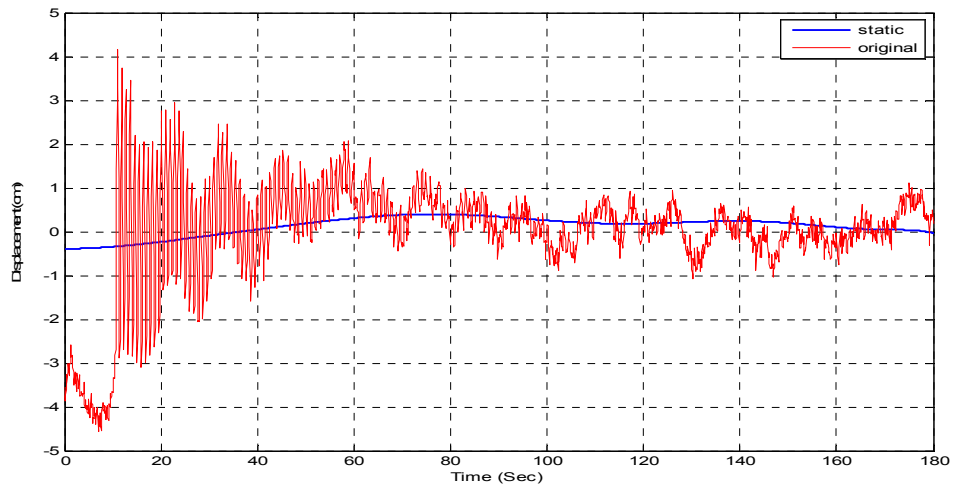


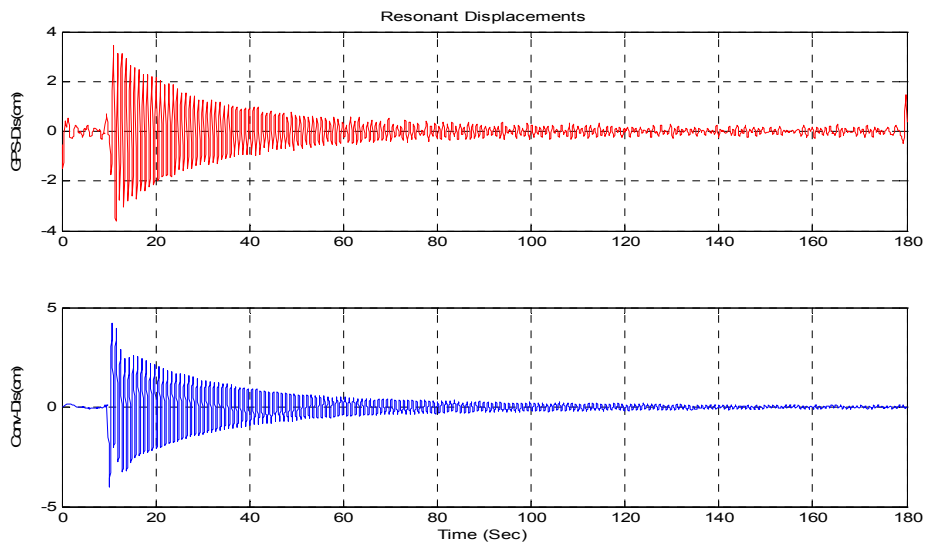
**Figure 3 Free vibration measuring experiment for GPS and accelerometer comparison**



(a)

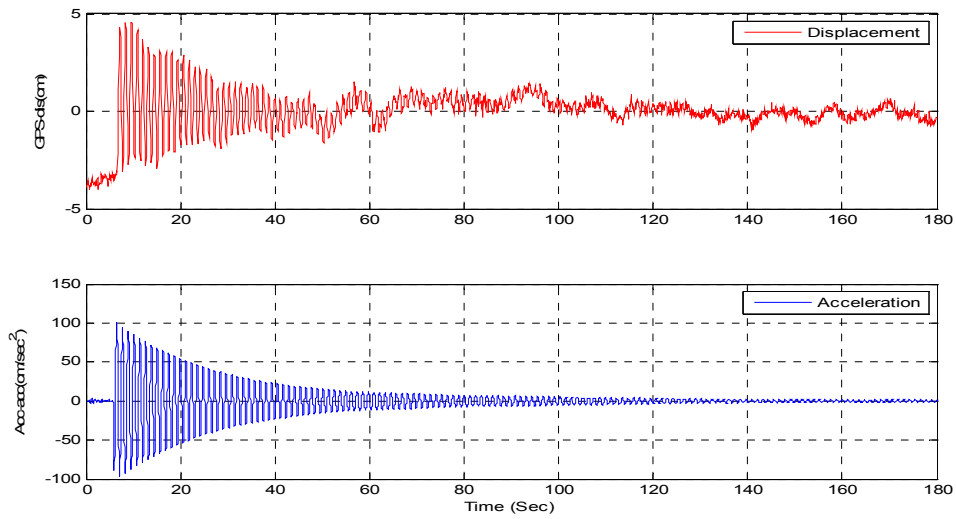


(b)

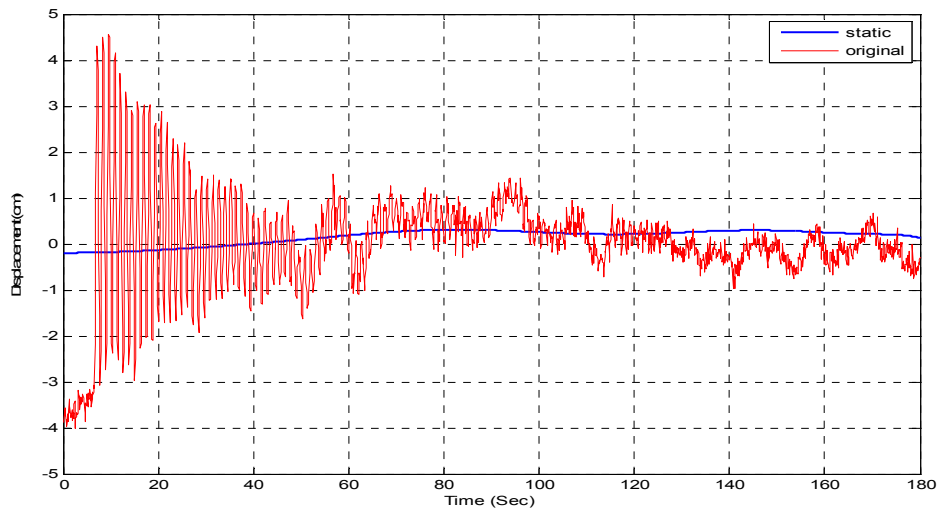


(c)

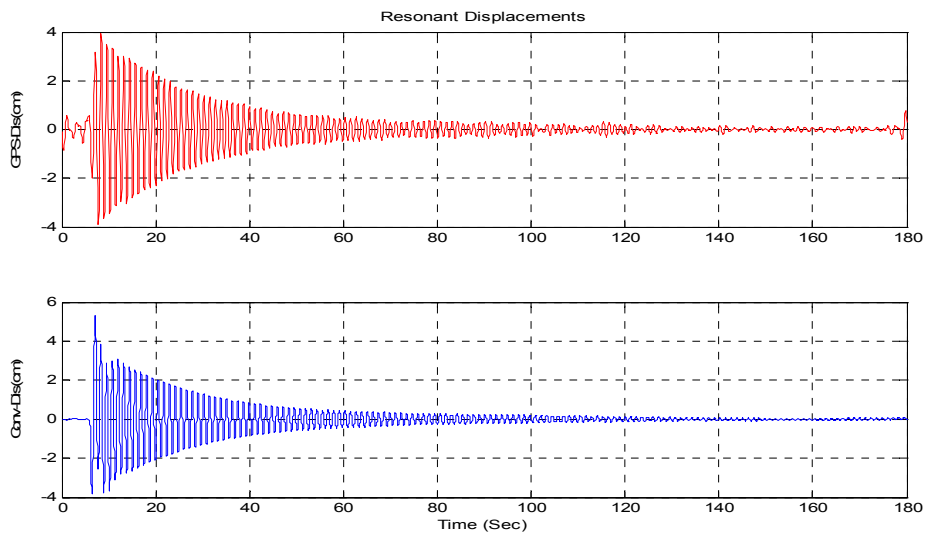
**Figure 4 Experiment 5 with initial input displacement of 3cm: (a) GPS and accelerometer raw measurements; (b) GPS raw measurement and its static component; and (c) extracted resonant displacements result from GPS (top) and converted displacement result from accelerometer (bottom)**



(a)

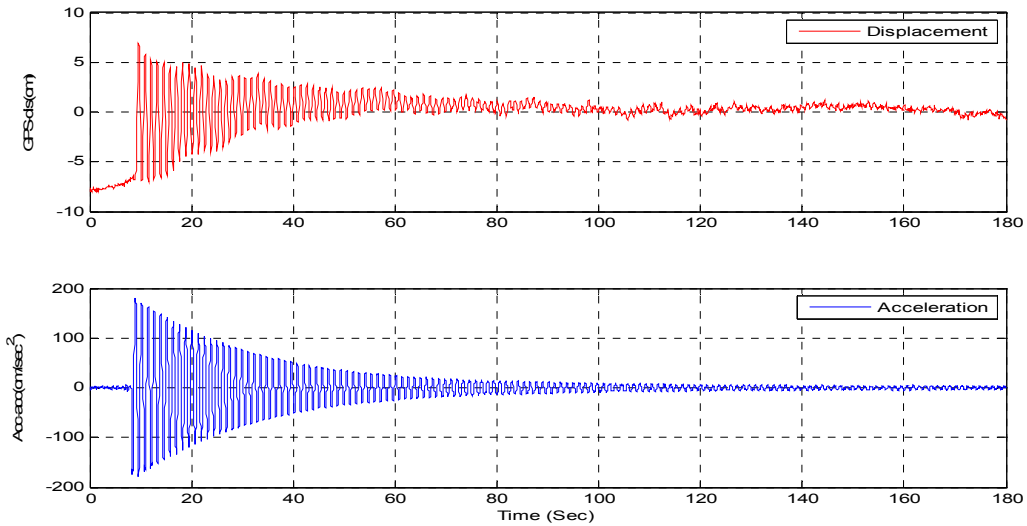


(b)

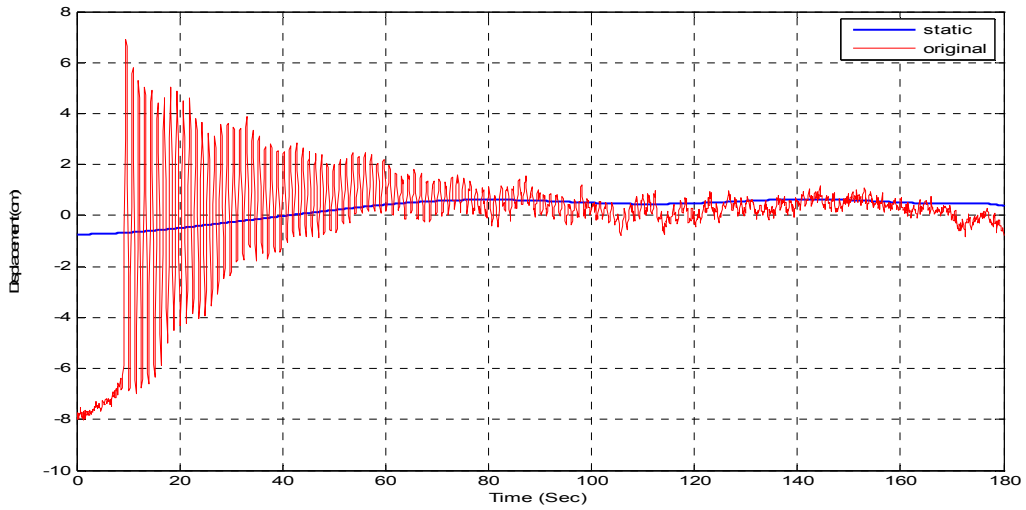


(c)

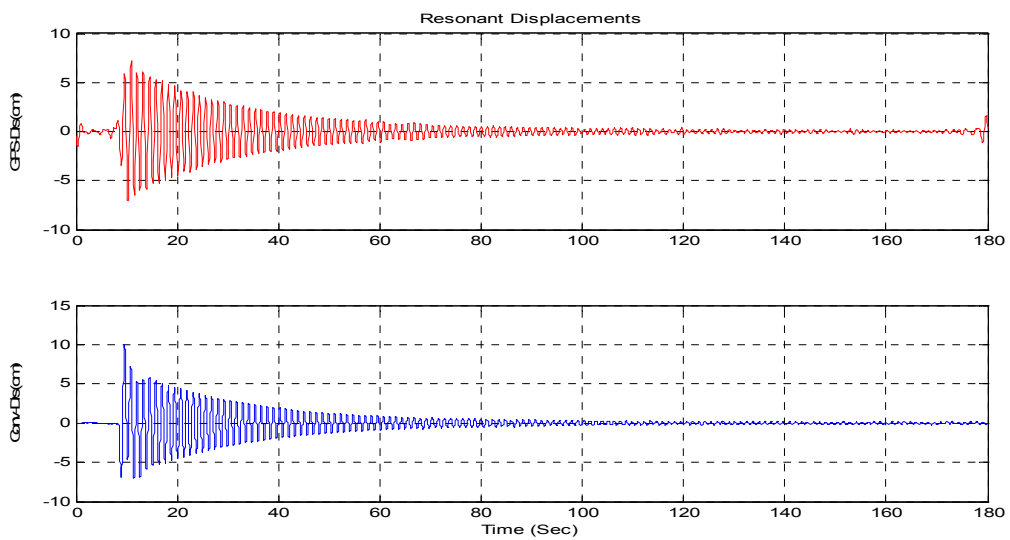
**Figure 5 Experiment 4 with initial input displacement of 4cm: (a) GPS and accelerometer raw measurements; (b) GPS raw measurement and its static component; and (c) extracted resonant displacements result from GPS (top) and converted displacement result from accelerometer (bottom)**



(a)



(b)



(c)

**Figure 6 Experiment 3 with initial input displacement of 8cm: (a) GPS and accelerometer raw measurements; (b) GPS raw measurement and its static component; and (c) extracted resonant displacements result from GPS (top) and converted displacement result from accelerometer (bottom)**

The damping ratio for a structure is an exponential decay envelope with an excited sine wave inside the envelope. When we deal with a real structural response to forces, in terms of its damping ratio, it is necessary to specify the relevant mode and frequency. Therefore, using digital filter to extract a single frequency signal from the wideband time series measurements is essential. The results of damping evaluation for the building model based on GPS and accelerometer data from the free vibration experimental are summarised in Table 1. It can be seen that the GPS displacements of resonant components for the model are in good agreement with the accelerometer's measurement, and its derived displacement from acceleration (presented by Conv-dis. in the table) through double integration transformation (based on the drift removal technique developed by the first author, Li, 2004). It is also evident that GPS is less reliable when the model vibrating amplitude was small, as in Experiment 5

**Table1 Damping ratios for the free vibration on building model**

Exp.	Frequency (Hz)			Damping ratio (%)		
	GPS	Acc.	Conv -dis.	GPS	Acc	Conv -dis.
3	0.81	0.81	0.81	0.8	0.8	0.8
4	0.82	0.82	0.82	0.9	0.9	0.9
5	1.10	1.10	1.10	0.7	0.6	0.7

GPS measurement is contaminated by its intrinsic noise and baseline error (Ge and Rizos, 2000; Rizos, 2002). The static component standard deviation (Table 2) illustrates the measurement error of the free vibration experiments. Because the 180sec window length used in data processing, we can ignore the very small static movement of the Yokohama Island Tower which would couple into the GPS measurement for the very short period. Another reason for ignoring the possible static motion of the building is that the experiment was done on a calm day. Based on the generally accepted GPS static error specifications for horizontal positioning of 0.1ppm+3mm, the error based on a 34km baseline should be as large as 6.4mm. Therefore a reference GPS station with baseline as short as possible is preferred. Furthermore, the integration of GPS with other sensors for full-scale building measurement is essential.

**Table 2 GPS static displacement evaluation of the free vibration experiments**

Exp.	Mean (mm)	Standard deviation (mm)	Initial input amplitude (cm)
3	2.81	4.25	8
4	1.55	1.61	4
5	1.27	2.14	3

#### ACCELEROMETER AND NIVEL FOR LOW AMPLITUDE VIBRATION DETECTION

Because the amplitude-dependent full-scale structural damping evaluation requires high quality data

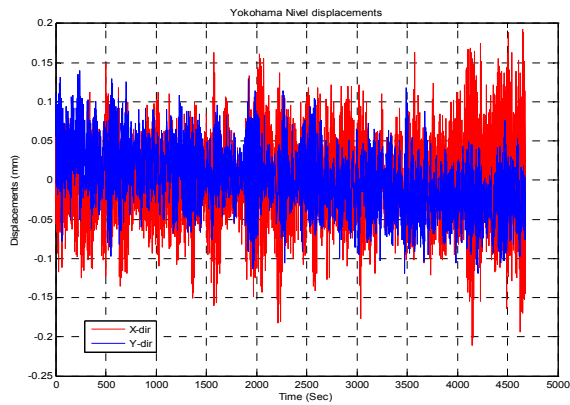
measurement, millimetre accuracy is needed. GPS-only measurement will not be able to satisfy this criterion. The Leica inclination sensor Nivel 220 was put on trial to overcome this weakness of GPS. The experimental data to be analysed were taken on a very calm day, 16 June 2008. There were no ambient forces like strong wind, or earthquake during this experiment, which means the Yokohama Island Tower could be very stable. The measurement range for the Nivel is limited to 1.5mrad, but no absolute static displacement can be measured. The resolution of the Leica Nivel 220 is 0.001mrad. We assume deformation of this building is linear with its height for the fundamental mode. Therefore, when setup at a height of 110m, its displacement resolution is 0.11mm. Its quantisation error is half of the resolution, i.e. 0.055mm. Comparing the two 200sec displacement plots in Figure 8 (a) and (b), it can be seen that the Nivel sensor reading error is about 0.05mm. It is evident that there was a linear trend in the raw data in the y-direction. This might be because of the temporary installation and the room temperature change during the experiment. Some peak points were missed because the sampling rate for Nivel was only 1Hz, it could not adequately track the vibrations of 0.33Hz and 0.34Hz (Figure 8 (c) and (d)).

Moreover, Nivel measurement is the inclination data. It can only measure the bending deformation pending on its installed location with angular change. The measured displacement by Nivel is considered linear with its setting height. But for a steel building, its deformation is formed by bending and shearing deformations. It can be observed that the transformed displacement at fundamental frequency from acceleration is larger than the displacement extracted from inclination through comparing Figure 8 (c) with Figure 9 (b), and Figure 8 (d) with Figure 9 (c). If we subtract the two different displacements, then the shearing deformation captured by accelerometer will be obtained. Therefore, the conversion of accelerometer measurement into displacement is another important complement to the hybrid system.

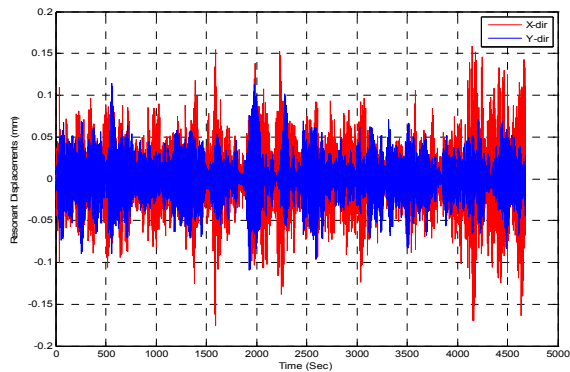
Because of all the above mentioned advantages and disadvantages of each individual sensor, hybrid GPS-based system from full-scale structural monitoring is necessary.



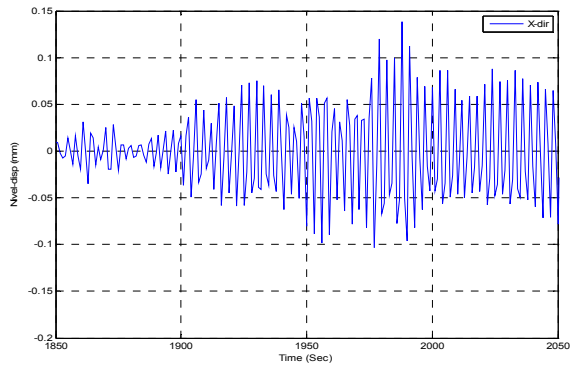
**Figure 7 Inclination sensor-NIVEL 220 on site.**



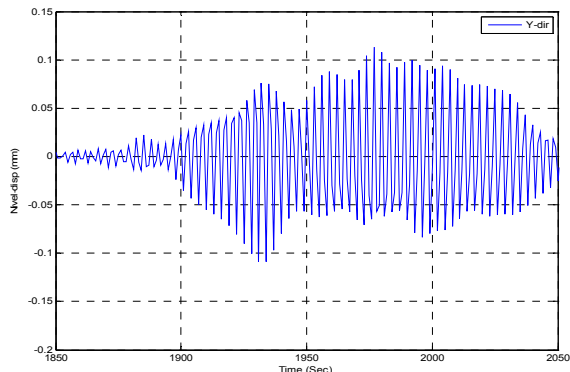
(a)



(b)

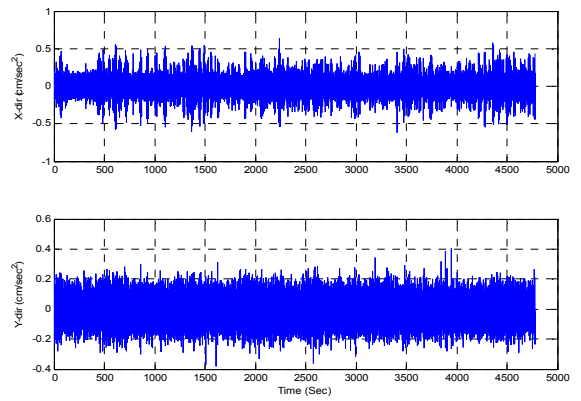


(c)

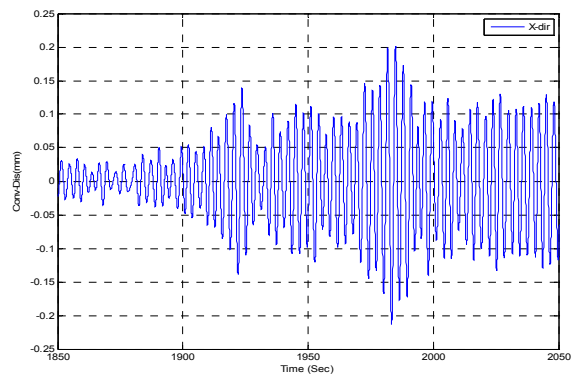


(d)

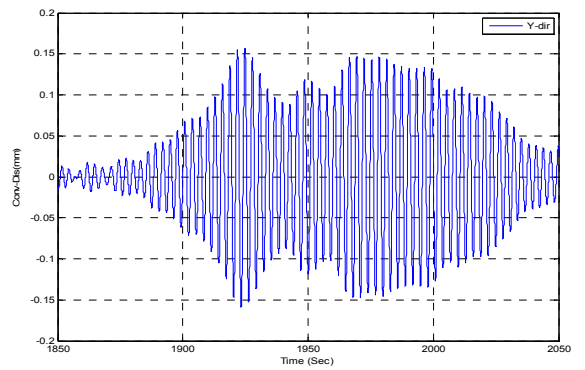
**Figure 8 Nível measurements: (a) raw time series; (b) measurements removed trend; (c) fundamental mode of displacement in x-direction; and (d) fundamental mode of displacement in y-direction**



(a)



(b)



(c)

**Figure 9 Accelerometer measurements: (a) raw wideband time series of accelerations; (b) converted time series of displacement at fundamental frequency in x-direction; and (c) converted time series of displacement at fundamental frequency in y-direction**

### EVALUATION OF DAMPING RATIO IN FULL-SCALE FOR STRAUCTURAL DESIGN

The Yokohama building is a steel building in a low-amplitude regime. Based on the Japanese Damping Database for such a building design, the fundamental natural frequency decreases with building height, and the regression line approximates the natural frequency as a simple linear function of building height:

$$f_1 = \frac{50}{H} \quad (1)$$

$H$  is the building height, and  $f_1$  is the fundamental natural frequency.

Therefore, by Eq (1), the predicted fundamental natural frequency of the tower at the accelerometer and Nivel setup height of 110m is 0.45Hz. The measured frequency is 0.33Hz for the x-direction and 0.34Hz for the y-direction of the building coordinate system, with the same results for both sensors from the full-scale monitoring. These are lower than the predicted values by 26% in the x-direction and by 24% in the y-direction.

Tip resonant displacement and the building's height are the key quantities for predicting the building's damping. Based on the Japanese Damping Database, and considering the amplitude dependency, the formula for predicting the fundamental damping ratios for a steel-building is given by:

$$\zeta_1 = 0.013f_1 + 400 \frac{x_H}{H} + 0.0029 \quad (2)$$

$$\zeta_1 = \frac{0.65}{H} + 400 \frac{x_H}{H} + 0.0029 \quad (3)$$

$\zeta_1$  is the predicted fundamental damping ratio of the building.  $x_H$  is the resonant displacement (in standard deviation in a measuring period) of the horizontal vibrations at the building's top.

The measurements standard deviations in displacement by both the Nivel and accelerometer sensors are listed in Table 3, also the fundamental natural frequency captured by the two different type sensors. Then using Eq (2) & (3) the predicted building damping for those displacements are given in Table 4. Table 4 shows that all the full-scale damping values are within the recommended design damping ratio range for a 100m steel building of 0.7%. The prediction formula Eq (3) results of 0.9% are higher than those using real full-scale data by random decrement (RD) or multi-RD techniques (He & Fu, 2001; Jeary, 1992), but all are within the standard design damping ratio of 1% for its habitability in Japan.

The prediction formula Eq (2) consists of a frequency dependent term, an amplitude dependent term, and a constant. But the frequency dependent term cannot be attributed to the pure frequency effect. It is likely to be due to the soil-structure-interaction (SSI) (Tamura, 2007). Eq (3) is an empirical result, where the natural frequency  $f_1$  is approximated by the building height based on Eq (1) for the steel buildings. It is therefore slightly biased with Eq (2) using the measured full-scale natural frequency in its application. And, Eq (2) and (3) are the regression line applied to buildings whose height

range is  $30m < H < 200m$  in Japan. Furthermore, the tip drift ratio of the non-dimensional displacement data are within the range  $x_H / H \leq 2 \times 10^{-5}$ . Therefore, the measured resonant displacement to be used to evaluate the damping of Yokohama Island Tower must be inside the range of 2.2mm for the equipments' setting height of 110m. This is why we called the predictor of Eq. (2) and (3) is for the low amplitude vibration of structure. Because the GPS is less accurate when resonant displacement is smaller than 5mm, it is necessary to use the Nivel sensor to measure the bending deformation in full-scale structure and its low amplitude damping characteristics. In the meantime, it is very important to complement Nivel with the conventional accelerometer for bending and shearing deformations measurement at fundamental mode, when assuming the fundamental mode deformation is linear with building's height. Again, this highlights the importance of combining GPS with accelerometer and Nivel sensors for full-scale structural monitoring.

**Table 3 Nivel & accelerometer measured standard deviation in displacement & fundament natural frequency**

	Fundamental Natural freq.		Displacement of rms	
	Nivel	Acc.	Nivel	Conv.-dis.
x	0.33Hz	0.33Hz	0.054mm	0.062mm
y	0.34Hz	0.34Hz	0.042mm	0.042mm

**Table 4 Accelerometer & Nivel full-scale measurements damping analysis vs. prediction**

	Predicted By Eq.(2)		Predicted By Eq.(3)		By MRD		By RD
	Nivel	Acc	Nivel	Acc	Acc	Conv.-dis.	Nivel
$\zeta_{1x}$ %	0.7	0.7	0.9	0.9	0.7	0.7	0.8
$\zeta_{1y}$ %	0.7	0.7	0.9	0.9	0.6	0.6	0.7

## CONCLUDING REMARKS

Structural monitoring is a rapidly advancing research area which strives to improve our understanding of structural performance, improve infrastructure asset management, and hopefully lead to safer and more economical building design. This paper has presented some topics relevant to wind resistant design of tall buildings in Japan, focusing on full-scale measurement in order to evaluate a building's tip deformation and damping. High quality full-scale damping data are required to establish an accurate damping predictor for assessing damping ratios for design. Recently, vibration-measuring techniques as well as data-processing techniques have significantly improved. Nevertheless, there are many unsolved problems that

have a pressing need for solution. Thus, this paper is also a call for surveyors and civil engineers to contribute their skills and knowledge to this research along side that of structural engineers.

## ACKNOWLEDGEMENT

The first author wishes to thank Australian Academy of Science for nominating her to JSPS as a research Fellow and JSPS for awarding her the fellowship which enabled this collaborative research with her host in TPU.

## REFERENCES

- Ashkenazi, V., & G.W. Roberts, 1997. Experimental monitoring of the Humber Bridge using GPS, *Civil Engineering*, Proceedings, Institution of Civil Engineers, 120, 177-182.
- Brownjohn, J., T.C. Pan, A. Mita, & K.F. Chow, 1998. Dynamic and static response of Republic Plaza, *Journal of the Institution of Engineers Singapore*, 38(2) 35-41.
- Ge, L., S. Han, & C. Rizos, 2000. Multipath mitigation of continuous GPS measurements using an adaptive filter, *GPS Solutions*, 4(2), 19-30.
- He, J., & Z.-F. Fu, 2001. Modal Analysis, Butterworth-Heinemann, Oxford, UK.
- Jeary, A.P., 1992. Establishing non-linear damping characteristics of structures from non-stationary response time-histories, *The structural Engineer*, 70(4), 61-66.
- Jeary, A.P., 1997. Damping in structures, *Journal of Wind Engineering and Industrial Aerodynamics*, 72, 345-355.
- Kilpatrick, J., T. Kijewski, T. Williams, D.K. Kwon, B. Young, A. Abdelrazaq, J. Galsworthy, D. Morrish, N. Isyumov, & A. Kareem, 2003. Full scale validation of the predicted response of tall buildings: Preliminary results of the Chicago monitoring project. In Proc. 11th Intern. Conf. on Wind Engineering, Lubbock, TX, USA, 2-5 June 2003. Lubbock, TX: Texas Tech University.
- Li, X., 2004. Integration of GPS, accelerometer and optical fiber sensors for structural deformation monitoring, *ION GNSS 17th International Technical Meeting of the Satellite Division*, Long Beach, California, 21-24 September, 211-224.
- Li, X., L. Ge, E. Ambikairajah, C. Rizos, Y. Tamura, & A. Yoshida, 2006. Full-scale structural monitoring using an integrated GPS and accelerometer system, *GPS Solutions*, 10(4), 233-247.
- Parkinson, B., & J. Spilker, 1996. Global Positioning System: Theory and Applications, Washington, DC: American Institute of Aeronautics & Astronautics, 793pp.
- Rizos, C., 2002. Network RTK research and implementation: A geodetic perspective, *Journal of Global Positioning Systems*, 1(2), 144-150.
- Satake, N., et. al. 2003. Damping evaluation using full-scale data of buildings in Japan, *Journal of Structural Engineering*, 129, 470-477.
- Song, Ch., & J.P. Wolf, 1997. The scaled boundary finite-element method - alias consistent infinitesimal finite-element cell method - for elastodynamics, *Comput. Methods Appl. Mech. Engrg.*, 147, 329-355.
- Tamura, Y., & S.Y. Sukanuma, 1996. Evaluation of amplitude-dependent damping and natural frequency of buildings during strong winds, *Journal of Wind Engineering and Industrial Aerodynamics*, 59, 115-130.
- Tamura, Y., M. Matsui, L.C. Pagnini, R. Ishibashi, & A. Yoshida, 2002. Measurement of wind-induced response of buildings using RTK-GPS, *Journal of Wind Engineering and Industrial Aerodynamics*, 90(12-15), 1783-1793.
- Tamura, Y., 2007. Wind resistant design of tall building in Japan, 1st International Conference on Modern Design, Construction and Maintenance of Structures, 10-11 December, Hanoi, Vietnam.
- Wolf, J.P., & Ch. Song, 1996. Finite-Element Modelling of Unbounded Media, John Wiley & Sons Ltd, UK.

# e-Analysis of High-Rise Buildings Subjected to Wind Loads

Dae-Kun Kwon<sup>1</sup>; Tracy Kijewski-Correa<sup>2</sup>; and Ahsan Kareem<sup>3</sup>

**Abstract:** The NatHaz Aerodynamic Loads Database (NALD) (<http://aerodata.ce.nd.edu>) introduced in 2000 has served an important first step in establishing an on-line experimental archive of high-frequency base balance (HFBB) data for use in the preliminary design of high-rise buildings subjected to wind loads. As a result, NALD was recently introduced in the Commentary of ASCE 7-05 (C6.5.8) as an alternative means of assessing the dynamic wind load effects on high-rise buildings. This paper presents NALD version 2.0 (v. 2.0), integrating the latest advances in data management and mining for interactive queries of aerodynamic load data and an integrated on-line analysis framework for determining the resulting base moments, displacements, and equivalent static wind loads for survivability and accelerations for serviceability (habitability). The key feature of NALD v. 2.0 is the flexibility its analysis module offers: Users may select not only the data from the on-line NatHaz aerodynamic loads database, but also may input desired power spectral density (PSD) expression or wind tunnel-derived PSD data set obtained from a HFBB experiment for the evaluation of wind load effects on high-rise buildings. Thus, it serves as a stand-alone analysis engine. Examples illustrate the capabilities of NALD v. 2.0 and provide comparisons of response estimates to demonstrate the flexibility of the analysis engine to provide a platform that can be readily expanded and supplemented to yield a comprehensive, simplified, and efficient avenue for e-analysis of high-rise buildings.

**DOI:** 10.1061/(ASCE)0733-9445(2008)134:7(1139)

**CE Database subject headings:** Aerodynamics; Wind loads; Wind tunnels; Buildings, high-rise; Building design; Structural response; Standards and codes; Internet; Information technology (IT).

## Introduction

One of the major challenges in any engineering discipline is the processing and archiving of large quantities of information. This is no exception in the field of structural engineering, where such stores of data include those generated by wind tunnel studies, laboratory experiments, material testing, and even full-scale monitoring. Recent developments in information technology (IT) offer attractive solutions to these challenges, allowing efficient means to collect, store, analyze, manage, and even share large data sets with the worldwide community (Kijewski et al. 2003; Kwon et al. 2005; Fritz and Simiu 2005). Not only do such approaches enable geographically dispersed researchers working on a similar topic to share data and findings, but it also provides a venue in which this information can be disseminated to other members of the design community around the world.

Most codes and standards traditionally have relied on reduc-

tive formats and simplifications, which often lead to tables and plots that describe wind loads on structures. The level of accuracy inherent in codification information in this format and the uncertainty associated with interpolation or extrapolation of information may compromise the overall accuracy in code-specified load effects. This has led to database-assisted design procedures, which offer convenient meshing with existing analysis software. Primarily, such databases rely on wind tunnel-derived data, which may be couched in analysis portals to provide desired load effects. One such example is described below.

The NatHaz Aerodynamic Loads Database Version 1.0 (NALD v. 1.0), established in the fall of 2000, is an example of Web-based archiving and distribution of wind tunnel test data for the determination of alongwind, acrosswind, and torsional response (Zhou et al. 2003). This site has served as an important first step in establishing an on-line experimental database for use in the preliminary design of high-rise buildings, which is being extensively consulted by a number of firms (McNamara 2005) and individual researchers (Chan and Chui 2006). This interactive database provides users with the RMS base bending moment coefficients and the nondimensionalized power spectra obtained from high-frequency base balance (HFBB) measurements on rigid building models of various aspect ratios and geometries, exposed to two typical boundary layers. One attractive feature in this package was the use of JAVA-based applets to provide a specific spectral value at a given nondimensional (reduced) frequency, negating potential errors associated with interpolation or curve fitting of spectral data. However, the structure of this prototype site was rather archaic in light of recent advances in data management and mining. This paper discusses the use of advances in the field of information technology to enhance, for the purposes of analysis and design, the accessibility, organization, dissemination, and utility of Web-archived wind tunnel data. The recently redesigned NALD v. 2.0 serves as an example of the application

<sup>1</sup>Postdoctoral Research Associate, Dept. of Civil Engineering and Geological Sciences, Univ. of Notre Dame, Notre Dame, IN 46556. E-mail: [dkwon@nd.edu](mailto:dkwon@nd.edu)

<sup>2</sup>Rooney Family Assistant Professor, Dept. of Civil Engineering and Geological Sciences, Univ. of Notre Dame, Notre Dame, IN 46556. E-mail: [tkjewsk@nd.edu](mailto:tkjewsk@nd.edu)

<sup>3</sup>Robert M. Moran Professor, Dept. of Civil Engineering and Geological Sciences, Univ. of Notre Dame, Notre Dame, IN 46556. E-mail: [kareem@nd.edu](mailto:kareem@nd.edu)

Note. Associate Editor: Kurtis R. Gurley. Discussion open until December 1, 2008. Separate discussions must be submitted for individual papers. To extend the closing date by one month, a written request must be filed with the ASCE Managing Editor. The manuscript for this paper was submitted for review and possible publication on December 1, 2006; approved on December 2, 2007. This paper is part of the *Journal of Structural Engineering*, Vol. 134, No. 7, July 1, 2008. ©ASCE, ISSN 0733-9445/2008/7-1139-1153/\$25.00.

of these new technologies. These changes were achieved using a combination of Web-based programming tools and popular engineering software, e.g., Apache Web servers, JAVA/JavaScript, hypertext preprocessors (PHP), structured query language databases (MySQL), and MATLAB. The revised site offers more attractive and user-friendly features to allow not only the retrieval of power spectral values at specific reduced frequencies, but also the on-line determination of resulting base moments, displacements, and equivalent static wind loads (ESWL) for survivability and accelerations for serviceability (habitability) considerations. Thus, in NALD v. 2.0, a dual purpose design aid is introduced: A database-driven Web archive of HFBB data and a stand-alone analysis engine that can be used independently or in tandem for estimating ESWL and building dynamic responses through a user-friendly analysis interface. The latter feature will be particularly useful for those who may not be very familiar with the details of the random vibration-based dynamic analysis procedure generally used in connection with HFBB measurements.

## Research to e-Analysis

Measurement of forces using HFBB and synchronous scanning of pressures have become widely accepted techniques for wind tunnel studies of buildings and other structures. The translation of wind tunnel data into ESWL and building response involves a random vibration-based analysis. Most wind tunnel study reports do not provide details of this process with the exception of a generic description in an appendix or a cited reference in the report. This practice has left designers largely in the dark surrounding the theory employed and completely unaware of the many published advances in the procedures for predicting wind-induced response. As such, they are generally not capable of repeating these analyses in house for parametric investigations of period and damping sensitivity that are essential when mitigation of wind-induced motion is required. Instead, design offices often have to engage either a testing laboratory or an external expert to conduct these additional parameter studies. To prevent these analysis procedures from languishing on the library shelves, the NatHaz Modeling and DYNAMO laboratories at the University of Notre Dame have mobilized their technology transfer using information technologies. In this context, this paper chronicles the development of an analysis portal that encompasses necessary features of random vibration analysis to predict building response based on wind tunnel derived data, existing databases, or established expressions for spectral loading, which does not require prior working knowledge of the subject by the user. First, a short history of this development is presented, which is followed by the latest developments.

### **NatHaz Aerodynamic Loads Database**

Aerodynamic loads on buildings may be derived through multiple point synchronous scanning of pressures or by measured forces on the model mounted on a high-frequency base balance. The simultaneously monitored pressure database offers great flexibility in deriving mode generalized loads for buildings with mode shapes that depart from linear or exhibit coupling. However, for tall buildings with dominant resonant response, both the mean and background components can be approximately quantified by modal analysis using integrated wind loads derived from HFBB. The HFBB measurements have been widely recognized for con-

veniently quantifying generalized wind forces on tall buildings with uncoupled mode shapes (Kareem and Cermak 1979; Tschanz and Davenport 1983; Reinhold and Kareem 1986; Boggs and Peterka 1989). The generalized forces are then utilized for estimating building response with given structural characteristics. The HFBB technique generally requires mode shape corrections, which are either based on empirical relationships or analytical formulations derived on the basis of assumed wind loading models (Vickery et al. 1985; Boggs and Peterka 1989; Xu and Kwok 1993; Zhou et al. 2002; Holmes et al. 2003; Chen and Kareem 2004, 2005).

Since its inception a few decades back at Shimizu Corporation's wind tunnel laboratory (Fujii et al. 1986; Kikuchi et al. 1997), synchronous pressure measurements (SPM) on building surfaces have been increasingly implemented in wind tunnel practice. This was largely facilitated by the availability of cheaper electronic pressure sensors and represented an advancement over the covariance-based integration methodology that involved several configurations of limited pressure measurements over a building surface (Kareem 1982). SPM offers the added advantage of providing more accurate estimates of generalized wind loads for buildings with nonlinear mode shapes, as approximate mode shape corrections are not required. Nonetheless, the HFBB maintains its attractiveness in cases where the mode shapes do not depart too far from linear.

Individual researchers (Chen and Kareem 2005; Huang and Chen 2007) and wind tunnel laboratories (Steckley et al. 1992; Ho et al. 1999) have their own favorite analysis format based on either SPM or HFBB. Some groups (Chen and Kareem 2004, 2005) prefer to establish equivalent static wind loads from either SPM or HFBB data for subsequent response analysis, while others directly employ the data for calculating response components (Steckley et al. 1992; Tamura et al. 1996; Ho et al. 1999; Fritz and Simiu 2005).

The NALD consists of results from 162 different tests, derived from nine cross-sectional shapes, three model heights, two exposure categories, and three response directions (alongwind, acrosswind, and torsion), as shown by the NALD Web selection menu in Fig. 1. While a detailed description of the test procedures can be found in Kareem (1990), Kijewski and Kareem (1998), and Zhou et al. (2003), a brief summary is now provided. Each of the balsa wood models was tested in a boundary layer wind tunnel with a 3 m (10 ft)  $\times$  1.5 m (5 ft) cross section, of 18 m (60 ft) length. The turbulent boundary layers simulated in this study were generated by the natural action of surface roughness added on the tunnel floor and upstream spires. Two typical boundary layers were simulated in this experiment, BL1 ( $\alpha=0.16$ , where  $\alpha$ =power law exponent of the mean wind velocity profile) and BL2 ( $\alpha=0.35$ ), similar to the conditions of open [Exposure C in the ASCE 7-05 (ASCE 2005)] and urban [Exposure A in ASCE 7-98 (ASCE 1998)] flow environments, respectively. The output of the sensitive, multicomponent base balance was analyzed using the fast Fourier transform (FFT) to determine the spectral and cross-spectral density functions, which were later nondimensionalized. This analysis was carried out for all 27 building models, in both boundary layers, and at various angles of wind incidence, though only the results from perpendicular approaching winds (zero degree angle of attack) were considered in the NALD v. 1.0. The authors plan to augment the 162 test cases currently housed in the NALD with data for other building shapes and aspect ratios, as they become available from other researchers and/or additional testing.

The reliability of the measured spectra within the NALD has

## User Interface to select inputs

**Step 1: Select Shape of Interest**

01 D=2" B=6"	02 D=3" B=6"	03 D=4" B=6"
04 D=4" B=4"	05 D=6" B=4"	06 D=6" B=3"
07 D=6" B=2"	08 4" 4"	D=4" 09 60° B=6"

↑ ↑ ↑ ONCOMING WIND ↑ ↑ ↑

**Step 2: Select Height of Interest**

16"  
20"  
24"

**Step 3: Select BL condition of Interest**

Open Urban

**Step 4: Select Response Component of Interest**

● Alongwind ● Acrosswind ● Torsional

Submit Reset

Fig. 1. NALD data selection menu

been established through verifications against datasets from other wind tunnel experiments. For example, the acrosswind spectra have been compared to a model derived from earlier measurements by Kareem (1990). Results in the torsional direction were also compared to those derived from pneumatic averaging, to overcome the uniform mode shape assumption inherent to the HFBB-derived torsional loads (Kareem 1990). More recently, Zhou et al. (2003) compared the NALD acrosswind loads with the empirical expression suggested by the Architectural Institute of Japan (AIJ 1996; Tamura et al. 1996). In addition, nondimensionalized base moment coefficients were compared to the empirical expressions given by AIJ for acrosswind and torsional directions (Zhou et al. 2003).

Since these previously reported comparisons, a number of new studies concerning HFBB and SPM have been published (Liang et al. 2002, 2004; Cheng and Wang 2004; Gu and Quan 2004; Ha et al. 2004; Lin et al. 2005; Flay and Bhat 2005). In particular, it is worth noting that Lin et al. (2005) have provided an in-depth comparison of the NALD to their HFBB and SPM. They found the NALD to be in close agreement with their studies with the exception of a few cases, stating: "With the linear mode shape assumption . . . integrated simultaneous point pressures and HFBB agree for base force and moment spectra. The [NALD] effectively provides the base moment spectra for preliminary design and can be expanded on the Internet by the dataset here and by the other experimental results in the future" (Lin et al. 2005). This speaks not only to the reliability of the NALD, but also the robustness of its framework for future expansion. The examples

in this paper offer additional verification of NALD against selected major studies, though these are by no means exhaustive or meant to serve as a systematic comparison of HFBB data from different laboratories, codes, and standards.

## Overview of NALD v. 2.0: from Theory to Practice

### Theoretical Background of NALD v. 2.0

To account for the gustiness of turbulent boundary-layer winds on structures, most international codes and standards including ASCE 7 have adopted the concept of gust loading factor (GLF), which was first introduced by Davenport (1967) based on statistical theory of buffeting. This traditional GLF is based on the ratio of the maximum structural displacement to the mean displacement (Davenport 1967; Solari and Kareem 1998). Although the traditional GLF ensures an accurate estimation of the displacement response, it may fall short in providing a reliable estimate of other response components. To overcome this shortcoming, Zhou and Kareem (2001) proposed a new GLF format that is based on the ratio between the maximum base bending moment and the mean obtained from HFBB experiments, rather than the displacements utilized in the conventional approach.

This new GLF format associated with base moments has been introduced in ASCE 7-05 (ASCE 2005) as well as the AIJ (2004) *Recommendations for Loads on Buildings*. Using the aerodynamic base bending moment or base torque as the input, the

wind-induced response of a building can be computed using random vibration analysis as detailed in Zhou and Kareem (2001). Utilizing the base bending moment, NALD v. 2.0 assists in evaluating the equivalent static wind loads and attendant response components. Due to relatively less sensitivity of the base moment to mode shapes, the mode shape correction may not be necessary in this approach. Application of this framework for the alongwind response has proven effective in recasting the traditional gust loading factor approach into a new format. This procedure has been extended to the acrosswind and torsional response in a 3D

gust loading factor approach (Zhou and Kareem 2001; Kareem and Zhou 2003).

Although the theoretical background adopted in NALD v. 2.0 has been introduced in Zhou and Kareem (2001), Zhou et al. (2003), Kareem and Zhou (2003), and Tamura et al. (2005), it is briefly described here for completeness. Assuming the response is a stationary Gaussian process, the expected maximum base bending moment response ( $\hat{M}$ ) in the alongwind and acrosswind directions or the base torque response can be expressed in the following form:

$$\hat{M} = \bar{M} + g \times \sigma_M \approx \bar{M} + \sqrt{M_B^2 + M_R^2} = \bar{M} + \sqrt{(g_B \times \sigma_{CM} \times \bar{M}')^2 + \left( g_R \times \sigma_{CM} \times \bar{M}' \times \sqrt{\frac{\pi}{4\zeta_1} C_M(f_{r1})} \right)^2} \quad (1)$$

where  $\bar{M}$ =mean moment;  $M_B$ ,  $M_R$ =background and resonant base moment or torque components, respectively;  $g$ ,  $g_B$ ,  $g_R$ =peak factors for total, background, and resonant moments, respectively;  $\sigma_M$ ,  $\sigma_{CM}$ =RMS of the fluctuating base moment/torque response and base moment/torque response coefficient ( $=\sigma_M/\bar{M}'$ );  $\bar{M}'$ =reference moment or torque depending on response component;  $\zeta_1$ =building damping ratio in the first mode;  $C_M(f_{r1})$ =nondimensional moment coefficient at  $f_{r1}$  ( $=f_{r1} \times S_M(f_{r1})/\sigma_M^2$ );  $f_{r1}$ =reduced frequency according to  $f_1$  ( $=f_1 B/\bar{U}_H$ );  $f_1$ =natural frequency of building in the direction of motion;  $S_M(f)$ =PSD of the fluctuating base moment or torque response;  $f$ =frequency [Hz];  $\bar{U}_H$ =mean wind velocity evaluated at building height  $H$ . In addition, since  $\sigma_{CM}$  and  $C_M(f_{r1})$  are obtained from the HFBB experiment, the mean, background, and resonant base moments can be computed in the alongwind, acrosswind, and torsional directions using respective building properties. This has led to the introduction of a 3D GLF approach to facilitate evaluation of response in three directions (Kareem and Zhou 2003). The gust loading factor  $G_M$  associated with base moment can be described as the following form:

$$G_M = \hat{M}/\bar{M}' = \bar{G} + \sqrt{G_{MB}^2 + G_{MR}^2} \quad (2)$$

Thus, mean ( $\bar{G}$ ), background ( $G_{MB}$ ), and resonant ( $G_{MR}$ ) GLF can be easily derived by comparing Eq. (2) to Eq. (1) (Kareem and Zhou 2003). Using Eqs. (1) and (2), the ESWL on a building in the alongwind, acrosswind, and torsional directions can be computed by distributing the base moments to each floor akin to the manner in which base shear is distributed in earthquake engineering. The mean base moment ( $\bar{M}$ ) has a relationship with the mean component of the ESWL as follows:

$$\bar{M} = \int_0^z \bar{P}(z) \times z dz \quad (3)$$

where mean component of the ESWL ( $\bar{P}$ ) is

$$\bar{P}(z) = \frac{1}{2} \rho \bar{U}_H^2 \left( \frac{z}{H} \right)^{2\alpha} B C_D \Delta H = \bar{M} \frac{2 + 2\alpha}{H^2} \left( \frac{z}{H} \right)^{2\alpha} \Delta H \quad (4)$$

Next, the background component for the alongwind and acrosswind responses can be obtained by using the background GLF as follows:

$$P_{B(D,L)}(z) = G_{MB(D,L)} \times \bar{P}(z) = M_{B(D,L)} \frac{2 + 2\alpha}{H^2} \left( \frac{z}{H} \right)^{2\alpha} \Delta H \quad (5)$$

Similarly, the background component for the torsional response ( $P_{B(T)}$ ) is expressed as

$$P_{B(T)}(z) = G_{MB(T)} \times \bar{P}(z) = M_{B(T)} \frac{1 + 2\alpha}{H} \left( \frac{z}{H} \right)^{2\alpha} \Delta H \quad (6)$$

where subscripts  $B$ ,  $D$ ,  $L$ , and  $T$ =background, alongwind, acrosswind, and torsional components;  $\rho$ =air density;  $z$ =elevation above the ground;  $B$ =building width;  $C_D$ =drag force coefficient;  $\Delta H$ =floor-to-floor height of building;  $\alpha$ =exponent of mean wind speed profile defined in ASCE 7.

For the resonant components, the ESWL in sway modes is given by

$$P_{R(D,L)}(z) = M_{R(D,L)} \frac{m(z)\varphi_{1(D,L)}}{\sum m(z)z\varphi_{1(D,L)}} \quad (7)$$

and in the torsional mode

$$P_{R(T)}(z) = M_{R(T)} \frac{I(z)\varphi_{1(T)}}{\sum I(z)\varphi_{1(T)}} \quad (8)$$

where subscript  $R$ =resonant component;  $m(z)$ =mass per unit height;  $\varphi_1$ =fundamental mode shape in the direction of motion ( $= (z/H)^\beta$ );  $\beta$ =mode shape exponent in the direction of motion, e.g., linear mode shape if  $\beta=1$ ;  $I(z)$ =mass moment of inertia per unit height ( $=m(z) \times \gamma^2$ );  $\gamma$ =radius of gyration.

For the acceleration response, only the resonant component is of interest. The peak accelerations for the three principle directions of motion, i.e., alongwind, acrosswind, and torsion, can be obtained by the following equations:

- Alongwind and acrosswind

$$\begin{aligned}\ddot{Y}_{\text{Peak}(D,L)}(z) &= \frac{P_{R(D,L)}^*}{K_{(D,L)}^*} \varphi_{1(D,L)} \times (2\pi f_1)^2 \\ &= \frac{\int_0^H P_{R(D,L)}(z) \varphi_{1(D,L)} dz}{\int_0^H m(z) \varphi_{1(D,L)}^2 dz} \varphi_{1(D,L)}\end{aligned}\quad (9)$$

- Torsion

$$\ddot{Y}_{\text{Peak}(T)}(z) = \frac{P_{R(T)}^*}{K_{(T)}^*} \varphi_{1(T)} \times (2\pi f_1)^2 = \frac{\int_0^H P_{R(T)}(z) \varphi_{1(T)} dz}{\int_0^H I(z) \varphi_{1(T)}^2 dz} \varphi_{1(T)}\quad (10)$$

where  $P^*$ =generalized force;  $K^*$ =generalized stiffness. The resulting RMS acceleration can then be determined by dividing the peak accelerations by the resonant peak factor  $g_R$ . Note that the angular accelerations in torsion may be resolved into the resultant alongwind and acrosswind components at the corner of the building, and these lateral accelerations induced by torsion can be combined with those generated by the sway motions to obtain the total lateral accelerations at the corner by the square root of the sum of the squares (SRSS) or complete quadratic combination (CQC) (Zhou et al. 2003; Chen and Kareem 2004, 2005).

The displacement response calculation can be computed by a modal analysis procedure. Assuming that building mass is uniformly distributed along the height, i.e., mass per unit height [ $m(z)$ ] being a constant value ( $m$ ), the mean and maximum displacements in the alongwind can be computed by the following expressions:

$$\begin{aligned}Y_{\text{mean}(D)}(z) &= \frac{P_{\text{mean}(D)}^*}{K_{(D)}^*} \varphi_1 = \frac{(2\beta + 1)\bar{M}}{mH^2(2\pi f_1)^2} \left(\frac{z}{H}\right)^\beta \\ Y_{\text{max}(D)}(z) &= G_M \times Y_{\text{mean}(D)}(z)\end{aligned}\quad (11)$$

Similarly, the maximum displacement in the acrosswind direction is computed by only including background and resonant displacements, since there is no mean displacement in this direction

$$\begin{aligned}Y_{B(L)}(z) &= \frac{P_{B(L)}^*}{K_{(L)}^*} \varphi_1 = \frac{M_{B(L)}(2\beta + 1)(2 + 2\alpha)}{mH^2(2\pi f_1)^2(2\alpha + \beta + 1)} \left(\frac{z}{H}\right)^\beta \\ Y_{R(L)}(z) &= \frac{P_{R(L)}^*}{K_{(L)}^*} \varphi_1 = \frac{M_{R(L)}(\beta + 2)}{mH^2(2\pi f_1)^2} \left(\frac{z}{H}\right)^\beta \\ Y_{\text{max}(L)}(z) &= \sqrt{Y_{B(L)}^2(z) + Y_{R(L)}^2(z)}\end{aligned}\quad (12)$$

Alternatively, if the RMS moment coefficient ( $\sigma_{\text{CM}(L)}$ ) and nondimensional moment coefficient [ $C_{M(L)}(f)$ ] in the acrosswind direction, which can be obtained from NALD as well, are known for given building properties, the background and resonant displacements in the acrosswind direction can be obtained from the following expressions in which Eq. (12) is expanded by using  $M_{B(L)}$  and  $M_{R(L)}$  [see Eq. (1)]:

$$\begin{aligned}Y_{B(L)}(z) &= \frac{1}{2} \rho \times \bar{U}_H^2 \times D \times g_B \times \sigma_{\text{CM}(L)} \\ &\quad \times \frac{(2 + 2\alpha)(2\beta + 1)}{m(2\alpha + \beta + 1)(2\pi f_1)^2} \times \left(\frac{z}{H}\right)^\beta \\ Y_{R(L)}(z) &= \frac{1}{2} \rho \times \bar{U}_H^2 \times D \times g_{R(L)} \times \sigma_{\text{CM}(L)} \\ &\quad \times \sqrt{\frac{\pi}{4s_1} C_{M(L)}(f_{r1})} \times \frac{(\beta + 2)}{m(2\pi f_1)^2} \times \left(\frac{z}{H}\right)^\beta\end{aligned}\quad (13)$$

Note that all parameters in Eqs. (11)–(13) are related to acrosswind properties, e.g.,  $f_1$  here is natural frequency of building in the acrosswind direction. Note that the displacement response is dictated by 50-year wind speeds, as this is the mean recurrence interval (MRI) for base moments and the ESWL (survivability design), while the acceleration response is governed by the 10-year wind speed (serviceability design).

### Database-Enabled Selection

NALD v. 1.0 (Zhou et al. 2003) provided users with wind tunnel measurements of RMS base moment coefficients and the nondimensional power spectral values requisite for the above response calculations for the 162 tests discussed previously. Upon entering the database, the user stepped through a series of hypertext markup language (HTML) links to identify the data of interest. Once the desired test case and response component were selected, a JAVA applet retrieved the exact nondimensionalized power spectral value corresponding to a user-specified reduced frequency. This automated process negates potential human errors that result from picking off values from hardcopy spectra and eliminates the uncertainty associated with curve-fit expressions that tend to generalize spectral features. However, since the NALD v. 1.0 could not support structured query language (SQL), the architecture associated with this prototype involved an expansive hierarchy of directories with duplicate HTML files, requiring the user to step through a sequence of at least five Web pages to reach the desired JAVA applet.

To reduce the redundancy in the architecture, several Web-based tools were utilized in NALD v. 2.0, now hosted by a dedicated Apache Web server available to the public at <http://aerodata.ce.nd.edu>. This hardware change now permits the use of PHP, a kind of common gateway interface (CGI) language, and MySQL for a database-oriented query to specify the desired test data, replacing the archaic and sequential HTML structure of the original site. This speeds the retrieval time and dramatically reduces the number of HTML files, directories, and total file sizes by eliminating unnecessary redundancies on the server. It also provides inherent scalability so the data archives can be readily expanded. The new user-friendly interface was shown in Fig. 1 and allows the selection of a desired test case in only one step, which is then followed by the launch of the appropriate JAVA applet from NALD v. 1.0 (Zhou et al. 2003), with the option for downloading data for further off-line analysis. It is worth noting that NALD v. 2.0 has been introduced in the commentary of ASCE 7-05 [C6.5.8] (ASCE 2005) as an alternative means to assess the dynamic wind-induced loads on typical isolated buildings in the preliminary design stages.

**Step 1 : Select Shape of Interest**

01 D=2" B=6"	02 D=3" B=6"	03 D=4" B=6"
04 D=4" B=4"	05 D=6" B=4"	06 D=6" B=3"
07 D=6" B=2"	08 4" 4"	D=4" 09 60° B=6"

↑ ↑ ↑ ONCOMING WIND ↑ ↑ ↑

**Step 2 : Select Height of Interest**

15"  
20"  
24"

**Step 3 : Select Exposure Category of Interest**

Urban Exposure A      Open Exposure C

**Step 4 : Options of Non-dimensional power spectral density (PSD)**

- Use PSD data tested by NatHaz (Default)
- Use User's PSD Expression ( $C_M(f) = f \cdot S_{RR}(f) / \sigma_M^2$ )
- Use User's PSD Data, X,Y pairs

Next      Reset

Fig. 2. NALD v. 2.0 data selection menu for on-line analysis, including PSD option

### On-Line Analysis of Wind Loads and Response

In NALD v. 1.0, users would retrieve relevant spectral properties for a given test case and then manually perform off-line calculations to obtain the building base bending moments, ESWL, and accelerations based on the equations introduced previously (Zhou et al. 2003). To minimize the calculations required on the part of the end user, an on-line analysis module was developed utilizing the theory presented in the previous section to supplement the existing JAVA interface and provide these and other response quantities automatically.

The new user interface developed for on-line analysis is shown in Fig. 2. It is similar to the reorganized selection menu (Fig. 1), but with additional options for specifying the input power spectral density (PSD). At present, three user options are available for prescribing a PSD for the analysis: PSD data from the NALD (default option), a user-specified PSD (curve-fitted or analytical expression) or user-supplied PSD data (X, Y data pairs). The user selections are handled by a combination of PHP and MySQL as inputs for the next stage in the process. After selecting these basic inputs, the module requests additional inputs for the full-scale system, including cross-sectional dimensions, height, exposure

category, and fundamental dynamic characteristics (Fig. 3). Either metric (SI) or English units may be specified for the structural inputs and calculated outputs. In addition, an on-line calculator is provided for user-friendly unit conversion (Fig. 4). It should be noted that ASCE 7 recommends a 50-year mean recurrence wind that is used in survivability design, e.g., ESWL evaluation, whereas, in serviceability design, a building's acceleration is generally based on a 10-year mean recurrence wind. Thus, it is required to include a MRI factor to convert 50-year winds into 10-year winds for serviceability design. For convenience, wind speeds for both survivability (50-year MRI) and serviceability (10-year MRI) in the exposure of interest are calculated on-the-fly in NALD v. 2.0 (Fig. 5) based on the relationships in ASCE 7-05 (ASCE 2005) utilizing the user-specified 3-sec gust 50-year reference wind speed ( $U_{10}$ ) in open terrain (Fig. 3). Nondimensional spectral values [ $C_M(f)$ ] are then calculated on-the-fly for all directions and mean recurrence intervals (Fig. 5). Thus, the JAVA applets are no longer required in this new on-line analysis module.

MATLAB provides an attractive programming framework for more complicated computations and can be easily extended to

Step 5 : Please select options and fill out input values. [On-line Unit Converter](#)

Please select the unit of input values (default : Metric)  
 If user would like to see English unit output, please select checkbox (default : Metric)

Metric(SI) unit [kg, m, m/s]  
  English unit [lb, ft, mph]  
  Output : English unit

Building width(B), depth(D) and height(H)  
 B [m, ft] :       D [m, ft] :       H [m, ft] :

Natural frequencies of building for three directions; alongwind( $f_x$ ), acrosswind( $f_y$ ) and torsional( $f_z$ ).  
 $f_x$  [Hz] :        $f_y$  [Hz] :        $f_z$  [Hz] :

Mode shape exponents( $\beta$ ) for three directions, ( $z/H$ ) <sup>$\beta$</sup>  (default : linear mode shape,  $\beta=1.0$ )  
 alongwind( $\beta_1$ ) :       acrosswind( $\beta_2$ ) :       torsional( $\beta_3$ ) :

Bulk density( $\rho_B$ ), average radius of gyration( $\gamma$ ) and damping ratio( $\zeta$ ) of building  
 $\rho_B$  [kg/m<sup>3</sup>, lb/ft<sup>3</sup>] :        $\gamma$  [m, ft] :        $\zeta$  :

Floor-to-floor height of building( $\Delta H$ ), Air density( $\rho_A$ ), drag force coefficient( $C_D$ )  
 $\Delta H$  [m, ft] :        $\rho_A$  [kg/m<sup>3</sup>, lb/ft<sup>3</sup>] :        $C_D$  :

From ASCE standard 7-98 (Fig. 6-1)  
 3-second basic wind speed( $U_{10}$ ), file name(.dat) for wind force output (default : w\_force),  
 select checkbox if this building is located in Alaska  
 $U_{10}$  [m/s, mph] :       file name :        Alaska

User selected to use NatHaz PSD data.

Fig. 3. Interface for user-supplied structural inputs

### On-line Unit Converter

<p><b>Length</b></p> <p><input type="text"/> <span style="border: 1px solid black; padding: 2px;">m</span></p> <table border="0" style="width: 100%;"> <tr> <td style="width: 50%;"><input type="text"/></td> <td style="width: 50%;"><input type="text"/></td> </tr> <tr> <td>m</td> <td>cm</td> </tr> <tr> <td><input type="text"/></td> <td><input type="text"/></td> </tr> <tr> <td>ft</td> <td>in</td> </tr> <tr> <td><input type="text"/></td> <td><input type="text"/></td> </tr> <tr> <td>yd</td> <td>mile</td> </tr> </table>	<input type="text"/>	<input type="text"/>	m	cm	<input type="text"/>	<input type="text"/>	ft	in	<input type="text"/>	<input type="text"/>	yd	mile	<p><b>Velocity</b></p> <p><input type="text"/> <span style="border: 1px solid black; padding: 2px;">m/s</span></p> <table border="0" style="width: 100%;"> <tr> <td style="width: 50%;"><input type="text"/></td> <td style="width: 50%;"><input type="text"/></td> </tr> <tr> <td>m/s</td> <td>cm/s</td> </tr> <tr> <td><input type="text"/></td> <td><input type="text"/></td> </tr> <tr> <td>ft/s</td> <td>in/s</td> </tr> <tr> <td><input type="text"/></td> <td><input type="text"/></td> </tr> <tr> <td>km/hr</td> <td>mph</td> </tr> </table>	<input type="text"/>	<input type="text"/>	m/s	cm/s	<input type="text"/>	<input type="text"/>	ft/s	in/s	<input type="text"/>	<input type="text"/>	km/hr	mph
<input type="text"/>	<input type="text"/>																								
m	cm																								
<input type="text"/>	<input type="text"/>																								
ft	in																								
<input type="text"/>	<input type="text"/>																								
yd	mile																								
<input type="text"/>	<input type="text"/>																								
m/s	cm/s																								
<input type="text"/>	<input type="text"/>																								
ft/s	in/s																								
<input type="text"/>	<input type="text"/>																								
km/hr	mph																								
<p><b>Density</b></p> <p><input type="text"/> <span style="border: 1px solid black; padding: 2px;">kg/m<sup>3</sup></span></p> <table border="0" style="width: 100%;"> <tr> <td style="width: 50%;"><input type="text"/></td> <td style="width: 50%;"><input type="text"/></td> </tr> <tr> <td>kg/m<sup>3</sup></td> <td>g/cm<sup>3</sup></td> </tr> <tr> <td><input type="text"/></td> <td><input type="text"/></td> </tr> <tr> <td>lb/ft<sup>3</sup></td> <td>lb/in<sup>3</sup></td> </tr> </table>	<input type="text"/>	<input type="text"/>	kg/m <sup>3</sup>	g/cm <sup>3</sup>	<input type="text"/>	<input type="text"/>	lb/ft <sup>3</sup>	lb/in <sup>3</sup>	<p><b>Acceleration</b></p> <p><input type="text"/> <span style="border: 1px solid black; padding: 2px;">m/s<sup>2</sup></span></p> <table border="0" style="width: 100%;"> <tr> <td style="width: 50%;"><input type="text"/></td> <td style="width: 50%;"><input type="text"/></td> </tr> <tr> <td>m/s<sup>2</sup></td> <td>ft/s<sup>2</sup></td> </tr> <tr> <td><input type="text"/></td> <td><input type="text"/></td> </tr> <tr> <td>milli-g</td> <td>gal</td> </tr> </table>	<input type="text"/>	<input type="text"/>	m/s <sup>2</sup>	ft/s <sup>2</sup>	<input type="text"/>	<input type="text"/>	milli-g	gal								
<input type="text"/>	<input type="text"/>																								
kg/m <sup>3</sup>	g/cm <sup>3</sup>																								
<input type="text"/>	<input type="text"/>																								
lb/ft <sup>3</sup>	lb/in <sup>3</sup>																								
<input type="text"/>	<input type="text"/>																								
m/s <sup>2</sup>	ft/s <sup>2</sup>																								
<input type="text"/>	<input type="text"/>																								
milli-g	gal																								
<p><b>Force</b></p> <p><input type="text"/> <span style="border: 1px solid black; padding: 2px;">N</span></p> <table border="0" style="width: 100%;"> <tr> <td style="width: 50%;"><input type="text"/></td> <td style="width: 50%;"><input type="text"/></td> </tr> <tr> <td>N</td> <td>kgf</td> </tr> <tr> <td><input type="text"/></td> <td><input type="text"/></td> </tr> <tr> <td>lbf</td> <td>kips</td> </tr> </table>	<input type="text"/>	<input type="text"/>	N	kgf	<input type="text"/>	<input type="text"/>	lbf	kips	<p><b>Moment</b></p> <p><input type="text"/> <span style="border: 1px solid black; padding: 2px;">N-m</span></p> <table border="0" style="width: 100%;"> <tr> <td style="width: 50%;"><input type="text"/></td> <td style="width: 50%;"><input type="text"/></td> </tr> <tr> <td>N-m</td> <td>kgf m</td> </tr> <tr> <td><input type="text"/></td> <td><input type="text"/></td> </tr> <tr> <td>lbf-ft</td> <td>kips-ft</td> </tr> </table>	<input type="text"/>	<input type="text"/>	N-m	kgf m	<input type="text"/>	<input type="text"/>	lbf-ft	kips-ft								
<input type="text"/>	<input type="text"/>																								
N	kgf																								
<input type="text"/>	<input type="text"/>																								
lbf	kips																								
<input type="text"/>	<input type="text"/>																								
N-m	kgf m																								
<input type="text"/>	<input type="text"/>																								
lbf-ft	kips-ft																								

Fig. 4. On-line unit conversion module

■ 1-hour mean wind speeds for designs

Survivability design (50-year return period) : $U_H = 51.30$ m/s
Serviceability design (10-year return period) : $U_H = 37.96$ m/s

■ RMS base moment coefficients ( $\sigma_{CM}$ ), reduced frequencies ( $f_r \cdot B / U_H$ ) and non-dimensional moment coefficients ( $C_M(f_r)$ )

	$\sigma_{CM}$	$f_r \cdot B / U_H$		$C_M(f_r)$	
		50-year	10-year	50-year	10-year
Alongwind	0.109	0.156	0.211	0.048	0.040
Acrosswind	0.133	0.156	0.211	0.192	0.073
Torsional	0.044	0.273	0.369	0.060	0.039

Fig. 5. NALD v. 2.0 output from on-the-fly calculation of wind speeds and nondimensional moment coefficients

more sophisticated numerical calculations due to many predefined function capabilities. For these reasons, MATLAB (version 6.5, R13) is used as the computational framework for this study, and the MATLAB Web server tool is internally utilized to supply user inputs to the server-side MATLAB analysis. A MATLAB code, running on the NALD server, determines the base moment/torque, the structural displacements and accelerations, in addition, to the ESWL for the mean, background, and the resonant components. The following quantities are then displayed on the Web portal: Nondimensional spectral base moment (Fig. 6), RMS base moment coefficient, nondimensional moment coefficient, base moment and the maximum lateral displacements for survivability design, 10-year RMS and peak lateral accelerations, corresponding lateral accelerations induced by torsion, and total lateral accelerations at the corner. All displacements and accelerations are calculated at the roof level. All these quantities, i.e., base bending moments, displacements, and accelerations are displayed for each of the three response components (Fig. 7). Finally, a plot of the mean, background, and resonant components of the ESWL on the building are displayed for the end user, as shown in Fig. 8. An option is also available to download this information as a text file for further off-line analysis and possible application to an existing structural finite element model or a spreadsheet-based building analysis. As such, the NALD v. 2.0 can also be used to express wind loads, i.e., the ESWL, in three directions in terms of 3D gust loading factors, akin to the alongwind GLF (Kareem and Zhou 2003; Tamura et al. 2005).

■ Non-dimensional PSD for alongwind, acrosswind and torsional ( $C_{Mf}(f) = f \cdot S_{Mf}(f) / \sigma_M^2$ )

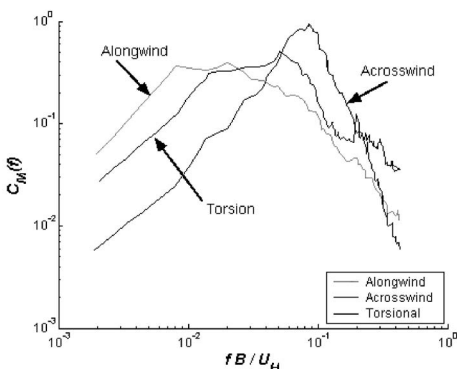


Fig. 6. Nondimensional base moment spectra display

■ Survivability Design (50-year wind) : Base moments

	Base Moment ( $10^6$ kN-m)			
	$\bar{M}$	$\bar{M}_B$	$\bar{M}_R$	$\bar{M}$
Alongwind	1.2828	0.9734	1.4828	3.0566
Acrosswind	-	1.1899	3.6403	3.8298
Torsional	-	0.0784	0.1386	0.1592

■ Survivability Design (50-year wind) : Maximum Displacements

	Maximum Displacements at roof
Alongwind	0.363 m
Acrosswind	0.455 m

■ Serviceability Design (10-year wind) : Peak and RMS Accelerations

	Peak Accelerations at roof	
Alongwind	14.19 milli-g	
Acrosswind	23.50 milli-g	
Lateral Accelerations at Corner Induced by Torsion	0.00476 rad/s <sup>2</sup>	Alongwind component : 9.70 milli-g
		Acrosswind component : 9.70 milli-g
Total Lateral Accelerations at Corner	Alongwind component : 17.19 milli-g Acrosswind component : 25.43 milli-g	

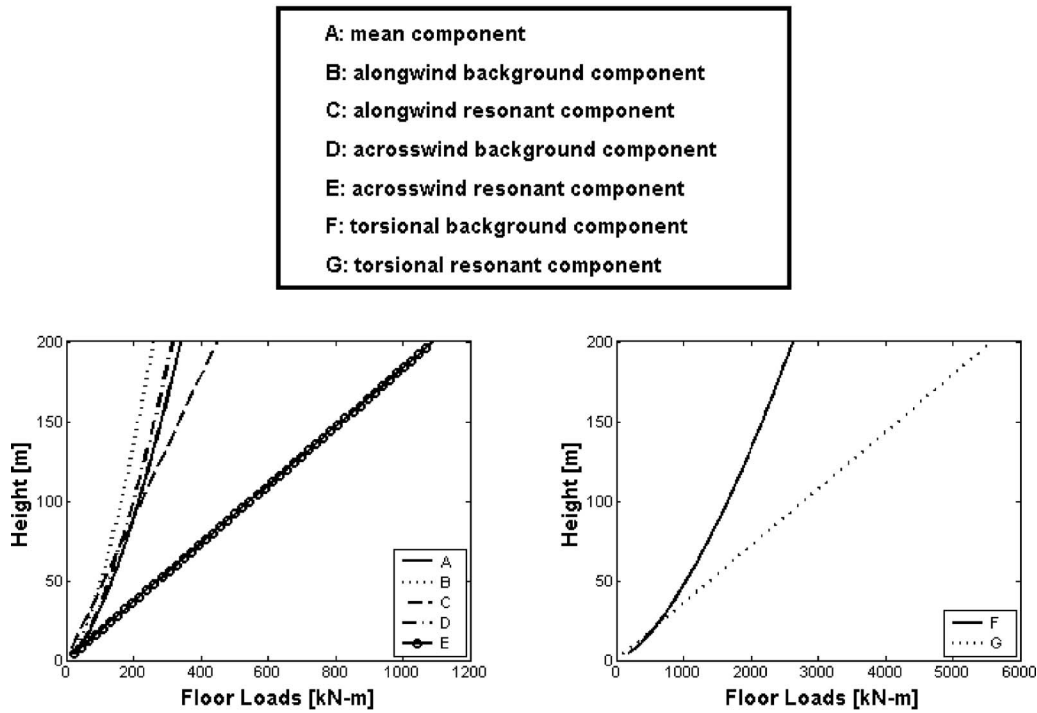
	RMS Accelerations at roof	
Alongwind	3.75 milli-g	
Acrosswind	6.21 milli-g	
Lateral Accelerations at Corner Induced by Torsion	0.00121 rad/s <sup>2</sup>	Alongwind component : 2.47 milli-g
		Acrosswind component : 2.47 milli-g
Total Lateral Accelerations at Corner	Alongwind component : 4.49 milli-g Acrosswind component : 6.68 milli-g	

Fig. 7. Display of on-the-fly calculated survivability and serviceability values

The architecture of NALD v. 2.0 and the role of various Web-based tools such as HTML/JAVA Script and PHP are summarized in Fig. 9. It is basically operated by Apache Web server with two main processes, i.e., external process and internal process. The external process includes user-friendly interfaces for the selection of a desired analysis case in Fig. 2 (interface 1), additional interfaces for design inputs such as structural parameters of building in Fig. 3 (interface 2), and display of analysis results for the user-specified building. On the other hand, the internal processes are server-side operations involving MySQL for database operations and MATLAB Web servers for the computational schemes implicitly utilized in NALD v. 2.0. The MySQL database server handles data transmissions between interfaces and if necessary, transmits information stored in the database. The MATLAB Web server functions as a numerical analysis engine for on-the-fly calculations, as well as serving as the nexus between interface 2 and the design results. The on-line analysis module performs the requisite calculations and then generates meaningful figures such as the nondimensional PSD and the ESWL, as well as the ESWL text file.

It should again be emphasized that one unique feature provided by this on-line analysis module is the user's nondimensional PSD options. As mentioned earlier, NALD v. 2.0 provides the user with three PSD options. Thus, the user can utilize not

■ Wind Force Components(mean, background and resonant components)



■ Download data file including all wind force components : w\_force\_all\_m100011.dat  
 (Column 1 : heights [m], Columns 2 to 8 : wind force component A to G [kN, kN-m])

Fig. 8. Display of on-the-fly calculated wind force components

only the PSD data offered by the NALD, but also any arbitrary PSD expression or data set for the on-line determination of wind load effects on high-rise buildings. Depending on the selected PSD option specified in Fig. 2, additional inputs will be requested following the prompt for structural inputs (interface 2 in Fig. 3). Fig. 10(a) shows the supplemental interface for user-supplied PSD expressions, while Fig. 10(b) shows the supplemental inter-

face for user-supplied PSD data sets of  $X$  (reduced frequency) and  $Y$  (nondimensional base moment PSD) pairs. Since this on-line analysis module mainly utilizes MATLAB, the aforementioned inputs should be MATLAB compatible. The “info link” displayed in the top line provides the user with simple guidelines to minimize unexpected input errors. The on-line analysis module also includes a simple error-detection scheme with pop-up error mes-

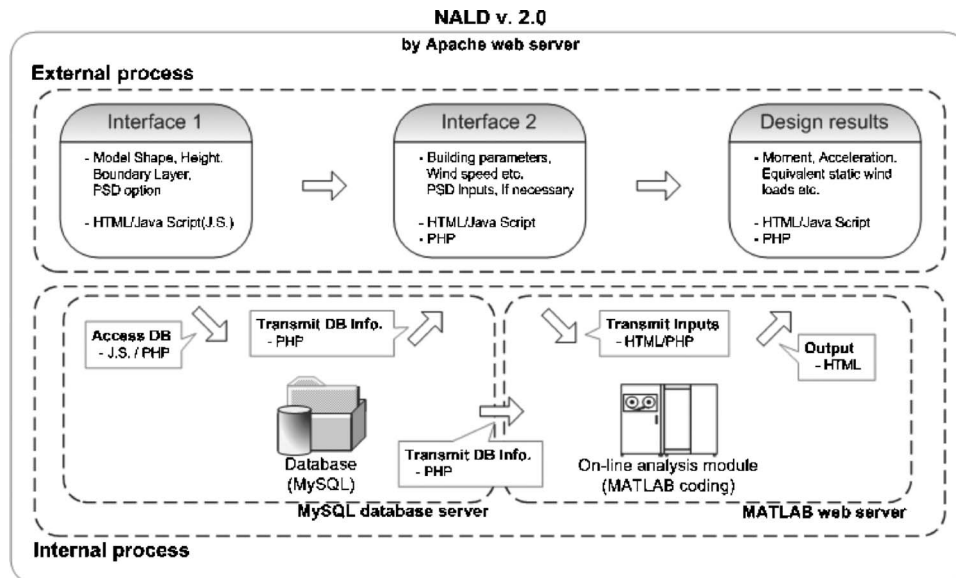


Fig. 9. Diagram of NALD v. 2.0 architecture



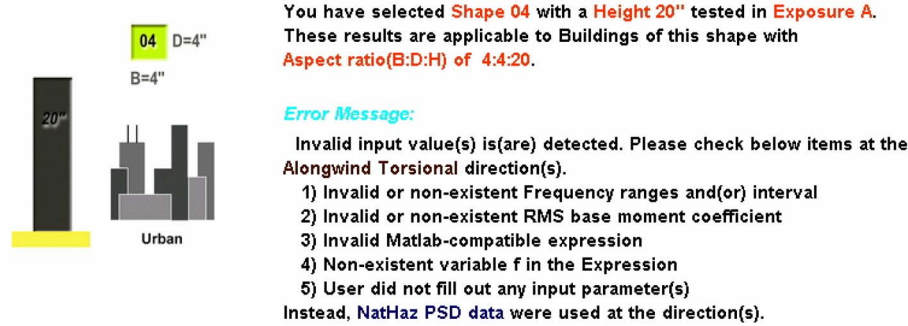


Fig. 11. An example of error message for user-supplied inputs

sponding alongwind, acrosswind, and torsional loading spectra based on the NALD experimental data were shown previously in Fig. 6 and the display of the corresponding response estimates automatically computed by the on-line analysis module were previously demonstrated in Fig. 7. These include: Mean, peak background, peak resonant, and total peak base moments, and the maximum alongwind and acrosswind displacements at the roof level for survivability design, and peak and RMS accelerations at the roof level for serviceability design. The moment and acceleration values match those manually computed by Zhou et al. (2003). The output also includes distributions of the equivalent static wind load components: Mean, background, and resonant, for all response directions, as shown previously in Fig. 8. These load distributions can be downloaded by the user for incorporation into models developed using various commercial software packages to allow for further analysis and design of structural members. This exercise reaffirms that the real-time analysis module provides response estimates that are consistent with manual calculations presented previously by Zhou et al. (2003).

### Example 2—User’s PSD Expression (PSD Option 2)

As mentioned earlier, NALD v. 2.0 provides the user with an opportunity to utilize the various types of empirical PSD expressions available. This permits comparative analyses to demonstrate the impacts of generalized spectral expressions versus precise spectral values drawn directly from PSDs of HFBB data. In this example, acrosswind PSD expressions specified by AIJ (1996, 2004) and Gu and Quan (2004), detailed in the Appendix, are considered.

The requisite inputs for this option were shown previously in Fig. 10(a):  $C_M(f)$ ,  $S_M(f)$ ,  $\sigma_M$ , in a MATLAB compatible format, the reduced frequency range ( $f_s$  to  $f_e$ ), reduced frequency interval ( $\Delta f$ ), and  $\sigma_{CM}$ . If the user leaves blank(s) for any loading direction, the analysis will default to the NALD experimental data for that direction, and an error message will be displayed, as shown in Fig. 11. Based on the aforementioned example parameters, a comparison between the NALD v. 2.0 experimental PSD data and other two aforementioned empirical PSD expressions was shown in Fig. 12. It should be noted that AIJ (1996, 2004) empirical expressions are not a function of boundary layer condition, terrain category, and building height, but are expressed mainly as a function of the side ratio ( $D/B$ ), whereas Gu and Quan (2004) incorporate the preceding attributes in their empirical expression (see the Appendix). This demonstrates a major drawback of empirical expressions: The need to incorporate an exhaustive set of variables in the expression in order to fully encompass various structural and flow features influencing response. Such considerations

were the motivating factors behind the on-line database approach represented by NALD v. 1.0. Despite the dependence on so many variables, the NALD result shows relatively good agreement with both empirical expressions with the exception of discrepancies in the low-frequency range, which are not of concern given the lack of their practical significance for typical high-rise buildings. Note also the high-frequency details lost in the empirical expressions.

To perform the on-line analysis, the reduced frequency range of the NALD experimental data is imposed on the two acrosswind PSD expressions, i.e.,  $f_s=0.0019$ ;  $f_e=0.43$ ;  $\Delta f=0.0001$ . The RMS base bending moment coefficients ( $\sigma_{CM}$ ) are automatically calculated from the respective empirical expressions (Appendix). For demonstrative purposes, the specifications of these empirical PSD expressions in a MATLAB compatible format are listed below:

$$4 * 0.85 * (1 + 0.6 * 0.1688) * 0.1688/\pi * (f/0.0901)^{2/} \\ ((1 - (f/0.0901)^2)^2 + 4 * 0.1688^2 * (f/0.0901)^2)$$

AIJ (2004)

$$4 * 0.85 * (1 + 0.6 * 0.2806) * 0.2806/\pi * (f/0.0901)^{2/} \\ ((1 - (f/0.0901)^2)^2 + 4 * 0.2806^2 * (f/0.0901)^2)$$

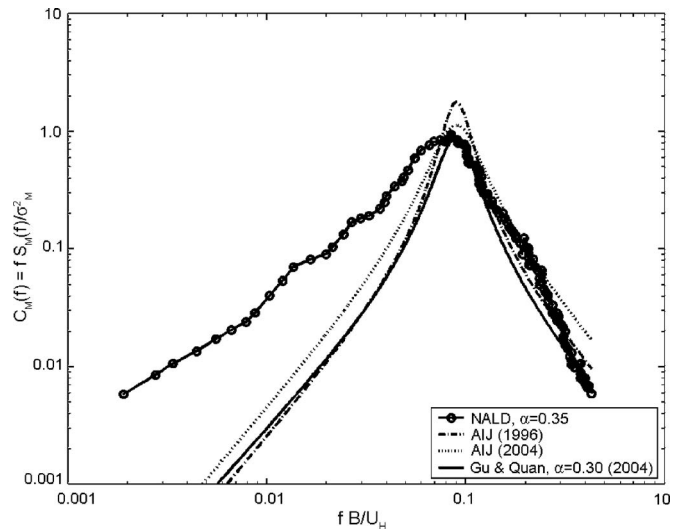


Fig. 12. Comparison of acrosswind spectra with empirical expressions of AIJ (1996, 2004) and Gu and Quan (2004) ( $D/B=1.0$ , Exposure A)

**Table 1.** Acrosswind Analysis Results for Empirical PSD Expressions in Example 2 ( $D/B=1.0, H/\sqrt{BD}=5$ )

	$\sigma_{CM}$	RMS acceleration [mg]	Base bending moment [ $10^6$ kN m]
NALD v. 2.0	0.1330	6.21	3.830
AIJ (1996)	0.1572	6.27	3.925
AIJ (2004)	0.1572	8.11	4.771
Gu and Quan (2004)	0.2122	7.34	4.692

Gu and Quan (2004)

$$1/0.2122^2 * (0.0396 * 0.1990 * (f/0.0897)^{1.8698}) / ((1 - (f/0.0897)^2)^2 + 0.1990 * (f/0.0897)^2)$$

The resulting RMS base bending moment coefficient ( $\sigma_{CM}$ ), total base moments ( $M_{total}$ ), and RMS accelerations ( $a_{RMS}$ ) derived from the four different PSDs [NALD default; user-specified AIJ (1996), AIJ (2004) and Gu and Quan (2004)] are summarized in Table 1. A quick review of the results suggests that those based on the NALD experimental data and AIJ (1996) compare well with one another. The same can be said for the results based on AIJ (2004) and Gu and Quan (2004), which take on slightly larger values than the former pair. It is important to note that RMS base bending moment coefficient ( $\sigma_{CM}$ ) is quite sensitive to the approach flow characteristics. Thus, it becomes evident that reliable estimates of the RMS coefficient and the spectral amplitude are critical to the accurate evaluation of aerodynamic load information. Though empirical fits to experimental data, such as those in AIJ (1996, 2004), provide compact representations for use in codes and standards, they cannot accurately represent experimental data for all possible building configurations and flow conditions, again motivating the on-line database philosophy of NALD v. 2.0. However, in light of these factors, the results are in reasonable agreement. Furthermore, it is also demonstrated here that the on-line analysis module works effectively for user-supplied PSD expressions.

**Example 3—User-Specified PSD Data (PSD Option 3)**

Another PSD option offered by NALD v. 2.0 is the user-specified PSD data in the form of  $X, Y$  pairs. The prompt for this data allows the user to implement his/her own PSD data derived from a wind tunnel experiment. As shown previously in Fig. 10(b), three inputs are requested in each direction: RMS base bending moment coefficient ( $\sigma_{CM}$ ),  $X$  coordinate [reduced frequency,  $f \times B/U_H$ ], and  $Y$  coordinate (nondimensional power spectrum  $C_M(f)$ ). All  $X$  and  $Y$  input should be separated by a comma (,) or single space, and the total number of  $X$  values should be the same

**Table 2.** Design Results for Data from NALD v. 2.0 and Cheng and Wang (2004) ( $D/B=1.0, H/\sqrt{BD}=5$ )

	Alongwind		Acrosswind	
	Base bending moment [ $10^6$ kN m]	RMS acceleration [mg]	Base bending moment [ $10^6$ kN m]	RMS acceleration [mg]
NALD v. 2.0	4.818	5.69	6.388	11.73
Cheng and Wang (2004)	5.158	6.29	6.639	11.17

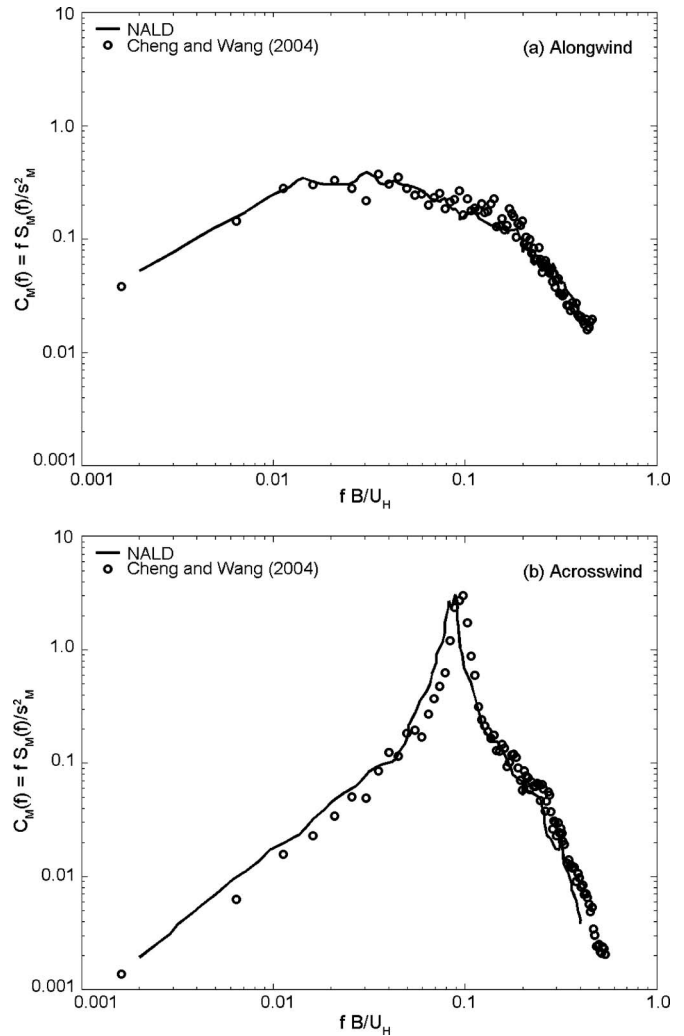


**Fig. 13.** Comparison of alongwind and acrosswind between NALD and Cheng and Wang (2004) ( $D/B=1.0, H/\sqrt{BD}=5$ , Exposure C)

as  $Y$  values. Should the user inputs be in error, the user is alerted and NALD PSD data will be retrieved by default, as shown previously by the error pop up in Fig. 11.

Fig. 10(b) shows an example of this PSD option, using the download of one of the test cases archived in NALD v. 2.0. As expected, the results exactly replicate the results obtained using PSD option 1 (Example 1) and presented by Zhou et al. (2003) and, thus, are not repeated here. This demonstrates the accuracy of an on-line module in evaluating building response based on user-specified spectral data values. Another example utilizing the data by Cheng and Wang (2004) (PSD option 3) is also compared to the NALD experimental data for the case of  $D/B=1.0, H/\sqrt{BD}=5$  under BL1 (Exposure C) for the alongwind and acrosswind directions. Table 2 summarizes the resulting base bending moments and RMS accelerations. Since the NALD spectra and Cheng and Wang (2004) data show a good agreement in the alongwind and acrosswind directions, as shown in Figs. 13(a and b), it is obvious that the response quantities correspondingly show a good agreement in Table 2.

These last two examples demonstrate the utility of the various PSD input options in this on-line analysis, providing the user with the versatility to perform an automated on-line analysis of wind

**Table 3.** Comparison of NALD v. 2.0 with AS 1170.2 and ASCE 7-05 for CAARC Building

		Responses	AS 1170.2	ASCE <sup>a</sup> exposure B	NALD v. 2.0		
					Average <sup>b</sup>	Exposure C	Exposure A
Case 1	Alongwind	Peak acceleration [mg]	8.24 <sup>c</sup>	6.97	8.60	7.67	9.52
		Base moment [10 <sup>6</sup> kN m]	2.80	2.42	2.31	2.16	2.46
	Acrosswind	Peak acceleration [mg]	15.53 <sup>c</sup>	— <sup>d</sup>	11.52	11.22	11.81
		Base moment [10 <sup>6</sup> kN m]	1.30	— <sup>d</sup>	1.47	1.11	1.83
Case 2	Alongwind	Peak acceleration [mg]	5.47 <sup>c</sup>	4.65	5.88	5.07 <sup>e</sup>	6.69 <sup>e</sup>
		Base moment [10 <sup>6</sup> kN m]	1.68	1.51	1.32	1.22	1.41
	Acrosswind	Peak acceleration [mg]	17.44 <sup>c</sup>	— <sup>d</sup>	11.83	11.04 <sup>e</sup>	12.62 <sup>e</sup>
		Base moment [10 <sup>6</sup> kN m]	1.89	— <sup>d</sup>	1.88	1.71	2.04

<sup>a</sup>ASCE 7-05 (ASCE 2005). Peak accelerations are calculated multiplying RMS acceleration by resonant peak factor and total moments are integrated wind loads determined by design wind pressure over full height of structure considering gust effect factor.

<sup>b</sup>It is obtained from taking averages of Exposures C and A results.

<sup>c</sup>Peak factor for 1 h is considered, instead of 10 min.

<sup>d</sup>ASCE only treats the alongwind direction.

<sup>e</sup>Extrapolated values, since ranges of reduced frequency are beyond acrosswind spectra.

effects on a high-rise building using his/her own data or an established expression for the base moment spectrum and evaluate various design options expediently.

#### Example 4—Comparison to Australian Standard

It is of interest to examine how the NALD v. 2.0 analysis compares with the dynamic response estimates of major building codes and standards. A *Commentary on the Australian Standard for Wind Loads* reported a detailed procedure for the dynamic analyses in the alongwind and acrosswind directions in Appendix C of that standard, using the Commonwealth Aeronautical Advisory Research Council (CAARC) standard tall building (Holmes et al. 1990). This CAARC building is analyzed by AS 1170.2, NALD v. 2.0, and ASCE 7-05 (ASCE 2005). The CAARC building's main characteristics are summarized here: Case 1.  $B=46$  m;  $D=30$  m; Case 2.  $B=30$  m;  $D=46$  m (Case 2 represents a 90 deg angle of incidence for the same building in Case 1);  $H=183$  m;  $f_x=f_y=0.2$  Hz;  $\rho_B=160$  kg/m<sup>3</sup>;  $\zeta=0.015$  for serviceability design and 0.050 for survivability design;  $C_D=1.3$  for Case 1 and 1.19 for Case 2; mode shapes for all directions are assumed linear. In Holmes et al. (1990), it was assumed that the CAARC building was located in Brisbane (terrain category 3), which corresponds to Exposure B in ASCE 7-05. Since NALD v. 2.0 handles Exposures A (BL2) and C (BL1) only, comparisons are made for both exposures, as well as their average, as they should provide upper and lower limits for the CAARC building. It should be pointed out that base moments in the AS 1170.2 were calculated for the ultimate limit state design, corresponding to wind speed of 1,000-year return period, while accelerations were

calculated for a 5-year return period, and the peak factor was evaluated for 10 min, instead of the 1-hour used in both NALD v. 2.0 and ASCE 7-05. On the other hand, NALD v. 2.0 observes the standards set by ASCE 7: 50-year return period for base moments (survivability design), and 10-year return period for accelerations (serviceability design). Thus, proper modifications to wind speed (to account for differences in return period) and peak factor (to account for differences in averaging interval) are required to compare AS 1170.2 with both NALD v. 2.0 and ASCE 7-05 results. As such, AS 1170.2 RMS results are translated to peak accelerations based on a peak factor calculated over 1 h. The design wind speed for NALD v. 2.0 and ASCE 7-05 are adjusted using the relationships in ASCE 7-05 for a 1,000-year return period in base moment calculations and a 5-year return period in acceleration calculations, so that they may be compared to the results of AS 1170.2 directly. As shown in Table 3, AS 1170.2 responses show relatively higher values (conservative) in comparison with NALD v. 2.0 and ASCE 7-05, except for the alongwind peak accelerations, which show good agreement. The discrepancies may in part be attributed to the measurement approach used to estimate aerodynamic loads. The data used in the Australian Standard are based on an aeroelastic model, and load spectra are estimated by an inverse approach, which may have inherent identification sensitivities. The other possible source may be the differences in the approach flow conditions, which have been observed to have notable influence on the acrosswind response. Another important advantage of NALD v. 2.0 is also underscored by this example; it provides a means to estimate the acrosswind response that ASCE 7 does not provide, outside of its commentary.

These examples demonstrate the capabilities and accuracy of NALD v. 2.0, providing a user-friendly procedure to reliably estimate building dynamic responses. The writers envision this capability to be particularly useful for those who may not be very familiar with the details of the dynamic analysis procedure typically employed in response estimation for wind-sensitive structures. In addition, the robust framework presented here is conveniently amenable to including additional data for other building cross sections and flow conditions.

## Concluding Remarks

The rapid development of information technologies has revolutionized many engineering applications. This study discusses the use of these advances to enhance, for the purposes of analysis and design, the accessibility, organization, dissemination, and utility of wind tunnel data. The second version of the NatHaz Aerodynamic Loads Database (NALD v. 2.0) (<http://aerodata.ce.nd.edu>) integrates these technologies for the purpose of wind-induced response prediction. NALD v. 2.0 offers more attractive and user-friendly features to allow on-line determination of not only the base moments, displacements, and the equivalent static wind loads for survivability design, but also accelerations for serviceability (habitability) design. Several Web-based tools such as PHP and MySQL are fused with MATLAB to create efficient yet computationally robust interfaces that process, convert, and analyze wind tunnel data on-the-fly with minimal user effort. The attractive feature of this on-line processing approach is that no user intervention is expended in the determination and display of wind loads and response quantities for the preliminary design of high-rise buildings. Moreover, this on-line analysis module provides the flexibility to utilize not only the NALD experimental PSD data, but also user-specified PSD expressions or data sets. This versatility provides users with a robust stand-alone, on-line analysis engine for high-rise buildings using various data sources. Further, the architecture used in this study permits easy extensions to more sophisticated numerical analyses by employing the many predefined function capabilities of MATLAB operating on the server side. While, the analysis capabilities offered by NALD v. 2.0 are not necessarily intended to replace customized wind tunnel testing in the final design stages, they do provide users with an efficient means to approximate the complete 3D response of buildings in the early design stage, which has not been fully treated in most codes and standards. Additionally, the analysis engine built into NALD v. 2.0 offers the option of utilizing user-supplied custom spectral description or wind tunnel test results to obtain final design estimates of wind load effects on buildings.

It should be noted that the Web-based tools used to establish the interface and analysis modules described in this study are continuously updated as evolving security and vulnerability issues are identified. Due to this constant updating, the interfaces are likely to experience some cosmetic changes since the publication of this manuscript.

## Acknowledgments

The writers wish to acknowledge Yin Zhou, formerly of Notre Dame, Chii-Ming Cheng, Tamkang University, Taipei, and Rachel Bashor, NatHaz Modeling Laboratory for their respective contributions. The writers are also grateful for the financial support in part by the National Science Foundation via Grant Nos. CMMI

03-24331, CMMI 06-01143, and CBET 07-42191, and a Postdoctoral Fellowship from Korea Science and Engineering Foundation (KOSEF).

## Appendix. Acrosswind PSD Expressions Used in Example 3

- AIJ Recommendations for Loads on Buildings (1996, 2004)

$$C_M(f) = \frac{f \times S_M(f)}{\sigma_M^2} = \sum_{j=1}^N \frac{4K_j(1 + 0.6\beta_j)\beta_j}{\pi} \frac{(n_0/n_{sj})^2}{\{1 - (n_0/n_{sj})^2\}^2 + 4\beta_j^2(n_0/n_{sj})^2}$$

where

$$N = \begin{cases} 1, & D/B < 3 \\ 2, & D/B \geq 3 \end{cases} \quad K_1 \approx 0.85 \quad K_2 \approx 0.02$$

$$n_0 = \frac{f \times B}{U_H} \quad n_{s1} = \frac{0.12}{\{1 + 0.38(D/B)^2\}^{0.89}} \quad n_{s2} = \frac{0.56}{(D/B)^{0.85}}$$

$$\beta_1 = \frac{(D/B)^4}{1.2(D/B)^4 - 1.7(D/B)^2 + 21} + \frac{0.12}{(D/B)} \quad (\text{AIJ 1996})$$

$$\beta_1 = \frac{(D/B)^4 + 2.3(D/B)^2}{2.4(D/B)^4 - 9.2(D/B)^3 + 18(D/B)^2 + 9.5(D/B) - 0.15} + \frac{0.12}{(D/B)} \quad (\text{AIJ 2004})$$

$$\beta_2 = 0.28(D/B)^{-0.34}$$

$$\sigma_{CM} = 0.0082(D/B)^3 - 0.071(D/B)^2 + 0.22(D/B)$$

- Gu and Quan (2004)

$$C_M(f) = \frac{f \times S_M(f)}{\sigma_M^2} = \frac{1}{\sigma_{CM}^2} \times \frac{S_p \beta (n_0/f_p)^\alpha}{\{1 - (n_0/f_p)^2\}^2 + \beta (n_0/f_p)^2}$$

where

$$n_0 = fB/U_H$$

$$f_p = 10^{-5}(191 - 9.48\alpha_w + 1.28\alpha_{hr} + \alpha_{hr}\alpha_w)(68 - 21\alpha_{db} + 3\alpha_{db}^2)$$

$$S_p = (0.1\alpha_w^{-0.4} - 0.0004e^{\alpha_w})(0.84\alpha_{hr} - 2.12 - 0.05\alpha_{hr}^2) \times (0.422 + \alpha_{db}^{-1} - 0.08\alpha_{db}^{-2})$$

$$\beta = (1 + 0.00473e^{1.7\alpha_w})(0.065 + e^{1.26 - 0.63\alpha_{hr}})e^{1.7 - 3.44/\alpha_{db}}$$

$$\alpha = (-0.8 + 0.06\alpha_w + 0.0007e^{\alpha_w})(-\alpha_{hr}^{0.34} + 0.00006e^{\alpha_{hr}}) \times (0.414\alpha_{db} + 1.67\alpha_w^{-1.23})$$

$$\alpha_w = 1(A), 2(B), 3(C), 4(D) \quad A, B, C, D : \text{Terrain categories}$$

$$\alpha_{hr} = H/\sqrt{BD}$$

$$\alpha_{db} = D/B$$

$$\alpha_{hr} = H/T \quad [T = \min(B, D)]$$

$$\sigma_{CM} = (0.002\alpha_w^2 - 0.017\alpha_w - 1.4)(0.056\alpha_{db}^2 - 0.16\alpha_{db} + 0.03) \\ \times (0.03\alpha_{ht}^2 - 0.622\alpha_{ht} + 4.357)$$

## References

- Architectural Institute of Japan (AIJ). (1996). "Recommendations for loads on buildings." Architectural Institute of Japan.
- Architectural Institute of Japan (AIJ). (2004). "Recommendations for loads on buildings." Architectural Institute of Japan.
- American Society of Civil Engineers (ASCE). (1998). "Minimum design loads for buildings and other structures." *ASCE 7-98*, ASCE, Reston, Va.
- American Society of Civil Engineers (ASCE). (2005). "Minimum design loads for buildings and other structures." *ASCE 7-05*, ASCE, Reston, Va.
- Boggs, D. W., and Peterka, J. A. (1989). "Aerodynamic model tests of tall buildings." *J. Eng. Mech.*, 115(3), 618–635.
- Chan, C.-M., and Chui, J. K. L. (2006). "Wind-induced response and serviceability design optimization of tall steel buildings." *Eng. Struct.*, 28(4), 503–513.
- Chen, X., and Kareem, A. (2004). "Equivalent static wind loads on buildings: New model." *J. Struct. Eng.*, 130(10), 1425–1435.
- Chen, X., and Kareem, A. (2005). "Dynamic wind effects on buildings with 3-D coupled modes: Application of high frequency force balance measurements." *J. Eng. Mech.*, 131(11), 1115–1125.
- Cheng, C.-M., and Wang, J. (2004). "Wind tunnel database for an intermediate wind resistance design of tall buildings." *Proc., 1st Int. Symp. on Wind Effects on Buildings and Urban Environment*, 10–25.
- Davenport, A. G. (1967). "Gust loading factors." *J. Struct. Div.*, 93(3), 11–34.
- Flay, R. G. J., and Bhat, J. (2005). "Cross-wind force spectra for building geometries commonly proposed for New Zealand cities." *Proc., 2nd Workshop on Regional Harmonization of Wind Loading and Wind Environmental Specifications in Asia-Pacific Economies (APEC-WW)*, 19–30.
- Fritz, W. P., and Simiu, E. (2005). "Probabilistic description of tall building response to wind: Database-assisted design, dynamics, and wind directionality effects." *Proc., 9th Int. Conf. on Structural Safety and Reliability (CD-ROM)*.
- Fujii, K., Hibi, K., and Ueda, H. (1986). "A new measuring system using electronically scanned pressure sensors (ESP) and some applications of the ESP system to a square building shape." *Proc., 9th National Symp. on Wind Engineering*, 313–318 (in Japanese).
- Gu, M., and Quan, Y. (2004). "Across-wind loads of typical tall buildings." *J. Wind. Eng. Ind. Aerodyn.*, 92(13), 1147–1165.
- Ha, Y. C., Kim, D. W., and Kil, Y. S. (2004). "Characteristics of the across-wind fluctuating force and spectral density of rectangular high-rise buildings with various side ratios." *Proc., CTBUH 2004*, 978–982.
- Ho, T. C. E., Lythe, G. R., and Isyumov, N. (1999). "Structural loads and responses from the integration of instantaneous pressures." *Wind Engineering into the 21st Century: Proc., 10th Int. Conf. on Wind Engineering*, A. Larsen, G. L. Larose, F. M. Livesey, eds., Balkema, Rotterdam, The Netherlands, 1505–1510.
- Holmes, J. D., Melbourne, W. H., and Walker, G. R. (1990). "A commentary on the Australian standard for wind loads: AS 1170 part 2." Australian Wind Engineering Society.
- Holmes, J. D., Rofail, A. W., and Aurelius, L. J. (2003). "High frequency base balance methodologies for tall buildings with torsional and coupled resonant modes." *Proc., 11th Int. Conf. on Wind Engineering*, 2381–2388.
- Huang, G., and Chen, X. (2007). "Wind load effects and equivalent static wind loads of tall buildings based on synchronous pressure measurements." *Eng. Struct.*, 29(11) 2641–2653.
- Kareem, A. (1982). "Fluctuating wind loads on buildings." *J. Engrg. Mech. Div.*, 108(6), 1086–1102.
- Kareem, A. (1990). "Measurement of pressure and force fields on building models in simulated atmospheric flows." *J. Wind. Eng. Ind. Aerodyn.*, 36(1), 589–599.
- Kareem, A., and Cermak, J. E. (1979). "Wind tunnel simulation of wind-structure interactions." *ISA Trans.*, 18(4), 23–41.
- Kareem, A., and Zhou, Y. (2003). "Gust loading factor—Past, present and future." *J. Wind. Eng. Ind. Aerodyn.*, 91(12–15), 1301–1328.
- Kijewski, T., and Kareem, A. (1998). "Dynamic wind effects: A comparative study of provisions in codes and standards with wind tunnel data." *Wind Struct.*, 1(1), 77–109.
- Kijewski, T., Kwon, D., and Kareem, A. (2003). "e-technologies for wind effects on structures." *Proc., 11th Int. Conf. on Wind Engineering*, 2217–2224.
- Kikuchi, H., Tamura, Y., Ueda, H., and Hibi, K. (1997). "Dynamic wind pressures acting on a tall building model—Proper orthogonal decomposition." *J. Wind. Eng. Ind. Aerodyn.*, 69–71, 631–646.
- Kwon, D., Kijewski-Correa, T., and Kareem, A. (2005). "e-analysis/design of tall buildings subjected to wind loads." *Proc., 10th Americas Conf. on Wind Engineering (CD-ROM)*, Paper No. 123, AAWE.
- Liang, S., Li, Q. S., Liu, S., Zhang, L., and Gu, M. (2004). "Torsional dynamic wind loads on rectangular tall buildings." *Eng. Struct.*, 26(1), 129–137.
- Liang, S., Liu, S., Li, Q. S., Zhang, L., and Gu, M. (2002). "Mathematical model of acrosswind dynamic loads on rectangular tall buildings." *J. Wind. Eng. Ind. Aerodyn.*, 90(12–15), 1757–1770.
- Lin, N., Letchford, C., Tamura, Y., Liang, B., and Nakamura, O. (2005). "Characteristics of wind forces acting on tall buildings." *J. Wind. Eng. Ind. Aerodyn.*, 93(3), 217–242.
- McNamara, R. J. (2005). "Some current trends in high rise structural design." *Structure Magazine*, September, 19–23.
- Reinhold, T. A., and Kareem, A. (1986). "Wind loads and building response predictions using force-balance techniques." *Proc., 3rd ASCE Engineering Mechanics Specialty Conf. on Dynamic Response of Structures*, ASCE, New York, 390–397.
- Solari, G., and Kareem, A. (1998). "On the formulation of ASCE 7-95 gust effect factor." *J. Wind. Eng. Ind. Aerodyn.*, 77–78, 673–684.
- Steckley, A., Accardo, M., Gamble, S. L., and Irwin, P. A. (1992). "The use of integrated pressures to determine overall wind-induced response." *J. Wind. Eng. Ind. Aerodyn.*, 42(1–3), 1023–1034.
- Tamura, Y., Kareem, A., Solari, G., Kwok, K. C. S., and Holmes, J. D. (2005). "Aspects of the dynamic wind-induced response of structures and codification." *Wind Struct.*, 8(4), 251–268.
- Tamura, Y., Kawai, H., Uematsu, Y., Marukawa, H., Fujii, K., and Taniike, Y. (1996). "Wind load and wind-induced response estimations in the 'Recommendations for loads on buildings,' AIJ 1993." *Eng. Struct.*, 18(6), 399–411.
- Tschanz, T., and Davenport, A. G. (1983). "The base balance technique for the determination of dynamic wind loads." *J. Wind. Eng. Ind. Aerodyn.*, 13(1–3), 429–439.
- Vickery, P. J., Steckley, A. C., Isyumov, N., and Vickery, B. J. (1985). "The effect of mode shape on the wind-induced response of tall buildings." *Proc., 5th U. S. National Conf. on Wind Engineering*, Vol. 1B, 41–48.
- Xu, Y. L., and Kwok, K. C. S. (1993). "Mode shape corrections for wind tunnel tests of tall buildings." *Eng. Struct.*, 15(5), 387–392.
- Zhou, Y., and Kareem, A. (2001). "Gust loading factors: New model." *J. Struct. Eng.*, 127(2), 168–175.
- Zhou, Y., Kareem, A., and Gu, M. (2002). "Mode shape corrections for wind load effects." *J. Eng. Mech.*, 128(1), 15–23.
- Zhou, Y., Kijewski, T., and Kareem, A. (2003). "Aerodynamic loads on tall buildings: Interactive database." *J. Eng. Mech.*, 129(3), 394–404.

# Next Frontiers of Innovation, Discovery and Learning in Wind Engineering: A Cyberinfrastructure Perspective

by

Ahsan Kareem<sup>1</sup>, Tracy Kijewski-Correa<sup>2</sup>, Yukio Tamura<sup>3</sup> and Greg Madey<sup>4</sup>

## ABSTRACT

Wind-related catastrophes inflict enormous devastation on the built environment and result in a staggering number of fatalities, which may continue to rise in the future given the increase in exposure as population migrates towards the coasts. To better manage the impact of extreme wind events, given the heavy reliance on empirical and experimental data in the design process, a new paradigm is required utilizing shared resources and global collaborations. An engineering virtual organization (EVO) would enable such a paradigm shift by offering real-time shared access to geographically dispersed resources for more effective research and education to achieve improved understanding and modeling of wind effects on structures. This paper summarizes such a program recently launched by the authors to develop a prototype EVO. The goals of this initiative are (i) to establish and sustain such a virtual community for wind hazard mitigation; (ii) to enhance this community's analysis and design capabilities to address next generation challenges posed by wind; and (iii) to facilitate education and training of the future workforce in the field. The steps toward the former goal have already been initiated through the collection of the field's leading universities, organizations, firms and government agencies to form this prototype collaboratory and their commitments to contribute their resources. The latter two goals will be accomplished through the formation of a virtual organization utilizing cyberinfrastructure technologies to stitch these geographically dispersed e-analysis and design modules encompassing *Database-Assisted Design, Full-Scale Data, Stochastic Tools, Tele-Experimentation, Uncertainty Modeling, and Computational Platforms*. The prototype EVO will allow access to the modules, while the fully functional EVO will also have the capability for automated, integrated analysis and design using multiple modules. In addition, both the prototype and full version of the EVO will offer an interactive knowledge base intended to aggregate and centralize the shared knowledge of the collaboratory, including a *wind-wiki, damage database, help desk/FAQ, bulletin boards* and *curriculum tools* to facilitate dissemination and education.

KEYWORDS: cyberinfrastructure, virtual organization, wind effects, analysis and design, database.

## 1 INTRODUCTION

Wind-related catastrophes (e.g., hurricanes, tornadoes, thunderstorms) inflict enormous devastation on the built environment and result in a staggering number of fatalities. The number of storms in 2005 was unprecedented in recent history and included major events such as Hurricanes Katrina, Rita, and Wilma, which took a heavy toll on human lives, the economy, and the social fabric of society [1, 3, 7, 38, 53]. In 2005, 80% of the total \$212 billion worldwide economic losses resulted from hurricanes. In 2006, 91% of the worldwide losses were weather-related, and wind-related losses made up 57% of the \$50 billion in US

---

<sup>1</sup> Robert M. Moran Professor, NatHaz Modeling Lab., University of Notre Dame, Notre Dame, IN 46556

<sup>2</sup> Rooney Assistant Professor, DYNAMO Lab., University of Notre Dame, Notre Dame, IN 46556

<sup>3</sup> Director, Global Center for Excellence, Tokyo Polytechnic University, Atsugi., Japan, 243-0297

<sup>4</sup> Research Professor, Computer Science and Engineering, University of Notre Dame, Notre Dame, IN 46556

total losses [38]. The enormity of the societal impact of storm activity can be appreciated by the realization that private insurers are currently fleeing the coasts, potentially leaving states to face the cost of insurance payoffs topping \$650 billion [55].

To better manage the impact of extreme wind events, a new culture of resilience needs to be developed based on innovative design solutions. By harnessing new technologies, quality of life and economic strength can be improved. In response to this, the research agenda in the planned National Wind Hazards Reduction Program (NWHRP) focuses on the utilization of emerging technologies for developing hazard resilient communities [41]. The concept of shared resources is at the center of this plan and includes the exchanging of databases, computational and experimental resources, and full-scale data, as well as participating in collaborative research [1, 5]. Current examples of networked facilities for hazard reduction are the Network for Earthquake Engineering Simulation (NEES) [51]. These facilities have made high-end resources accessible to groups otherwise limited by their personal research tools allowing them to expand the scope of their research to address complex problems. A similar model in the area of wind effects that shares resources and includes global engagement with centers of research, education, and design would result in similar productive advances.

The interdisciplinary nature of wind effects on structures requires a knowledge base from a number of subject areas, including structural engineering, engineering mechanics, probabilistic methods, fluid dynamics, turbulence, structural dynamics, experimental methods and risk and reliability, to better quantify the load effects (e.g., [29, 46]). Under this umbrella, reliance is on analytical [10-11], computational [15, 26, 54, 61], and experimental tools [4, 7-8, 14, 44], full-scale measurements [9, 16, 23-25, 30-31, 34-35, 45, 48-49], codes and standards [2, 22, 50], and databases [10, 30, 35, 40, 44]. This presents a large set of subject areas and topics worthy of an Engineering Virtual Organization (EVO) to help assimilate information and resources into a publicly-accessible collaboratory. The resulting EVO would serve as an end-to-end system that integrates domestic and international community resources to facilitate an effective, transformative, and conveniently accessible venue for the acceleration of advances in research and development, as well as teaching and learning, in the area of wind effects.

Despite many advances in the area of wind effects on structures in recent decades, research has been conducted with limited resources scattered physically throughout universities, government, and private research laboratories as well as industry and trade organizations. With the trend toward increasingly complex designs such as free form architectures and the escalating potential for losses in coastal communities, the old paradigm is no longer optimal and requires the pooling of resources through a virtual organization reliant on cyberinfrastructure (CI). By centralizing tools and services within a flexible CI architecture to support research and education objectives in real-time, this synergistic, integrative approach offers efficacious tools that the community can use to minimize windstorm damage and meet the challenges posed by burgeoning emergence of wind sensitive structures in expanding urban and suburban locales.

Interestingly, other technology fields are fast recognizing the potential impact of virtual organizations, as evidenced by digital airports and, more recently, digital oil fields, which involve effective gathering, analyzing, and visualization of data in real-time during drilling to quickly react to problem spots as they are detected [20]. This is serving as a catalyst to gain competitive advantage over others in a business with astronomical stakes. Similarly, the structural engineering field is currently at the dawn of a new information technology (IT) known as Building Information Modeling (BIM), which promises to revolutionize the design and construction of buildings. Building Information Models are 3-D, smart, parametric e-models of buildings that are shared by a team of designers and builders to facilitate the exchange and interoperability of information in a digital format. BIM covers geometry, spatial relationships, geographic information, quantities, and properties of building components. BIM can be used to demonstrate the entire

building lifecycle. While BIM addresses the visualization and information exchange associated with structural projects, it possesses limited if any advanced analytical resources requisite for the design process. Certainly, the enormous reported losses from wind-related events and the increased sensitivity of freeform and super tall buildings, long-span bridges, and deep water offshore platforms to wind make it an ideal hazard for an EVO providing these much needed design tools. Furthermore, if such an EVO can be digitally linked with BIM, there is great potential for transformative and rapid technology transfer to both the design and construction industries, as well as universities and other educational institutions.

## 2 OVERVIEW OF VORTEX-WINDS EVO

In order to mitigate escalating damage to property, loss of lives and disruption of local economies [1, 3, 7], a new research, teaching and design paradigm is proposed addressing wind effects on structures through the formation of a virtual organization utilizing an integrated cyberinfrastructure technologies. Wind hazards would particularly benefit from this paradigm given the reliance on experimental and empirical data in the design process. The following sections detail a **Virtual Organization for Reducing the Toll of EXtreme Winds (VORTEX-Winds)**, its organization and various levels of functionality, followed by a description of a prototype EVO that will demonstrate real-time shared access to geographically dispersed resources, as well as providing a publicly accessible knowledge-base.

### 2.1 Vision & Goals

The basic vision of VORTEX-Winds is the development a comprehensive gateway for research and education to achieve improved understanding and modeling of wind effects on structures to counter the escalating loss of property and associated indirect losses and the increase in the sensitivity of emerging structural systems to winds. In response to this vision, the authors have established a virtual organization employing integrated cyberinfrastructure-based system that facilitates real-time, shared access to integrated design aids and services using geographically dispersed databases, specialized design/analysis tools, experimental facilities and full-scale monitoring networks, as well as providing a knowledge-base, with the following goals:

- (i) To establish and sustain a community contributing to and employing the resources integrated by cyberinfrastructure technologies to facilitate the mitigation of escalating damage, loss of lives and disruption of local economies posed by wind;
- (ii) To enhance analysis and design capabilities to address the challenges of innovative structural systems needed to realize, in a cost effective manner, buildings with ever increasing heights, bridges that span oceans, and offshore platforms tapping hydrocarbons in deeper waters exposed to weather extremes like hurricanes;
- (iii) To facilitate education and training of the future workforce in the field so that the growing competition in the global market is met through a cadre of well trained professionals and educators.

### 2.2 Structure & Shared Resources

The EVO structure is conceptually defined in Figure 1 as having two branches: the e-analysis and design modules and the Knowledge Base. The e-analysis and design modules are harvested from the independent work of a number of universities (largely supported by federal funding) and NIST and will be classified into six divisions. These six divisions are *Database-Assisted Design*, *Full-Scale/Field Site Data Repository*, *Statistical/Stochastic Toolboxes*, *Tele-Experimentation Services*, *Uncertainty Modeling*, and *Computational Platforms*. Examples of the modules offered within each of the divisions are shown in Figure 1. As discussed later in this paper, the modules can be interrogated independently or automatically queried and

input into an integrated analysis and design approach. This integrated approach mimics the traditional off-line analysis and design processes schematically depicted in Figure 2, pooling contributions from a number of different disciplines. The second branch of VORTEX-Winds is the knowledge base intended to aggregate and centralize the shared knowledge of the collaboratory. Services in this area include the virtual encyclopedia or *wind-wiki* encompassing basic terminology and concepts pertaining to wind-structure interaction, a *damage database* (curated archives of post-disaster reconnaissance, e.g., [24-25]), a *help desk*, where users can submit a question to the collaboratory and where past responses are archived as FAQs, *bulletin boards* hosting open discussions, *email list servers* for rapidly circulating announcements and other information, and *curriculum tools* to provide educators a means to formally integrate EVO services into their teaching. The knowledge base material will be broadly classified into 4 major areas: *Engineering Micrometeorology*; *Aerodynamics/Aeroelasticity*; *Structural Dynamics*; *Experimental Methods*; *Performance Evaluation* (encompassing Risk/Reliability and Codes/Standards).

### 2.3 Participants and Recruitment

Members: *Members* of the EVO will explicitly provide some shared resource in support of the stated mission. This diverse collection of resources includes aerodynamic and damping databases [e.g., 12, 28, 32, 42, 45, 47, 52, 62], wind load and response simulators and tunnels [e.g., 7, 8, 14, 44], computational fluid dynamics (CFD) platforms [e.g., 15, 54, 55] and real-time streaming meteorological (met) data [e.g., WS13]. Most of these resources will come from leading universities in the area of wind effects on structures and generally have been the result of federal or state funding. A number of federal agencies are also poised to contribute to the EVO, including National Institute of Standards and Technology (NIST) and National Oceanic and Atmospheric Agency (NOAA). Members obtain this status after successfully contributing to the EVO. As a result, they will take a primary role in the governance of the organization.

End Users: While the collaboratory members will certainly also use the shared resources to further their own research and educational missions, a number of other end users have also been identified within the community. *End users* are defined as those accessing the various services offered by the EVO, but not directly contributing to them. This class of participants is primarily associated with designers of structures with particular sensitivity to wind effects, such as tall buildings; however, the EVO will also reach out to educators as another category of end users. Other private sector entities, such as wind tunnels and risk analysis firms, may also become end users of various modules within VORTEX-Winds. All persons accessing the EVO (as end users or members) will be required to register, which will not only streamline operations, but will also gather data important to the evaluation and assessment of the EVO's impacts.

Stakeholders: *Stakeholders* indirectly benefit from the EVO through the actions of members and end users using the VORTEX-Winds' services to improve wind-resistant design. These stakeholders represent all who benefit from safer civil infrastructure. Obvious examples of stakeholders include risk management firms like Aon, Institute of Business and Home Safety (IBHS) and Risk Management Services (RMS), the wider professional community representing end users, such as Council on Tall Buildings and Urban Habitat (CTBUH), American Association for Wind Engineering (AAWE), and American Society of Civil Engineers' (ASCE) committee on Tall Buildings and Technical Council on Wind Engineering, and organizations dealing with codes and standards, such as the International Code Council (ICC). However, all of society, as users of civil infrastructure, would benefit from more wind-resistant structures and thus also become indirect stakeholders.

Recruitment: The success of any EVO lies in its ability to attract and engage leading researchers and practitioners within the community. Initially, VORTEX-Winds membership will be formulated by invitation, as discussed later in the prototype development plan. Subsequently, the EVO will build its ranks

through presentations, technical sessions and even exhibitor displays at the major conferences within the field, e.g., ASCE Structures Congress and assorted wind Engineering Conferences (Americas Conference on Wind Engineering (ACWE), International Conference on Wind Engineering (ICWE)). These venues will also be used to hold working group meetings to determine user requirements and community needs. Stakeholder organizations (ASCE, AAWA, CTBUH) will also assist in recruitment by circulating announcements to their constituents, as well as online surveys for community feedback on requirements and directions. In parallel, through the development of high quality services and a transparent and equitable governance system, it is believed that the reputation and notoriety of the EVO will spread at the grass roots level to insure sustainability and growth beyond the initial recruitment phase.

While this strategy may be effective for professional recruitment, it will reach only certain segments of the academic end user community. For this reason, American Association for Engineering Education (AAEE) will be used to advertise VORTEX-Winds to its constituents, including the provision for working groups/presentations at AAEE meetings.

### 3 ORGANIZATIONAL AND GOVERNING STRUCTURE

An effective strategy for self-organization and governance is required to insure a collaboratory that is reputable, sustainable and technically reliable. This aspect of the EVO is particularly important due to the unique challenges that arise when pooling diverse resources that span institutional, cultural and professional boundaries. As such, VORTEX-Winds will adopt many of the proven organization and governing strategies that have already been accepted in professional circles around the world. In terms of organization, VORTEX-Winds will be led by a director, elected to multi-year terms by the collaboratory. Serving under the director will be three elected directors, two of whom will respectively supervise the content of e-analysis & design modules and the knowledge base. These directors will respectively appoint 6 division leaders, an editor-in-chief and 4 subject area editors from the collaboratory membership. The third director will be the CI director ultimately responsible for the maintenance, updating and development of the CI tools. This structure is shown schematically in Figure 3. As the collaboratory includes two distinct branches: the e-analysis and design modules and the knowledge base, two different forms of internal governance are then required for each.

The primary concern with the e-analysis and design branch is the soundness of the technologies. Some form of quality-control is required, particularly when modules are submitted to the collaboratory in response to open calls, as opposed to direct invitation. Within academic circles, technical soundness is generally gauged through peer-review processes that are generally confidential and sometimes accused of being political. What is envisioned for this collaboratory is a transparent, anonymous version of the peer-review process on any analysis/simulation tool, experimental resource or data repository to be included in the collaboratory. Contributors wishing to add a module to one of the six divisions in Figure 1 must complete a standardized application form detailing the scientific methodologies and verifications performed to date. The application will be forwarded by the EVO Module Director to the appropriate module division leader. The division leader will select three appropriate collaboratory members within that division to review and issue anonymous comments on the application. The division leader will then consider the reviews and submit a decision to the EVO Module Director to invite or decline the contribution.

Within the knowledge base, the primary governance issues are associated with the wind-wiki. Like most wikis, registered users may contribute to the wind-wiki under any of these subject areas. However, given the technical nature of the material, each subject area's content will be managed by the subject area editor associated with that topic. The subject area editor will receive email notification when wiki-content

in his/her subject area has been modified and will have the duty of reviewing and ultimately authorizing any revisions or additions. The knowledge base editor-in-chief will have overall oversight and guide the editorial content. Certainly there is the potential within the collaboratory for power abuses, particularly when potential contributions are perceived to refute or undermine the work of others in the collaboratory. Therefore, an appeals process will be available to any contributors, and these appeals will be posted on a public bulletin board and an email call to all collaboratory members will open a discussion on the item under appeal. A majority vote within the collaboratory will determine the success of any appeal. While academic review and appeals processes are normally confidential, the full disclosure and participation is important to maintain the integrity of the EVO. This appeals process will be openly disclosed in the collaboratory literature, along with all relevant forms and policies for submission, as has been done in other EVOs like the Integrated Primate Biomaterials and Information Resource (IPBIR) [33].

#### 4 CONCEPTUAL CI DESIGN

VORTEX-Winds will include on all aspects of cyberinfrastructure support capabilities for the wind effects on structures research and engineering community, including: 1) communication tools to support collaboration, 2) high performance computational infrastructure, including access to TeraGrid services [40], 3) data storage, data mining, visualizations, and data warehousing, and 4) access to remote sensors and tele-experimentation. As a result, VORTEX-Winds will ultimately offer three levels of functionality:

1. Level 1: knowledge base queries, which would be handled within the Knowledge Base's resources such as the help desk, wind-wiki or bulletin boards;
2. Level 2: utilization of specific e-analysis and design modules, e.g., retrieval of wind field data from the data repository for a specific region;
3. Level 3: integrated analysis and design using multiple modules, e.g., online execution of basic wind-resistant design with computation hosted by the EVO and automated queries to multiple modules.

These services will be hosted on the front-side by a single gateway server, with computation and analysis conducted on backside parallel servers. This section will detail the commercially/publicly available CI tools and services required to facilitate these three levels of functionality, including similar features of EVOs in related areas.

##### 4.1 Level 1: Knowledge Base Queries

End users will be supported by a combination of asynchronous communication tools, including wikis, web-conferencing/bulletin-board-systems, online content, document servers, and synchronous communication tools such as video conferencing (e.g., WebEx or AccessGrid) and chat services. Whenever possible, we will employ well-supported, "ready-to-use-out-of-the-box" open source software for rapid deployment and ease of maintenance. Examples include Drupal and Plone for distributed content management (CMS), MediaWiki or tWiki for the wind-wiki, ePrints for document archival of pre- and postprints, and phpBoard, WebEx or Ikonboard for web conferencing services. Note that while the software used for databasing in EVOs like the IPBIR [33] or for general communication, documentation and support from EVOs like NEESit [51] can be readily adapted, most do not provide the unique knowledge base driven by the *wind-wiki* concept.

#### *4.2 Level 2: Module Stitching/Integration*

Development of VORTEX-Winds will involve the integration (or module-stitching) of existing and new databases, tools, and services. This is a unique challenge of this project since other popular repositories like NEEScentral [51] and EarthScope [13] had specific schemas established before being populated with data. In the case of VORTEX-Winds, most of the data and modules are pre-existing and thus software and service interoperability must be achieved by a cross-section of standard integration techniques, such as: 1) use of standard database schemas where possible, 2) development of standard (but simplified) ontologies, XML Schema, and schema conversion using XML parsing tools between interoperating services and databases, and 3) web services, especially for complex workflows or data analysis pipelines. Those workflows and analysis pipelines can be enabled using open-standards web services (SOAP/XML/WSDL) and associated open source workflow design and execution tools such as Taverna and its associated modules. Additional open source tools that may be employed include Weka for data mining, and the statistical package R for analysis and visualization of archived data, including the provision for realistic 3D visualization of both load and response details [39]. Popular open source databases that will be used include MySQL and PostgreSQL. Since some of the existing services use commercial/proprietary tools (e.g., Matlab, SAP2000) we will use those products' published API's for integration, or wrap them as a web services for standard access. In this case, licensing issues will be evaluated, using free "players" rather than the licensed development versions when available. Finally, meta-data, including authorship, documentation sources, "data pedigree", and data provenance, will be supported in the EVO both by 1) direct provision in the database schema and 2) through annotations on the wikis and/or web sites for each analysis or data module by the VORTEX-Winds leadership. Additional cyber related information on EVOs can be found in e.g., [3, 21, 17-19, 36, 56-60].

#### *4.3 Level 3: Integrated Analysis and Design*

Given that wind effects are highly sensitive to dynamic properties, geometry and surroundings, design strategies for them make use of a number of experimental and empirical resources that do not reside in any shared international repository. Although final design of some structures requires specialized testing, the preliminary design and analysis of most structures could benefit from access to such resources. An attempt in this context was initiated by researchers at the University of Notre Dame through the development of the NatHaz Aerodynamic Loads Database (NALD) [62]. Initially introduced in 2000, this database has served an important first step in establishing an on-line experimental archive of high frequency base balance (HFBB) data for use in the preliminary design of high-rise buildings subjected to wind loads. As a result, NALD was introduced in the Commentary of ASCE 7-05 (C6.5.8) [2] as an alternative means of assessing the dynamic wind load effects on high-rise buildings. More recently, NALD v. 2.0 has been re-designed to integrate the latest advances in data management and mining for interactive queries of aerodynamic load data and an integrated on-line analysis framework for survivability and serviceability design considerations of tall buildings [32]. These changes were achieved using a combination of web-based programming tools and popular engineering software, e.g., Apache web servers, JAVA/JavaScript, Hypertext Preprocessors (PHP), Structured Query Language databases (MySQL) and Matlab. The power of NALD v. 2.0 is the flexibility it's analysis module offer: users may select not only the data from the on-line aeroloads database, but also may implement any arbitrary power spectral density (PSD) expression or wind tunnel-derived PSD data set for the evaluation of wind load effects on high-rise buildings. Thus it serves, a dual purpose design aid: a database driven web archive of wind tunnel data and a stand-alone analysis engine that can be used independently or in tandem to yield a comprehensive, simplified and efficient platform for e-analysis of high-rise buildings.

While the NALD focuses only on the preliminary design loop in the wind-resistant design process, the CI of VORTEX-Winds will provide access to communication, data, computational, and remote sensing

and tele-experimentation services using launch-pad web pages (portals) to generate a comprehensive, interactive design aid. Users will be able to launch either individual services, or composite services integrated from multiple atomic services. This integration of multiple modules, as shown in Figure 4, will be enabled using prepackaged workflows designed using tools such as Taverna, stored using XML/Scufl files, and executed using a workflow engine such as FreeFluo. A researcher or engineer will be able to select individual modules and manually conduct an analytical workflow using a “cut & paste” process, or when provided, a semi-automated prepackaged workflow. Both approaches will require format conversion of data; those conversion modules will be provided as stand-alone services on the launch-pad portal, or directly integrated into the prepackaged web-services workflows. Demanding computation services will be provided on the Notre Dame Center for Research Computing cluster, with possible extensions into appropriate TeraGrid computer clusters. It should be noted that the interactive design aid takes the notion of hybrid simulation a step further by utilizing databases, experiments, full-scale measurements and analytical models through a repeated queries and multi-stage analyses. Further, unlike other EVOs like NEES or Time-sharing Experiments for the Social Sciences (TESS), the integrated design tools offered by VORTEX-Winds can be publicly available and are not restricted to funded proposals, due to their nature and small scale.

## 5 PROTOTYPE DEPLOYMENT

With the organizational and governance structure of VORTEX-Winds already defined, the primary technical hurdle is in achieving the three levels of functionality introduced in the previous section. This will require significant effort and coordination, particularly with respect to the integrated design feature. As a result, the prototype deployment that will be pursued in this study will establish the basic components of the Knowledge Base and stitch together a number of geographically distributed resources representative of the six module divisions identified in Figure 1. As such Level 2 functionality would be achieved at the conclusion of this two year study. If additional funding is secured, all existing services will be expanded and the third and most complex level of functionality will be developed.

## 6 IMPLEMENTATION PLAN

In order to achieve Level 2 functionality, seven tasks have been identified, as shown in Table 1 along with a timeline for completion. Note that separate evaluation and development servers will be established to allow parallel activities without conflict. Details of each task are as follows:

### *6.1 Task 1. Collaboratory Development*

As will be detailed in a later section, the authors have already received commitments from a number of leading universities and design firms to form the prototype VORTEX-Winds. Thus, minimal effort is needed at this stage in recruitment, and the primary collaboratory development activity will be the coordination of the members, establishment of the organization itself, and an inventory of the member resources and their formats for module development. Additionally, collaboratory development will call upon the key professional organizations (ASCE, CTUBH, AAWE) to circulate web-surveys to determine user requirements and community needs. These needs will help to prioritize the modules introduced in the prototype deployment and will help to chart the long-term strategic plan of the EVO.

### *6.2 Task 2. Module Formatting*

This is the primary technical task associated with the Year 1 development and will be concerned with insuring that the databases and various technologies identified as high-priority modules from Task 1 are standardized, appropriately formatted and complete before they are centralized in the EVO infrastructure.

### *6.3 Task 3. CI Development*

This task will involve the literal construction of the cyber-infrastructure to stitch together the formatted modules from Step 2 and develop basic data mining and visualization tools.

### *6.4 Task 4. Beta Testing*

Collaborating design firms and educators will serve as the end user community and will be given access to the prototype of VORTEX-Winds at the conclusion of Task 3 to begin testing the modules and providing feedback for redesign. A similar beta testing period will be launched once the knowledge base is populated.

### *6.5 Task 5. Knowledge Base Design*

This CI task will physically develop the knowledge base tools (wind-wiki, bulletin boards, help desk, etc.).

### *6.6 Task 6. Knowledge Base Population*

The assembled membership will begin contributing to the wind-wiki and other knowledge base features in the first and second years of this program.

### *6.7 Task 7. Assessment and Redesign*

Based on the feedback from Task 4, two periods of assessment and redesign will be executed. It is envisioned that the first period, concerned with the module side of the EVO, will be more intensive, than the knowledge base revision. Once any major redesigns are concluded, VORTEX-Winds will be opened for educational use. At the conclusion of Task 7, a Level 2 functioning prototype will be available.

## 7 SECURITY AND CHALLENGES

The CI Director for VORTEX-Winds will have responsibility to ensure the integrity, security, and responsible implementation and operation of all services in the EVO. This will include the development of security policies, guidelines and regulations, including a required end user agreement to acknowledge VORTEX-Winds in any publication or other product that results from its use. Guidance will be obtained from the TeraGrid program, including TeraGrid guidelines and user responsibility policies. Proper use of encryption for data files and email will be expected of the EVO community. User authentication, digital certificates, and encrypted connections (e.g., ssl, ssh/scp, vpn's) will be implemented and used where needed. All developers (and users) will be expected to respect intellectual property rights, including software licenses of both open and closed source products. To manage costs, free "player versions" (e.g., the free Mathematica Player) or clones of commercial products (e.g., Scilab, Octave or Rlab in place of Matlab) will be used where appropriate. Legal disclaimers will also be instituted to protect the collaboratory itself whenever its features are used in the context of design.

The entire development team will work toward the goal of ensuring sustainability. Approaches include building a community of volunteers who will maintain documentation, provide end-user support, and participate in annotation of the data. It is hoped that this community will parallel the many successful projects in the open source software and open content communities (e.g., Apache, Wikipedia, etc.), whose “volunteers” are often paid employees of firms, government laboratories, universities, and other organizations who see it in their institutions’ interest to contribute the time of their employees to such collaboratories.

## 8 INITIAL PROJECT TEAM

In order to facilitate early development of the collaboratory, the initial core leadership of the prototype EVO will draw from Notre Dame with active participations from the membership. However, as we build the initial EVO, these leadership positions will be filled based on elections.

The initial membership of the EVO has already been populated by NIST and many of the world’s leading university research centers and laboratories specializing in wind effects on structures, as listed in Table 2, along with a synopsis of the tentative shared resource they will provide: modules and/or contributions to the knowledge base. A select group of end users and stakeholders have also been identified and will help to drive the services and features of the EVO and beta-test the prototype developed. These private sector end users are leading design firms: Skidmore Owings and Merrill LLP (Chicago), Samsung Corporation (Seoul), LERA (New York), Shimizu Corporation (Tokyo), McNamara-Salvia (Boston) and Weidlinger (Los Angeles). The stakeholders include: AAWE, ASCE, AON Corp., IBHS. In addition, an educational end user community has been assembled to evaluate the EVO’s suitability as an academic resource.

## 9 EDUCATION PLAN

While this EVO’s introduction of a Knowledge Base will indirectly serve as an educational tool to countless professional end users, it is equally important that this EVO take an active role in developing formal curriculum tools based on EVO services for use in K-12 and post-secondary education [43]. This is particularly important considering the general shortage of engineers formally educated in wind effects in this country and requires intervention with students as early as possible. As many of the EVO members are also educators (see Table 2), they have already volunteered to use VORTEX-Winds in their course offerings. However, a formal education plan will also be executed at the University of Notre Dame. This will begin with early interactions in the Expanding Your Horizons (EYH) Program, targeting middle school girls and using the visualization tools of VORTEX-Winds to supplement its “Reach for the Sky” building competition. A more substantive use of the EVO services will come from interactions with Clay High School’s AP Calculus students, who will make use of the e-design aids to demonstrate the role of mathematics in predicting response. At the post-secondary level, both the visualization and e-design aids will be integrated into the first module of Notre Dame’s introductory engineering course at the freshman level and revisited in Introduction to Structural Engineering. Additionally, a joint project will be hosted between Civil Engineering and Architecture students using these aids to emphasize the cross-disciplinary nature of modern design. The aerodynamics load databases will also be used in the senior Steel Design project for comparison to ASCE 7 specifications. At the graduate level, the EVO will serve as a vital resource for the Wind Engineering and Structural

Systems courses. Finally, it should be noted that the educational partners will not only be asked to help beta-test the prototype EVO, but also to develop curriculum tools. These will be archived in the Knowledge Base for access by other educators nationwide so that VORTEX-Winds will provide an effective pedagogical tool to teach a highly technical subject, which has its roots in a host of interdisciplinary fields, through the use of cyberspace and visualization capabilities. The Knowledge Base Director will oversee all education and outreach activities and resources.

## 10 DISSEMINATION

In addition to announcing the existence and promoting the availability of VORTEX-Winds at conferences, e.g., Structures Congress or ACWE/ICWE, and in journals within the Structural Engineering and Wind Engineering communities, e.g., *ASCE Journal of Structural Engineering* or *Journal of Wind Engineering and Industrial Aerodynamics*, the leadership will utilize web announcements and email list servers of integral professional organizations like ASCE, IAWE, AAW, JAW, COE/TPU and CTBUH. In parallel, cyberinfrastructure features of the EVO will be described in computing journals such as *IEEE Computer*, *CTWatch Quarterly*, *IEEE Computing in Science and Engineering* and at conferences such as the TeraGrid annual conference and the International Conference on Computational Sciences.

## 11 CONCLUDING RELAMRKS

Despite many advances in the area of wind effects on structures in recent decades, research has been conducted with limited resources scattered physically throughout universities, government, and private research laboratories as well as industry and trade organizations. This has not permitted the community to fully benefit from the collective physical, computational and intellectual resources dedicated to this topic. This paper summarized the vision, scope, goals, objectives and initial accomplishments of a recent project concerning the development of a prototype EVO to meet these needs, entitled, **Virtual Organization for Reducing the Toll of EXtreme Winds (VORTEX-Winds)**. Through a collection of tools and services networked with a flexible architecture and interfaces to support research and education objectives in real-time, VORTEX-Winds promises to enhance the capability of each individual participant beyond their current resources through a synergistic, integrative approach to understanding and modeling the complex wind-structure interactions. The result will be a community as a whole better positioned to address the next frontiers in the field. Accordingly, VORTEX-Winds would serve as an end-to-end system that integrates domestic and international community resources related to wind effects on structures. It would facilitate an effective, transformative, and conveniently accessible venue for the acceleration of advances in research and development, as well as teaching and learning, in this area and would have a revolutionary impact on this field due to its unprecedented dissemination of knowledge and resources.

## 12 ACKNOWLEDGEMENTS

The authors are grateful for the financial support in part by the National Science Foundation via grant CBET 07-42191 and the matching support provided by the University of Notre Dame. Support of the Global Center of Excellence: New Frontiers of Education and Research in Wind Engineering at Tokyo Polytechnic University, Ministry of Education, Culture, Sports, Science and Technology (MEXT), Japan, is gratefully acknowledged. The authors are also thankful to Dr. D-K Kwon, NatHaz Modeling Laborato-

ry, Notre Dame and Mr. Alec Pawling of the Computer Science and Engineering, Notre Dame for their contributions.

### 13 REFERENCES

1. AAWE (2004), "Wind Engineering Research and Outreach Plan to Reduce Losses due to Wind hazards." Report prepared by the American Association for Wind Engineering in Collaboration with American Society of Civil Engineers, February 2004, Revised May 2004, 37 pp.
2. American Society of Civil Engineers (ASCE) (2005). Minimum design loads for buildings and other structures, ASCE 7-05, ASCE, Reston, VA.
3. Becerra-Fernandez, M. Prietula, G. Madey, and D. Rodriguez, "Project Ensayo: a Virtual Emergency Operations Center for Disaster Management Research, Training, and Discovery," in The International Conference on Global Defense and Business Continuity (ICGDBC 2007) San Jose, CA: IEEE, 2007.
4. Bi, A., and Smith, D. A. (2005). "Wall-Area-Averaged Pressure Coefficients Measured in Full-Scale." 10th Americas Conference on Wind Engineering, Baton Rouge, LA.
5. Bienkiewicz, B., Testimony before Committee on Science, U.S. House of Representatives, 108 Congress, 2nd Session, Hearing: "Strengthening Windstorm Hazard Mitigation: An Examination of Public and Private Efforts," February 9, 2004, Serial No. 108-40 [www.house.gov/science].
6. Bienkiewicz, B., M. Endo, J.A. Main, W.P. Fritz (2007) "Comparative inter-laboratory Study of Wind Loading on Low Buildings", extended abstract submitted during Twelfth International Conference on Wind Engineering (ICWE12). Cairns, Australia, July 1-6, 2007.
7. Burton, M., K.C.S. Kwok, P.A. Hitchcock, & R.O. Denoon, (2006) "Frequency dependence of human response to wind-induced building motion," J Str Eng, 132.
8. Butler, K. & Kareem, A., (2007) "Physical and Numerical Modeling of Downburst Generated Gust Fronts," Proceedings of the 12th International Conference on Wind Engineering, Cairns, Australia, July 1-7.
9. Campbell, S., Kwok, K.C.S. and Hitchcock, P.A. (2004) "Full-scale Measurements of Two High-rise Residential Buildings in Hong Kong during a Typhoon", Proceedings of 5<sup>th</sup> International Colloquium on Bluff Body Aerodynamics and Applications, Ottawa, 11-15 July, 2004, pp. 313-316.
10. Chen, X. and Kareem, A. (2003) "New Frontiers in Aerodynamics of Long-span Bridges: An Advanced Analysis Framework," Journal of Wind Engineering and Industrial Aerodynamics, Vol. 91, pp. 1511-1528.
11. Chen, X. and Kareem, A. (2005) "Dynamic Wind Effects on Buildings with 3-D Coupled Modes: Application of HFFB Measurements," Journal of Engineering Mechanics, ASCE, Vol. 131, No. 11.
12. Cheng, C.-M., and Wang, J. (2004). "Wind Tunnel Database for an Intermediate Wind Resistance Design of Tall Buildings." Proc. 1st International Symposium on Wind Effects on Buildings and Urban Environment, Tokyo, Japan.
13. Dalton, "Deep Thoughts," Nature, May 25, 2000, Vol. 405, Issue 6785, pp. 390. [www.earthscope.org]
14. Denoon, R.O., Kwok, K.C.S. and Roberts, R.D. (2001) "The Use of Motion Simulators in the Investigation of Occupant Response to Wind-induced Building Motion", Proceedings of 5th Asia Pacific Conference in Wind Engineering, Kyoto, Journal of Wind Engineering, No. 89, October 2001, pp. 97-100.
15. Fluent 6.3 Documentation, Fluent, Inc. (2006).
16. Gurley, K., F. Masters, D. Prevatt and T. Reinhold. "Hurricane data collection," FCMP deployments during the 2004 Atlantic Hurricane Season, Tenth Americas Conference on Wind Engineering, Baton Rouge, Louisiana, May 31-June 4, 2005.
17. Huang, H., Madey, G., "Building Self-Managing Data Warehouses for Scientific Simulations," in 38th Annual Simulation Symposium San Diego, 2005.
18. Huang, Y., Xiang, X., Madey, G., Cabaniss, S. E., "A Self Manageable Infrastructure for Supporting Web-based Simulations," in 37th Annual Simulation Symposium at the Advanced Simu-

- lation Technologies Conference 2004 (ASTC'04), T. Znati, Karatza, H., Ed. Arlington, VA: Society for Modeling and Simulation International, 2004.
19. Huang, Y., Madey, G., "Autonomic Web-Based Simulation," in 38th Annual Simulation Symposium San Diego, 2005.
  20. Holland, D. and Campbell, M. (2007), "The DOF Wave is Here – Who Can Hang Ten?" *Offshore Engineer*, May 2007, pp. 43-45.
  21. Gao, Y., M. van Antwerp, S. Christley, and G. Madey, "A Research Collaboratory for Open Source Software Research," in Proceedings of the 29th International Conference on Software Engineering + Workshops (ICSE-ICSE Workshops 2007), International Workshop on Emerging Trends in FLOSS Research and Development (FLOSS 2007) Minneapolis, MN, 2007. [[http://zerlot.cse.nd.edu/ICC\(2007\)SMARTcodes](http://zerlot.cse.nd.edu/ICC(2007)SMARTcodes), [www.smartcodes.org](http://www.smartcodes.org)].
  22. ISO (2006) Bases for design of structures - serviceability of buildings and walkways against vibrations, ISO.
  23. Jain, S., and D. A. Smith (2003). "A Comparison of Load Effects on a Frame Using Full and Model Scale Data." 11th International Conference on Wind Engineering, Lubbock, TX.
  24. Kareem, A. (1985) "Structural Performance and Wind Speed-Damage Correlation in Hurricane Alicia," *Journal of Structural Engineering*, ASCE, Vol. 112, No. 12, pp. 2596-2610, December.
  25. Kareem, A. (1986) "Performance of Cladding in Hurricane Alicia," *Journal of Structural Engineering*, ASCE, Vol. 112, No. 12, pp. 2679-2693.
  26. Kareem, A., (1987) "Wind Effects on Structures: A Probabilistic Viewpoint," *Probabilistic Engineering Mechanics*, Vol. 2, No. 4, pp. 166-200, December, 1987.
  27. Kareem, A., and Allen, R. (1990) "Development of Knowledge-Based Systems in Wind Engineering," *Journal of Wind Engineering and Industrial Aerodynamics*, Vol. 36, pp. 1245- 1258, December.
  28. Kareem, A., Kijewski, T. and Tamura, Y. (1999) "Mitigation of Motions of Tall Buildings with Specific Examples of Recent Applications," *Wind and Structures*, Vol. 2, No. 3, pp. 132-184.
  29. Kareem A. (2005) "Bluff Body Aerodynamics and Aeroelasticity: A Wind Effects perspective," Proceedings of the Fourth European & Africa Conference on Wind Engineering, July 11-15, Prague, Czech Republic.
  30. Kijewski-Correa, T., Kareem, A. and Kochly, M. "Experimental Verification and Full-Scale Deployment of Global Positioning Systems to Monitor the Dynamic Response of Tall Buildings," *Journal of Structural Engineering*, ASCE, 132(8), 2006, 1242-1253.
  31. Kijewski-Correa, T., Kilpatrick, J., Kareem, A., Kwon, D.K., Bashor, R., Kochly, M., Young, B.S., Abdelrazaq, A., Galsworthy, J., Isyumov, N., Morrish, D., Sinn, R.C. and Baker, W.F. (2005), "Validating the Wind-Induced Response of Tall Buildings: A Synopsis of the Chicago Full-Scale Monitoring Program," *Journal of Structural Engineering*, ASCE, 132(10), 2006, 1509-1523. [<http://windycity.ce.nd.edu>]
  32. Kwon, D.K., Kijewski-Correa, T. and Kareem, A. (2008), "e-Analysis of High-Rise Buildings Subjected to Wind Loads," *ASCE Journal of Structural Engineering*, in press.
  33. Lorenz, J.G., W.E. Jackson, J.C. Beck, and R. Hanner, "The Problems and Promise of DNA Barcodes for Species Diagnosis of Primate Biomaterials," *Philosophical Transactions of the Royal Society B – Biological Sciences*, October 29, 2005, Vol. 360 (1462), pp. 1869-1877.
  34. Masters, F., K. Gurley, and T. Reinhold. "Ground level wind characteristics of Isidore and Lili", 11th International Conference on Wind Engineering, Lubbock, Texas, June 2-5, 2003.
  35. Main, J.A. and N.P. Jones, (1999) "Full-Scale Measurements of Stay Cable Vibration," Proceedings of the 10th International Conference on Wind Engineering, 2: 963-970.
  36. Madey, G., A.-L. Barabasi, N. V. Chawla, M. Gonzalez, D. Hachen, B. Lantz, A. Pawling, T. Schoenharl, G. Szabo, P. Wang, and P. Yang, "Enhanced Situational Awareness: Application of DDDAS Concepts to Emergency and Disaster Management " in International Conference on Computational Science, Y. Shi, G. D. van Albada, J. Dongarra, and P. M. A. Sloot, Eds. Beijing: Springer, 2007.
  37. Munich Re Group (2005), "Hurricanes-More Intense, More Frequent" Knowledge Engineering Series # 302-04891, Munich, Germany.
  38. Munich Re Group (2006), "Natural Catastrophes 2006: Analysis, Assessments, Positions," Knowledge Series # 302-05217, Munich, Germany.
  39. Naeim, F., Lee, H., Bhatia, H., Hagie, S. and Skliros, K. (2004) "CSMIP Instrumented Building Resposne Analysis and 3-D Visualization System (CSMIP-3DV)," SMIP04 Seminar Proceedings, p. 83-102.
  40. "NSF TeraGrid," *Physics Today*, Oct. 2001, Vol. 54, Issue 10, pp. 31 [[www.teragrid.org](http://www.teragrid.org)].

41. NSTC (2006), "Windstorm Impact Reduction Wind Plan," A Report of the National Science and Technology Council, Executive Office of the President of the United States, April 2006, 29 pp.
42. Sadek, F., and Simiu, E., (2002), "Peak Non-Gaussian Wind Effects for Database-Assisted Low-Rise Building Design," *Journal of Engineering Mechanics*, ASCE, Vol. 128(5), pp. 530-539.
43. Sarkar, P.P. and Mehta, K.C. (1997). "Educational Modules on Wind Engineering," Multimedia CD-ROM, Texas Tech University, August 1997.
44. Sarkar, P.P, F. L. Haan, V. Balaramudu, A. Sengupta, Laborators Simulation of tornado and microburst to assess wind loads on buildings, ASCE 2006 Structures Congress (2006) St. Louis, MO.
45. Satake, N., Suda, K., Arakawa, T. Sasaki, A., and Y. Tamura, "Damping evaluation Using Full-Scale Data of Buildings in Japan," (2003) *Journal of Structural Engineering*, Vol. 129(4), pp. 470-477.
46. Simiu, E. and Scanlan, R.H. (1996) *Wind Effects on Structures*, Wiley Interscience.
47. Simiu, E., Sadek, F., Whalen, T. M., Jang, S., Lu, L.-W., Diniz, S., Grazini, A., and Riley, M. A., (2003), "Achieving Safer and More Economical Buildings through Database-Assisted, Reliability-Based Design for Wind," *Journal of Wind Engineering and Industrial Aerodynamics*, Vol. 91(12-15), pp. 1587-1611.
48. Smith, D. A., Mehta, K. C., Letchford, C., and Zhu, H. (2005) "Testing of Structures Using the Prop-Wash of a C-130 Aircraft." Ninth International Conference on Structural Safety and Reliability, Rome, Italy.
49. Tamura, Y., Matsui, M., Pagnini, L.-C., Ishibashi, R. and Yoshida, A. (2002). "Measurement of wind-induced response of buildings using RTK-GPS." *J. of Wind Eng. & Industrial Aerodynamics*, 90, 1783-1793.
50. Tamura, Y., A. Kareem, G. Solari, K.C.S. Kwok, J.D. Holmes (2005) "Aspects of the dynamic wind-induced response of structures and codification," *Wind and Structures*, Vol.8, No.4, pp.251-268.
51. Van Den Einde, L., Kinderman, T.L., Masuda, M. and Elgamal, A. (2007) "NEES IT Tools to Advance Earthquake Engineering Research," *Proceedings of Structures Congress 2007*, May 17-19, Long Beach, CD-ROM.
52. Whalen, T. M., Sadek, F., and Simiu, E., (2002), "Database-Assisted Design for Wind: Basic Concepts and Software Development," *Journal of Wind Engineering and Industrial Aerodynamics*, Vol. 90(11), pp. 1349-1368.
53. Willoughby, H. and F. Masters. "Early 21st century hurricane threats: maximum potential intensity, the Atlantic multidecadal oscillation, global warming, and chance," Tenth Americas Conference on Wind Engineering, Baton Rouge, Louisiana, May 31-June 4, 2005.
54. WindPerfect – V3.5: 3-Dimensional CFD Analysis Code, Environmental Simulation, Inc. [<http://www.env-simulation.com>]
55. WSJ (2007), "As Insurers Flee Coast, States Face New Threat," *Wall Street Journal*, Front Page Vol. CCXLIX No. 132, June 7, 2007.
56. Xiang, X., Huang, Y., Madey, G., Cabaniss, S.E., "A Web-based Collaboratory for Supporting Environmental Science Research," in Xiang, X. and G. Madey, "Improving the Reuse of Scientific Workflows and Their By-Products," in *Proceedings of the IEEE International Conference on Web Services Salt Lake City: IEEE, 2007*.
57. Xiang, X., Huang, Y., Madey, G., Cabaniss, S.E., G. Madey, and J. Romero-Severson, "A Service-oriented Data Integration and Analysis Environment for In-Silico Experiment and Bioinformatics Research," in *Hawaii International Conference on system Science Kona, HI: ACM, 2007*. [[www.vectorbase.org](http://www.vectorbase.org)]
58. Yu, D. and Kareem, A. (1998) "Parametric Study of Flow Around Rectangular Prisms Using LES," *Journal of Wind Engineering and Industrial Aerodynamics*, Vols. 77-78, pp. 653-662.
59. Zhou, Y., Kijewski, T. and Kareem, A. (2003), "Aerodynamic Loads on Tall Buildings: An Interactive Database," *Journal of Structural Engineering*, ASCE, 129(3): 394-404. [<http://aerodata.ce.nd.edu>]
60. Workshop on Web-based Support Systems at the Joint International Conference on Web Intelligence and Intelligent Agent Technology, J. Yao, T., Yao, Y. Y., Ed. Halifax, Canada: IEEE, 2003, pp. 29-36. [<http://www.nd.edu/~nom/>]
61. Xiang, X., Madey, G., "A Semantic Web Services Enabled Web Portal Architecture," in *IEEE International Conference on Web Services (ICWS 2004) San Diego, 2004*.

62. Xiang, X., Madey, G., Huang, Y., Cabaniss, S.E., "Web Portal and Markup Language for Collaborative Environmental Research," in *Environmental Online Communication*, A. Scharl, Ed. London: Springer, 2004, pp. 113-126.

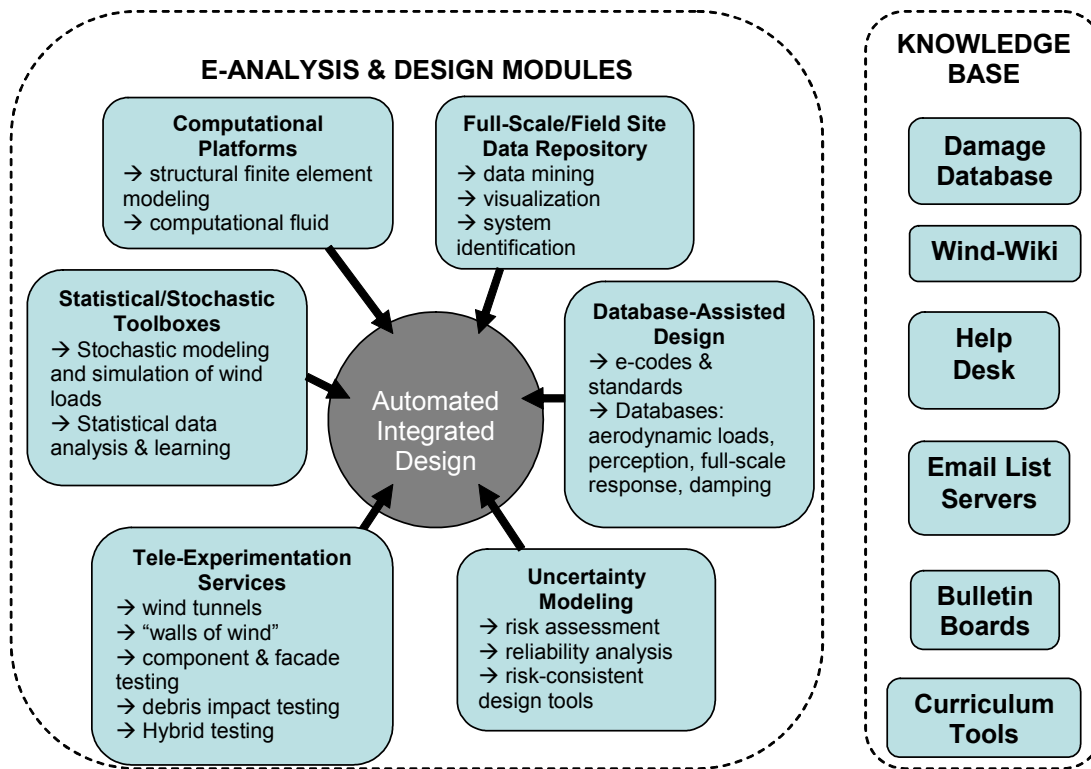


Figure 1. Schematic of VORTEX-Winds Capabilities.

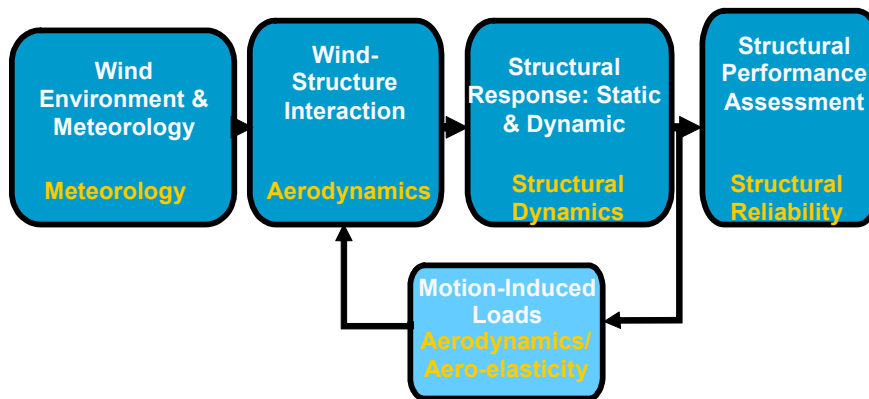


Figure 2. Schematic of Analysis and Design Processes for Wind.

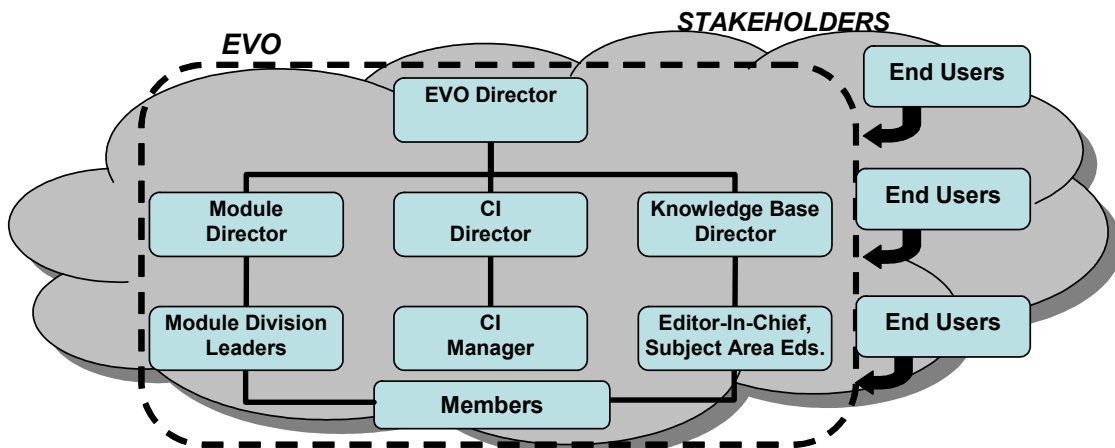


Figure 3. VORTEX-Winds Organizational Structure.

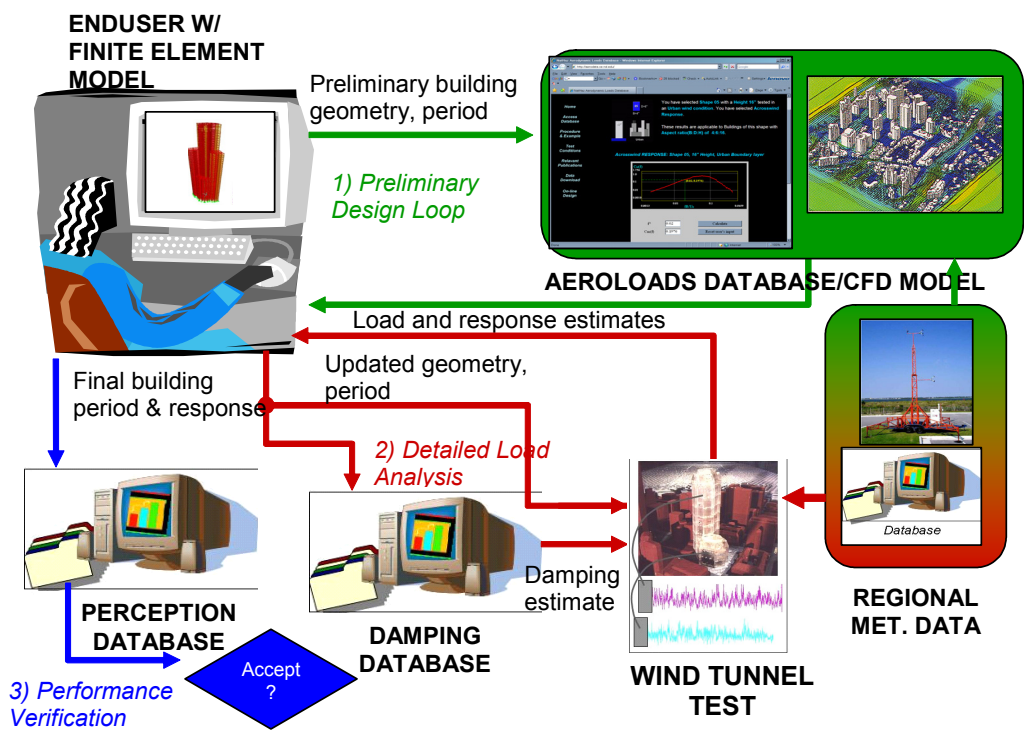


Figure 4. Schematic of Integrated Analysis and Design Concept.

Table 1. Initial Prototype Project Schedule by Quarters.

TASKS	DEVELOPMENT PHASE				DEPLOYED PROTOTYPE			
	4/07	1/08	2/08	3/08	4/08	1/09	2/09	3/09
1. Collaboratory Development	█	█	█	█	█	█	█	█
2. Module Formatting	█	█	█	█	█	█	█	█
3. CI Development	█	█	█	█	█	█	█	█
4. Beta Testing	█	█	█	█	█	█	█	█
5. Knowledge Base Design	█	█	█	█	█	█	█	█
6. Knowledge Base Population	█	█	█	█	█	█	█	█
7. Assessment and Redesign	█	█	█	█	█	█	█	█
K-12 Outreach and Education	█	█	█	█	█	█	█	█

Table 2. Initial EVO Membership and Their Potential Contributions.

	Databases/e-Design Aids	Gust, Tornado Simulator	Large-Scale Wind Simulator	CFD Platform	Real-Time Met. Data	Full-Scale Monitoring	Wind Tunnel Facility	Education
Univ. of Notre Dame	✓	✓		✓		✓	✓	✓
Univ. of Florida			✓		✓	✓		✓
Colorado State Univ.				✓			✓	✓
Iowa State Univ.		✓		✓			✓	✓
Texas Tech Univ.					✓	✓	✓	✓
Johns Hopkins Univ.						✓	✓	✓
Hong Kong UST						✓	✓	✓
Tokyo Polytechnic Univ.	✓	✓		✓	✓	✓	✓	✓
Tamkang Univ., Taipei	✓			✓		✓	✓	✓
Univ. of West. Ontario	✓		✓	✓		✓	✓	✓
Tongji Univ., Shanghai	✓			✓		✓	✓	✓
IIT Roorke, India	✓					✓		✓
Univer. of Genoa, Italy	✓				✓	✓	✓	✓
NIST	✓			✓				



# Numerical simulation of wind effects: A probabilistic perspective

Ahsan Kareem\*

*NatHaz Modeling Laboratory, University of Notre Dame, Notre Dame, IN 46556, USA*

Available online 28 April 2008

---

## Abstract

Numerical simulations of wind loads and their effects are critical in the design of structures to ensure their safety under winds. The simulations range from generation of time histories of wind velocity, pressure and force fluctuations to structural response and assessment of attendant functionality and safety under service and design loads, respectively. Typically these schemes employ Monte Carlo-based approaches that encompass model-based simulations or information derived from observed data. The scope of simulations spans uni-variate to multi-variate processes; uni-dimensional to multi-dimensional fields; Gaussian to non-Gaussian; stationary to non-stationary; conditional and unconditional cases. In order to accomplish these tasks, methods based on the time, frequency, or time–frequency domains are employed. This paper summarizes a historical perspective, recent developments and future challenges. Also included in the discussion are computational tools employed for data analysis, response analysis and its management, and prediction. Examples are presented to illustrate some of the topics discussed.

© 2008 Elsevier Ltd. All rights reserved.

*Keywords:* Monte Carlo; Simulation; Stationary; Gaussian; Non-Gaussian; Non-stationary; Transient events, time, frequency, and time–frequency domains

---

## 1. Introduction

Simulation of wind-related processes is essential for time-domain analysis of structures under wind loads, e.g., long-span bridges, offshore structures, or tall buildings. Besides numerical analysis, digitally simulated data is also needed to drive computer controlled test

---

\*Tel.: +1 574 631 6648; fax: +1 574 631 9236.

*E-mail address:* [kareem@nd.edu](mailto:kareem@nd.edu)

facilities involving any type of setup, e.g., multiple fans or controlled damping systems for mitigation of motion. Typically these simulations are based on models describing the process to be simulated, which may be an exact theoretical model, phenomenological or empirical model or observed data. These schemes can be broadly categorized into two classes: (1) methods based on the summation of trigonometric functions (wave superposition); (2) methods based on convolution of white noise with a kernel function or integration of a differential equation driven by white noise (digital filtering). These techniques vary in their applicability, complexity, computer storage requirements and computing time.

Some of the key issues involving simulations surface from the need to simulate: a very large number of points such as along the span of a long span bridge, which requires appropriate modeling and inclusion of imperfect correlation of the random processes/fields; modulations in both time and frequency in the case of transient wind field of a downburst; non-Gaussian features observed in the pressure fluctuations under separated flow regions; conditional simulation of data in the presence of a limited measurements, or loss of measured data. In some cases, it may become important to include all these features in a single simulation. Hurricanes passage is a potential example of this since extreme, imperfectly correlated, non-Gaussian loads impinge on structures and where limited observations be available.

Initially, the simulation techniques focused on the generation of uni-variate and one-dimensional processes. The simulation of processes more than single variate, or dimension, was first addressed by [Borgman \(1969\)](#), [Shinozuka \(1971\)](#) and [Shinozuka and Jan \(1972\)](#).

The simulation schemes are characterized as: conditional or unconditional; Gaussian or non-Gaussian; stationary/homogenous or non-stationary/non-homogeneous; univariate/uni-dimensional; multi-variate/multi-dimensional. The conditional simulations, or stochastic interpolation schemes, can be used to simulate, or interpolate, data in between measured locations. These schemes are discussed in the following sections.

## **2. Wave superposition (spectral)-based schemes**

### *2.1. Spectral representation approach*

One of the traditional approaches for simulation is to utilize a superposition of trigonometric functions with random phase angles, which has been the most popular, perhaps due to its simplicity ([Shinozuka, 1971](#)). Using large numbers of terms in the summation, the contiguous target energy spectrum is approximated by its discrete form. The Gaussianity of the simulated data is established by virtue of the Central Limit Theorem. The process, in principle, is applicable to multi-variate/multi-dimensional processes/fields. However, this approach for a large number of variates becomes computationally very inefficient. In this context, the summation of trigonometric functions may be carried out by utilizing a fast Fourier transform (FFT). The use of FFT improves the computational efficiency drastically, but not without the expense of increased demand on computer storage. The level of difficulty increases significantly for the simulations that involve long-duration multi-variate or multi-dimensional processes ([Samaras et al., 1985](#)). Significant progress has been made over the last several decades in the simulation of uni- and multi-variate, uni- and multi-dimensional, conditional and unconditional processes based on wave superposition schemes ([Shinozuka and Deodatis, 1991](#); [Shinozuka et al.,](#)

1990; Li and Kareem, 1991, 1993, 1995; Grigoriu, 1993; Mann, 1999; Chen and Kareem, 2005, Carassale and Solari, 2006).

The Cholesky decomposition of the cross power spectral density matrix (XPSD) has been widely utilized in digital simulation of multi-variate and dimensional schemes (Shinozuka and Jan, 1972). Li and Kareem (1989, 1993, 1995) introduced the concept of “stochastic decomposition” of the XPSD matrix for the simulation of stationary random processes, which was further extended to the simulation of non-stationary processes (Li and Kareem, 1991, 1997). Central to the stochastic decomposition is the decomposition of a correlated vector-valued random process into a set of vector-valued subprocesses, such that any two component processes from the same subprocess are statistically fully coherent, while any two component processes from different subprocesses are non-coherent. Therefore, the simulation of the parent process is simplified by the simulation of non-coherent subprocesses. The Schur decomposition is often more attractive than the Cholesky decomposition as the former permits a relatively small number of modes to be utilized in the simulation (Shinozuka et al., 1990; Di Paolo and Gullo, 2001; Li and Kareem, 1993). Similar gains are also possible with Cholesky decomposition through truncation of terms (Li and Kareem, 1995).

Regardless of the attractiveness of the FFT approach, concerns remain regarding the limitations imposed on the large number of simulation locations and the length of the time-series dictated by the computer memory available as noted in Samaras et al. (1985) and Li and Kareem (1993) and recently Chen and Kareem (2002). To address this shortcoming, Li and Kareem (1993) introduced a numerical simulation scheme that combines the advantages of the wave superposition techniques and digital filtering to simulate continuous long-duration multi-variate random processes. This approach offers the simple convenience of conventional FFT-based schemes; however, it does not suffer from the drawbacks of the required large computer memory that, in the past, has precluded the generation of long-duration time-series utilizing FFT. Central to this approach is a simulation of a large number of time-series segments by utilizing the FFT algorithm, which are subsequently synthesized by means of a digital filter to provide the desired duration of simulated processes. It offers computational efficiency, convenience, and robustness. This scheme has immediate applications to the simulation of real-time processes. Other measures are possible to reduce the computational effort for a large number of simulation locations, e.g., ignoring of higher modes in the case of Schur decomposition and reducing the order in the case of Cholesky decomposition. Additionally, decomposition at limited frequency locations and larger time steps may also reduce computational effort with subsequent interpolations. In order to facilitate the use of stochastic simulation in the design office, the NatHaz Modeling Laboratory has developed a web-based simulation portal, which would allow simulation of multi-variate Gaussian random processes with prescribed spectral characteristics. An example of the portal is give in Fig. 1, which is available at <http://windsim.ce.nd.edu/> (Kwon et al., 2005).

### 3. Digital filtering (time-series approach)-based schemes

#### 3.1. Parametric time-series methods

The digital filtering based schemes offer efficient methods of simulating random processes. Typical schemes are: autoregressive (AR), moving average (MA), and their



### NatHaz on-line wind generation : Interface

**User Inputs :** Please select options and fill out input values. [On-line Unit Converter](#)

Please select the unit of input values (default : Metric)  
 If user would like to see English unit output, please select checkbox (default : Metric)

Metric(SI) unit [m, m/s]    
  English unit [ft, mph]    
  Output : English unit

Generation points, i.e., Heights (z)  
 (Acceptable formats : Delimited by comma(,) or Matlab-compatible, e.g., 4,8,12 or 4:4:12)

z [m, ft] :

Number of sampling points (N), cut-off frequency ( $f_c$ )

N :       $f_c$  [Hz] :

Exposure Category (A,B,C,D based on ASCE 7-98) (EC),  
 3-second basic wind speed ( $U_{10}$ ) from ASCE 7-98 (Fig. 6-1)

A    
  B    
  C    
  D    
  $U_{10}$  [m/s, mph] :

For fluctuating wind force calculation (If leave blank, the force will not be calculated)  
 Air density ( $\rho_A$ ), Drag force coefficient ( $C_D$ ), Width of structure (B) - same format with Height (z)  
 (At this time, the area will be assumed as rectangular shape)

$\rho_A$  [kg/m<sup>3</sup>, lb/ft<sup>3</sup>] :     
 $C_D$  :     
 B [m, ft] :

Wind generation methods [Theoretical background \[PDF\]](#)

Cholesky decomposition with discrete frequency function and FFT  
 Schur decomposition with polynomial approximation and AR(Autoregressive) model  
 Cholesky decomposition with SRM(Spectral Representation Method) and FFT

Fig. 1. NatHaz internet simulation portal (<http://windsim.ce.nd.edu/>).

combination autoregressive and moving averages (ARMA) (Samaras et al., 1985; Mignolet and Spanos, 1992; Li and Kareem, 1989, 1990, 1991, 1993; Carassale, 2005). The ARMA representation entails weighted recursive relations that connect the random quantity being simulated at successive time increments. Unlike the FFT-based approaches, this scheme does not demand large computer memory; rather, only a limited amount of information (e.g., coefficient matrices) is stored and long-duration time series may be simulated at successive time increments. The matching of an ARMA model for certain applications may not be very straightforward, especially for those processes with filtered white noise as a spectral description. In lieu of this difficulty in selecting suitable model order, Aas-jakobson and Strommen (2001) decided to use a spectral approach (Chen and Kareem, 2002b). The estimation of optimal model parameters is also sensitive to the time increment selected (Mignolet and Spanos, 1992; Li and Kareem, 1990, 1993).

Based on the system's dynamic characteristics, the time-integration schemes require that the time increment should not exceed a prescribed value. This concern has been noted even in a recent study by Chay et al. (2006) dealing with the response of structures to downbursts where they resorted to linear interpolation, which introduces its own shortcomings. In order to efficiently simulate realizations of wind loads at the prescribed time increments, Li and Kareem (1990) offered two approaches. The first involved an

ARMA algorithm based on a three-stage-matching method and the other was based on a scheme, which combines ARMA and a digital interpolation filter. This topic has been revisited by Wang (2007) and offered an improved interpolation filter and demonstrated the shortcoming of the linear interpolation often used in practice.

The digital filtering approached can be directly implemented for multi-variate and dimensional processes/fields or they can be used in conjunction with a decomposition approach, Cholesky or Schur, in which the component processes are simulated as univariate processes. In Li and Kareem (1990), the dynamic response of structural systems to a variety of random excitations using recursive models was presented. The methodology permitted analysis of stationary, non-stationary, or transient response of structures under stochastic multi-input correlated processes, e.g., wind loads. For non-stationary or transient excitation, the analysis involved a direct computation of the output covariance from a given non-stationary correlation structure of the input. The concept of the ARMA system was also addressed in which the ARMA representation of the response was obtained in terms of the ARMA description of the stationary excitation. The usefulness of the recursive approach was also highlighted for nonlinear systems.

The time-series approach also offers many useful recipes for numerical evaluations of commonly used operations. For example, discrete convolution models can be employed for linear transformation of a given time history, discrete differentiation models for obtaining derivatives, and discrete interpolation models for interpolating time-series intermediate time increments and their hybrid combination (Li and Kareem, 1993). In a hybrid model, combined attractive features of the discrete convolution and differentiation models can be realized. This type of scheme is very effective in evaluating structural response with a displacement feedback, e.g., the response of a large floating platform exposed to ocean waves and winds which requires that the loads be formulated at the instantaneous displaced position of the platform (Li and Kareem, 1993).

### 3.2. State space modeling

In most modern control and dynamics studies, the state space is the format of choice. In this format, a state space model of the loading is needed which is augmented to the structural state space representation for the overall dynamic response analysis. Due to a large number of correlated wind-related processes with prescribed spectral characteristics, researchers have had difficulty in finding a state space model for wind (Gossman and Waller, 1983; Kareem, 1999). Models for special applications have been tailored to meet problem-focused needs. One such approach involves a combination of stochastic decomposition and AR models to formulate a state space representation of wind effects (Kareem and Mei, 2000). The XPSD matrix of wind-related process is decomposed utilizing Proper Orthogonal Decomposition (POD). Each component process is then modeled as an AR model, which is subsequently expressed in terms of state space format. By stacking these component models, the overall model for the entire system can be obtained in a straightforward manner. Details are available in Kareem and Mei (2000).

One of the most elegant applications of the state space model has recently presented in Chen and Kareem (2001) that addresses aeroelastic analysis of bridges under multi-correlated winds. An integrated state space model of a system with a vector-valued white noise input is presented to describe the dynamic response of bridges under the action of multi-correlated winds (Fig. 2). Such a unified model has not been developed before due to

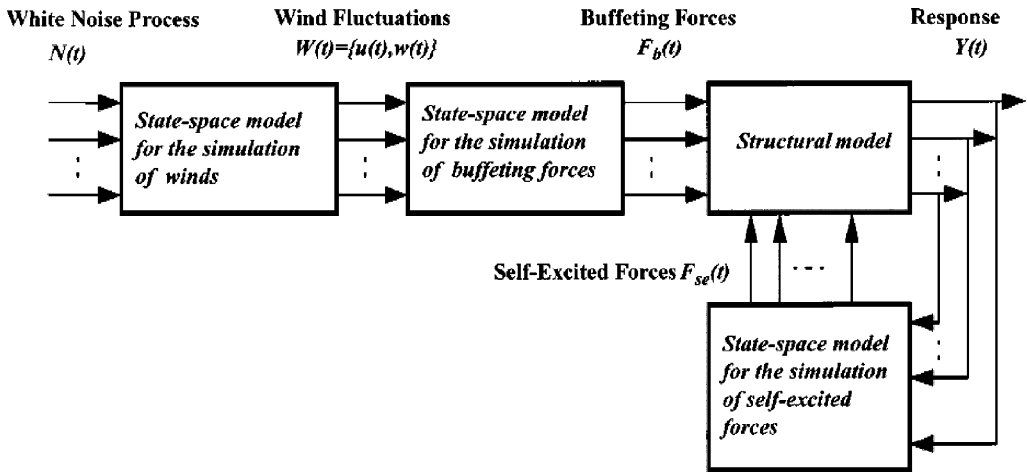


Fig. 2. Integrated modeling of dynamic response of wind-excited structures (Chen and Kareem, 2005).

a number of innate modeling difficulties. The integrated state space approach is realized based on the state space models of multi-correlated wind fluctuations, unsteady buffeting and self-excited aerodynamic forces, and bridge dynamics. Both the equations of motion at the full order in the physical coordinates and at the reduced-order in the generalized modal coordinates are presented. The state space model allows direct evaluation of the covariance matrix of the response using the Lyapunov equation, which presents higher computational efficiency than conventional spectral analysis approach. This state space model also adds time-domain simulation of multi-correlated wind fluctuations, the associated unsteady frequency-dependent aerodynamic forces and the attendant motion of the structure. It is important to note that frequency dependence of buffeting forces are maintained, unlike most time-domain bridge aerodynamic studies which employ instead a straightforward quasi-steady approach. The structural and aerodynamic coupling effects among structural modes, which are critical for the multi-modal response of bridges, can be easily included in the analysis. The model also permits consideration of various nonlinearities, of both structural and aerodynamic origins, in the response analysis. Fig. 3 shows an example simulation of wind fluctuations, buffeting, self-excited forces and bridge response.

#### 4. Simulation of inflow conditions

Inflow conditions are important for developing large eddy simulation (LES) scheme for modeling the flow around an isolated structure or a group of buildings. In earlier studies, smooth uniform inflow conditions were introduced and combined with periodic boundary conditions to avoid difficulties associated with inflow and outflow conditions. For direct comparison with experimental results, it is highly desirable to perform simulations with inflow conditions, which are comparable to those employed in experiments. One such approach is to utilize stochastic simulations of homogenous turbulence by statistical methods like those discussed here and in the preceding sections. Kondo et al. (1997) utilized the wave superposition approach in conjunction with FFT to simulate velocity

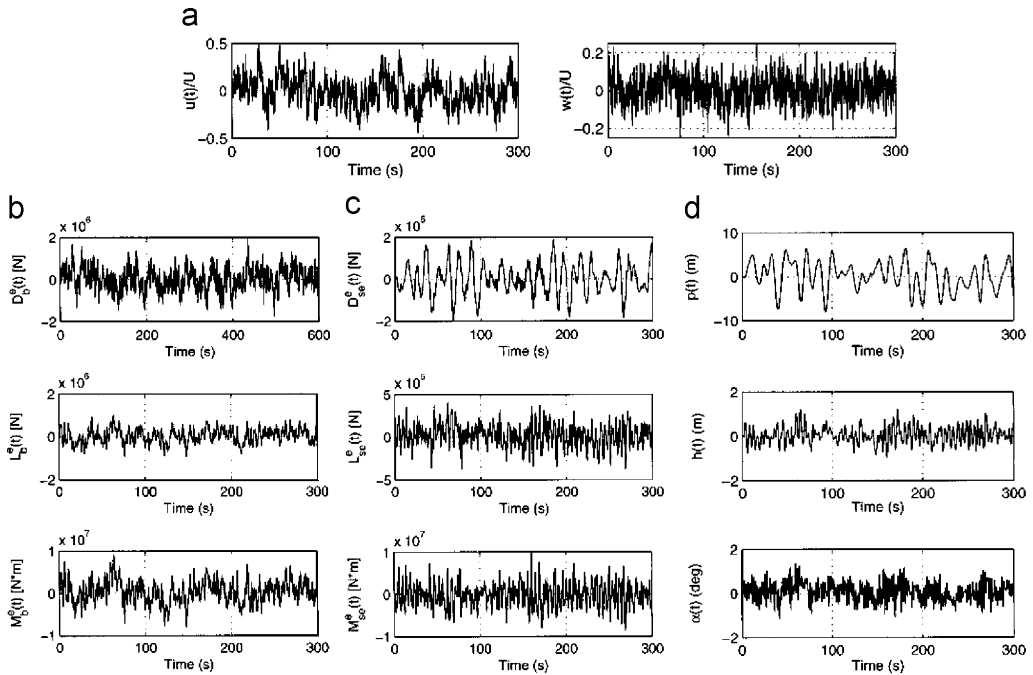


Fig. 3. Simulation of wind fluctuations, buffeting and self-excited forces, and bridge response ( $U = 60$  m/s, at midpoint of main span): (a) wind fluctuations, (b) buffeting forces, (c) self-excited forces, (d) bridge response (Chen and Kareem, 2001).

fluctuations for the LES scheme, which were then used by Tamura and Ono (2003) to study the influence of turbulence on the aerodynamics of prisms. One of the issues for these simulations is to ensure that the flow is divergence free, which may require an iterative approach and should also consider the decay of turbulence as the flow moves into the computational domain. The addition of a boundary layer profile combined with turbulent fluctuations adds more complexity. More realistic inflow conditions can be simulated by generating flow over rectangular blocks whose size is adjusted based on the built conditions. This flow is then imposed on the computational domain for estimation of wind effects (Tamura et al., 2002). Other approaches deal with conditional simulations, which are based on utilizing measurements of inflow turbulence in the wind tunnel and then conditionally simulating flow at all grid points as discussed in the section on conditional simulations.

## 5. Non-stationary/non-homogenous processes

The statistical description of severe wind events changes over the duration of the storm. The wind speed and turbulence intensity of hurricane and thunderstorm winds are in a constant flux as the storm passes over a fixed location. Wind models that account for this evolutionary behavior at multiple scales are just beginning to be realized. Non-stationarity has been particularly a difficult phenomenon to capture. Not only do the load statistics

change with time and frequency, but the direction in which these loads impinge structures also changes, thus further complicating the load and performance assessment process.

Non-stationarity in wind-storms stems from a number of origins, i.e., time-varying mean, time-varying variance and frequency-dependent changes in variance. Typically, the time-varying mean has been treated as a trend in the signal and, once removed, the remaining process is treated as stationary if other sources of non-stationarity are not present. The next level of non-stationarity stems from the time-varying amplitude of the signal (amplitude modulation (AM)) which introduces time-varying variance to fluctuations in wind. Further complications result from frequency modulations (FM) in which the variance varies with frequency contents. Finally, there are cases in which both AM and FM features are present.

Most simulations of the non-stationary processes have evolved around the generation of ground motion records known to be highly non-stationary. Following the introduction of the concept of evolutionary power spectrum (Priestly, 1965), a variety of non-stationary stochastic models have been adopted to generate non-stationary ground motion records including the modulated filtered Poisson process (Shinozuka and Sato, 1967; Amin and Ang, 1968), the modulated stationary process (Iyengar and Iyengar, 1969) and filtered modulated stationary process (Levy et al., 1971). The development of non-stationary time-series models like AR, MA and ARMA has evolved over the years for the simulation of ground motion records (Cakmak et al., 1985; Deodatis and Shinozuka, 1988). Despite the computational expediency, the time series-based models for non-stationary processes may not be straightforward due to the elusive definition of the time-varying correlation and spectral function combined with the difficulty associated with the selection of the model order.

Li and Kareem (1991) introduced for the first time an FFT based simulation scheme for multi-variate non-stationary processes. The utilization of FFT was made possible through the application of the stochastic decomposition advanced by the author and discussed earlier in this paper. A decomposed spectral matrix was expanded into a weighted summation of basic functions and time-dependent weights that are simulated by the FFT based algorithm. The effectiveness of the proposed technique was demonstrated using ground motion records that could be separated into time- and frequency-dependent components as well as for those in which both AM and FM modulations are present.

The addition of both AM and FM adds considerable complexity and temporal variation in frequency contents that can have a significant effect on structural response, especially in the inelastic range for earthquakes. This has made it critical to capture the transient features of both amplitude and frequency associated with earthquake, and potentially for wind, in order to make reliable predictions of structural response under extreme conditions.

In order to better model the temporal variations of frequency, estimates of evolutionary power spectral density have been made by decomposing a signal at various bands of frequencies using multiple band filtering (Kameda, 1975; Sherer et al., 1982; Der Kiureghian and Crempien, 1989). This can be viewed as the beginning of time-frequency analysis and modeling of transient signals. Further additions to this approach have been made based on short-time multiple window spectrum estimators in Conte and Peng (1997). These models have provided a sought out path for better modeling of temporal variations in both amplitude and frequency. Later, with the introduction of wavelets as a time-frequency analysis framework, researchers have explored it for the simulation of

non-stationary processes (Gurley and Kareem, 1999). Empirical mode decomposition offers an alternate to wavelet-based techniques, which has its advantages and shortcoming in comparison with the wavelet transform-based approaches (Kijewski-Correa and Kareem, 2006).

Non-stationary analysis of wind-excited structures has been rather limited. Recently, interest in this area has developed in the aftermath of increasing damage to structures in extreme winds induced by tornados, thunderstorms winds and downbursts/microburst and hurricanes. The significance of transient wind events and their load effects can be readily surmised from an analysis of thunderstorm databases both in the US and around the world, which suggest that these winds of gusts associated with convective gust-fronts differ significantly from conventional turbulence both in its kinematics and dynamics, e.g., their contrasting velocity profile and their transient nature. Accordingly, one should question the appropriateness of using design based on conventional representation of the design wind speed for many locations. It is important to note that the mechanics with gusts associated with these transient events differ significantly from conventional turbulence both in its kinematics and dynamics, i.e., their contrasting velocity profile and their transient nature. Further, extreme loads on structures are potentially sensitive to the influence of transient flows, i.e., the load coefficients may be enhanced based on the gust form and the resulting localized, rapid changes in the surrounding flow. In addition, the characteristics of these flow structures suggest that the resultant load effects are likely to be correlated over larger areas than in conventional flows. These aerodynamic consequences clearly point at the prospect of higher loads on structures than would be predicted by the present codes and standards, calling for a careful examination of these procedures.

The recognition of the significance of wind loading on structures during the passage of thunderstorms has prompted research aimed at modeling and simulation of the downburst wind field based on measurements. However, the non-uniformity and non-stationarity of the wind field in downbursts in both time and space have posed challenges in their modeling and simulation. Wang and Kareem (2004, 2005) have examined the evolutionary behavior of measured records of a thunderstorm outflow winds in a time-frequency framework involving the Wavelet and the Hilbert transforms. An efficient simulation model has been proposed on the basis that the instantaneous frequency of wind fluctuations at various frequency bands follows the Gaussian distribution. Without invoking any assumption associated with parametric models, this approach helps to characterize and simulate thunderstorm downburst winds based on a single sample measurement. Analytical expressions for the statistical properties of the underlying random processes are formulated. Examples concerning the simulation of actual full-scale downburst wind data are presented to demonstrate the efficacy of the proposed simulation that captures the evolutionary characteristics of measured data and preserves the correlation between measurements at different locations. In Fig. 4, a sample of measured, time-varying mean and simulated records are presented (Wang and Kareem, 2005). Verification of time histories with measured data was demonstrated by means of their time/frequency characteristics, e.g., co-scalograms.

Alternative models for downburst type winds have been obtained using a commercial software packages, e.g., FLUENT (Kim et al., 2005; Chay et al., 2006), and based on amplitude-modulated processes, which capture the time-varying mean utilizing wavelet shrinkage and amplitude-modulated fluctuations based on a separable time and frequency features (Chen and Letchford, 2005, 2005a). Other attempts have relied on the use of

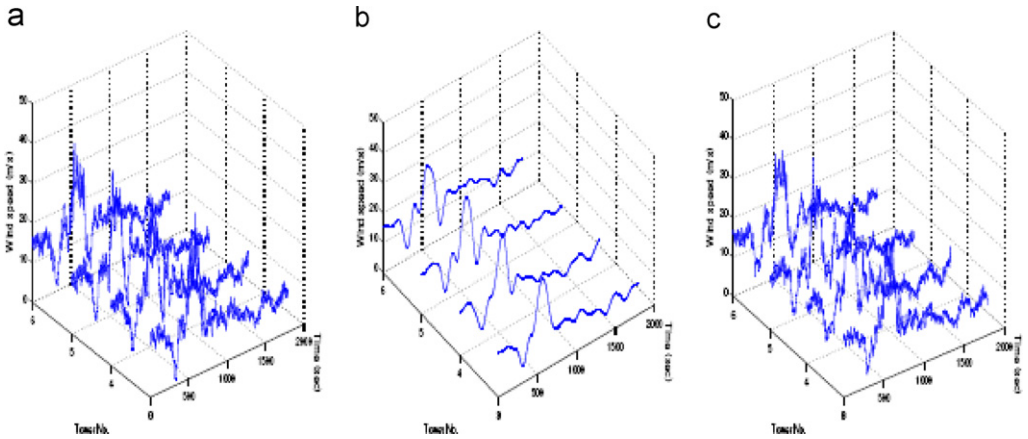


Fig. 4. Example simulation of full-scale downburst winds (Wang and Kareem, 2005). (a) Measurement; (b) time-dependent-mean; (c) simulations.

time-varying ARMA models for the simulation of non-stationary features of downburst type winds (Chay et al., 2006). Similar type of models have been advanced for capturing the non-stationary features of hurricanes (Wang and Kareem, 2005; Xu and Chen, 2004).

## 6. Non-Gaussian simulation

Significant progress has been made over the last decade in the modeling and simulation of Gaussian scalar, multi-variate and multi-dimensional conditional or unconditional random processes, but work in the area of non-Gaussian processes has been rather elusive (Yamazaki and Shinozuka, 1988; Grigoriu, 1984, 1998). The most commonly used approach to the simulation of non-Gaussian processes is based on the static transformation that relates the underlying Gaussian process to the non-Gaussian process being simulated. This approach does not have any memory, whereas schemes based on transformations with memory retain this feature, but there is very limited progress in this direction.

### 6.1. Static transformation schemes

Early work based on correlation distortion has been based on an inverse mapping of the desired probability density function, a summary of which may be found in Gurley et al. (1996). In Gurley and Kareem (1997), a simulation approach which is significantly more robust than the correlation distortion schemes was presented. The non-Gaussian features and the frequency contents in the form of the first four moments and the target power spectral density of the process were used; alternatively, analytical expressions or other estimates of the distribution may be employed. The approach is named the “spectral correction method” and it relies on a few iterations to match both the spectral and probabilistic features.

Fig. 5 shows an example of a simulation run based on a measured time history of a highly skewed full-scale pressure measurement. Also included are the probability density function (PDF) and power spectral density function (PSD) of the target and the simulated

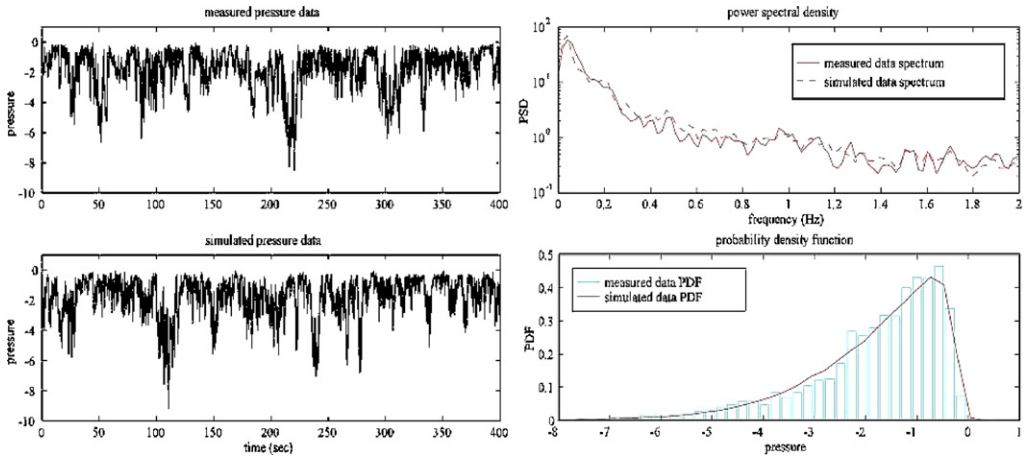


Fig. 5. Measured and simulated pressure time histories (left); comparison of PSD and PDF of simulated and measured time histories (right) (after Gurley et al., 1997).

records which show good agreement. Additional follow-up work in this broad framework can be found in Grigoriu (1998), Deodatis and Micaletti (2001) and Masters and Gurley (2003). This approach has been extended to multi-variate processes, including conditional simulations and random fields (Gurley and Kareem, 1998, 1998a; Gurley et al., 2001).

## 6.2. Transformation schemes with memory

Inasmuch as the preceding memoryless techniques are based on static transformations, they may fail to encapsulate any memory that may be present in the target signals. A Volterra series-based scheme offers an alternative that ensures preservation of memory. The Volterra based models in the frequency domain lend themselves to the simulation of non-Gaussian wind-related processes for which the Volterra kernels are available or estimated (Gurley et al., 1997; Kareem et al., 1998). The challenge remains in that the development of Volterra kernels needed for such simulation may not always be available (Gurley and Kareem, 1997).

## 6.3. Other approaches

A class of single point non-Gaussian processes, e.g., pressure fluctuations at a location, can also be simulated through manipulation of the phase (Seong and Peterka, 1998). Gurley et al. (1996) utilized Neural networks to simulate non-Gaussian pressure time histories and demonstrated that due to the static nature of the approach, the simulated time history did not reflect the memory in the process as evidenced by the lack of good comparison with the target bi-spectra and the bi-spectra of the simulated record using Volterra kernel of Neural networks (Gurley et al., 1996, 1997).

Future challenges in this area lie in the simulation of large vectors of data, which may be used in a design database, and in simulations that preserve memory inherent to the process. In the former case some space reduction techniques combined with linear stochastic

estimation may be invoked to accomplish the task of simulating very large correlated data sets.

## 7. Conditional simulations

### 7.1. Gaussian processes

Simulation of random velocity and pressure time series at un-instrumented locations conditioned on the measured records are often needed in evaluating wind-related studies. For example, malfunctioning instruments may leave a hole in a data set or information may be lacking due to limited number of sensors. The concept is similar to conditional sampling in experiments or numerical simulations. Fundamentally, two approaches have been introduced and the simulation is either based on linear estimation or kriging, or on a conditional probability density function (Krige, 1966; Borgman, 1990; Kameda and Morikawa, 1992). These approaches, being equivalent for uni-variate uni-dimensional processes (Shinozuka and Zhang, 1996), permit generation of time histories at new locations when one or more time series for the full length interval are available, and extension of existing records beyond the sampling time for cases where conditioning time series is limited to small subintervals. Gurley et al. (1997) have utilized the conditional probability density function approach to simulate one of the measured velocity records based on the availability of the other three on a full-scale tower. Fig. 6 shows these records including the conditionally simulated. The comparison of the co-spectra between the simulated and measured records and the power spectral density, though not shown here for brevity, provides good agreement. In Fig. 7(a), measured record up to 2500 s shown in the top figure is assumed to be only available up to 980 s, indicated by the darkened portion of the record. The remaining record from 980–2500 s is simulated, as shown in lighter color in the bottom figure, based on the information derived from the first 980 s of data. Both examples demonstrate the effectiveness and utility of conditional simulation of Gaussian processes. An interesting application of this approach has been noted in developing inflow

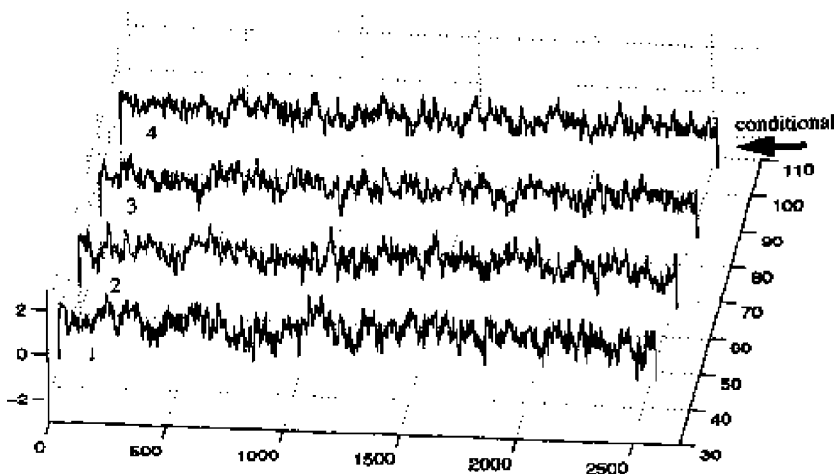


Fig. 6. Example of conditionally simulated time history (Gurley et al., 1997).

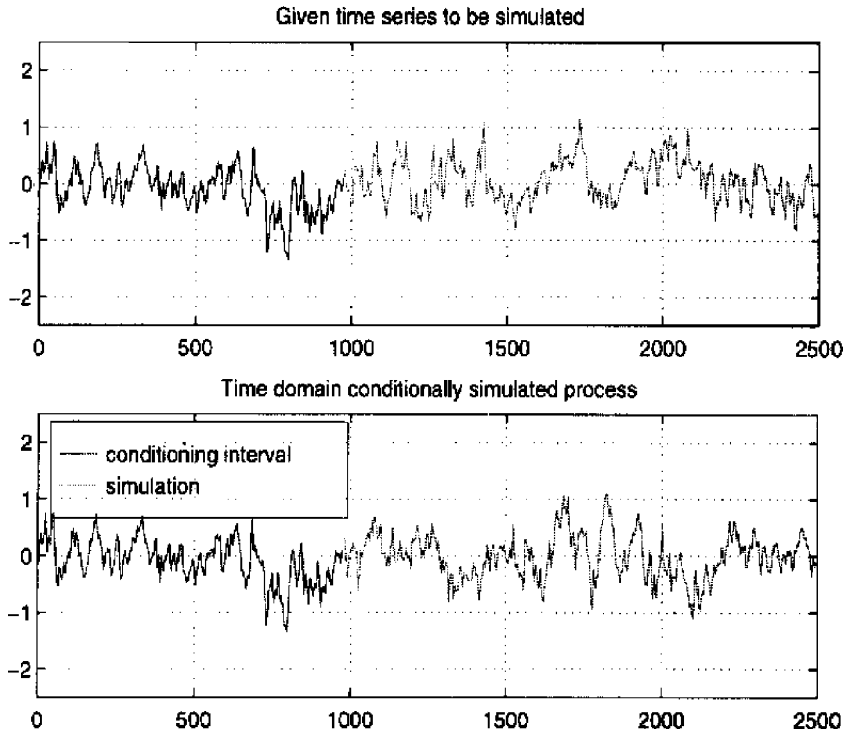


Fig. 7. Example of a simulated time history record (Gurley et al., 1997).

conditions for a computational fluid dynamics study in which measured turbulence at limited locations was expanded to the entire grid through conditional simulation (Maruyama and Morikawa, 1995).

Similar schemes are possible using linear stochastic estimation (LSE) in which conditional information at reference points are used to estimate information over the entire flow domain (Adrian, 1994). In this approach, estimated values of the flow field at points conditioned on measurements at reference locations and time are expressed in terms of the Taylor's series expansion. By minimizing the mean quadratic error, involving cross-correlation, and retaining the first-order terms, desired estimates are obtained. Essentially, LSE estimates a random variable as a linear combination of some known reference variables. LSE has the ability to reconstruct the entire random field by using a few reference variables in conjunction with attendant correlations. This approach can also help to couple experiments with CFD in which the experimental time histories, measured at limited locations, are interfaced with the inlet section of a time-varying numerical simulation of a spatially developing flow (Delville et al., 2000). Applications in wind engineering have been explored in Chen et al. (2003) in which LSE was utilized to reconstruct wind-induced pressure time series from the covariance matrix for structural load analyses on a low building roof. It is noted that this approach helps to reduce data storage for large scale databases, where one may reconstruct data based on stored covariance matrices and few reference measured pressures. It should be noted that the

authors were unable to faithfully reproduce individual time series, but the integrated effect of several time histories resulting in a panel load were successfully replaced. This difficulty in matching individual time history may have resulted from the non-Gaussian nature of the data.

## 7.2. Non-Gaussian processes

The preceding discussion was based on conditional simulations of Gaussian variates. Here, this concept is extended to non-Gaussian cases often experienced in wind engineering concerning pressure fluctuations in separated flow regions or velocity fluctuations in extreme atmospheric flow conditions. A non-Gaussian conditional simulation given in Elishakoff et al. (1994) addressed problems related to wide-band processes. In Gurley and Kareem (1998), a multi-variate non-Gaussian simulation based on a spectral correction scheme was extended to conditional simulation utilizing the conditional probability density function approach which is applicable to both narrow- and wide-banded processes. Details of the simulation scheme are available in Gurley and Kareem (1998). An example of the conditional simulation given in Gurley and Kareem (1998) involves pressure fluctuations given at three locations and at the fourth location the results we simulated. The left side of Fig. 8 shows the three records and the simulated fourth record. The right side of the figure shows the target and measured coherence between locations 1 and 4, 2 and 4, and 3 and 4. The top far right in Fig. 8 is a comparison of the PDF of the missing record and its replacement. This example and another dealing with extension of a single non-Gaussian pressure record, not shown here, demonstrates that the conditional simulation scheme presented in Gurley and Kareem (1998) ensures excellent agreement between the target and simulated marginal distribution and spectral descriptions. Similar to the conditional

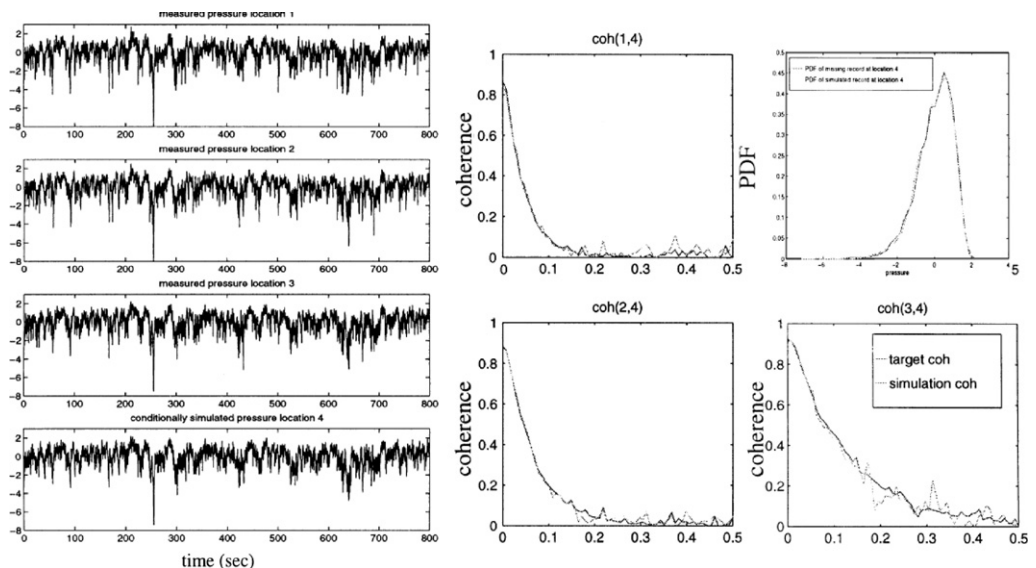


Fig. 8. Example of a simulated signal for a non-Gaussian process (Gurley and Kareem, 1998).

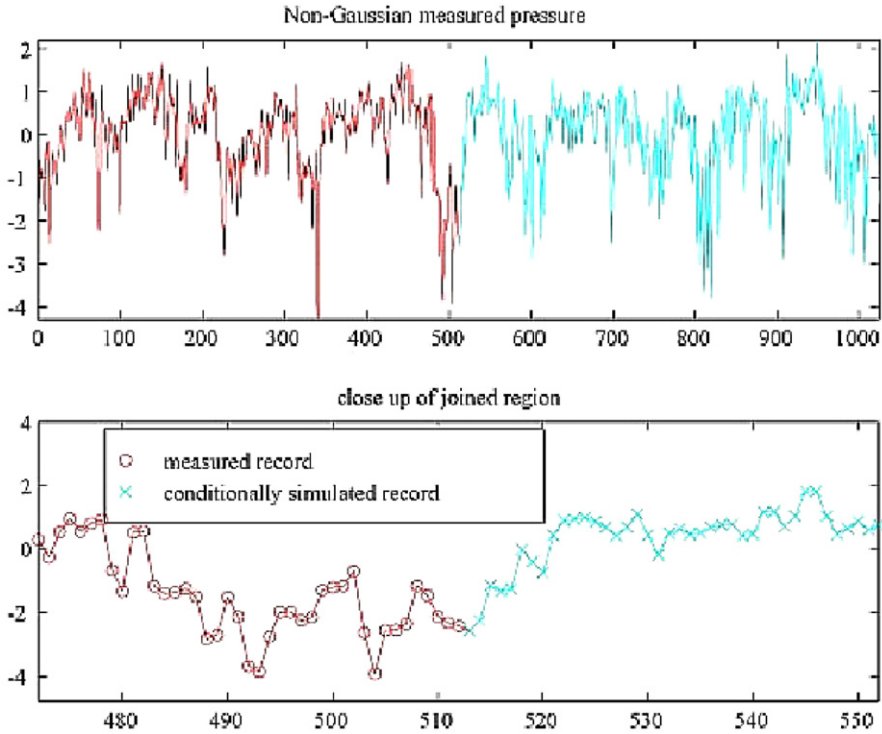


Fig. 9. Example of extended data record and close-up of extension region (Gurley and Kareem, 1998).

simulation in Fig. 7, extension of a missing record is shown in Fig. 9, with a close-up of the transition from measured to simulated data location, in the bottom figure, to illustrate continuity.

### 7.3. Non-stationary processes

In the previous two sections, discussion was focused on the conditional simulation of Gaussian and non-Gaussian vector-valued processes, which is extended to non-stationary vector-valued processes. Application of the conditional simulation of ground motion records marked by non-stationary behavior are available in the literature (Vanmarcke and Fenton, 1991; Hoshiya, 1995; Shinozuka and Zhang, 1996; Kameda and Morikawa, 1992; Heredia-Zavoni and Santa-Cruz, 2000). These techniques are based on Kriging, conditional probability density function or their combination. Wang (2007) invoked the time–frequency framework to the conditional simulation of non-stationary processes. This scheme utilizes evolutionary cross-correlation in terms of cross wavelet coefficients, which extends the application of Kriging method to time–frequency domain. A numerical example of the conditional simulation of downburst wind velocities was presented to demonstrate the efficacy of the proposed scheme. This scheme has been extended to conditionally simulate non-Gaussian and non-stationary processes.

## 8. Computational modeling tools

### 8.1. Proper orthogonal decomposition

Multicorrelated stationary random processes/fields, such as wind velocity and pressure fluctuations, on structures can be transformed into a set of subprocesses by diagonalizing their covariance or cross power spectral density (XPSD) matrices through either the Cholesky (lower or upper triangular) or Schur (eigenvector) decomposition. The eigenvector decomposition offers physically meaningful insight into the process as each eigenvector (eigenmodes) may be characterized on the basis of its spatial distribution. It is also recognized that only a small number of eigenmodes corresponding to eigenvalues with larger magnitudes are dominant, such that one may ignore some of the eigenmodes associated with small eigenvalues in the description of a large-size random field. Accordingly, this technique provides a unique tool for data compression and facilitates a reduced-order modeling of large-size random fields. The eigenvector decomposition is theoretically based on the Karhunen–Loeve expansion, which is also known as the proper orthogonal decomposition (POD) (Loeve, 1963).

The POD technique based on the covariance matrix has been widely used in many fields, such as fluid mechanics, image processing, signal analysis, data compression, and others. A comprehensive review on the subject is available in Solari et al. (2005). Lumley (1970) and Armit (1968) introduced this technique to address turbulence and wind-related problems, respectively, and it was later used by many researchers in describing pressure fluctuations on buildings and structures and a host of wind-related problems (Lee, 1975; Kareem and Cermak, 1984; Holmes et al., 1997; Kareem, 1999; Tamura et al., 1999; Carassale et al., 2001). In stochastic structural mechanics, the POD technique based on the covariance matrix has been utilized for the simulation of spatially varying correlated random variables (Yamazaki and Shinozuka, 1990), stochastic finite element analysis (Ghanem and Spanos, 1991), and stochastic dynamics (Li and Kareem, 1989, 1995; Vasta and Schueller, 2000).

The numerical advantage of the POD technique, akin to the modal analysis in structural dynamics, relies on the reduced-order representation through truncation of the higher eigenmodes associated with small eigenvalues. This reduced-order representation, of course, must warrant that the important characteristics of the random field and related quantities remain unchanged, or the modification resulting from the approximate representation is acceptable. Several studies on the covariance matrix-based POD technique have demonstrated that truncating higher wind loading modes helps to expedite computations of global wind loads and their effects, (Tamura et al., 1999; Chen and Kareem, 2006). However, truncation of higher modes may not work effectively in the case of local response, which may lead to an underestimation of the local wind loads and their effects (Chen and Kareem, 2005).

### 8.2. Time-frequency representation and system identification

Like many physical processes of interest, wind effects manifest non-stationary and nonlinear features and their complete characterization may not be accomplished via Fourier transforms, necessitating a new analysis framework in the time-frequency domain. The dual nature of wavelet transforms, being a simultaneous transform in time and

frequency, justifies its recent extension to the analysis of interest to civil engineering, adapting the transform to a number of situations where Fourier transforms (for frequency domain analysis) or Hilbert transforms (for time-domain system identification) were traditionally used to define quantities of interest. When considering the time and frequency information in tandem, wavelets can be used to determine the times and frequencies at which signal energy content is strongest through examination of scalograms and co-scalograms (Gurley et al., 1997; Gurley and Kareem, 1999; Kareem and Kijewski, 2002). Fig. 10 displays a co-scalogram comparison for full-scale pressure measured on a building and the two upstream wind velocity records: the first record monitored simultaneously as the pressure time history under consideration and the second from a different wind event. The left column in Fig. 10 shows the scalogram and co-scalograms of wind pressure and the first wind velocity that are knowingly correlated. Note the pockets of white beyond 250 s revealing time-varying pockets of correlation in different frequency bands. This may be compared to a similar analysis for wind pressure and velocity that are known to be uncorrelated, for which no marked white pockets, indicative of correlation, are present (right column in Fig. 10). The presence of subtle light pockets, indicative of spurious

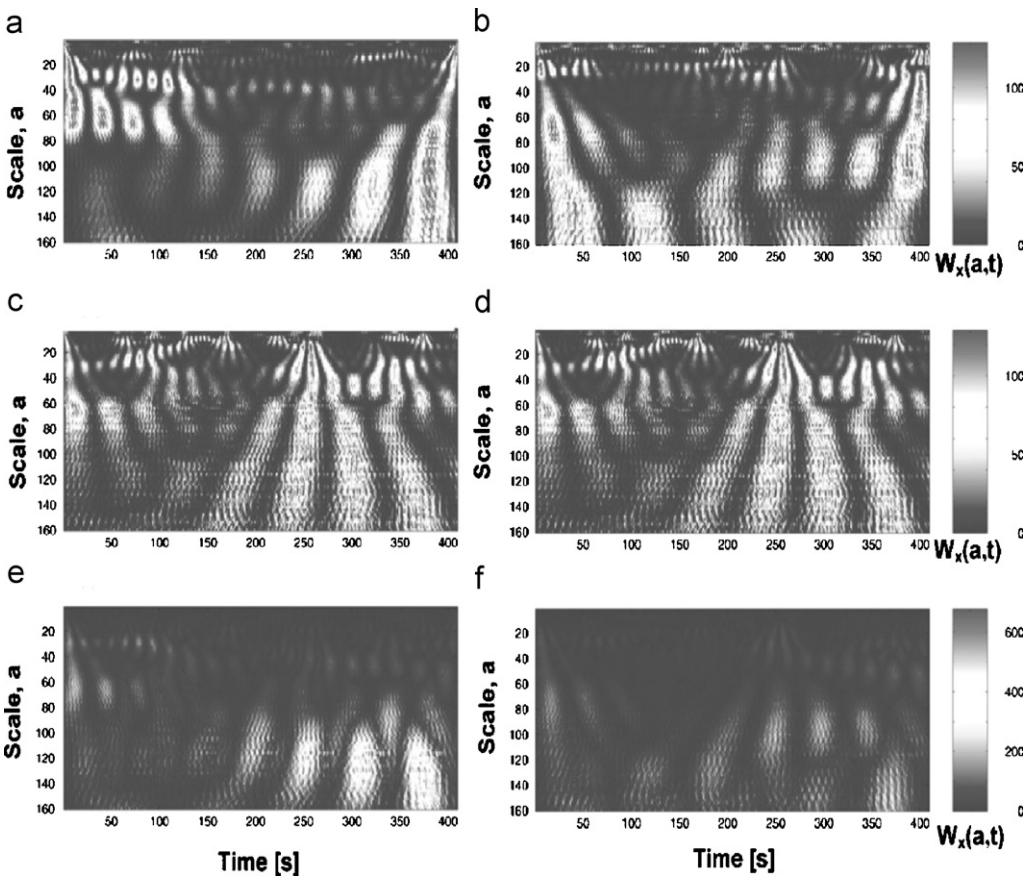


Fig. 10. Example wavelet scalograms and co-scalograms of wind pressure (Kareem and Kijewski, 2002).

correlation, present in both the correlated and uncorrelated examples in Fig. 10 is due to lack of ensemble averaging (Kareem and Kijewski, 2002).

More specific insights into the linear and quadratic interplay between two signals in both time and frequency can be gained utilizing wavelet coherence and bi-coherence measures (Gurley et al., 2003). However, by exploiting the dual potential of wavelets, other analysis based primarily in either the time or frequency domain can also be performed. By tracking the variation of wavelet transform coefficients in the time domain, system identification can be readily performed (Kijewski and Kareem, 2003). Similarly, the distribution of wavelet coefficients with frequency at a window in time provides a familiar spectral representation whose evolutionary properties can be monitored to provide insights into nonlinear behavior (Kareem and Kijewski, 2002).

Recently, in order to capture intermittent correlation, a wavelet coherence measure was introduced to produce a time-frequency display of the coherence between signals intermittently correlated, e.g., pressure and velocity fluctuations (Kareem and Kijewski, 2002; Gurley et al., 2003). In this study, the analysis developed for first-order correlation detection was further extended to higher-order correlation through a bi-coherence measure, as some of the processes under investigation may not have been linearly related, e.g., wind velocity fluctuations and associated pressure fluctuations. Detailed examples given in (Kareem and Kijewski, 2002; Kijewski and Kareem, 2003) affirm that the wavelet-based technique is capable of identifying both first- and second-order correlation while effectively reducing the presence of noise in both simulated and measured data. The robustness of the provided thresholding techniques is further established, as it is shown to alleviate the presence of spurious coherence, even in cases where variance and leakage are prevalent. Though relatively intensive, this approach facilitates the removal of significant levels of all of the various contributing noise sources.

Wavelet-based system identification and instantaneous spectral analysis offer very valuable tools that permit the tracking of nonlinear characteristics in structural frequency and damping. Such tracking of time-varying frequency content is typically accomplished by monitoring the instantaneous frequency of the signal and extracting ridges from wavelet scalograms to form the wavelet instantaneous frequency spectra discussed in (Kareem and Kijewski, 2002; Kijewski and Kareem, 2003). The complex coefficients associated with these ridges can be used directly in a traditional system identification approach based on analytic signal theory to identify the instantaneous frequency, and in the case of free vibration decay or random decrement signatures, damping. Frequency domain perspectives from the wavelet coefficients are also insightful, as the wavelet instantaneous frequency and bandwidth can be respectively tracked to monitor the mean frequency and its deviation as they evolve in time. This basic analysis framework coupled with analysis schemes like SVD and PCA would help to facilitate delineation of aerodynamic, aeroelastic or structural parameters.

## 9. Time-domain analysis of structures

### 9.1. Time-domain approach for coupled flutter

The prediction of wind-induced buffeting response and flutter instability is of major concern in the design of long span bridges. The analytical approach has predominantly been conducted in the frequency domain. This is primarily due to computational efficiency

offered by the frequency domain, particularly when handling the unsteady forces that are functions of frequency. The flutter analysis is generally conducted by complex eigenvalue analysis, whereas the buffeting response analysis is typically handled using a mode-by-mode approach that ignores the aerodynamic coupling among modes (Chen and Kareem, 2002a). More recently, a coupled multi-mode flutter analysis framework has been introduced (Chen et al., 2000). This has led to a convenient transformation of the equations into a frequency independent state space format. A significant feature of this approach is that an iterative solution for determining flutter conditions is unnecessary because the equations of motion are independent of frequency. In general, the frequency domain approach is restricted to linear structures excited by the stationary winds without aerodynamic or structural non-linearities.

One of the challenges in aeroelastic analysis remains in the modeling of aerodynamic forces that take into consideration non-linearities in both structural dynamics and aerodynamics and the ubiquitous issues related to turbulence (Chen and Kareem, 2003, 2003a). Traditional analysis approaches are not suitable for accommodating these computational challenges. To include nonlinearities of structural and aerodynamic origins, the time-domain approach is more appropriate (Chen et al., 2000 and the references cited). Most of the studies concerning the buffeting response have used the quasi-steady theory for modeling the aerodynamic forces, thus ignoring the frequency-dependent characteristics of unsteady aerodynamic forces in the numerical scheme, potentially impacting the accuracy of the response estimates.

Time-domain approaches also require input time histories of multi-dimensional multi-variate wind fields, which can be simulated as discussed in earlier sections on simulation. In Chen et al. (2000, 2000a), a comprehensive treatment of the time-domain simulation of aerodynamic response of bridges was reported. Unsteady aerodynamic forces are expressed in terms of the convolution integrals involving the aerodynamic impulse functions and the structural motions or wind fluctuations. Subsequently, the aerodynamic impulse functions and the associated aerodynamic transfer functions (i.e., the flutter derivatives, admittance function and spanwise coherence) are approximated in terms of rational functions. A detailed parameter study was conducted in which the response of a bridge was modeled with and without modal coupling and the use of the quasi-steady aerodynamic force formulation for comparison with frequency-dependent functions. For the case when buffeting forces are modeled by the quasi-steady theory, the forces are overestimated and hence the response is conservative. However, when the self-excited forces are also modeled by the quasi-steady theory, as most of the time-domain simulations have been, the aerodynamic damping will be overestimated and this leads to an underestimation of the response. For further details please refer the cited papers.

## 9.2. *Nonlinear aerodynamic response of bridges*

Innovative aerodynamic tailoring of deck sections and advanced aeroelastic analysis frameworks are fundamental to the cost-effective design of bridges with increasing complexity and span. Recent experiences have clearly demonstrated that traditional truss and box sections cannot be extended economically to longer spans. Further, the innovative sections with attractive aerodynamic performance, meant to take the place of more traditional sections, tend to exhibit aerodynamic nonlinearities. This situation is complicated by the fact that there is no conclusive evidence concerning the stabilizing or

destabilizing effects of turbulence on the aerodynamics of bridges. While current analytical methods have proven their utility for past and current designs, their inability to fully analyze bridges with innovative sections and long spans, which are characterized by aerodynamic nonlinearities, turbulence effects and the spanwise coherence of aerodynamic forces, limits the utility of state-of-the-art analysis procedures, thus requiring a comprehensive nonlinear analysis framework. The design of future, longer spans will require a multi-mode, coupled framework for flutter and buffeting analysis, which can accommodate the effects of turbulence, aerodynamic and structural nonlinearities, as discussed later in this section. Certainly, these analytical tools must be complemented by extensive wind tunnel and full-scale testing.

For many innovative bridge sections, even at low levels of turbulence, the effective angle of incidence due to structural motion and incoming wind fluctuations may vary to a level such that the nonlinearities in the aerodynamic forces may no longer be neglected. Wind tunnel studies using full-bridge, aeroelastic models have often shown flutter onset velocity boundaries to be sharply defined in smooth flows, whereas it exhibits rather gradual flutter boundaries in turbulent flows. A recent experimental study supports the full correlation of self-excited forces tacitly assumed in most current analytical approaches (Haan et al., 1999, 2000). This implies that the turbulence-induced changes in flutter instability of bridges cannot be explained entirely due to a decrease in the coherence of self-excited forces, as suggested in Scanlan (1997). Therefore, one may conclude that current linear force models have proven their utility for a number of practical applications; however, these fail to completely address the challenges posed by aerodynamic nonlinearities and turbulence effects. Diana et al. (1999) proposed a nonlinear aerodynamic force model based on the so-called “Quasi-static corrected theory,” which led them to analytically investigate the turbulence effects on flutter and buffeting response. This nonlinear force model attempted to incorporate frequency-dependent characteristics by decomposing the total response into components with different frequencies. A recent study utilizing an active turbulence generator, demonstrated the validity of the approach in modeling bridge response to incoming turbulence (Diana et al., 2005).

An advanced nonlinear aerodynamic force model and attendant analysis framework has been presented by Chen and Kareem (2003, 2003a) that focused on the needs for modeling of aerodynamic nonlinearity and effects of turbulence on long span bridges. The nonlinear force model separates the forces into the low- and high-frequency components in accordance with the effective angle of incidence corresponding to the frequencies lower than and higher than a critical frequency, e.g., the lowest natural frequency of the bridge. The low-frequency force component can be modeled based on the quasi-steady theory due to its reduced velocity, while the high-frequency force component is separated into self-excited and buffeting components which are modeled in terms of the frequency-dependent unsteady aerodynamic characteristics at the low-frequency spatiotemporally varying effective angle of incidence. The nonlinear analysis framework is summarized in Fig. 11 along with the conventional linear scheme. Within this framework, the effects of the low-frequency component of turbulence on flutter and buffeting responses can be analytically investigated. The effects of turbulence on flutter are modeled through the changes in the effective angle of incidence caused by turbulence and its influence on the self-excited forces and the flutter instability.

The application of this framework to a long-span suspension bridge, with aerodynamic characteristics sensitive to the angle of incidence, revealed a gradual growth in response

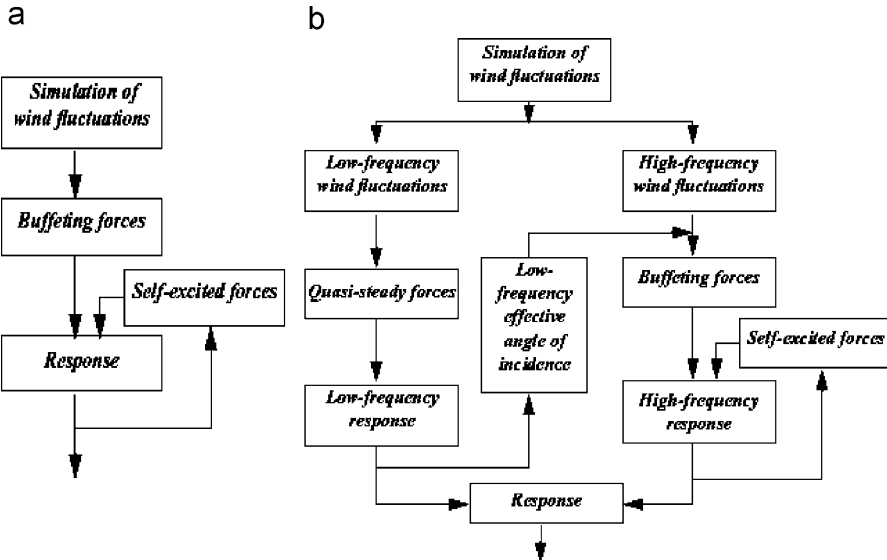


Fig. 11. (a) Traditional and (b) nonlinear aeroelastic analysis framework (Chen and Kareem, 2003, 2003a).

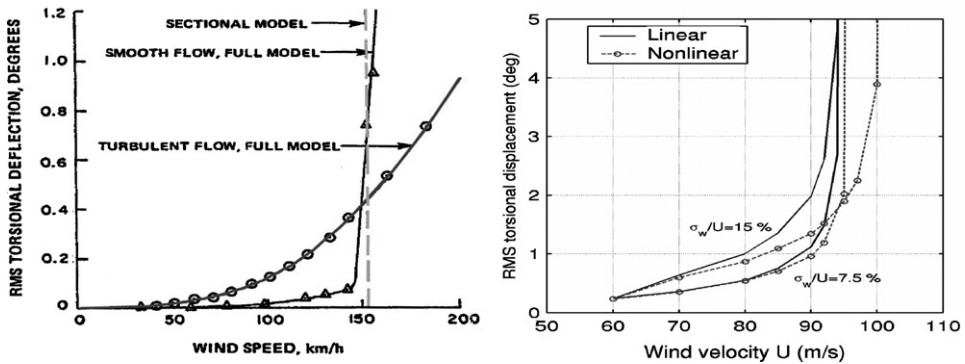


Fig. 12. (Top) Torsional response of Lions’ Gate Bridge (Irwin, 1977); (bottom) linear and nonlinear predicted response of a bridge (Chen and Kareem, 2003, 2003a).

with increasing wind velocity around the flutter onset velocity, which is similar to the wind tunnel observations of full-bridge, aeroelastic models in turbulent flows (Fig. 12). This suggests that the effects of turbulence on the flutter of full-bridges may in part be attributed to aerodynamic nonlinearities, i.e., nonlinearities in the self-excited forces.

9.3. Time-domain response of buildings

Wind loads and the associated response of buildings have primarily been examined utilizing the high-frequency base balance (HFBB) (Chen and Kareem, 2005; Zhou et al., 2003). The wind-tunnel-based aerodynamic load data are utilized in conjunction with the building’s computational model to estimate building response, which is then couched in a

directional statistical description in terms of probability of exceedence of wind speed to arrive at the building's performance analysis for service and strength limit states. Typically these computations are done in the frequency domain due to its expediency. One can utilize the spectral description of aerodynamic loads derived from the HFBB and simulate a mode generalized time history of the corresponding load if it becomes necessary to use the time-domain approach due to consideration of any nonlinear load effects. Additionally, multi-point synchronous measurements of pressure, which upon weighting with the tributary area of the respective tap, results in the overall integral loads as a function of time which can be interfaced with the appropriate structural model to derive time histories of response. The pressure approach offers more flexibility in terms of buildings with nonlinear mode shapes, and the complexity of model building these days can be avoided through computer controlled lithographic machines to construct complex model configurations with embedded pressure taps. Regardless, the HFBB has the advantage of permitting fast turn around in examining different external geometries at nominal cost for detuning the building shape to avoid adverse loading on the building, e.g., a case study reported in Abdelrazak et al. (2005).

## 10. Concluding remarks

This paper outlines developments in computational stochastic modeling of wind load effects beginning with some historical perspectives and discussing recent developments, improvements and challenges. The topics discussed include simulation of random processes that range from multi-variate to multi-dimensional cases involving Gaussian, non-Gaussian, stationary, non-stationary, conditional and unconditional. These tools are becoming increasingly important in the analysis of wind-excited structures that are exposed to a wide range of loads with attendant dynamic effects. Also discussed are customary time and frequency domain approaches and the emerging time-frequency analysis framework particularly important for non-stationary and non-homogenous processes/fields. Applications of these computational techniques to the analysis of buildings and bridges are highlighted, including the role of stochastic simulation in providing inflow conditions for a computational wind engineering studies.

## Acknowledgments

The support of the work reported has been made possible in part by the recent NSF Grants CMS03–24331, CMMI 06–01143 and CMMI 07–42191 and earlier grants including many other sponsors over the years. The author is indebted to the contributions of his former students and post-doctoral fellows on the subject of this paper. Without their contributions this would not have been possible. Kyle Butler and Rachel Bashor, current graduate students, are thanked for their assistance in the preparation of this manuscript.

## References

- Aas-jakobson, K., Strommen, 2001. Time domain buffeting response calculations of slender structures. *J. Wind Eng. Ind. Aerodyn.* 89, 341–364.

- Abdelrazak, A.K., Kijewski-Correa, T., Song, Y.-H., Case, P., Isyumov, N., Kareem, A., 2005. Design and full-scale monitoring of the tallest building in Korea: Tower palace III. In: Proceedings of the Sixth Asia-Pacific Conference on Wind Engineering.
- Adrian, R.J., 1994. Stochastic estimation of conditional structure: a review. *Appl. Sci. Res.* 53, 291–303.
- Amin, M., Ang, A.H.S., 1968. Nonstationary stochastic model of earthquake motions. *J. Eng. Mech. ASCE* 94 (2), 559–583.
- Armitt, J., 1968. Eigenvector analysis of pressure fluctuations on the west instrumented cooling tower. Internal Rep. RD/L/N114/68, Central Electricity Research Laboratories, UK.
- Borgman, L.E., 1969. Ocean wave simulation for engineering design. *J. Waterways Harbor Div. ASCE*, 557–583.
- Borgman, L.E., 1990. Irregular waves: kinematics and force. The sea, Prentice Hall, Englewood Cliffs, NJ.
- Cakmak, A.S., Sherit, R.I., Ellis, G., 1985. Modeling earthquake ground motions in California using parametric time series methods. *Soil Dyn. Earthquake Eng.* 4 (3), 124–131.
- Carassale, L., 2005. POD-based filters for the representation of random loads on structures. *Probab. Eng. Mech.* 20, 263–280.
- Carassale, L., Solari, G., 2006. Monte Carlo simulation of wind velocity fields on complex structures. *J. Wind Eng. Ind. Aerodyn.* 94, 323–339.
- Carassale, L., Piccardo, G., Solari, G., 2001. Double modal transformation and wind engineering applications. *J. Eng. Mech. ASCE* 127 (5), 432–439.
- Chay, M.T., Albermani, F., Wilson, R., 2006. Numerical and analytical simulation of downburst wind loads. *Eng. Struct.* 28, 240–254.
- Chen, X., Kareem, A., 2001. Aeroelastic analysis of bridges under multi-correlated winds: integrated state-space approach. *J. Eng. Mech. ASCE* 127 (11).
- Chen, X., Kareem, A., 2002. Advances in modeling of aerodynamic forces on bridge decks. *J. Eng. Mech. ASCE* 128 (11), 1193–1205.
- Chen, X., Kareem, A., 2002a. Advanced analysis of coupled buffeting response of bridges: a complex model decomposition approach. *Prob. Eng. Mech.* 17 (2), 201–213.
- Chen, X., Kareem, A., 2002b. Discussion on time domain buffeting response calculations of slender structures by K. Aas-Jakobson and E. Strommen. *J. Wind Eng. Ind. Aerodyn.* 90, 639–642.
- Chen, X., Kareem, A., 2003. New frontiers in aerodynamic tailoring of long span bridges: an advanced analysis framework. *J. Wind Eng. Ind. Aerodyn.* 91, 1511–1528.
- Chen, X., Kareem, A., 2003a. Aeroelastic analysis of bridges: turbulence effects and aerodynamic nonlinearities. *ASCE J. Eng. Mech.* 129 (8).
- Chen, X., Kareem, A., 2005. POD based modeling, analysis and simulation of dynamic loads. *J. Eng. Mech. ASCE* 131 (4), 325–339.
- Chen, X., Kareem, A., 2006. Revisiting multimodal coupled bridge flutter: some new insights. *ASCE J. Eng. Mech.* 132 (10), 1115–1123.
- Chen, L., Letchford, C.W., 2005. Proper orthogonal decomposition of two vertical profiles of full-scale nonstationary downburst wind speed. *J. Wind Eng. Ind. Aerodyn.* 93 (3), 187–216.
- Chen, L., Letchford, C.W., 2005a. Simulation of extreme winds from thunderstorm downbursts. In: Proceedings of the 10th Americas Conference on Wind Engineering. Baton Rouge.
- Chen, X., Matsumoto, M., Kareem, A., 2000. Time domain flutter and buffeting response analysis of bridges. *J. Eng. Mech. ASCE* 126, 7–16.
- Chen, X., Matsumoto, M., Kareem, A., 2000a. Aerodynamic coupling effects on flutter and buffeting of bridges. *J. Eng. Mech. ASCE* 126, 17–26.
- Chen, Y., Kopp, G.A., Surry, D., 2003. The use of linear stochastic estimation for the reduction of data in the NIST aerodynamic database. *Wind Struct.* 6 (2), 107–126.
- Conte, J.P., Peng, B.F., 1997. Fully nonstationary analytical earthquake ground-motion model. *J. Eng. Mech.* 123 (1), 15–24.
- Delville, J., Lamballais, E., Bonnet, J.-P., 2000. POD, LODS and LSE: their links to control and simulations of mixing layers. *ERCOFTAC Bull.* 46.
- Deodatis, G., Shinozuka, M., 1988. Auto-regressive models for non-stationary stochastic processes. *J. Eng. Mech. ASCE* 114 (11), 1995–2012.
- Deodatis, G., Micaletti, R.C., 2001. Simulation of highly skewed non-Gaussian stochastic processes. *J. Eng. Mech. ASCE* 127 (12), 1284–1295.
- Der Kiureghian, A., Crempien, 1989. An evolutionary model for earthquake ground motion. *Struct. Saf.* 6, 235–246.

- Diana, G., Cheli, F., Zasso, A., Boccione, M., 1999. Suspension bridge response to turbulent wind: comparison of a new numerical simulation method results with full scale data. In: Larsen, et al. (Eds.), *Wind Engineering into the 21st Century, Proceedings of the Tenth International Conference on Wind Engineering*. Balkema, Rotterdam, pp. 871–878.
- Diana, G., Bruni, S., Rocchi, D., 2005. Experimental and numerical methodologies to define the response of a long span bridge to wind. In: *Proceedings of the Sixth Asia-Pacific Conference on Wind Engineering*.
- Di Paolo, M., Gullo, I., 2001. Digital generation of multivariate wind field processes. *Probab. Eng. Mech.* 16, 1–10.
- Elishakoff, I., Ren, Y.J., Shinozuka, M., 1994. Conditional simulation of non-Gaussian random fields. *Eng. Struct.* 16 (7), 558–563.
- Ghanem, R., Spanos, P., 1991. *Stochastic Finite Elements: A Spectral Approach*. Springer, Berlin.
- Gossman, E., Waller, A.H., 1983. Analysis of multicorrelated wind excited vibrations of structures using the covariance method. *Eng. Struct.* 5, 264–272.
- Grigoriu, M., 1984. Crossings of non-Gaussian translation processes. *J. Eng. Mech. ASCE* 110 (4), 610–620.
- Grigoriu, M., 1993. On the spectral representation method in simulation. *Prob. Eng. Mech.* 8, 75–90.
- Grigoriu, M., 1998. Simulation of stationary non-Gaussian translation processes. *J. Eng. Mech. ASCE* 124 (2), 121–126.
- Gurley, K., Kareem, A., 1997. Analysis, interpretation, modeling and simulation of unsteady wind and pressure data. *J. Wind Eng. Ind. Aerodyn.* (67–71), 657–669.
- Gurley, K., Kareem, A., 1998. A conditional simulation of non-normal velocity/pressure fields. *J. Wind Eng. Ind. Aerodyn.* (67–68), 673–684.
- Gurley, K., Kareem, A., 1998a. Simulation of correlated non-Gaussian pressure fields. *MECCANICA* 33 (3), 309–317.
- Gurley, K., Kareem, A., 1999. Applications of wavelet transforms in earthquake, wind and ocean engineering. *Eng. Struct.* 21, 149–167.
- Gurley, K., Kareem, A., Tognarelli, M.A., 1996. Simulation of a class of non-normal random processes. *J. Nonlinear Mech.* 31 (5), 601–617.
- Gurley, K., Tognarelli, M.A., Kareem, A., 1997. Analysis and simulation tools for wind engineering. *Probab. Eng. Mech.* 12 (1), 9–31.
- Gurley, K., Jacobs, J., Kareem, A., 2001. Simulation of multidimensional non-Gaussian stochastic fields. In: Schueller, Spanos (Eds.), *Proceedings of the Monte Carlo Simulation*. Balkema, Rotterdam.
- Gurley, K., Kijewski, T., Kareem, A., 2003. First and higher-order correlation detection using wavelet transforms. *ASCE J. Eng. Mech.* 129 (2), 188–201.
- Haan, F.L., Kareem, A., Szewczyk, A.A., 1999. Influence of turbulence on the self-excited forces on a rectangular cross section. In: Larsen, et al. (Eds.), *Wind Engineering into the 21st Century, Proceedings of the Tenth International Conference on Wind Engineering*. Balkema, Rotterdam, pp. 1665–1672.
- Haan, F.L., Kareem, A., Szewczyk, A.A., 2000. Experimental measurements of spanwise correlation of self-excited forces on a rectangular cross section, Volume of Abstracts. In: *Fourth International Colloquium on Bluff Body Aerodynamics and Applications (BBAA IV)*, pp. 439–442.
- Heredia-Zavoni, E., Santa-Cruz, S., 2000. Conditional simulation of a class of non-stationary space-time random fields. *J. Eng. Mech. ASCE* 126 (4), 398–404.
- Holmes, J.D., Sankaran, R., Kwok, K.C.S., Syme, M.J., 1997. Eigenvector modes of fluctuating pressures on low-rise building models. *J. Wind Eng. Ind. Aerodyn.* 69–71, 697–707.
- Hoshiya, M., 1995. Kriging and conditional simulation of a Gaussian field. *J. Eng. Mech. ASCE* 121 (2), 181–186.
- Irwin, P., 1977. Wind tunnel and analytical investigation of the response of Lions Gate Bridge to turbulent wind, NRC of Canada, NAE-LTR-LA-210.
- Iyengar, R.N., Iyengar, K.T.S.R., 1969. A nonstationary random process model for earthquake accelerograms. *Bull. Seismol. Soc. Am.* 59 (3), 1163–1188.
- Kameda, H., 1975. Evolutionary spectra of seismogram by multifilter. *J. Eng. Mech. ASCE* 101 (6), 787–801.
- Kameda, H., Morikawa, H., 1992. An interpolating stochastic process for simulation of conditional random fields. *Prob. Eng. Mech.* 7 (4), 242–254.
- Kareem, A., 1999. Analysis and modeling of wind effects: numerical techniques. In: Larson, Lindsey, Livesey (Eds.), *Wind Engineering into the 21st Century*. Balkema, Rotterdam.
- Kareem, A., Cermak, J.E., 1984. Pressure fluctuations on a square building model in boundary-layer flows. *J. Wind Eng. Ind. Aerodyn.* 16, 17–41.

- Kareem, A., Mei, G., 2000. Stochastic decomposition for simulation and modal space reduction in wind induced dynamics of structures. In: Melchers, R.E., Stewart, M.G. (Eds.), *Applications of Statistics and Probability*. Balkema, Rotterdam, pp. 757–764.
- Kareem, A., Kijewski, T., 2002. Time–frequency analysis of wind effects on structures. *J. Wind Eng. Ind. Aerodyn.* 90, 1435–1452.
- Kareem, A., Tognarelli, M.A., Gurley, K., 1998. Modeling & analysis of quadratic term in the wind effects on structures. *J. Wind Eng. Ind. Aerodyn.* (74–76), 1101–1110.
- Kijewski, T., Kareem, A., 2003. Wavelet transforms for system identification: considerations for civil engineering applications. *Comput. Aided Civ. Infrastruct. Eng. Int. J.* 18, 341–357.
- Kijewski-Correa, Kareem, A., 2006. Efficacy of Hilbert and wavelet transform for the time–frequency analysis. *J. Eng. Mech. ASCE* 132 (10), in press.
- Kim, J., Ho, T.C.E., Hangan, H., 2005. Downburst induced dynamic responses of tall building. In: *Proceedings of the 10th Americas Conference on Wind Engineering*.
- Kondo, K., Mochida, A., Murakami, S., 1997. Generation of velocity fluctuation for inflow boundary condition of LES. *J. Wind Eng. Ind. Aerodyn.*, 67–68.
- Krige, D.G., 1966. Two-dimensional weighted moving average trend surfaces for ore evaluation. In: *Proceedings of the Symposium on Math. Stat. and Comp. Appl. for Ore Evaluation* J. South Africa Inst. Mining Metall., 13–38.
- Kwon, D., Kijewski-Correa, T., Kareem, A., 2005. e-Analysis/design of tall buildings subjected to wind loads. In: *Proceedings of the 10th Americas Conference on Wind Engineering*.
- Lee, B.E., 1975. The effect of turbulence on the surface pressure field of a square prism. *J. Fluid Mech.* 69, 263–282.
- Levy, R., Kozin, F., Moorman, R.B.B., 1971. Random processes for earthquake simulation. *J. Eng. Mech. ASCE* 97 (2), 495–517.
- Li, Y., Kareem, A., 1989. On stochastic decomposition and its application in probabilistic dynamics. In: Ang, A.H.-S., Shinozuka, M., Schueller, G.I. (Eds.), *Proceedings of the Fifth International Conference on Structural Safety and Reliability (ICOSSAR'89)*. ASCE, New York.
- Li, Y., Kareem, A., 1990. ARMA system in wind engineering. *Prob. Eng. Mech.* 5 (2), 50–59.
- Li, Y., Kareem, A., 1991. Simulation of multi-variate non-stationary random processes by FFT. *J. Eng. Mech. ASCE* 117 (5), 1037–1058.
- Li, Y., Kareem, A., 1993. Simulation of multi-variate random processes: a hybrid DFT and digital filtering approach. *J. Eng. Mech. ASCE* 119 (5), 1037–1058.
- Li, Y., Kareem, A., 1995. Stochastic decomposition and its applications to probabilistic dynamics. *J. Eng. Mech. ASCE* 121 (1), 162–174.
- Li, Y., Kareem, A., 1997. Simulation of multivariate non-stationary random processes: hybrid DFT and digital filtering approach. *J. Eng. Mech.* 123 (12), 1302–1310.
- Loeve, M., 1963. *Probability Theory*. Van Nostrand, Princeton, NJ.
- Lumley, J.L., 1970. *Stochastic Tools in Turbulence*. Academic, San Diego.
- Maruyama, T., Morikawa, H., 1995. Digital simulation of wind fluctuation in a turbulent boundary layer using experimental data. *Proc. 9ICWE (New Delhi) I*, 659–670.
- Mann, J., 1999. Wind field simulation. *Probab. Eng. Mech.* 13 (4), 269–282.
- Masters, F.J., Gurley, K., 2003. Non-Gaussian simulation: cumulative distribution function map-based spectral correction. *J. Eng. Mech. ASCE* 129 (12), 1418–1428.
- Mignolet, M.P., Spanos, P.D., 1992. Simulation of homogenous two dimensional random field; Part I, AR and ARMA models; Part II. *J. Appl. Mech. ASME* 59, 260–277.
- Priestly, M.B., 1965. Evolutionary spectra and non-stationary processes. *J. R. Stat. Soc. Ser. B* 27, 204–237.
- Samaras, E., Shinozuka, M., Tsurui, A., 1985. ARMA representation of random processes. *J. Eng. Mech. ASCE* 111 (3), 449–461.
- Scanlan, R.H., 1997. Amplitude and turbulence effects on bridge flutter derivatives. *ASCE J. Struct. Eng.* 123 (2), 232–236.
- Seong, S.H., Peterka, J.A., 1998. Digital generation of surface-pressure fluctuations with spiky features. *J. Wind Eng. Ind. Aerodyn.* 73, 181–192.
- Sherer, R.J., Riera, J.D., Schueller, G.I., 1982. Estimation of the time-dependent frequency content of earthquake accelerations. *Nucl. Eng. Des.* 71 (3), 310.
- Shinozuka, M., 1971. Simulation of multivariate and multidimensional random processes. *J. Acoust. Soc. Am.* 49, 357–367.

- Shinozuka, M., Sato, Y., 1967. Digital simulation of nonstationary random processes. *J. Eng. Mech. ASCE* 93 (1), 11–40.
- Shinozuka, M., Jan, C.M., 1972. Digital simulation of random processes and its applications. *J. Sound Vib.* 25 (10), 111–128.
- Shinozuka, M., Deodatis, G., 1991. Simulation of stochastic processes by spectral representation. *Appl. Mech. Rev.* 44 (4), 191–203.
- Shinozuka, M., Zhang, R., 1996. Equivalence between KRIGING and CPDF methods for conditional simulation. *J. Eng. Mech. ASCE* 122 (6), 530–538.
- Shinozuka, M., Yun, C.-B., Seya, H., 1990. Stochastic methods in wind engineering. *J. Wind Eng. Ind. Aerodyn.* 36, 829–843.
- Solari, G., Carassale, L., Tubino, F., 2005. POD methods and applications in wind engineering. In: *Proceedings of the Sixth Asia-Pacific Conference APCWE-VI*, September 2005, Seoul, Korea.
- Tamura, T., Ono, Y., 2003. LES analysis on aeroelastic instability of prisms in turbulent flow. *J. Wind Eng. Ind. Aerodyn.* 91, 1826–1827.
- Tamura, Y., Suganuma, S., Kikuchi, H., Hibi, K., 1999. Proper orthogonal decomposition of random wind pressure field. *J. Fluids Struct.* 13, 1069–1095.
- Tamura, T., Okuda, Y., Okada, H., 2002. LES estimation of wind characteristics in the surface layer over various grounds—urban roughness effects and terrain effects. In: *Proceedings of the UJNR Panel on Wind and Seismic Effects (Task Committee D)*, 2002, Seattle.
- Vanmarcke, E.H., Fenton, G.A., 1991. Conditional simulation on local fields of earthquake ground motion. *Struct. Saf.* 10 (1–3), 247–263.
- Vasta, M., Schueller, G.I., 2000. Phase space reduction in stochastic dynamics. *J. Eng. Mech.* 126 (61), 626–632.
- Wang, L., 2007. Stochastic modeling and simulation of transient events, Ph.D. Dissertation, Department of Civil Engineering and Geological Sciences, University of Notre Dame, Notre Dame, IN.
- Wang, L., Kareem, A., 2004. Modeling of non-stationary winds in gust fronts. In: *Proceedings of the Ninth Joint Specialty Conference on Probabilistic Mechanics and Structural Reliability*, July, Albuquerque.
- Wang, L., Kareem, A., 2005. Modeling and simulation of transient winds: downbursts/hurricanes. In: *Proceedings of the 10th American Conference on Wind Engineering*, Baton Rouge, LA.
- Xu, Y.L., Chen, J., 2004. Characterizing nonstationary wind speed using empirical mode decomposition. *J. Struct. Eng. ASCE* 130 (6), 912–920.
- Yamazaki, F., Shinozuka, M., 1988. Digital generation of non-Gaussian stochastic fields. *J. Eng. Mech. ASCE* 114 (7), 1183–1197.
- Yamazaki, F., Shinozuka, M., 1990. Simulation of stochastic fields by statistical preconditioning. *J. Eng. Mech. ASCE* 116 (2), 268–287.
- Zhou, Y., Kijewski, T., Kareem, A., 2003. Aerodynamic loads on tall buildings: an interactive database. *ASCE J. Struct. Eng.* 129 (3), 394–404.

# Wind-Induced Vibrations of Tall Buildings: The Role of Full-Scale Observations in Better Quantifying Habitability

Audrey Bentz, Graduate Student, University of Notre Dame, Department of Civil Engineering,  
156 Fitzpatrick Hall, Notre Dame, IN, 46556

Tracy Kijewski-Correa, PhD, Associate Professor, University of Notre Dame, Department of  
Civil Engineering, 156 Fitzpatrick Hall, Notre Dame, IN, 46556

## TABLE OF NOMENCLATURE

$\phi_i(z)$	Overall mode shape
$\phi_{i,A}(z)$	Axial mode shape component
$\phi_{i,V}(z)$	Frame racking mode shape component
$\phi_{i,PZ}(z)$	Panel zone mode shape component
$\tilde{\phi}(z)_i$	Approximate mode shape
$z$	Elevation
$h$	Total building height
$\alpha$	Mode shape power
$\xi$	Critical damping ratio
$f$	Frequency

## Abstract

The design of tall buildings, in many cases, is governed by habitability considerations whose satisfaction depends significantly upon two key aspects: first are the criteria used to establish the target limit state. These criteria are based on occupant comfort and can have a considerable effect on the efficiency and economy of modern tall building design, though there remains uncertainty surrounding the appropriate criteria, including the physical measures and waveforms best quantifying motion stimulus. Further, the ability of any design to meet these target criteria depends largely on the equivalent viscous damping levels assigned to the building. The basis for this assignment is rather qualitative and raises considerable uncertainty in the resulting acceleration response predictions. These and other lingering challenges prompted a long-term full-scale monitoring effort in Chicago by the authors and their colleagues, extending now internationally. This paper addresses several issues related to the perception issue in tall buildings: determination of realistic occupant comfort criteria, assessment of the faithfulness of predicted acceleration responses by current approaches, development of a more intuitive predictive model for damping, and the ability to calibrate this model using full-scale data, particularly for buildings featuring coupled response. This paper therefore canvasses these issues and value of full-scale observations in resolving them.

## Introduction

As building systems become taller, more lightweight, and efficient, they become increasingly sensitive to the effects of wind. As a result, habitability limit states often govern the design of tall structures, as wind-induced accelerations increase and become more perceptible to occupants. Human perception of motion is dependent upon many factors, some of which are more difficult to quantify than others. While researchers have studied the

effects of frequency, amplitude, duration of motion, and waveform (peak factors) on human comfort using motion simulators, there are still other factors beyond these that contribute to motion perception and are difficult to accurately capture within motion simulators. In many cases, motion is not actually perceived until awareness is triggered by visible signs of motion, sounds generated by the motion, and even by word of mouth. In addition, the extent to which each contributing factor causes perception and/or discomfort varies from person to person, and the means to best quantify these accelerations (peak vs. RMS) is still contested [8]. The subsequent section will discuss some of these environmental factors that strongly influence the onset of perception based on full-scale observations.

Clearly the limit states associated with occupant comfort have their own uncertainties, and this is unfortunately compounded by uncertainties surrounding the prediction of dynamic response in the design stage. This paper will discuss two items in this regard: first is the fact that energetic transient events cannot be neglected in the assessment of structures for habitability. The second is the fact that regardless of whether transient or stationary response is being evaluated in design, neither can be done without an accurate estimate of damping. Damping plays a vital role in reducing acceleration responses. However, unlike mass and stiffness, the determination of damping is riddled with ambiguity. This problem arises from the many sources contributing to a building's inherent structural damping, which cannot be directly quantified and are generally dependent upon amplitude. In lieu of a theoretical means to determine damping in the design stage, empirical efforts have been undertaken by a number of researchers using databases of full-scale measurements [3,7,10]. Initially the parameterization of damping databases was performed with respect to height or period, after categorizing the data by primary construction material (steel or concrete). Although material and height are certainly important considerations in damping estimation, the significant amount of scatter observed in these parameterizations suggests that other variables should be explored. The authors have previously proposed a more intuitive model for damping estimation based on the dominant deformation mechanism of a structure, taking the structural system into consideration as well as building height and material [1]. Preliminary findings confirmed that shear-based deformations dissipate more energy than axial shortening associated with global cantilever behavior, and the relative contribution of these two components was shown to be a viable parameter for damping data regression. This paper will discuss this more intuitive model along with some of the fundamental challenges associated with the estimation of damping from full-scale data, particularly in the presence of modal coupling.

### **Quantifying Human Perception Criteria**

The establishment of reliable occupant comfort criteria is an important goal toward the achievement of economic and efficient tall building design. Ideally, the permissible acceleration levels would be quantified through interviewing processes in realistic building environments instrumented so that the exact response of the building is known. Since it is impractical to extensively study the effects of building motion on human comfort in-situ, largely due to a lack of accessibility, studies have instead been historically performed in motion simulators. While these efforts have been underway for decades, many simulator studies utilize only sinusoidal motions. However, recent efforts have attempted to create more faithful testing environments, capable of simulating various waveforms on multiple axes to explore the influence of frequency, amplitude, duration, and peak factor [2]. The findings from these studies have particularly underscored the influence of waveform in human perception, exploring various peak factors on the simulated motions to achieve sinusoidal, narrowband and even transient events associated with gust fronts or thunderstorms. When considering actual building motion, these findings indicate that transient events may cause greater perception issues due to their sudden onset and high amplitude, but perhaps are not severely disruptive or negatively influencing comfort due to their short duration.

Although the motion simulator experience provides valuable information on the factors most influencing occupant comfort and perception, they may not capture the environmental factors that may cue motion at lower acceleration levels in actual buildings. Visual and audio cues in particular play a significant role in the perception of motion, but are difficult to reproduce in controlled simulator studies. In fact, an informal on-line survey ([www.nd.edu/~tallbldg/survey.html](http://www.nd.edu/~tallbldg/survey.html)) was developed by the authors and their colleagues to collect qualitative data on the perception issue in tall buildings. Initial findings presented in Kijewski-Correa et al. [5] chronicled multiple responses to a particular wind event where 70% of the respondents were looking out the window at the time they first perceived the motion. Interestingly, while 20% were first alerted by these visual cues, 80% did acknowledge the role of others in triggering their own perception. This factor is often not captured in controlled motion simulators, and since it is only achieved in group environments, perhaps becomes office buildings. 47% of solitary respondents (residential) indicate that they first perceived motion through audio cues such as squeaking, cracking and whistling, while 42% indicate that they felt the motion first. The remaining respondents indicated visual cues

as their first perception mechanism, with 6% citing “External motion cue: looking out the window” and another 6% citing “Internal motion cue: object swaying, liquid sloshing, etc”. It is interesting to note that visual cues were not a common perception trigger for the respondents, even though 57% of respondents were looking out a window while experiencing the motion.

### **Dynamic Response to Transient Events**

Clearly waveform has some influence on perception; however, this presently is not accounted for in design-stage acceleration response prediction. For decades, wind tunnel testing has served as an important design tool for quantifying wind loads and ensuing acceleration responses; however, it is interesting to note that in some countries, particularly the United States, the most severe wind events, outside of hurricanes, are actually the result of gust front and thunderstorm activities not captured in the traditional boundary layer wind tunnel testing. Within the context of the Chicago Full-Scale Monitoring Program, transient wind events have been recorded and independent anecdotal evidence published in local papers confirms that occupant comfort or at minimum perception can be adversely affected in these transient events. Though not as common, similar transient events have been observed for another building in the program: a 264 m tall building located in Seoul, South Korea. This building has been instrumented with three orthogonal pairs of accelerometers attached to girders on the 64<sup>th</sup> floor, whose locations are shown in Figure 1. Pirnia et al. [9] investigated the dynamic properties of the building with a focus on amplitude dependence and closely spaced modes. These factors complicate system identification and extraction of dynamic properties in each direction.

Recent data from this building has shown significant responses to thunderstorm events, whose transient nature provides an impulsive-type stimulus to the building, exciting multiple modes with its broadband energy. Figure 1 shows the responses of the building to one such event that occurred on April 25<sup>th</sup>, 2008, through inset acceleration time histories and power spectral densities (PSD). Note that several of the higher modes are evident in the response, affirming the impulsive nature of this transient event, clearly visible at  $t \approx 40$  minutes, particularly for the y-response. In this event, the wind before the transient was approaching from the East, moving parallel to the x-axis of the building. During the event, the wind changed direction rapidly, approaching parallel to the y-axis of the structure with markedly higher speeds. This may explain the greater impulse like responses at  $t \approx 40$  minutes in this direction, particularly at Location 2 on the leeward edge. The full-scale observation of these types of events then raises important questions surrounding occupant comfort and its quantification: considering that the sudden onset of these events does cause perception complaints, should they be considered as design limit states for habitability and if so, how should they be predicted in design as deviants from the traditional wind tunnel testing protocols?

### **New Models for Damping**

While both laboratory and full-scale perception studies continue in attempts to determine the most appropriate accelerations for habitability design, including the role of waveform, work needs to continue in hopes of predicting more faithful acceleration responses in the design stage so habitability requirements can be met in the formative stages of a project, without the need for costly retrofits later. Regardless of whether stationary events will remain the sole basis for design, any dynamic response analysis depends significantly on the specified damping ratio. Recognizing this, the authors [1] have worked toward improved damping models noting the influence of a structural system’s primary deformation mechanism on energy dissipation. It was found that buildings with a high contribution of frame racking, characterized by shear deformations in beams, columns and panel zones, had greater damping levels than buildings dominated by cantilever action, where the majority of deflections come from the axial lengthening and shortening of columns. These findings suggest that structural systems associated with taller, more slender buildings (tending to have dominant axial deformations) have less damping and therefore are more susceptible to occupant comfort issues. Since in-situ damping values are often less than those assumed in design, as affirmed by the full-scale case study on 9 tall buildings [7], designers are often confronted with buildings that meet perception criteria on paper, but in practice do not. It is hoped that the ability to better estimate damping levels in the design stage, based on the relative participation of shear vs. axial deformations, will allow designers to more accurately predict accelerations to enable pro-active redesign as needed.

This intuitive damping model was developed by analyzing the in-situ damping levels of numerous buildings worldwide, assuming the structural mode shapes consist of three components:

$$\phi_i(z) = \phi_{i,A}(z) + \phi_{i,V}(z) + \phi_{i,PZ}(z) \quad (1)$$

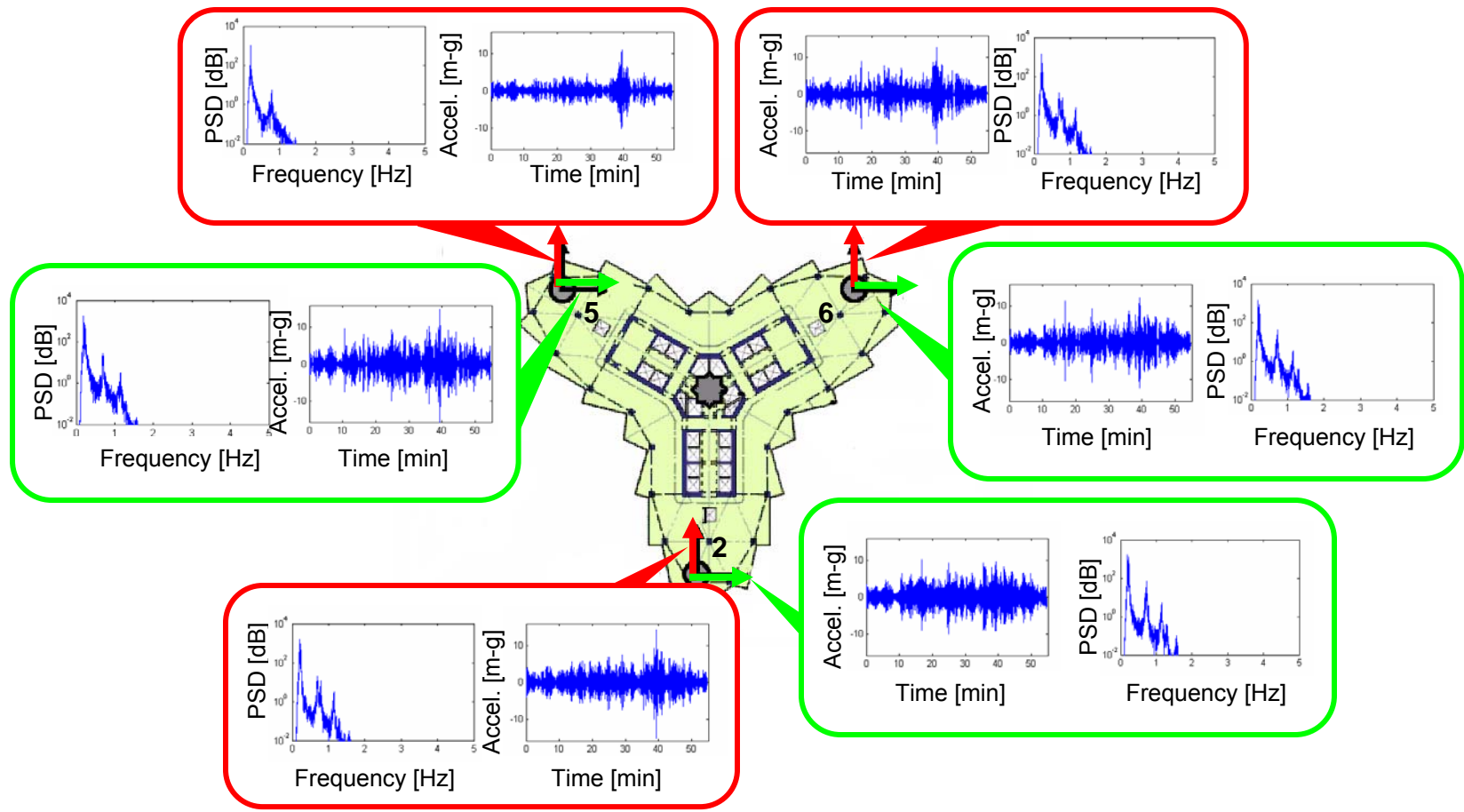


FIGURE 1- 64<sup>TH</sup> FLOOR PLAN SHOWING INSTRUMENT LOCATIONS AND DECOUPLED RESPONSE MEASUREMENTS AT EACH LOCATION, WITH INSET TIME HISTORY AND POWER SPECTRAL DENSITIES

Soliciting the help of the designers of the buildings, the authors have initiated campaign to determine the various components in (1) for all buildings for which in-situ damping levels are available. In cases where finite element models are not available or cannot be readily constructed from the public record, a basic fit to the overall mode shape by a power-law expression is used to provide qualitative estimates of the degree of cantilever action present [1]. In this case, the  $i^{\text{th}}$  mode shape is described by

$$\tilde{\phi}(z)_i = (z/h)^\alpha \quad (2)$$

and least squares minimization can be used to identify a best-fit power ( $\alpha$ ). For  $\alpha \sim 1$ , there is a general lack of cantilever action and as  $\alpha \rightarrow 2$ , there is an increasing presence of cantilever action. Often,  $\alpha = 1$  is termed a “shear building” and  $\alpha = 2$  is termed a “cantilever building,” as these signify benchmarks where around 75-80% of the deformations are contributed by the namesake. As such, the authors have adopted the following characterization of buildings based on the mode shape power [1]:

$$\begin{aligned} \text{Type V (Shear): } & \alpha \leq 1.25 \\ \text{Type A-V (Interactive): } & 1.25 < \alpha < 1.5 \\ \text{Type A (Cantilever): } & \alpha \geq 1.5 \end{aligned} \quad (3 \text{ a,b,c})$$

The effectiveness of this approximate characterization was verified in [1] using the FEM mode shapes of moment resisting frames with different aspect ratios. The approximation was then applied to actual building systems, including four structures from the Chicago Full-Scale Monitoring Program, with results affirming the general hypothesis previously stated [1]. At present, the authors are expanding the database of structures used in this new parameterization, again seeking the help of designers to better quantify the relative contributions of these deformation mechanisms.

The development of these predictive models is entirely reliant on the accuracy with which damping levels are specified. It can be rightfully argued that the scatter observed in full-scale damping databases is as much a function of the lack of appropriate parameterization as it is errors in the estimation of damping itself. Its estimation in lightly damped systems, in the presence of coupled modes and amplitude dependence is particularly challenging and requires sophisticated analysis techniques. To demonstrate this point, system identification was performed for stationary events occurring before and after the transient event previously documented in Figure 1. Despite the use of bandpass filtering and algebraic manipulation of sensor outputs assuming rigid body motion in plane, the individual responses on the building’s primary axes cannot always be isolated, depending on the response level and the degree of amplitude dependence that facilitates beating of modes [6]. In particular, the aforementioned Korean Tower had been previously analyzed in [9] using traditional filtering and decoupling approaches to isolate the contributions in both lateral directions and torsion. However, revisiting this same building for other wind events often results in residual coupling, despite these efforts. An example of this is shown in Figure 2, where random decrement signatures (RDS) extracted using the same methodology as Pirnia et al. [9] demonstrate clear beat phenomena between the lateral and torsional responses. As traditional filtering cannot be used to isolate these components, the wavelet transform paradigm introduced by Kijewski and Kareem [4] was instead consulted to visualize the intermittent presence of torsional response and effectively separate these two modes. Therefore, each random decrement signature was processed using time-frequency transforms with appropriate corrections for end effects [4]. Stationary wind events from west and southwesterly directions were considered. The westerly event generated the strongest responses for the x-direction, while the more southwesterly wind event generated the strongest responses for the y-direction. The mean frequency and damping estimates obtained by the random decrement technique with local averaging [9] are spatially depicted in Figure 2, with an example of the random decrement signatures. Visually the beating between sway and torsion is very evident, particularly in the x-direction (in fact, note that one of the y-responses shows no evidence of coupling) and becomes more pronounced at the leeward extremes of the structure due to the “fishtailing” similarly observed in a skyscraper in Boston [6]. The extent of coupling is very much dependent on the wind direction and amplitude, being largely facilitated by the amplitude-dependence previously noted by Pirnia et al [6]. Excellent repeatability is noted for the lateral frequencies at all three locations in Figure 2. The torsional frequency also shows good agreement, though generally taking on slightly larger values in the x-axis responses, perhaps due to differing amplitudes in the event analyzed for that direction. Interestingly, Pirnia et al. [9] provided expressions for amplitude dependent frequency in this building. Evaluating them for the amplitude levels herein:  $f_x = -0.0027(0.2)+0.1992 = 0.198 \text{ Hz}$  and  $f_y = -0.0023*0.2 + 0.2076 = 0.207 \text{ Hz}$ . Thus in the presence of considerable coupling, the frequencies of vibration in individual modes appear to be somewhat softened.

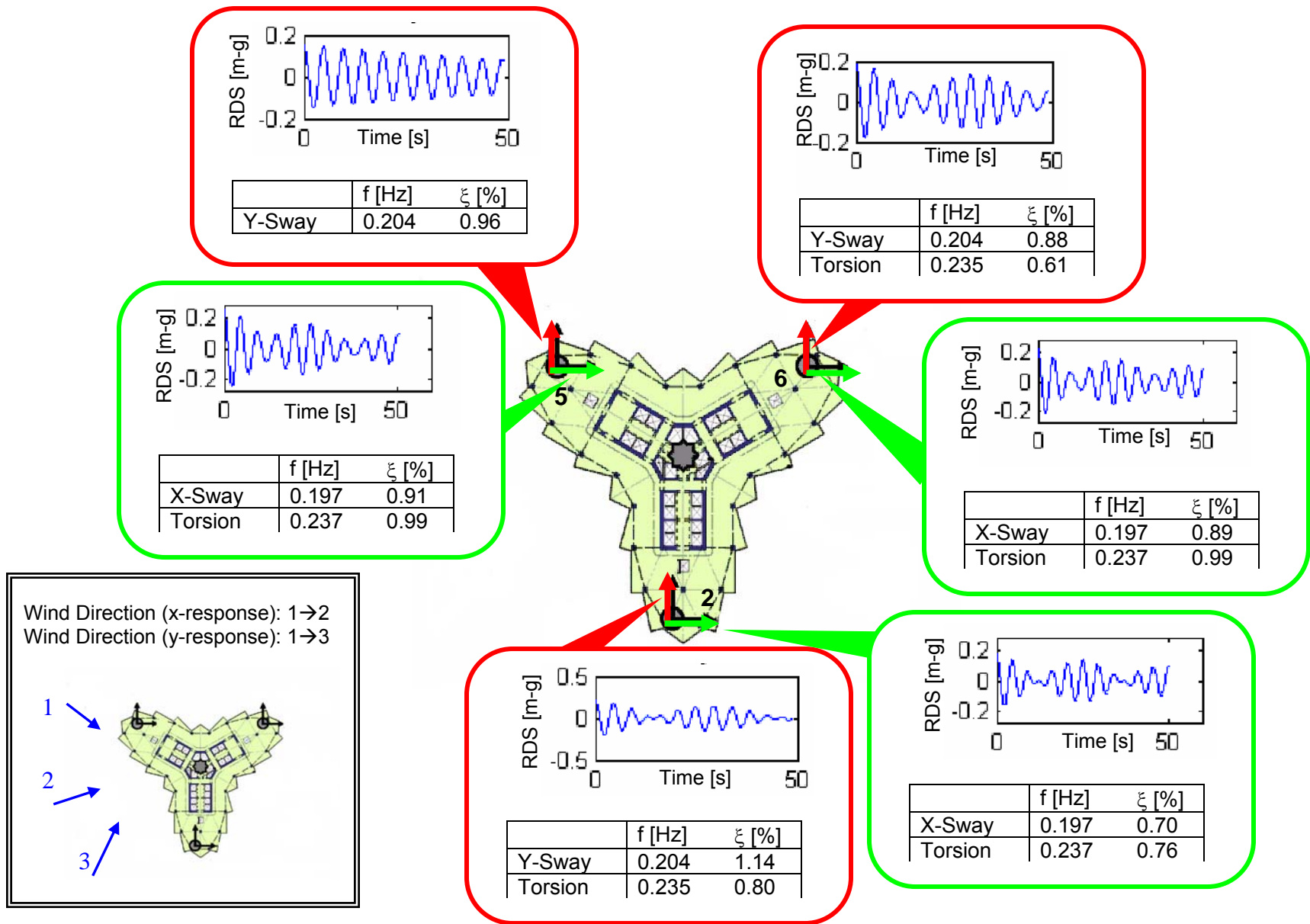


FIGURE 2- RESULTS OF SYSTEM IDENTIFICATION, DISPLAYED AT INSTRUMENT LOCATIONS (WIND DIRECTION SHOWN AS INSET)

Damping on the other hand shows an expected variability. Mode 1 (X-sway) shows an average damping of 0.83% critical (CoV 14%), while Mode 2 (Y-sway) shows an average damping of 0.99% critical (CoV 13%). Torsion was separately observed in two different events. In the first event, damping was an average of 0.7% critical (CoV 19%). In the second event, torsional damping was an average of 0.91% critical (CoV 15%). These events correspond to what would be in the lower-amplitude regime of Pirnia et al.'s [6] amplitude-dependent study. That study interestingly found damping values in this low amplitude regime to be highly variable and inflated. For example, damping values easily exceeded 1.5% in this regime for X-sway and then stabilized to a value of around 0.8% critical [6]. This prior study did not make use of any wavelet-based decoupling strategy to accommodate the coupled modes, and it is hypothesized, particularly at the lower amplitudes, that both modes were equally present in the response, leading to inflated damping values that are actually the aggregate of two closely spaced modes. As response increased, a particular mode may begin to dominate, such as lateral sway, allowing it to be readily isolated in the analysis. Thus it can be viewed that the 0.8% critical damping value is [6] probably is more representative of the inherent damping in the X-sway mode. This would then be consistent with what is observed in Figure 2: the wavelet analysis was successful in isolating the X-sway and extracting its damping value of approximately 0.83% critical. Applying similar metrics to the Y-sway response, Pirnia et al. [6] found that damping values stabilize at much lower amplitudes. Thus inflated values of damping (0.7% critical) rapidly stabilized with increasing amplitude to a value of 0.6% [6]. Considering that the effect of coupling was observed to be less prevalent in the Y-direction, these observations make intuitive sense: the inflated, coupled behavior would occupy a more limited amplitude range and the Y-sway response would rapidly dominate and be easily extracted, even without time-frequency aids. Note the low amplitude damping level in Figure 2 was 0.99%, in reasonable agreement with [6]. It should also be noted that Pirnia et al. [6] were unable to effectively isolate the torsional response, due to its minor and intermittent contributions, a capability now enabled by the wavelet analysis herein.

The effect of beating in building responses raises an interesting question regarding how damping should be specified. Generally, damping is assigned separately for each mode, however, in coupled buildings the internal tuning between modes can itself be an energy dissipative behavior, as clearly seen is the case in the decrement signatures in Figure 2. Therefore, should the modes be viewed in isolation, as the wavelet analysis permits, or should their aggregate effect be considered as the true measure of energy dissipative capability? Similar questions were raised in [6] and with respect to the issue of amplitude dependence in [9]. In fact, amplitude dependence, coupling and exchange of energy between modes generally go hand in hand. Damping estimates that do not consider time or amplitude dependent characteristics will not account for the role of intermittent coupling and beat phenomena or the exaggeration of spectral bandwidth that results when frequency content varies with amplitude. Instead they will provide an inflated damping value that may or may not be representative of the energy dissipation within the system or even more importantly the inherent damping associated with an individual mode. Furthermore, in the case of coupling, motions can even be amplified, as shown in [6], which in essence constitutes a negative damping contribution. Thus the one parameter that remains an enigma is often difficult to quantify even when full-scale data is available.

## **Conclusions**

This paper has discussed the uncertainties surrounding human comfort criteria and efforts being made to better establish realistic design guidelines for accelerations, including the use of web-based occupant surveys, and the need to insure that design predictions of acceleration response are accurate reflections of in-situ behavior. In particular, this requires the need for more intuitive and accurate damping models, as well as an ability to assess the effects of transient events and their role in perception. This study additionally addressed the challenges that are faced when extracting damping values that become the bases for response predictions, particularly in the presence of coupling. Clearly human perception will continue to drive the design of tall buildings for many years to come, requiring refocused efforts at understanding the in-situ dynamic interactions between human and structure and more effective means to mitigate any adverse effects in the design stage to avoid costly retrofits and public scrutiny. As this study has demonstrated, full-scale observations have played and will continue to play a vital role in this regard.

## **Acknowledgements**

The authors wish to acknowledge the financial support of the National Science Foundation, Grant CMMI 06-01143, and the first author's support by the Schmitt Presidential Fellowship from the Graduate School of the University of Notre Dame. Damping values and structural system characteristics were also made available to the authors through wider collaborations with the Chicago Full-Scale Monitoring Program (PI: Dr. Ahsan Kareem of the University of Notre Dame; NSF Grant CMS-00-85109).

## References

1. Bentz, A., and Kijewski-Correa, T., "Predictive Models for Damping in Buildings: The Role of Structural System Characteristics" Proceedings of the 8<sup>th</sup> Annual Structures Congress, 18<sup>th</sup> Analysis and Computation Specialty Conference, Vancouver, Canada, CD-ROM, 2008
2. Burton, M. D., Hitchcock, P. A., Kwok, K. C. S., and Roberts, R.D., "Acceptability Curves from Motion Simulator Investigations and Previous Experience with Building Motion," Tenth Americas Conference on Wind Engineering, p. 286, 2005
3. Jeary, A. P., "Damping in Tall Buildings- A Mechanism and Predictor," *Earthquake Engineering and Structural Dynamics*, 14, p.733-750, 1986
4. Kijewski, T. and Kareem, A., "Wavelet Transforms for System Identification in Civil Engineering", *Computer-Aided Civil and Infrastructure Engineering*, Vol. 18, No.5, p.339-355, 2003
5. Kijewski-Correa, T., Pirnia, J.D., Bashor, R., Kareem, A., Kilpatrick, J., Young, B., Galsworthy, J., Isyumov, N., Morrish, D. and Baker, W. "Full-Scale Performance Evaluation of Tall Buildings Under Winds," Proceedings of 12<sup>th</sup> International Conference on Wind Engineering, July 2-6, Cairns, Australia, Vol. 1, p.351-358, 2007
6. Kijewski-Correa, T. and Pirnia, J.D., "Dynamic Behavior of Tall Buildings Under Wind: Insights from Full-Scale Monitoring," *The Structural Design of Tall and Special Buildings*, 16, p.471-486, 2007
7. Lagomarsino, S., "Forecast Models for Damping and Vibration Periods of Buildings," *Journal of Wind Engineering and Industrial Aerodynamics*, 48, p.221-239, 1993
8. McNamara, R., Kareem, A. and Kijewski, T., "Ask the Experts...Perception of Motion Criteria for Tall Buildings Subjected to Wind," Proceedings of Structures Congress, ASCE, Denver, 2002
9. Pirnia, J.D., Kijewski-Correa, T., Abdelrazaq, A., Church, J., and Kareem, A., "Full-Scale Validation of Wind-Induced Response of Tall Buildings: Investigation of Amplitude-Dependent Dynamic Properties," Proceedings of the 7<sup>th</sup> Annual Structures Congress, Long Beach, CA, CD-ROM, 2007
10. Satake, N., Suda, K., Arakawa, T., Sasaki, A., and Tamura, Y., "Damping Evaluation Using Full-Scale Data of Buildings in Japan," *Journal of Structural Engineering*, 129, 4, 470-447, 2003

# Efficacy of Damage Detection Measures from Digital Images

Jim Thomas<sup>1</sup>, Joe Jeray<sup>2</sup>, Ahsan Kareem<sup>3</sup>, Kevin Bowyer<sup>4</sup>

<sup>1</sup>*Computer Science and Engineering, University of Notre Dame, Notre Dame, USA, [jthoma14@cse.nd.edu](mailto:jthoma14@cse.nd.edu)*

<sup>2</sup>*Civil Engineering, University of Notre Dame, Notre Dame, USA, [jjeray@nd.edu](mailto:jjeray@nd.edu)*

<sup>3</sup>*Civil Engineering, University of Notre Dame, Notre Dame, USA, [kareem@nd.edu](mailto:kareem@nd.edu)*

<sup>4</sup>*Computer Science and Engineering, University of Notre Dame, Notre Dame, USA, [kwb@cse.nd.edu](mailto:kwb@cse.nd.edu)*

## INTRODUCTION

Estimating the extent of damage caused by natural disasters is necessary for implementing effective relief measures in the affected areas. Remote-sensing through satellite or aerial means have enabled engineers to easily obtain digital images of such areas. A careful analysis of these images facilitates rapid detection and assessment of the damage that has occurred. Significant research has been done in the past towards development of automated algorithms to compare images from before and after the disaster to assess the damage. In this study we evaluate the efficacy of existing measures used to detect damage is evaluated. Determining the efficacy of these damage measures in definitive assignment of damage states is necessary for the automated assessment of windstorm damage.

## DAMAGE DETECTION

Building damage and debris spread can be identified and classified by applying change-detection algorithms to before-and-after images. In this comparison building damage appears as changes in shape, lines, colors, texture, etc. The automatic damage detection process is usually a sequence of operations. First step is image pre-processing which involves image registration and radiometric image pre-processing. The next step is to identify objects that have been damaged. For example in windstorm damages the objects are buildings and damage is indicated by changes in roofing structure. We can identify such objects manually or by using image segmentation techniques. change detection algorithms to identify whether change has occurred between before and after images. The next step is to compute damage metrics which quantify and measure extend of damage. The efficacy of these measurements can then be determined by comparing with qualitative descriptions obtained from field surveys. For windstorm damages the rating is done qualitatively ranging from RS-A (no damage) to RS -D (Roof structure collapsed or removed) as discussed in [2].

## DAMAGE MEASURES FROM CHANGE DETECTION

Change detection algorithms use different criterion to classify pixels in before and after images as changed or not changed. By counting the number of pixels or groups of pixels that have changed, we obtain damage measures for before windstorm and after windstorm images. A survey of existing change detection algorithms were presented in [1]. The simplest change detection algorithm is based on a simple differencing of each pixel. This technique simply thresholds a difference image to obtain a change mask. A more complicated class uses significance tests where decisions at each pixel depends on small blocks of pixels in its neighborhood. Algorithms based on Shading models use intensity at pixels. In our study we apply each of these algorithms to find changed pixels in images and use them to compute damage measures.

## **DAMAGE MEASURES FROM SPECTRAL BANDS**

Commercial imaging satellites presently offer spatial resolutions which have been refined to 50cm (4 spectral bands B-G-R-NIR). Each pixel in a digital image is assigned an integer value (digital number or "DN") for each separate spectral band, reflecting average reflectance of that pixel in that band. Digital images are thus composed of multiple arrays of DN values (one array for each band). For Windstorm damages, Womble describes statistical measures [2] which are computed for the separate spectral bands of each roof-facet object, using the intensity (DN) values extracted from the before-and-after images. These statistical measures are: (1) Standard Deviation is commonly used to describe the dispersion of a statistical distribution. It is a measure of the deviation from the mean and is a measure of the width of the statistical distribution. (2) Variance is the second moment of a probability distribution and can be used to describe relative smoothness. It is commonly used to describe the variability of a given value from its mean. (3) Average deviation is also a measure of dispersion but does not utilize a squared deviation term; hence, it is less sensitive to extreme deviations than the standard deviation or variance. (4) Skewness is a third-order-moment term which measures the degree of asymmetry of a probability distribution around its mean. (5) Uniformity is a textural measure. Previously mentioned non-illumination-based metrics are desired for the identification of windstorm damage to roofs. Textural measures are a common and powerful type of non-illumination-based metric and can thus be useful to our purpose. Uniformity, is used to describe the coarseness of an object based on its histogram. While a non damaged roof typically has a fairly uniform texture, a damaged roof is expected to have a less-uniform texture, shown quantitatively as a decrease in the uniformity. (6) Entropy is a measure of the randomness or disorder within an object. Damage metrics are formed by comparing the post-windstorm and pre-windstorm values of the above statistical measures for each roof-facet object in each spectral band. We extend Womble's study to to identify individual damage metrics or combinations (permutations) of damage metrics that are well correlated with damage states.

## **DAMAGE MEASURES BASED ON FEATURE ORGANIZATION**

An alternative method [3] is to use quantitative measures which measure change based on feature organization. Damages bring about a disorganization in the visual features of an Image. The feature used commonly is edge segments. By finding the relationships between edge segments and how they get disorganized when a disaster occurs, the image can be classified. First a relation graph is constructed followed by eigenvalues, eigenvectors and eigenclusters for this graph. A set of four change detection measures are then calculated from these values and used to classify the extent of damage in the image. These measures are: (1) Total lengths of the edges in the eigenclusters, (2) Number of eigenclusters, (3) Sum of positive eigenvalues, (4) Distance measure of spectra from two images.

These measures are applied to a set of before and after images of a hurricane affected area. The efficacy of the measures is determined by comparing damage assessment with the results of the automated algorithms that use these measures. The effectiveness of each measure for different damage scenarios is delineated.

## **REFERENCES**

- [1] R.J Radke , S Andra , O Al-Kofahi , B Roysam, Image Change Detection Algorithms: A Systematic Survey, IEEE Trans Image Process. 2005 Mar;14(3):294-307.
- [2] J. A Womble, Remote-Sensing Applications to Windstorm Damage Assessment, Doctoral Dissertation in Civil Engineering, Texas Tech University, December 2005.
- [3] S.Sarkar, K.L Boyer, Quantitative Measures of Change based on Feature Organization: Eigenvalues and Eigenvectors, Computer Vision and Image Understanding (71), No. 1, July 1998, pp. 110-136.

# Outline of Conventional Construction Systems for Pitched Roofs in Eastern Asia

Takashi Ohno<sup>1</sup> and Wang Xihui<sup>2</sup>

<sup>1</sup>*Faculty of Engineering, Tokyo Polytechnic University, Tokyo, 243-0297 Japan*  
(Corresponding author: Email: oono@arch.t-kougei.ac.jp)

<sup>2</sup>*Tokyo Technology Department, Sekisui House Ltd. Tokyo, 107-0052 Japan*

**ABSTRACT:** Roof construction is one of the most important building construction issues in relation to wind and rain. Government policy dictates that most new buildings have flat roofs, but many conventional existing ones have pitched roofs. These are the subjects of this study. The authors' research focuses on the following four items.

1) Conventional construction systems for pitched roof systems that reflect supply conditions in each area.

University and technical college textbooks on building construction and literature on traditional building construction were collected and compiled. The authors also visited construction sites and surveyed students in each area to obtain relevant information.

2) Climate data on wind velocity, especially combined with rainfall, and the probability of simultaneous occurrence.

3) Distribution factors regarding wind pressure on roof surfaces with eaves and rakes that happened during wind.

4) Reinforcing methods considering wind with rain for existing construction systems.

**KEY WORDS:** Conventional construction system, pitched roof, Eastern Asia, Eaves, Rake

## 1. INTRODUCTION

The development of construction systems requires a grasp of legal constraints, weather and other environmental conditions, conditions of use, related policies and cultural aspects, as well as production and construction conditions. Production and construction conditions are composed of various elements, including building materials usable for construction and type of labor. Actual situations are clearly indicated by conventional construction systems.

## 2. SCOPE

### 2.1 *Consideration of dwellings as conventional construction systems*

As might be expected, construction systems for large buildings expected to have new functions, for example, office buildings and commercial facilities, are almost the same as those used in Ja-

pan. These kinds of buildings use global standard construction systems that are almost the same anywhere in the world. Conventional construction systems are suitable for buildings that serve functions that do not change for a certain period of time, and dwellings are typical of such buildings. In many countries, dwellings account for the major part of building construction, and they are likely to reflect the actual situations of conventional construction systems, or production and construction conditions, in each country and area.

## 2.2 Focus of roof construction system

It is said that wind damage is greater than seismic damage. In the case of earthquakes, some breakage of non-structural members in various parts of a building is acceptable, however, breakage of such members as a result of wind can be critical, because it may lead to complete collapse of the building. Many coastal areas in Eastern Asia are hit by typhoons almost regularly from summer to autumn. (For inland areas, frequent occurrence of tornados has been reported recently with the influence of global warming or unknown causes.) In Eastern Asia, most dwellings generally have masonry walls on all external perimeters, and roofs become the focus of study concerning wind resistance.

Assuming that full collapse-resistant measures are taken for buildings, the major damage by wind is caused by negative pressure and wind updraft.

It is generally assumed that wind damage to buildings with flat roofs comprising a reinforced concrete slab is rare. However, damage to buildings with pitched roofs has been reported in many countries and areas, and it is a problem that cannot be ignored.

Fig.1. shows some patterns of damage and collapse of buildings due to wind. The target of this research is to develop reinforcing measures to prevent the effects shown in Fig.1.2 (roof parts) and Fig.1.3 (roof structure and roof frame).

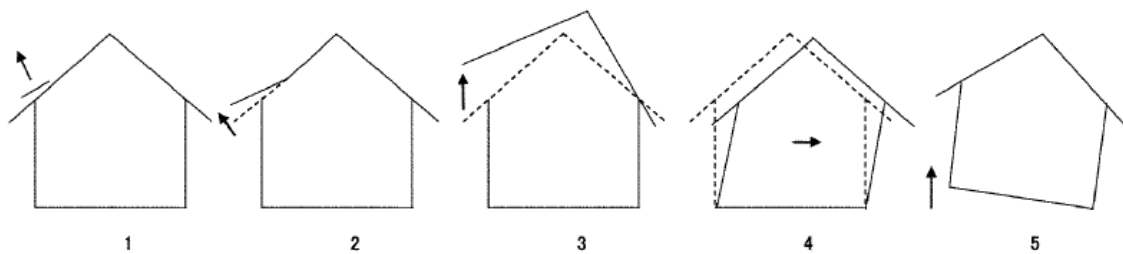


Fig.1. Building Damage by Wind

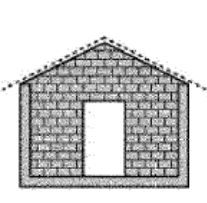
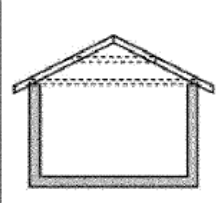
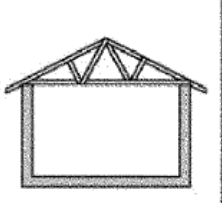
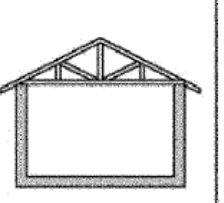
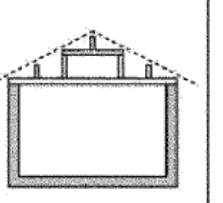
				
1 Masonry	2 Couple roof (Principle rafter)	3 Trussed rafter	4 Roof truss	5 Post frame

Fig.2. Frame (Structure) Type of Pitched Roof

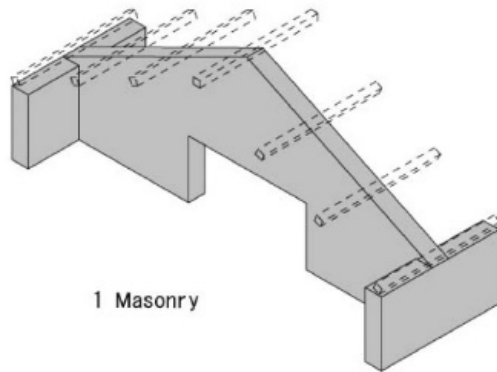


Fig.2.1 iso. Masonry as Roof Structure

### 3. SYSTEM OF STUDY

At the beginning of this research, existing pitched roof systems were investigated as follows.

- 1) Textbooks on building construction of university and technical college were collected and information was compiled to determine common conventional construction systems.
- 2) Literatures were collected on the pitched roofs of some traditional construction systems on which most such systems are based, as well as various kinds of related materials including production and construction conditions, to complement the above information 1.
- 3) Construction sites and housing estates were visited to determine which construction systems were actually implemented in each area and to hear opinions from students with knowledge and interest in the building construction of pitched roof systems, to complement the above information 1 as well as 2.

The authors have not yet collected sufficient material and have visited only a few places in the centers of cities for short periods. As a result, this paper describes only part of the actual situation.

### 4. RESULTS AND DISCUSSIONS

#### 4.1. Roof structure

Fig.2. shows typical roof structures or roof frames that appear in textbooks that were collected. The masonry systems shown in Fig.2.1 are used in many countries and areas other than Japan. The trussed rafter systems shown in Fig.2.3 are peculiar to Singapore and Malaysia with trusses made of wooden boards such as 2×4. A couple roof, as shown in Fig.2.2, and similar systems consist of wooden boards like those used for the wooden trussed rafter system (Fig.2.3), or of round or square timber. The former roof frames are closely spaced as a roofing substrate, like rafters for the trussed rafter system. However, the latter roof frames are more widely spaced, like other roof framing structures.

Fig.2.4 shows a roof truss system that can be engineered with large spans, and is widely used. The post frame systems shown in Fig.2.5 are very common in Japan and are also seen in many other countries and areas.

## 4.2 Roof layer construction

Fig.3. shows typical layered construction systems from roofing to underlay on roof structures only. Roof frames are widely spaced for types from Fig.3.1 to Fig.3.10 with purlins. However, for types shown from Fig.3.11 to Fig.3.15, roof frames are closely spaced, such as trussed rafter systems with wooden boards, couple roofs, and other similar systems. Although the authors think the vertical battens shown in Fig.3.1 (Fig.3.1 iso) are very effective in discharging rainwater, they are rarely seen in Japan, and the type shown in Fig.3.5 is used widely in Eastern Asia including Japan. Types using galvanized metal sheets as roof sheathing, as shown in Fig.3.7 (Fig.3.7 iso) and Fig.3.8, are peculiar to the Philippines and are also seen in Taiwan. Types using thick roofing felts as substitutes for roof sheathings, shown in Fig.3.9 and Fig.3.11, are conventional roof systems in Singapore and Malaysia.

In general, it is expected that systems with more roofing layers can be easily adapted for varied performance. Roofing layers are determined in accordance with the level of precipitation, one of the most important elements in each region, so it is considered that overall roofing construction methods are connected with weather conditions in each region. However, according to the results of The authors' previous investigation, it seems that the distribution of pitched roof construction methods is related to spatial formation (styles) and types of materials, and is not necessarily related to weather conditions. Pitched roof systems made of cast-insitu concrete are excluded from this paper.

## 4.3 Support system for eaves

As most construction systems with eaves and rakes projecting from the building are cantilevered, they are the weakest points against wind. Fig.4 shows typical support systems at eaves in Eastern Asia. The systems are related to the roof structures or roof frames and layer constructions, and the Common Rafter systems of Fig.4.2 can be seen in many countries and areas including Japan. For systems with roof sheathing shown in Fig.4.3, the eaves are short and the Principal Rafter systems shown in Fig.4.1 allow long eaves.

Fig.4.1 3iso is an isometric drawing showing their details. The systems of Fig.4.5 combine various horizontal materials with roof sheathing or common rafter. Every system is expected to be effective in providing structural stability at the eaves. The systems of Fig.4.6 use other special materials for the eaves and it is considered that all of these systems were devised for not only structural reasons but also for their details.

## 4.4. Support system for rakes

Fig.5. shows typical support systems at rakes in Eastern Asia. The systems are also related to the roof structure or roof frame and layer construction. Other members of Fig.5.2 (Fig.5.2 iso) are used in the case of roof layer construction without purlins, Fig.3.11 or 3.12 and the roof frame type is the Couple roof (Fig.2.2) or Trussed rafter (Fig.2.3).

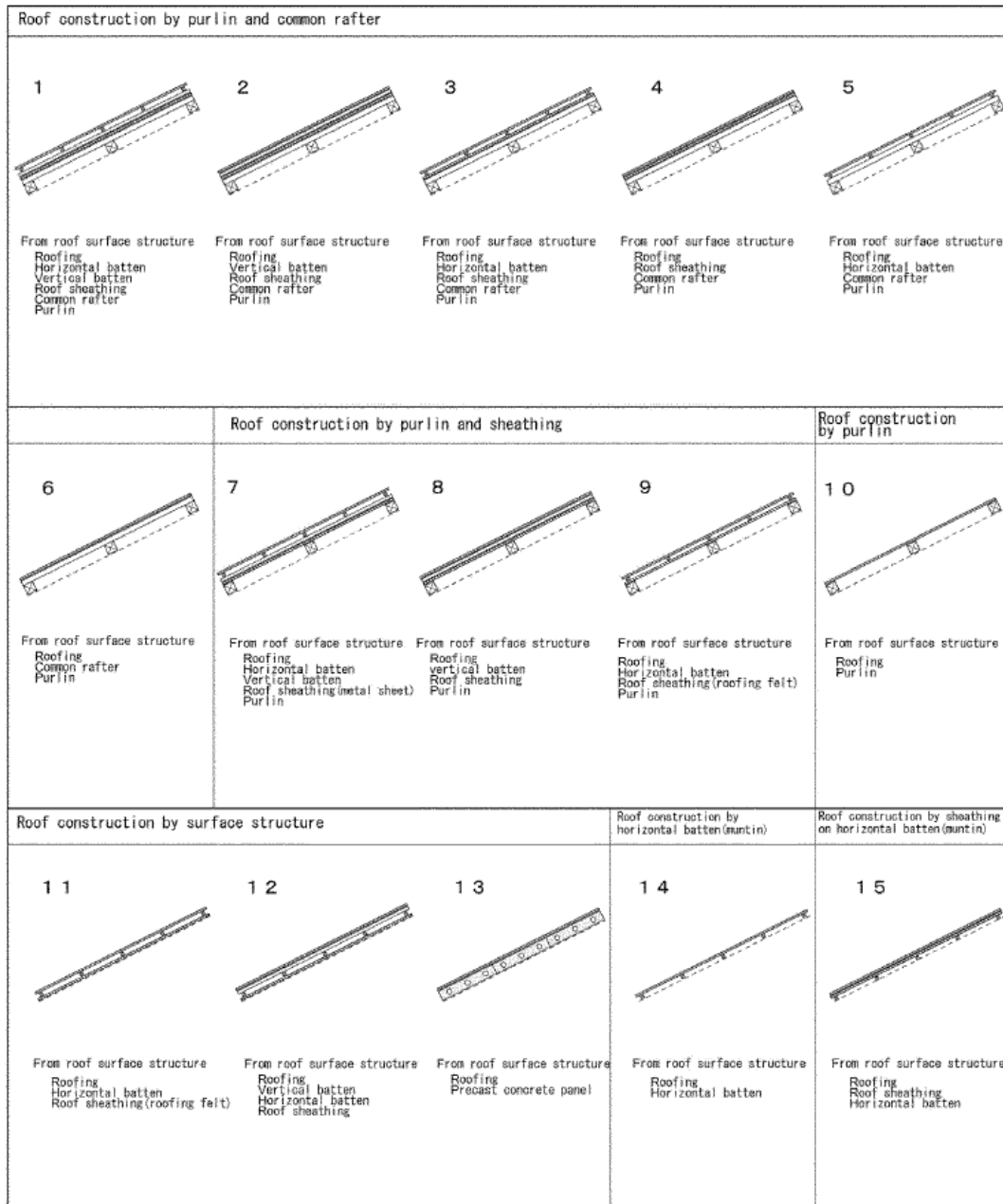


Fig.3. Layer Construction of Pitched Roof

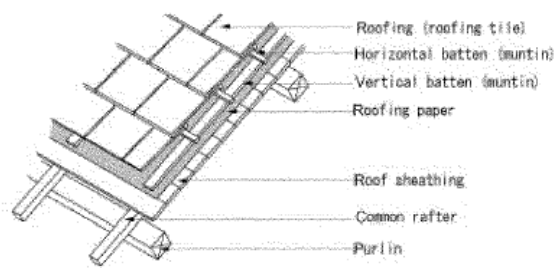


Fig.3.1 iso. Horizontal Batten on Vertical Batten

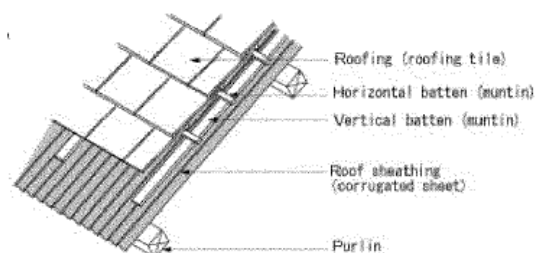


Fig.3.7 iso. Corrugated Sheet as Roof Sheathing

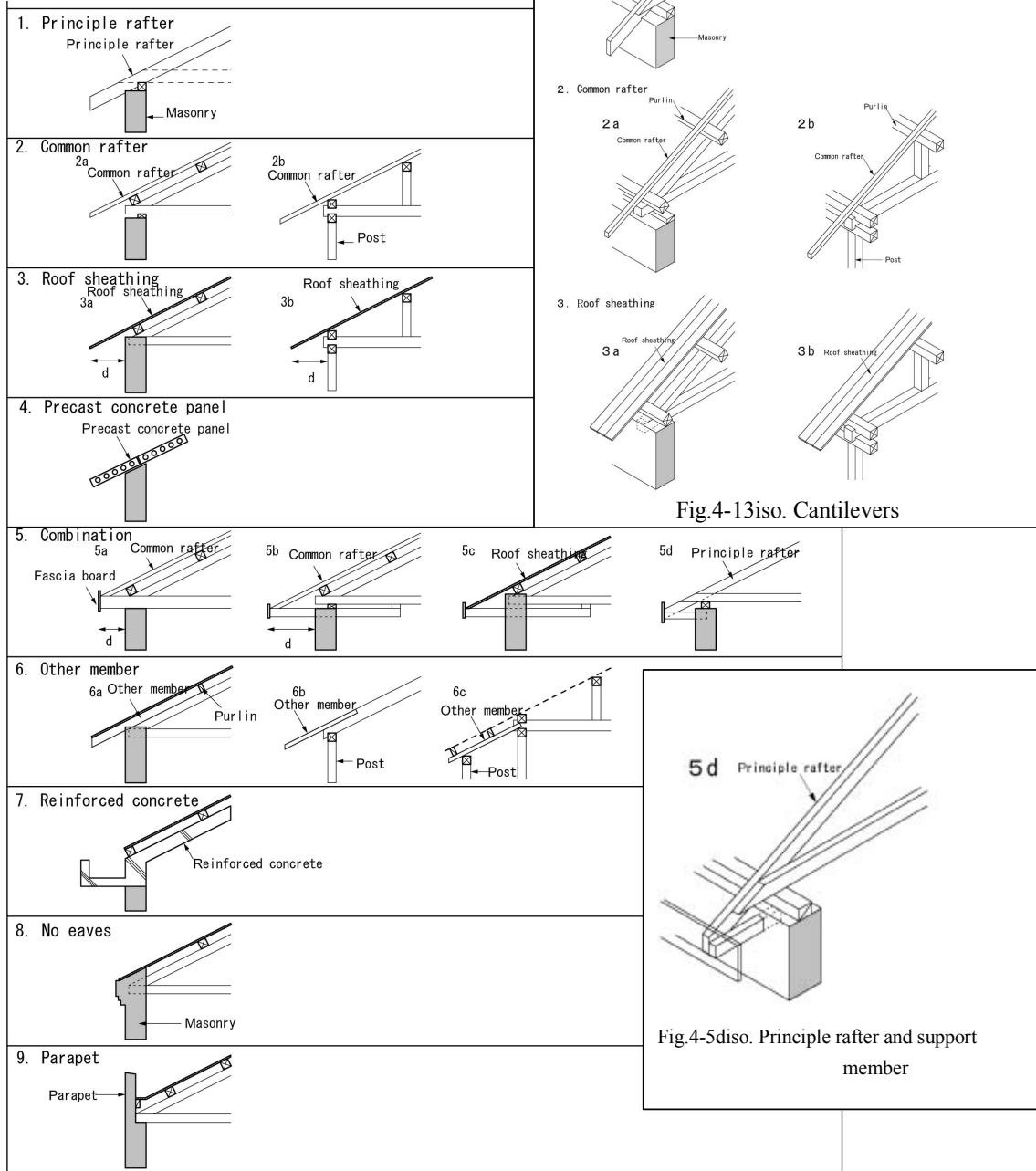


Fig.4. Support Type of Eaves

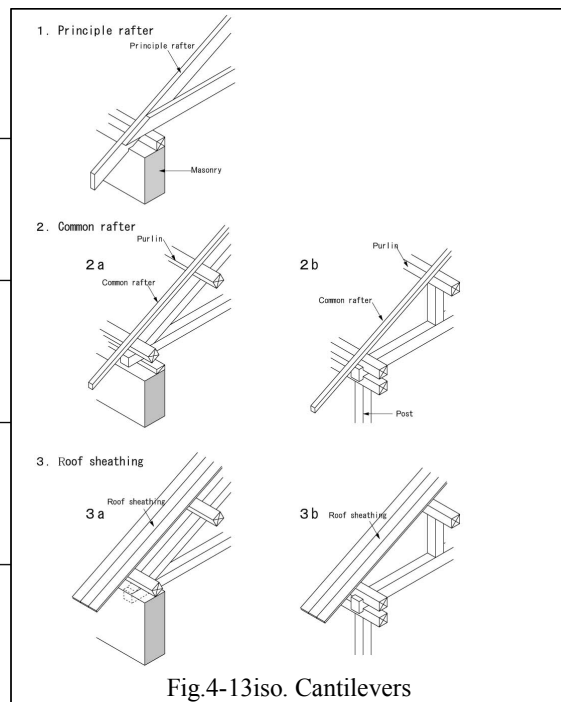


Fig.4-13iso. Cantilevers

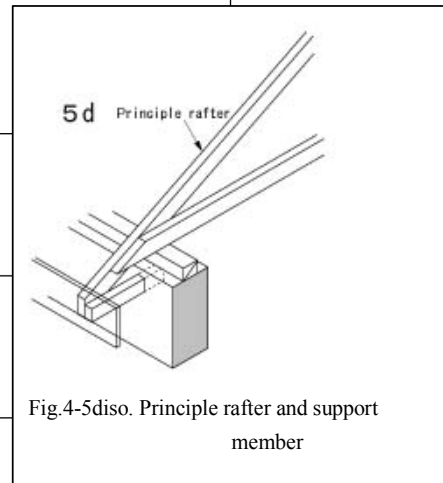


Fig.4-5diso. Principle rafter and support member

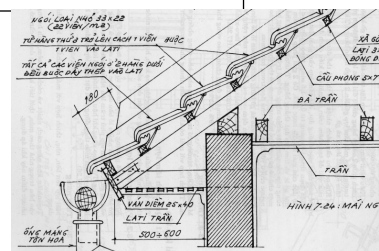


Fig.4-5dtx. Figure<sup>2)</sup> in Vietnamese Textbook

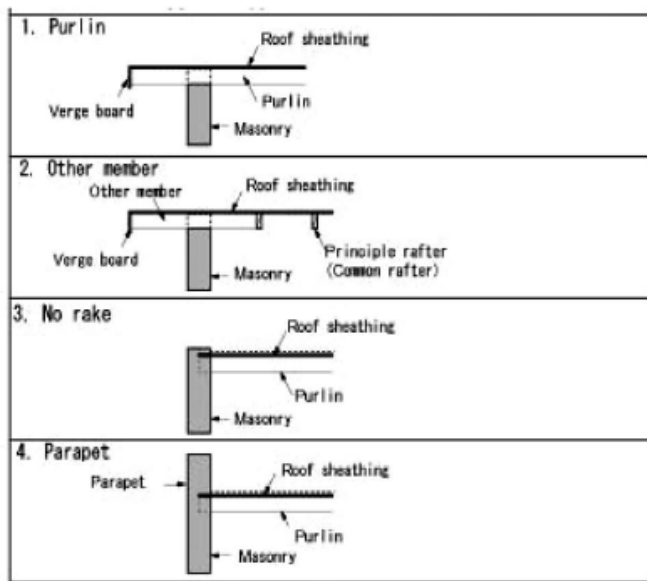


Fig.5. Support Type of Rakes

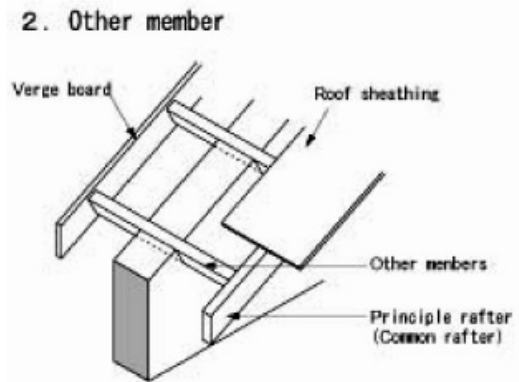


Fig.5.2 Other Member

#### 4.5 Comparison

Table 1. shows structures and framing types of pitched roof identified through textbooks and so on for each country or area in Eastern Asia, Table 2. shows layer construction of roof surface, and Table 3. shows support types for eaves and rakes.

China has a very large land area, and covers most kinds of roof construction systems in Southeast and East Asia. In Malaysia and Singapore, teaching materials of Western countries are used as textbooks and this significantly affects their construction systems.

The authors' identifying work covers a limited range through a limited number of documents, students and visited areas. Thus, the results of Table 1., 2. and 3. are not comprehensive and are subject to error. The authors expect various opinions from experts in building construction in each country and area following this contribution to the Journal.

#### 5. CONCLUSION

Eaves and rakes which project from a building itself are the most important points. However, there are no acknowledged distribution factors of wind pressure on roof surfaces with eaves and rakes and there are no accepted simultaneous probabilities of wind velocity and rainfall. A proposal for standard reinforcing methods for existing conventional construction systems will be decided through a study based on climate data of wind velocity and rainfall, and engineering data of wind force coefficient, as discussed above.

It is effective not only to rigidly connect each member with the roof structure or roof frame through the use of hardware, but also to increase member structural stability in existing construction systems. At the present time, the authors are interested in construction systems using an additional member such as that shown in Fig.4.5diso.

Fig.4.5dtex shows the original figure in a textbook from Vietnam.

Table 1. Frame (Structure) Type of Pitched Roof

	M	P	T	R	F	M+P	M+R	M+F	P+R
	Masonry	Principle Rafer (Couple roof)	Trussed Rafter	Roof Truss	Post Frame				
Japan		○		○	○				○
China	○	*		○	○		○	○	
Korea	○		○	○	○			○	
Taiwan	○				○				
Thailand		○	○	○					
Vietnam	○	○		○	○			○	
India	○	○		○	○	○	○		
Philippine	○	○		○	○	△	△		
Malaysia	○	○	○	○		○			○
Singapore	○	○	○	○		○			○
Indonesia	○	○	○	○	○				○

○ : Textbooks( and so on) △ : Others (visiting and surveying)

Table 2. Layer Construction of Roof Surface

	Purlin and Common Rafter					Purlin and Sheathing			Pur- lin	Surface Structure			Horizontal Batten		
	1	2	3	4	5	6	7	8	9	10	11	12	13	14	15
Japan		○		○	○						○				
China	○				○		○				○		○		
Korea		○	○	○	○	*									
Taiwan		○	○	○				○							
Thailand														○	
Vietnam					○		○		○	○			○	○	
India				○	○		○		○	○			○	○	○
Philippine						*	○	○		○		○		○	
Malaysia		○	○						○		○				
Singapore											○				
Indonesia					○	*									
(Figure)	1	2	3	4	5	6	7	8	9	10	11	12	13	14	15

○ : Textbooks \* : Traditional?

Table 3. Support Type for Eaves and Rakes

	Eaves							Rakes		
	Principle Rafter/ Roof Truss	Common Rafer	Roof Sheathing	Precast Concrete Panel	Combination	Other Member	Parapet/ (Fascia)	Purlin	Other Member	Parapet/ (Verge)
Japan		○			*		○	○		○
China		○	○	○	○	○	○	○	○	○
Korea	△	○			○					
Taiwan		○	△			○	○			○
Thailand	○	△					△			
Vietnam	○	○	○	○	○	○	○	○		○
India	○	○			○		○	○		○
Philippine	○	○			○	○	○	○		○
Malaysia	○	○			○		○		○	○
Singapore	○				○		○		○	○
Indonesia	○	○			○	○	○	○		○
(Figure)	1	2	3	4	5	6	7,8	1	2	3,4

○ : Textbooks △ : Others \* : Traditional?

## ACKNOWLEDGEMENT

The authors would like to thank Yasuhide Segawa (Archi Shop) for drawing many standardized figures other than Fig.4.5dtext, and would also like to introduce the following students and others who researched teaching materials, collected them, and complemented various information.

China: Li Yuan Qi (Tongji University), Akira Natori (Toyo University)

Korea: Yongsun Kim (Tokyo University), Sungil Hong (Wonkwang University)

Philippine: Ronwaldo E.R. Aquino (VIbrametrics inc), Caryn G. Paredes

Thailand: Waricha Wongphyat, Areemit Narongwit

Vietnam: Nguyen Ngoc, Ly The Dan, Thanh Trung Vu

India: K.M.Parammasivam (Anna University), Rajeev Gupta (Indian Institute of Technology)

Indonesia: Pandita (JI. Tanjung), Yuji Katoh (Sumitomo Corporation)

This paper describes a part of the study that was made under the 21st Century COE program implemented by the Ministry of Education, Culture, Sports, Science and Technology (over a period from fiscal 2003 to 2007).

## NOTES

1) It is especially difficult to judge whether each foreign construction system is conventional or not.

2) This figure is quoted from pp. 245 of the Vietnamese Textbook in References.

## REFERENCES

Many reference books were used for this paper. The following are the representative textbooks or literatures of each country and area.

China: Han Shinwa, "The Principle and Design of Building Construction"(Tianjin University Press, 2004) and others: dozens of books.

Korea: Jeong-Hyen Kim, Hyong-Dai Kim, other, "The Newest Learning for Building Construction Method" (Kimoondang, 2003) and others: a few books.

Taiwan: Ji-dong Ye, Jhuo-fu Wu, Li-chang Huang, "building methods and construction", (Morion Co., Ltd., 1991) and other.

Thailand: Triwat Viriyasiri and Suriyon Siridhampiti, "Introduction to Building Design and Construction Drawing", (Bangkok: Chulalongkorn University Press, 2005) and other.

Vietnam: Phan Tan Hai, Vo Dinh Diep, Cao Xuan Luong, "PRINCIPLE OF ARCHITECTURAL DETAIL DESIGN", (Statistical Publisher, 2003) and others: a few books.

India: S.C.Rangwala, K.S.Rangwala, P.S.Rangawla, "Building Construction", (S.B.Patle, Charotar Publishing House, 2004) and others: a few books.

Philippine: Max B. Fajardo Jr. "Simplified Methods on Building Construction" (5138 Merchandising Publisher, 2001) and others: a few books.

Malaysia: Ivor H. Seeley "Building Technology Fifth Edition" (Pal grave Publishers Ltd, 1995) and other.

Singapore: Roy Chudley, Revised by Roger Greeno "Construction Technology Third Edition" (Pearson Education Limited, Addison Wesley Longman Limited, 1999) and other.

Indonesia: Reimar Schefold, Peter J.M. Nas and Gaudenz Domenig, "Indonesian Houses Tradition and transformation in vernacular architecture", (Singapore University Press, 2003).

# Prediction of lower pressures on a porous roof cover sheet

Vu Thanh Trung<sup>1</sup>, Yukio Tamura<sup>1</sup> and Akihito Yoshida<sup>1</sup>

<sup>1</sup>*Wind Engineering Research Center, Tokyo Polytechnic University, Tokyo, 243-0297 Japan*

**ABSTRACT:** This paper describes a computational method for predicting the lower pressures on a porous roof cover sheet with respect to two porosities and various wind angles from known upper pressures. The resulting computational results are shown to closely model experimental results. The method is based on the unsteady form of the Bernoulli equation.

**KEY WORDS:** Porous roof cover sheet, low-rise building, unsteady Bernoulli equation, wind tunnel experiment

## 1 INTRODUCTION

Thermal reduction is always a problem for building roofing systems, especially profiled steel sheet systems, and roofing systems with porous roof cover sheets have been applied to overcome it. A few experimental studies have been carried out on wind loading on permeable roofing systems (Kramer et al.[1, 2]; Kind and Wardlaw[3]; Cheung and Melbourne[4]; Amano et al.[5]; N. Chino et al[6]; B. Bienkiewicz and Y. Sun[7, 8]).

Some studies have also been carried out on internal pressures. Holmes[9] carried out a study on internal pressures in low-rise buildings with both windward and leeward wall openings using wind tunnel experiments and numerical techniques. Liu and Saathoff[10, 11] used the Bernoulli equation approach to predict the variation of internal pressure induced by wind in a single-room building with a single opening, and extended this to multi-room buildings with multiple openings.

Unlike wind loadings on conventional building roofs, wind loadings on porous roof cover sheets comprise a combination of wind pressures on both porous roof cover sheet surfaces. In this study, the authors used a method based on the unsteady form of the Bernoulli equation to compute the lower pressures on a porous roof cover sheet from known upper pressures and compared the computational results with experimental results.

## 2 EXPERIMENT SET UP

A model 200 mm high ( $H$ )  $\times$  470 mm wide ( $B$ )  $\times$  710 mm deep ( $D$ ) with porous roof cover sheets was tested in a Boundary Layer Wind Tunnel 2.2 m wide by 1.8 m high located at Tokyo Polytechnic University, Japan. The length and velocity scales were 1/50 and 1/4, respectively. Terrain category III (power law index 0.2) in AIJ-RFLB (2004)[12] was chosen for the tests. The

turbulence intensity at height 200 mm was 0.26 and the wind speed was 7m/s.

There were 2 test model cases to consider the effect of porosities of the sheets (5% and 10%) with a total of 41 wind direction angles ( $0^\circ$  to  $360^\circ$  in  $10^\circ$  steps and four wind directions angles:  $45^\circ$ ,  $135^\circ$ ,  $225^\circ$  and  $315^\circ$ ). The model had sixteen sheets one of which was porous with 128 holes, while four had pressure taps (A, B, C and D) (see Fig. 1). Models 1 (porosity 5%) and 2 (porosity 10%) had sheets with holes of diameter 2.8 mm and 4 mm, respectively. The gap between the sheet and the top of the profiled roof was 1 mm (see Fig. 1). Fig. 2 shows some pictures of the test model in the wind tunnel.

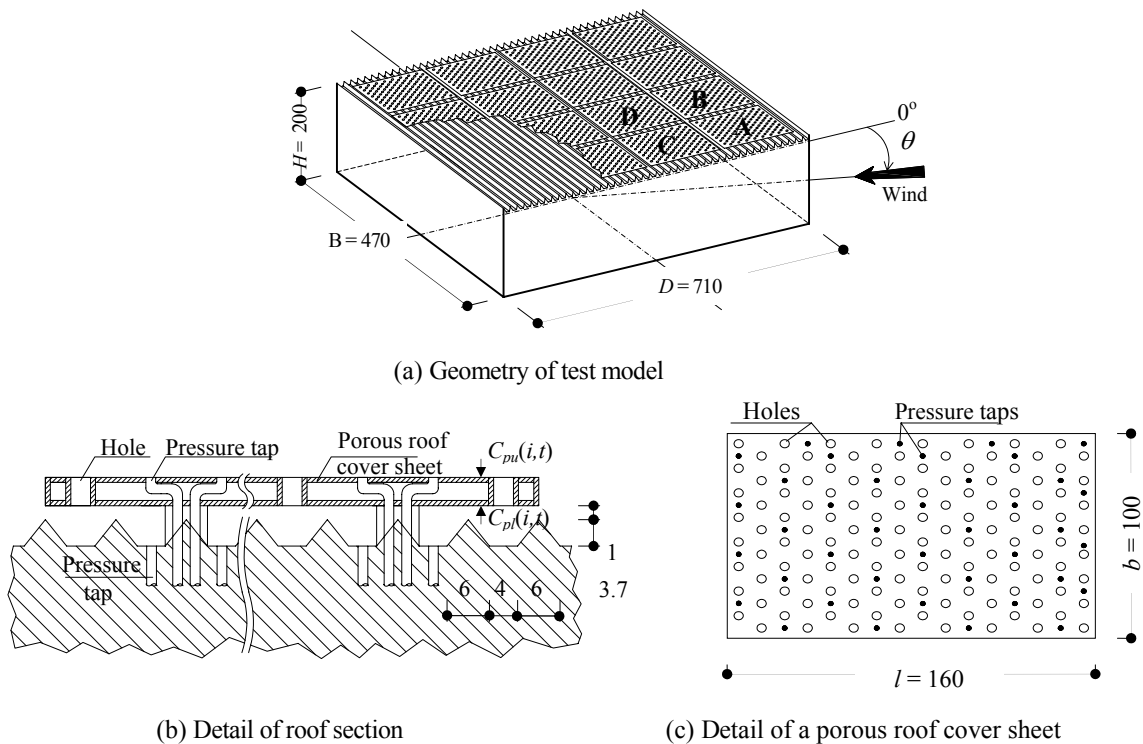
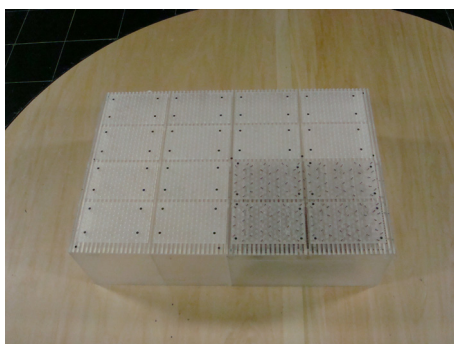


Fig. 1. Test model (all dimensions in mm)



(a) Test model in the wind tunnel



(b) Close-up view of a porous roof cover sheet

Fig. 2. Some pictures of test model in the wind tunnel

### 3 THEORETICAL BACKGROUND

The lower pressures on the sheet depend on the upper pressures and the surrounding pressures. The computational theory was based on the unsteady Bernoulli equation proposed by Liu and Saathoff[11].

Fig. 3 shows the computational model for the sheet. The authors divided the underneath volume of the sheet into small rooms, as shown in Fig. 3.

Assuming that the air flow through the opening was similar to an air jet, the relation between the upper pressure at the  $i$ th opening and lower pressure in the  $i$ th room is as shown in Eq. 1.

$$\rho_a l_{e,i} \dot{V}_{e,i} = P_{e,i} - P_i - \frac{1}{2} \rho_a V_{e,i} |V_{e,i}| - \frac{32\mu t}{d^2} V_{e,i} \quad (1)$$

where  $\rho_a$  is air density,  $l_{e,i}$  is equivalent length of the slug of air at  $i$ th opening ( $l_{e,i} \cong t + 0.8\sqrt{3.14d^2/4}$ ),  $P_{e,i}$  is upper pressure at  $i$ th room,  $P_i$  is lower pressure at  $i$ th room,  $V_{e,i}$  is velocity of the air-flow through  $i$ th opening,  $\mu$ : the viscosity of air,  $d$  is diameter of hole (opening),  $t$  is thickness of sheet. The symbol  $\dot{\bullet}$  above a variable denotes time differentiation. The last term on the right-hand side of Eq. 1 represents pressure drop due to Poiseulle flow.

The relation between the lower pressure in the  $i$ th room and that in the  $(i+1)$ th room is shown in Eq. 2.

$$\rho_a l_{i,i+1} \dot{V}_{i,i+1} = P_i - P_{i+1} - \frac{1}{2} \rho_a V_{i,i+1} |V_{i,i+1}| - \frac{1}{2} K \rho_a V_{i,i+1} |V_{i,i+1}| - \frac{12\mu L}{a W} V_{i,i+1} \quad (2)$$

where  $l_{i,i+1}$  is equivalent length of slug of air at opening between  $i$ th room and  $(i+1)$ th room,  $P_i$ ,  $P_{i+1}$  are lower pressures in  $i$ th room and  $(i+1)$ th room respectively,  $K$  is loss coefficient (= 46),  $a$  is gap between cover sheet and roof,  $L$  is length of imaginary room,  $W$  is width of imaginary room, and  $V_{i,i+1}$  is velocity of air-flow between  $i$ th room and  $(i+1)$ th room. The fourth term on the right-hand side of Eq. 2 represents pressure drop due to orifice. The last term on the right-hand side of Eq. 2 represents pressure drop due to surface friction along the length of the sheet.

The relation between the lower pressure in the  $i$ th room and that in the  $(i+3)$ th room is shown in Eq. 3.

$$\rho_a l_{i,i+3} \dot{V}_{i,i+3} = P_i - P_{i+3} - \frac{1}{2} \rho_a V_{i,i+3} |V_{i,i+3}| - \frac{12\mu W}{a L} V_{i,i+3} \quad (3)$$

where the last term on the right-hand side of Eq. 3 represents pressure drop due to surface friction along the width of the sheet.

In addition, assuming compressibility of air in the  $i$ th room under adiabatic conditions, the relation between the lower pressures and the flow velocity from the continuity equation is as shown in Eq. 4.

$$\dot{P}_i = (nP_a/U_i)(A_{e,i}V_{e,i} + A_{i-1,i}V_{i-1,i} + A_{i-3,i}V_{i-3,i} - A_{i,i+1}V_{i,i+1} - A_{i,i+3}V_{i,i+3}) \quad (4)$$

where  $n$  is polytrophic exponent (is - 1.4 for adiabatic air),  $P_a$  is atmospheric pressure,  $U_i$  is volume of  $i$ th room,  $A_{*,**}$  is cross-sectional area of opening between  $(*)$ th room and  $(**)$ th room.

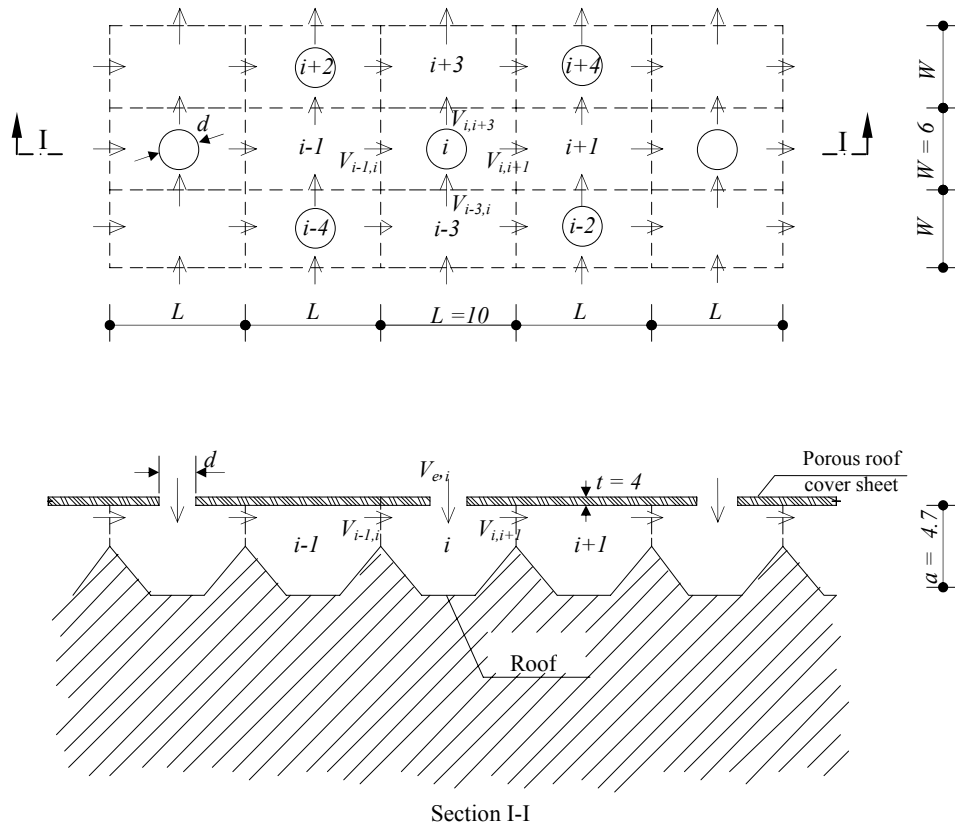


Fig. 3. Computational model (all dimensions in mm)

The first-order, simultaneous equations for the upper pressures at the openings and the lower pressures in the rooms are derived from Eqs 1, 2, 3 and 4 for each room. The lower pressures can be obtained from the known values of the upper pressures by solving the differential equations. In this study, the lower pressures were obtained by solving the differential equations under the experimental values of the upper pressures using the 4th Runge-Kutta method. The computational results were compared with the experimental results of the lower pressures.

#### 4 RESULTS AND DISCUSSION

In this study, the authors calculated the lower pressures on sheet A (corner region) with two porosities 5% and 10% for 17 wind direction angles ( $0^\circ$  to  $360^\circ$  in  $30^\circ$  steps and four wind directions angles:  $45^\circ$ ,  $135^\circ$ ,  $225^\circ$  and  $315^\circ$ ).

The contour plots of the experimental and computational results for the lower mean and rms wind pressure coefficients ( $\bar{C}_{pl}$  and  $C'_{pl}$ ) for sheet A for porosities 5% and 10% at wind angle  $\theta = 0^\circ$  are shown in Fig. 4. Comparison between the experimental and computational results shows good agreement for the distribution of  $\bar{C}_{pl}$  and  $C'_{pl}$ .

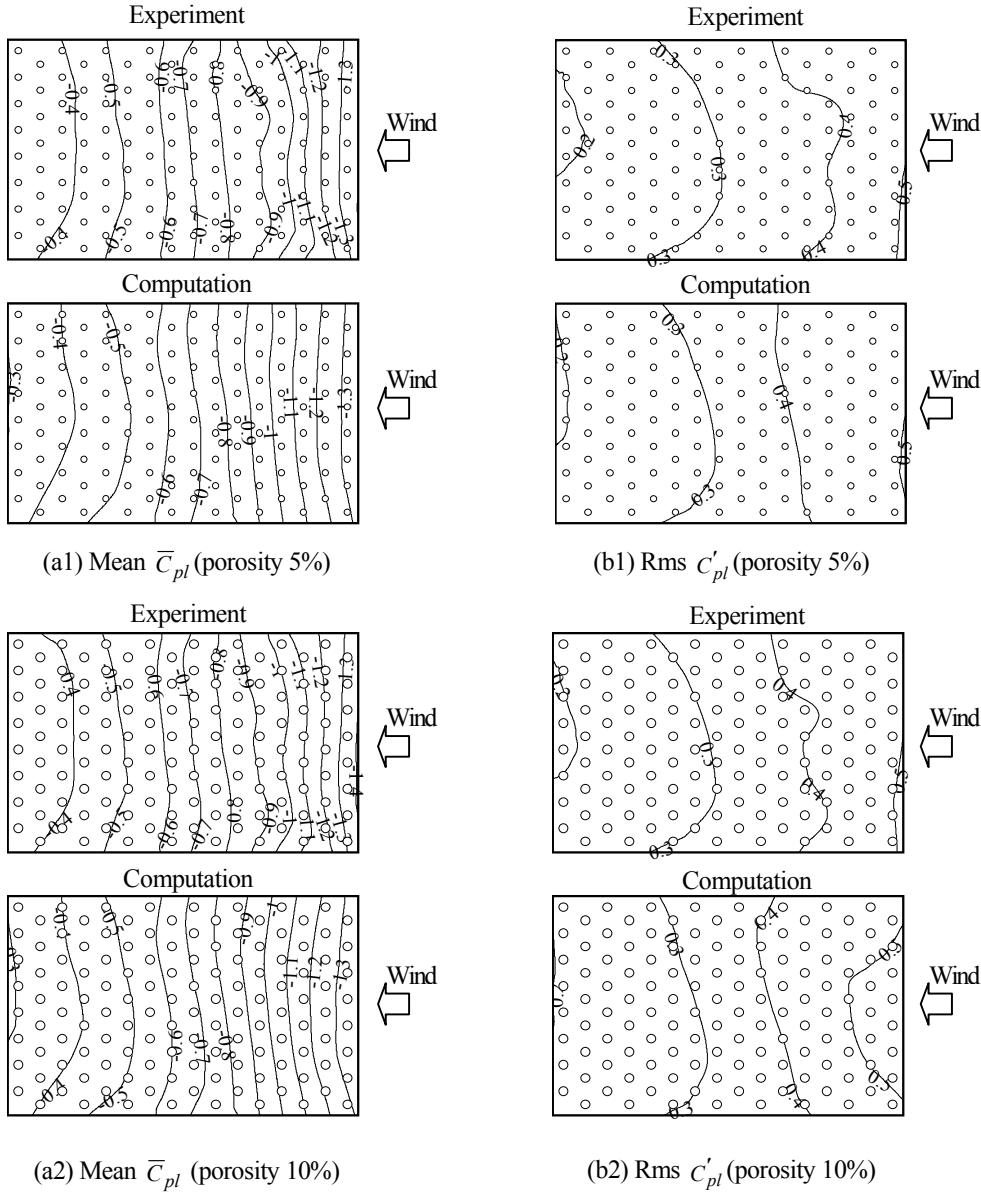


Fig. 4. Comparison between experimental and computational results for mean and rms pressure coefficients ( $\bar{C}_{pl}$  and  $C'_{pl}$ ) on the lower surface of porous roof cover sheet A with porosity at wind angle  $\theta=0^\circ$

The panel wind pressure coefficient  $C_{psl}$  on the lower surface of sheet A was calculated as follows.

$$C_{psl}(t) = \sum_{i=1}^N (C_{pl}(i,t) \cdot F_i) / F \quad (5)$$

where  $C_{psl}(t)$  is panel wind pressure coefficient on the lower surface of sheet A at time  $t$ ;  $C_{pl}(i,t)$  is the wind pressure coefficient at point  $i$  at time  $t$  on the lower surface of sheet;  $F_i$  is the effective area on which wind pressure acts measured at point  $i$ ;  $N$  is the number of measurement points on sheet A; and  $F$  is the area of sheet A ( $= l \cdot b$ ) (see Fig. 1).

Fig. 5 compares computational and experimental results for  $C_{psl}$ . From this figure, it is apparent that:

(1) For porosity 5%, overall agreement between the present computational results and the available experimental data is actually quite good. At wind angles  $\theta$  from  $30^\circ$  to  $90^\circ$ , there are slight differences (about 0.1 and 0.03 for mean and rms panel wind pressure coefficients ( $\bar{C}_{psl}$  and  $C'_{psl}$ ) on the lower surface of the sheet, respectively) between computational results and experimental data, particularly for wind angle  $\theta = 45^\circ$ . For the rest, the difference is very small.

(2) For porosity 10%, the present computational results are very similar to those of the experiment except for those for wind angles  $\theta$  from  $30^\circ$  to  $90^\circ$  and the differences are less than those for porosity 5%.

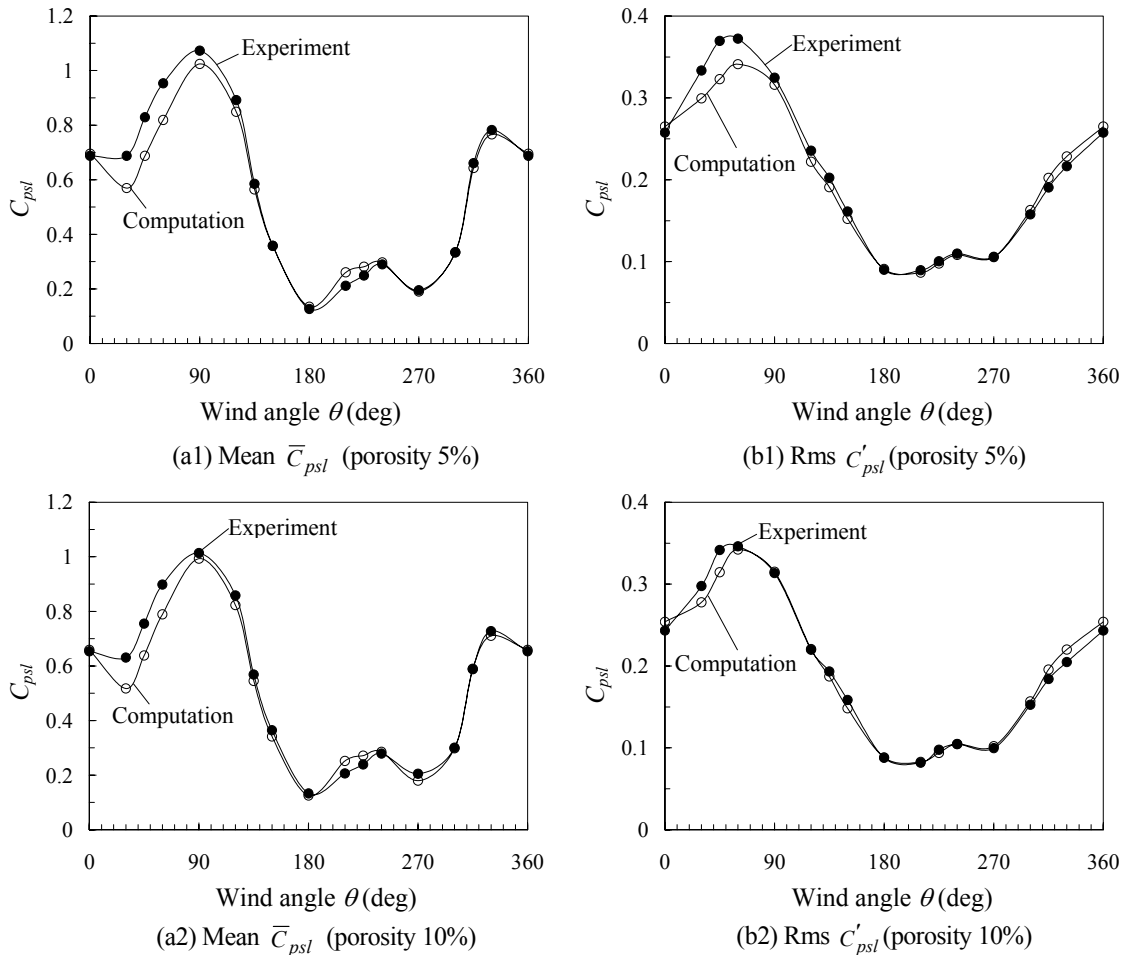


Fig. 5. Comparison between experimental and computational results for mean and rms panel wind pressure coefficients ( $\bar{C}_{psl}$  and  $C'_{psl}$ ) on the lower surface of porous roof cover sheet A with porosity for all wind angles  $\theta$

Fig. 6 shows time series of the panel wind pressure coefficients  $C_{psl}$  on the lower surface of sheet A at wind angles  $\theta = 0^\circ$  and  $45^\circ$ . Good agreement can be seen between the computational and experimental results.

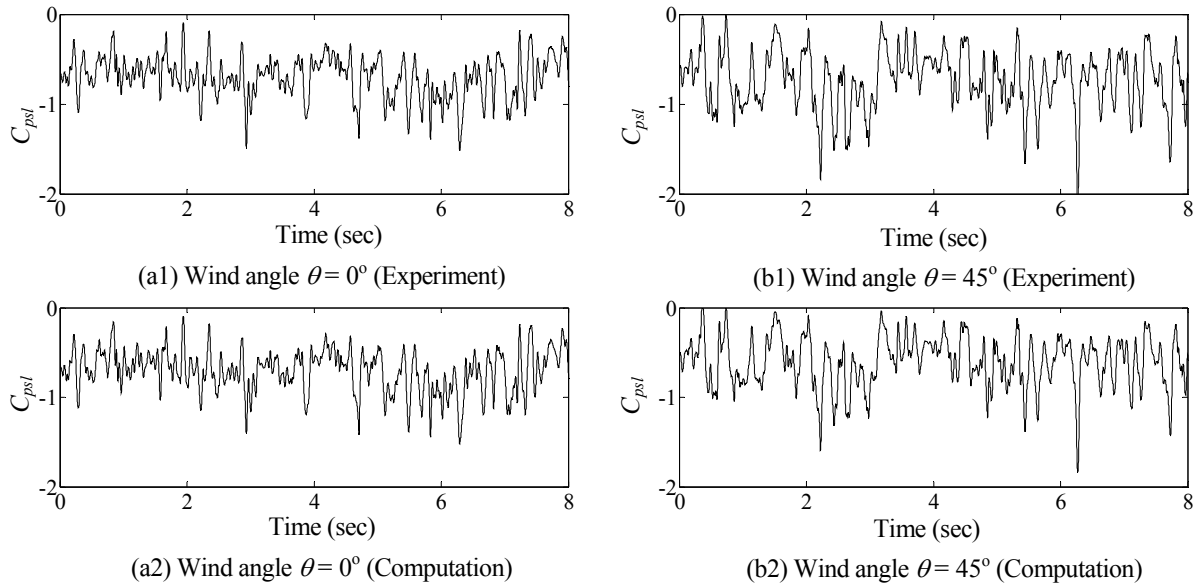


Fig. 6. Comparison between experimental and computational results for time series of the panel wind pressure coefficients  $C_{psl}$  on the lower surface of porous roof cover sheet A, with porosity 5% and wind angle  $\theta$

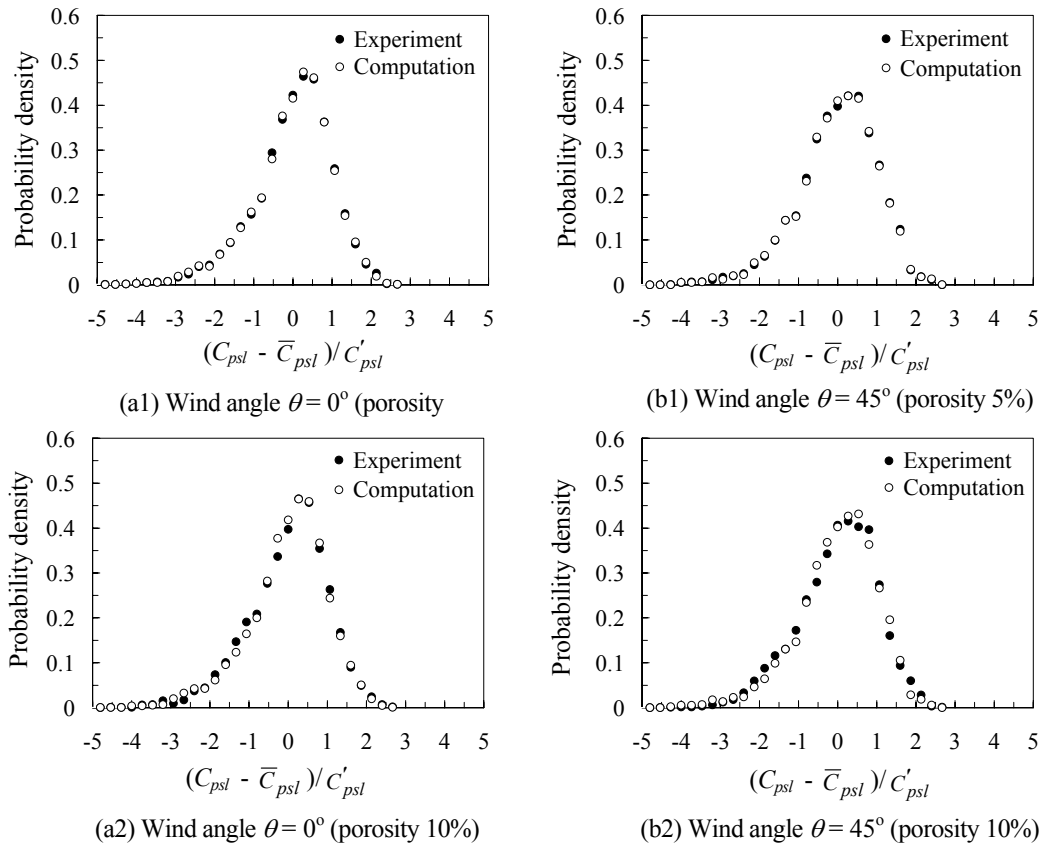


Fig. 7. Comparison between experimental and computational results for probability density function of the panel wind pressure coefficients  $C_{psl}$  on the lower surface of porous roof cover sheet A, with porosity and wind angle  $\theta$

Furthermore, Fig. 7 compares the computational and experimental results of the probability density function of the panel wind pressure coefficients  $C_{psl}$  on the lower surface of sheet A at wind angles  $\theta = 0^\circ$  and  $45^\circ$ . It is clear that the computational results closely model the experimental results.

Fig. 8 shows spectra of both computation and experiment. This also shows good agreement.

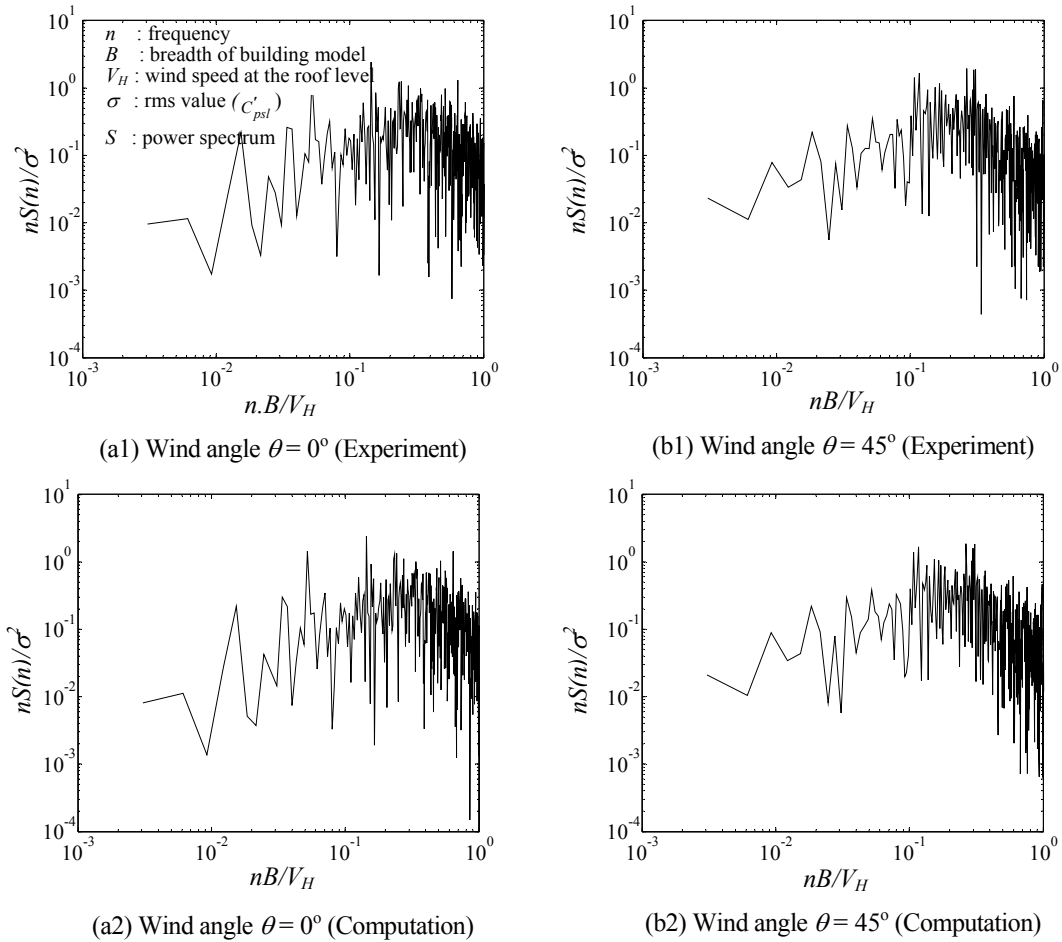


Fig. 8. Comparison between experimental and computational results for spectrum of the panel wind pressure coefficients  $C_{psl}$  on the lower surface of porous roof cover sheet A, with porosity 5% and wind angle  $\theta$

## 5 CONCLUSIONS

The lower pressures of a porous roof cover sheet with respect to two porosities and various wind angles were predicted by a computational method based on the unsteady form of the Bernoulli equation. The computational results closely model the experimental results. Lastly, this method will be valuable for predicting the lower pressures on a porous roof cover.

## ACKNOWLEDGEMENTS

This study was funded by the Ministry of Education, Culture, Sports, Science and Technology, Japan, through the Global Center of Excellence Program, 2008-2013, which is gratefully acknowledged. The authors would also like to thank to SAWAYA Co., Ltd, Japan.

## REFERENCES

1. Kramer, C., Gerhardt, H.J. and Kuster, H.W. (1979). "On the wind-loading mechanisms of roofing elements", *J. Wind Eng. Ind. Aerodyn*, 4, 415-427.
2. Gerhardt, H.J. and Kramer, C. (1983). "Wind loads on wind-permeable building facades", *J. Wind Eng. Ind. Aerodyn*, 11 1-20.
3. Kind, R.J. and Wardlaw, R.L. (1982), "Failure Mechanisms of Loose-Laid Roof-Insulation Systems", *J. Wind Eng. Ind. Aerodyn*, 9, 325-341.
4. Cheung, J.C.K. and Melbourne, W.H. (1988), "Wind loading on a porous roof", *J. Wind Eng. Ind. Aerodyn*, 29, 19-28.
5. Amano, T., Fuji, K., and Tazaki, S. (1988), "Wind loads on permeable roof-blocks in roof insulation systems", *J. Wind Eng. Ind. Aerodyn*, 29, 39-48.
6. Chino, N., Iwasa, Y., Mataka, Y., Hagiwara, T. and Sato, H. (1991), "Internal pressure of double composite exteriors", *J. Wind Eng. Ind. Aerodyn*, 38, 381-391.
7. Bienkiewicz, B. and Sun, Y. (1992), "Wind-tunnel study of wind loading on loose-laid roofing systems", *J. Wind Eng. Ind. Aerodyn*, 41-44, 1817-1828.
8. Bienkiewicz, B. and Sun, Y. (1997), "Wind loading and resistance of loose-laid roof paver systems", *J. Wind Eng. Ind. Aerodyn*, 72, 401-410.
9. Holmes, J.D. (1979), "Mean and fluctuating internal pressures induced by wind", *Proc. 5th Int. Conf. on Wind Engineering*, Fort Collins, CO, 435-450.
10. Liu, H. and Saathoff, P.J. (1981), "Building internal pressure: Sudden change", *J. Eng. Mech. Div. ASCE*, April, 309-321.
11. Saathoff, P.J. and Liu, H. (1983), "Internal pressure of multi-room buildings", *J. Eng. Mech. Div. ASCE*, June, 908-919.
12. AIJ-RFLB (2004), "AIJ Recommendations for Loads on Buildings", Architectural Institute of Japan.